

An investigation into the surface chemistry of
supported gold phosphine clusters

A thesis submitted in partial fulfilment of the requirements for
the degree of

Doctor of Philosophy in Chemistry

By

David Philip Anderson

University of Canterbury

New Zealand

2013

[This page was intentionally left blank]

Table of Contents

| | |
|---|--------|
| Acknowledgments..... | -VI- |
| Collaborators..... | -VIII- |
| Abstract..... | -IX- |
| Abbreviations..... | -X- |
| Chapter 1 – Introduction | |
| Overview | - 1 - |
| Motivation..... | - 1 - |
| Nanoparticles and clusters | - 4 - |
| Catalysis | - 8 - |
| Heterogeneous oxidation catalysis | - 12 - |
| Gold: a surprising catalyst. | - 14 - |
| Characterisation methods..... | - 19 - |
| Scope of this dissertation..... | - 24 - |
| References..... | - 27 - |
| Chapter 2 – Preparation of phosphine stabilised gold clusters | |
| Ligand protected metal clusters | - 32 - |
| Phosphine and thiol stabilised gold clusters | - 34 - |
| Synthesis of phosphine stabilised gold clusters..... | - 36 - |
| Characterisation of the gold phosphine clusters | - 44 - |
| Summary..... | - 51 - |
| Bridge..... | - 51 - |
| References..... | - 52 - |

Chapter 3 – Far infrared of phosphine stabilised gold clusters

| | |
|-----------------------------|--------|
| Objectives..... | - 55 - |
| Introduction..... | - 55 - |
| Experimental | - 59 - |
| Results and discussion..... | - 63 - |
| Summary..... | - 69 - |
| References..... | - 70 - |

Chapter 4 – Preparation of supported phosphine stabilised gold clusters

| | |
|--|---------|
| Objectives..... | - 72 - |
| Preparation of active heterogeneous catalysts | - 72 - |
| Experimental | - 81 - |
| Characterisation of the supported gold clusters..... | - 87 - |
| Summary..... | - 98 - |
| Bridge..... | - 99 - |
| References..... | - 101 - |

Chapter 5 – Photoelectron spectroscopy of supported gold clusters

| | |
|------------------------------|-----|
| Objectives..... | 104 |
| Introduction..... | 105 |
| Experimental | 116 |
| Results and Discussion | 122 |
| Conclusions..... | 145 |
| Bridge..... | 146 |
| References..... | 147 |

Chapter 6 – Catalytic behaviour of supported gold phosphine clusters

| | |
|--------------------|-----|
| Objectives..... | 152 |
| Introduction..... | 153 |
| Experimental | 163 |
| Results..... | 173 |
| Discussion | 190 |
| Conclusion | 193 |
| Bridge..... | 194 |
| References..... | 195 |

Chapter 7 – Further applications of supported gold clusters

| | |
|--|-----|
| Hydrogen gas sensors based on gold clusters..... | 199 |
| Photocatalytic hydrogen production from ethanol..... | 212 |
| References..... | 215 |

Chapter 8 –Concluding summary

| | |
|--|-----|
| Concluding summary and further research..... | 218 |
|--|-----|

Acknowledgements

Beyond a shadow of doubt the completion of this PhD thesis has been one of the most challenging and rewarding experiences so far in my life. During the past few years at the University of Canterbury, I have been privileged to have been given a range of opportunities to get involved in a series of collaborative research projects, provided access to a wide range of quality research apparatus, and also been allowed to attend an assortment of research conferences. I have little doubt that the experiences garnered throughout my studies will provide a great stepping stone to a variety of great new opportunities in the coming years.

All the academic experiences and successes referred to here were made possible by the academics and staff of the Chemistry Department, the MacDiarmid institute and also my parents. From the very start of my PhD, it was apparent that many aspects of this research would need to be started from scratch, and without the skilled help from Nick Oliver, Danny Leonard, Wayne Mackay and Robert McGregor, none of this would have been possible. Thanks to Nick and Danny for designing and manufacturing the catalytic batch reactors and the gas manifold system, that were essential for safe and convenient handling of various flammable gases. Thanks to Rob who skilfully made all the glass apparatus and delicate vacuum manifolds used in this thesis. Thanks to Wayne and Bruce Reid who helped get the 8th floor laboratory up and going from an empty shell on my first day to a fully functioning research lab by the time I had finished my experiments. Thanks to Marie Squire and Matt Polson who ensured that the characterisation my various compounds and reaction mixtures in the Chemistry Department was fast and accurate during the duration of my thesis. I would like to also thank Dr. Milo Kral from Department of Mechanical engineering for access and help to HRTEM facilities.

A special thanks to the whole technical staff of the Department of Chemistry and to their tremendous response to the Canterbury earthquakes. Thanks to Nick, Rob, Wayne and Matt who not only repaired our damaged earthquake battered equipment, broken glassware but also gave us hope that the department would reopen at some point. Thanks to Sato and Mike at the electron microscopy suite in the mechanical engineering department who ensured that the microscopes were running and repaired after the wobbles.

Above all, I can't express my thanks enough to the contributions of my dear supervisor Dr. Vladimir Golovko, whose enthusiasm and passion for this research project was second to none from day one. Throughout my time under his supervision, I gained a great deal of research experience despite the various delays and issue that arose.

Thanks to the Golovko group which has grown over the last four years to be truly *United Nations* of graduate research students. Thanks to Jan-Yves Ruzicka, who started with me in our empty lab at the very start of this project, and understands well the trials and tribulations that we have encountered in the last few years. During the growth of the Golovko research group, I have also had the great pleasure of being involved in a wide range of international collaborations some that have already produced some great work and others that still have a lot of potential. Special thanks to Dr. Gunther Andersson at the Flinders University, and Dr. Greg Metha from the University of Adelaide whom, with Dr. Golovko, have started a truly unique interdisciplinary research collaboration that is generating some truly novel research. Thanks to the team at the SXR Beamline, at the Australian Synchrotron, at which we were able to perform a wide range of photoelectron experiments. Particular thanks to Dr. Lars Thomsen for his insights and help, during the initial phases of these experiments.

I must also acknowledgment the support of my friends and flatmates. Arriving from Europe, I had no idea that I would make such great friendships, which have helped drag me over the finishing line in the last 18 months. Thanks to you all.

Lastly, my eternal gratitude to my parents, Ruth and Shane, who have supported me through 9 years of tertiary education and for providing that extra spark during the tough days of study, and for having the confidence that I could pull this off. This thesis is dedicated to you, and hoping that the next decade will be even more exciting and thrilling than the last.

Thanks you all,

David

Collaborators

During my PhD studies, I was fortunate to be able to collaborate with a wide range of researchers from around the world. Without their input, advice and help, I would not have been able to have done aspects of the work described in several chapters of this thesis.

Chapter 2

EXAFS results were collected and modelled by Professor Gregory Metha, Jason Alvino and Dr. Hugh Harris from the University of Adelaide.

Chapter 3

Far infrared spectroscopy was conducted at the Australia under the guidance Dr Dominique Appadoo. The data was collected inconjunction with Jason Alvino from the University of Adelaide and Baira Donevan from the Golovko research group. The modelling of the far IR data was conducted by Jason Alvino and Professor Gregory Metha.

Chapter 4

HRTEM was conducted at the Department of Mechanical Engineering, University of Canterbury with support from Professor Milo Kral and Mike Flaws. Several samples were also studied HAADF STEM at Monash University by Shery Chang, which help immensely understanding the size and shape of our gold particles on various metal oxide supports.

Chapter 5

Photoelectron spectroscopy experiments were done in coloboration with Dr. Gunther Andersson and Professor Greg Metha. Data analysis and collection was shared amongst all of the collaborators over four trips two the synchrotron. Our work on the electronic structure of supported gold clusters was aided immensely by the contributions of Dr. Lars Thomsen and Dr. Bruce Cowie, who advised us at the Soft Xray Beamline at the Australian Synchrtron.

Chapter 7

Hydrogen gas sensing studies were conducted at the RMIT university by Professor W. Wlodarski and Dr. M. Ahmad. HRTEM and XPS data was collected and analysed by David Anderson. Catalytic hydrogen production was conducted by Dr. Geoff Waterhouse at University of Auckland.

Abstract

This thesis describes the preparation and study of a wide range of supported gold catalysts based on atomically-precise triphenyl phosphine stabilised gold clusters. This selected range of ligand-stabilised gold clusters were prepared in attempt to study the effect of increasing cluster nuclearity on the electronic and catalytic properties of these materials. A novel far-infrared study was conducted on the pure cluster materials in attempt to understand the metal-metal and the metal–ligand vibrations, which was also compared to the simulated spectra for each cluster. The design and activation of these novel catalysts based on gold clusters was discussed and the factors that influence activity were described. A comprehensive photoelectron study of the catalysts was conducted in an attempt to understand the electronic structure of the supported gold clusters and the effect of various activation conditions have on the electronic structure of the gold clusters. A selection of the prepared supported gold catalysts were tested for their catalytic activity for the partial oxidation of styrene and the influence of the several activation conditions on the reactivity of the catalyst is also examined. In collaboration, the application of a selection of ligand-stabilised gold clusters as hydrogen sensors and as catalysts for the photocatalytic generation of hydrogen from ethanol is also investigated.

Abbreviations

Commonly used abbreviations in this thesis:

| | |
|------|--|
| AFM | Atomic force microscopy |
| ALD | Atomic layer deposition |
| ANBF | Australian National Beamline Foundation |
| AS | Australian Synchrotron |
| BE | Binding energy |
| ESD | Electron-stimulated desorption |
| FWHM | Full width half-maximum |
| HBP | High binding energy peak |
| KE | Kinetic energy |
| LBP | Low binding energy peak |
| PES | Photoemission spectroscopy or Photoelectron spectroscopy |
| PVP | Polyvinylpyrrolidone |
| SXR | Soft X-Ray Beamline |
| TEM | Transmission electron microscopy |
| UHV | Ultra high vacuum |
| UPS | Ultra-violet spectroscopy |
| XPS | X-Ray photoelectron spectroscopy |
| RBF | Round bottomed flask |
| TBHP | Tert-butyl hydroperoxide |
| PTFE | Polytetrafluoroethylene |
| RF | Radio Frequency |
| DI | Deionised water |

1 Introduction

Overview

The introductory chapter to this thesis will aim to discuss the motivation for undertaking this research; we will define catalysis and then discuss catalytic oxidation reactions. We will then delve in to the crux of this dissertation, gold catalysis, where an overview of the important milestones in gold chemistry will be examined. The origins of the unique, low temperature oxidation chemistry of gold catalysts will be explored; also highlighting aspects of gold chemistry that are still to be explored. To end with, an overview of this dissertation, with a brief summary of each chapter, will be presented.

Motivation

The twenty first century is shaping up to be a pivotal period for the global community, with a vast array of environmental, energy, resource and population issues being identified as potential flash points in the coming century.¹ The twentieth century had been characterised by significant growth of the human population and by significantly increased exploitation of the available natural resources. Current population growth models are predicting further population growth by the end of the current century, possibly reaching 12 billion inhabitants by the end of this century.^{2,3} Global poverty levels have been steadily decreasing in the last twenty years, mainly in mainland China, resulting in a growing middle class. The increasing size of the middle class has, consequentially, increased the consumption of resources and also increased the pressures exerted on the environment. Parallel to this population explosion, there has also been a wide range of technological developments that have also increased the efficiencies of agriculture production, energy production and provided new technologies that have superficially facilitated this growth to date.⁴

The current economic paradigm is dependent on economic growth, leading to gradual increases in the resources required to sustain the economic growth.⁴ The increasing demands for land to exploit for agriculture, water for irrigation, minerals for high tech applications, is putting us at a tipping where there is insufficient resources to sustain this economic growth much longer. The full consequences of such exploitation of the environment, and consequently on us, was recognised as early as 1962.⁵ The most pessimistic predictions of the current environmental catastrophe have highlighted:

- The acidification of the oceans, leading to coral bleaching;⁶
- The continued release of greenhouse gases, which have recently tipped the levels of carbon dioxide to prehistoric levels (> 400 ppm);⁷
- The accelerating loss of ecosystems in every corner of the globe, leading to a significant decrease in biodiversity;^{8,9}
- The effect of man-made pollutants on the environment and on the ecosystem.

In Jared Diamond's discussion on the factors influencing the demise of a particular society or community, it was argued that a society, which recognises the potentially hazardous consequences of their lifestyle, such as over-exploitation of resources or overpopulation of an island, is able to develop new methods, technology and behaviour to deal with such issues.¹⁰ If we are to avoid many of these gloomy predictions, a range of political steps, in parallel to developments in new technologies, need to be taken.

Many small steps have been made to begin to deal with many of these issues such as the Kyoto protocol, but politically, many of these issues have become toxic even though the scientific consensus is that the effects of climate change will be or are already a significant influence.¹¹ Many European countries have introduced strong policies in an attempt to deal with these issues, but as the problems facing us are global issues that are interconnected, the solution also needs to be implemented globally. Many chemical manufactures from the western sphere have, over the last thirty years, outsourced their production to China and other poorly regulated regions.¹² In effect, the environmental and pollution issues are being exported to the less developed zones of the earth from the developed nations.

There have been discussions about the need to refocus the global economy towards pseudo steady-state type model, or towards a model which favours a larger services industry which is significantly less reliant on environmental resources and more reliant on skilled labour.⁴ Fundamentally there is a need to do *more with less*, to become less dependent on carbon based fuel sources and to develop technologies that are more chemically efficient *i.e.* little or no unusable by-products. False

dawns, such as the potential of biofuels as a sustainable source of chemical energy, will need to be avoided if progress is to be made.^{13,14}

Hence, there is a massive requirement for new technologies and materials that can only be facilitated by catalytic materials.

Catalysts can be employed in many possible solutions to these issues:

- for use in alternative energy sources and new conversion technologies e.g. fuel cells and devices for photolytic splitting of water,
- for the large scale production of chemicals with minimal energy input and without environmentally damaging side products,
- for the manufacture of new materials such as polymers with precisely controlled, tailored macroscopic properties suited for desired applications,
- for the stereospecific synthesis of organic molecules.

Nanoclusters of metals and metal oxides have been shown to have unique electronic properties, different from those of the bulk and unique, single-site catalytic properties.¹⁵ Preparation of these nanoclusters on supports, especially when they are uniform and/or present in structured arrays, are leading to new catalytic properties, including coordinative unsaturation, defects, novel redox properties, and precisely controlled acidity and basicity.¹⁶ These properties can be varied over wide ranges and controlled by selection of the sizes and compositions of the nanoclusters and their interactions with supports. Even extremely subtle changes in the electronic structure of a catalyst can trigger large changes in its performance, and a major challenge is to tune the catalytic properties by varying the catalyst structure on the atomic, and consequently the nanoscale from a bottom up approach.¹⁶

Nanoparticles and clusters

As heterogeneous catalysts are dependent on the various size dependant properties of metal nanoparticles, the next short section is dedicated to defining and clarifying what is meant by the terms nanoparticle, nanocluster and cluster that are found in the literature. Nanoscience concerns itself with the study of materials that have at least one dimension in the nano domain, 1 – 100 nm; hence, nanoparticles are materials that have all dimensions in the nano domain. The unique properties of materials with nanosized dimensions arises from the confinement of the movement of the electrons in the material leading to unique electronic properties *i.e.* quantum size effect.

The first description of materials of with nano sized dimensions was by Richard Feynman in a 1959 talk titled “There’s plenty room at the bottom”.¹⁷ This seminal talk was the first to consider that new materials could be prepared by direct manipulation of single atoms. Although, a wide range of materials have been previously made that would now be considered nanomaterials such as metal colloids, polymers and micelles. The properties of a nanoparticle differ significantly from the bulk material in numerous ways such as melting point, fluorescence, electrical conductivity, magnetic properties and chemical reactivity. The surface area of nanoparticles increases greatly as compared to similar mass of the bulk material, increasing the area that is able to react. As particle size is decreased, there is an increase in the ratio of the surface atoms to the interior atoms. Consequently, the surface of the material becomes much more influential in the chemical properties of the material. The unique properties of metal nanoparticles can be tuned by:

- the surface atoms at the interphase between the nanoparticle and gas/liquid substrate.
- the core atoms of nanoparticle which can be used to tune the electronic band gap of the material
- the control of the particle size and organic capping groups.

The colour of colloidal suspensions of gold nanoparticles have demonstrated substantial size dependant properties, which was first illustrated by Michael Faraday in the 1857 Bakerian lecture, but has been exploited for decorative purposes for the staining of glass since Egyptian times.¹⁸

The benefits of the nano domain are now truly coming to fruition. There is now a tidal wave of applications of new technologies and science, based not only on nanoparticles, but also on other one and two dimensional nanomaterials such as nanotubes and nanofilms. In recent years, there has been a range

of novel applications of metal nanoparticles as cancer treatments, drug delivery vectors, gas sensors, computing, and pharmaceuticals. ^{19: Murty, 2012 #2527}

The exploitation of the nanodomain has been facilitated by recent developments in the synthetic methodologies of metal and metal oxide nanoparticles *i.e.* improved control of composition, size and, increasingly, the shape of the nanoparticles.²⁰⁻²³ Nanoparticles can be prepared via a top-down or a bottom up method. From the view point of a chemist, metal nanoparticles are typically prepared by the reduction of a metal salt in the presence of a capping agent that controls the growth of the nanoparticles, in contrast to laser ablation and other physical methods that are characterised top-down procedures. The unique size dependant properties of the resultant nanoparticles, prepared in solution, are determined by careful control of the reductant, metal precursor, the capping agent and reaction conditions. The capping agent consists of a monolayer of organic molecules that stabilise the core and hinder the aggregation of the nanoparticles. Further functionalisation of the outer layer of the capping agent can add another layer of complexity, such as chemical markers, fluorescent tags, and reaction functionalities.

The mechanism for the formation of metal nanoparticles, with precisely controlled dimensions, is commonly described by LaMer theory, first introduced to describe the formation of sulfur sols in 1950.²⁴ In this approach, the formation of a colloidal solution of a stable suspension of an insoluble material in a solvent is dominated by concentration-dependant nucleation and subsequent growth processes (*i.e.* Ostwald ripening, agglomeration) that determine the final product. LaMer theory was applied more thoroughly to the formation of metal nanoparticles in solution by Sugimoto in 1987, in order to generate

monodisperse metal nanoparticle with specific properties.

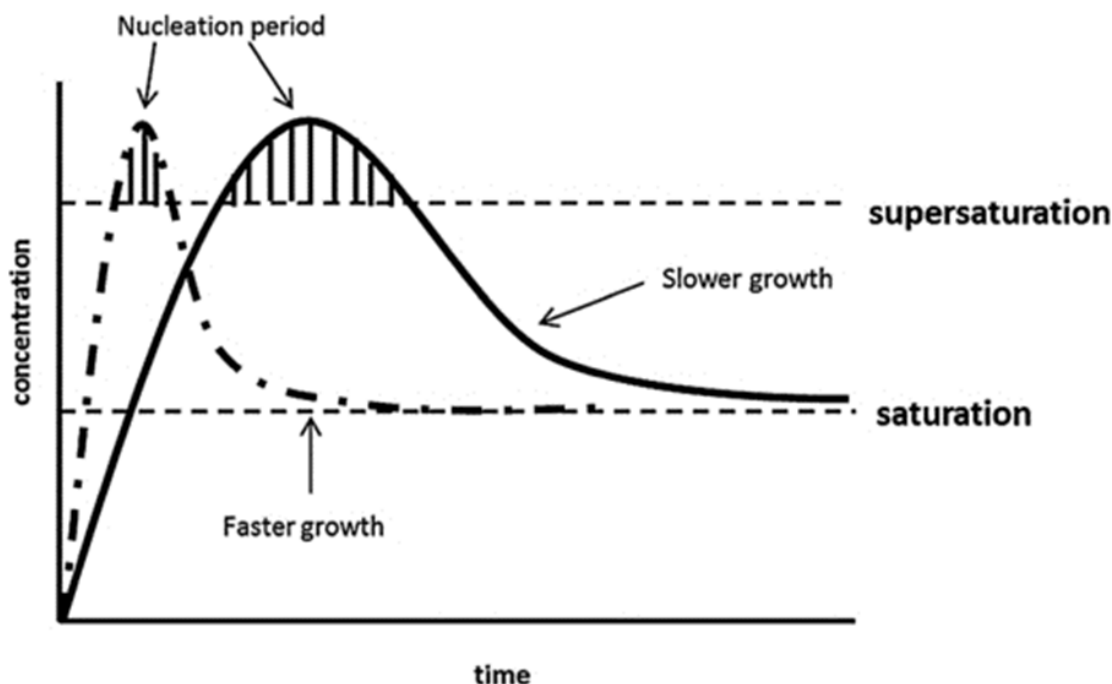


Figure 1 : Concentration of metal precursor over time for a monodisperse and polydisperse metal nanoparticle sample

During the idealised synthesis of metal nanoparticles, the initial reaction species are formed by the reduction of the metal precursor, the concentration of which increases to the point supersaturation. At a critical concentration, sudden nucleation occurs leading to a decrease in the concentration of the reactive species in solution. At a concentration lower than the nucleation concentration, the reactive species now deposit on the surface of nuclei already present, rather than form any new nucleation centres, leading to the growth of the particle size. The final phase of the formation of the nanoparticles is dominated by diffusive growth so long as the concentration of the reactive species remains above a threshold saturation concentration. The presence of a capping agent or passivating agent prevents agglomeration, although the nature of this organic compound can influence the particle size of the final product.

The unique optical and electronic properties of gold nanoparticles have been shown to be significantly size dependant. Hence, by careful tuning of the synthetic conditions it is possible to tune for the selected electronic or optical properties required. Whilst gold nanoparticles with large gold core sizes have a range of unique optical properties, it is the gold particles with core sizes < 2 nm that are of concern to us due to their unique electronic and catalytic properties. Atomically precise gold clusters

with gold cores with < 30 metal atoms have been of interest for catalysis due to their unique electronic properties as opposed to larger colloidal gold nanoparticles. Catalytic materials, derived from such small metal nanoparticles, can be termed as nanocatalysts, which are currently experiencing explosive growth in a wide range of applications in heterogeneous and homogeneous catalysis. Nanocatalysts promise to be significantly more efficient catalytic converters for cars, nano-engineered batteries, and provide a range of new, cleaner sources of energy such as novel fuel cell technologies. At such small sizes, the active sites of these nanocatalysts could be influenced by the presence or absence of a single atom, or contained within a nanopore to further influence selectivity.

Metal clusters

Metal nanoparticles with < 30 atoms that are atomically precise are often termed as metal clusters, often viewed as a specific class of metal nanoparticles, which are commonly stabilised by the presence of an organic ligand. These metal clusters are defined as an atomically precise, discrete molecular species that have metal–metal bonding interactions. The term *metal cluster*, first used by Cotton in 1960, is used to describe a wide range of cluster type materials such as transition metal carbonyl clusters, metal halide clusters and molecular clusters.²⁵ For the scope of this dissertation, the term metal cluster will refer to ligand stabilised metal clusters. Even though gold nanoparticles have been prepared for many years, the synthesis of precisely controlled gold clusters (0.8 nm – 2 nm) is still a relatively small area, which has only become of interest in the last decade due to the unique tuneable catalytic properties of gold clusters. There are two main classes of gold clusters:

- Phosphine stabilised gold clusters
- Thiol stabilised gold clusters

Gold phosphine stabilised clusters were first prepared in the 1960s, whilst thiol-stabilised gold clusters have become a popular choice in recent years. Typically, gold phosphine clusters can be isolated as single crystals and characterised by single crystal X-ray crystallography whilst gold-thiol clusters are much more difficult to isolate as single crystals, except for one recent example by Jadzinsky *et al.*^{26,27} Recent advances in electrospray ionisation mass spectrometry (ESI-MS) have helped facilitated the characterisation of monodisperse gold-thiol clusters. A more complete discussion on ligand-stabilised gold clusters will be presented in Chapter 2.

Interest in heterogeneous catalysis with such small, atomically precise metal clusters supported on various supports has dramatically increased in recent years. Nanocatalysts with such small

nanostructured features are at the frontier between homogeneous and heterogeneous systems. Developing catalysts with such small structural features can lead to significant issues when characterising and identifying the active catalytic species in the either gas or liquid phase reactions. Investigating the relationship between catalyst structure, reaction rates and selectivity of the elementary reaction steps has proved to be very difficult, even with the significant improvements in characterisation methods and models in last the twenty years.

Characterisation of clusters, nanoparticles and supported metal nanoparticles

The accurate determination of the atomic structure of a novel material is essential for the understanding of the properties of the new material, and for the further development of new materials and applications in new technologies. Discrete molecules, which can be isolated, can be reliably characterised quantitatively by X-ray diffraction or nuclear magnetic resonance which can give average atomic distances. However, the characterisation of nanostructured materials is much more difficult due to the short-range changes of the structure in the material. The wide range of characterisation methods either provides structural details on a specific, local scale (*i.e.* electron microscopy or atomic force microscopy) or on larger, bulk average systems such as photoelectron spectroscopy, X-ray absorption spectroscopy.²⁸ Due to the wide range of materials prepared for these studies, no single method of characterisation would be able to characterise the discrete gold clusters (0.8–1 nm), the larger gold nanoparticles (1.4–2.0 nm) and the supported gold nanoparticles. The techniques which are ideal for characterising the small clusters, such as nuclear magnetic resonance (NMR), becomes much less effective for gold nanoparticles that have gold core of more than 50 atoms. For the characterisation of the nanostructured gold catalysts, no single technique provides a complete structural determination; hence, a wide range of methods need to be explored for their suitability with these materials.

Catalysis

A catalyst is defined as a material that can lower the activation energy for a thermodynamically allowed reaction, resulting in an increase of the reaction rate for one or more possible reaction pathways. The un-catalysed reaction route from the substrate (S) to the product (P) goes through a high-energy transition state (TS). The catalysed pathway proceeds via a different, lower energy transition state(s), which are now possible due to the binding to the catalyst. Catalysis, a term coined by Jöns Berzelius in

1836, has been applied for thousands of years in the fermentation process, a prime example of bio-catalysis.²⁹

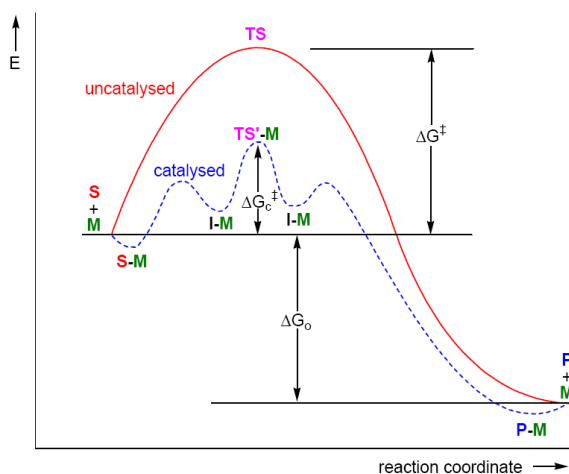


Figure 2: Schematic of how a catalyst works

Early chemists, such as Berzelius, noted certain materials appear to stimulate the reaction of other compounds, although the exact mechanism of this catalytic force was still unknown. The earliest studies, during the eighteenth and nineteenth centuries, were focused on how metals and metal oxides could influence the oxidative decomposition of various organic compounds and gasses. Even at this early stage, it was shown that metals would give very different products depending on the reagents used. The first practical application for this new catalytic concept was the development of the Davy Lamp, which was used as a miner's safety lamp. The new lamp used had a fine mesh of catalytic material (platinum) that surrounded a flame; the wire mesh catalysed the oxidation of the coal gas (CO, methane) in a controlled manner. During the development of the Davy lamp, a wide range of metals were shown to be inactive such as copper, silver and gold, whilst platinum and palladium were shown to be active.³⁰ However, catalysis was still not understood at a molecular level. In 1843, Michael Faraday proposed that the starting materials have to adsorb simultaneously at the surface; however, it wasn't until the contributions of Ostwald that the definition of a catalyst and its influence on the rates of the chemical reaction rather than the thermodynamic equilibrium of the reactants and the products.³¹

Since the early twentieth century, nearly all industrial processes are catalysed by a catalyst(s) at some point. There are three main types of catalyst: heterogeneous, homogenous and bio-catalysis which have been summarised in Table 1. Heterogeneous catalysts are the main type of catalytic material employed in the chemical industry, due to their reliability, ease of separation from the products. The catalyst typically consists of finely divided metal (20 – 100s nm) supported on a metal oxide support

material or in some cases a carbon support. In the early examples, the support material could vary from crushed animal bones or beach sand; however, the influence of the support on the catalytic reaction means that the support material is a precisely controlled facet of the catalyst.

Homogenous catalysts typically consist of soluble metal complexes, where the selectivity of the reaction can be controlled precisely by the chemistry of the ligands. The catalysts are very active and selective, but issues of product separation have prevented the wide spread use of these homogenous systems in industry. The most common homogenous process is palladium catalysed cross coupling.³² Tethering metal complexes to solid supports have also been shown to hold promise as industrial catalysts, but issues with leeching and stability of the catalysts still arise.³³

Bio-catalysts have been used for fermentation by yeast for many generations; other applications of enzymes in industry have been limited. In the last decade, the use of algae for applications in the production of carbon based fuels has become a massive area of research.³⁴

Table 1: Comparison of the three main types of catalytic materials

| Catalyst type: | Heterogeneous | Homogeneous | Bio-catalysis |
|-------------------------|---|--|---|
| Active component | Metals Metal Oxides | Soluble Complexes Metal | Complex Enzymes |
| Active site: | Poorly defined, Surface difficult to study | Well-defined, Discrete molecules are easy to study | Well-defined, Discrete molecules often difficult to study |
| Phase: | Gas/Solid or Liquid/Solid | Liquid | Liquid |
| Temperature: | High (250 °C – 1000 °C) | Low (<250 °C) | < 0 °C to 100 °C) |
| Selectivity | Low | High | VERY High |
| Product separation: | Facile | Difficult | Problematic |
| Catalyst recycle: | Simple | Difficult | Not required |
| Cost | Relatively cheap | Expensive | Getting cheaper |
| Reaction mechanisms: | Difficult to study | Easy to study | Easy to study for models, not so easy in <i>in-vivo</i> |

In recent years, the boundary between homogenous and heterogeneous catalysts has become blurred.³⁵ Unsupported, naked metal clusters in the liquid phase have also been shown to be active for range of important industrial reactions; however, whether these materials are classed as homogenous or heterogeneous catalysts can be difficult as with homogenous systems, similar issues with product separation and catalyst recyclability are encountered.³⁶ Metal clusters, with small nanometer size dimensions could prove to be a significant environmental issue due to their small size, and unique electronic properties. A range of recent studies have highlighted the possible detrimental size effects of nanometer size metal nanoparticles could have on the growth of various agricultural crops.³⁷ The usage of such small, reactive materials should be limited until the affects of these novel materials on the environment are more fully understood. However, supported metal clusters on various metal oxide and carbon supports can avoid many of these possible detrimental affects on the enviroment.

Overall, heterogeneous type catalysts are the primary catalyst in industry due to their high tolerance to heat, easy separation and relatively low cost. The heterogeneous catalysts are still relatively poorly understood, due to the complex issues of studying metal/metal oxide surfaces in situ. However, there is still great potential for improving heterogeneous systems. In the last twenty years, gold based catalysts have shown a range of surprising and novel reactivity in a wide range of systems, such as propylene epoxidation, CO oxidation.³⁸

Heterogeneous oxidation catalysis

The catalytic oxidation of organic substrates is an important tool for the functionalisation of molecules which are of great commercial and synthetic importance such as ketones, aldehydes, esters, carboxylic acids and alcohols.^{38,39} The selective and partial oxidation of the precursor molecules is a key requirement for many of these industrial processes; complete oxidation of organic molecules has many environmental applications.⁴⁰

A common thread throughout recent developments in selective oxidation catalysis has been the chemical nature of the source of active oxygen.⁴¹ A wide variety of oxygen sources have been explored, as summarised in Table 2. Typically, the oxidants used in metal catalysed oxidations have very low active oxygen content. Another serious drawback is generation of a large quantity of waste by-products. Hence, from an environmental perspective, molecular oxygen is an ideal oxidant because of its high abundance and high active oxygen content. However, it has been shown that catalytic processes involving molecular oxygen often demonstrate poor product selectivity. Furthermore, there is a limited number of catalysts that have been shown to activate molecular oxygen efficiently at industrial scale. Although, silver clusters have been used as effective catalysts for the epoxidation of ethylene with only molecular oxygen in several large scale industrial plants.⁴² Hydrogen peroxide is a commonly used oxidant as it only produces water as a by-product. Another common oxidant is the so-called sacrificial aldehyde which acts as an oxygen transfer agent. This method is relatively safe and benign but does have the disadvantage of generating considerable waste.⁴³

Table 2: Summary of oxidants for metal catalysed oxidations, comparing calculated active oxygen content and typical products (data from reference ⁴³)

| Oxidant | Active oxygen content (wt. %) | By-product |
|--|--|-----------------------------------|
| O ₂ | 100 % | H ₂ O / not present |
| O ₂ /Reductant (<i>i.e.</i> H ₂) | 50 % | H ₂ O |
| H ₂ O ₂ | 47 % | H ₂ O |
| NaOCl | 21.6 % | NaCl |
| CH ₃ CO ₃ H | 21.1 % | CH ₃ CO ₂ H |
| t-BuOOH | 17.8 % | t-BuOH |
| KHSO ₅ | 10.5 % | KHSO ₄ |
| PhIO | 7.3 % | PhI |

Stoichiometric metal oxidants are still widely used in industry, such as chromates and permanganates, leading to large amounts of toxic metal waste. Even with improved methods for reusing some of the waste, disposal of such quantities of material is becoming more and more difficult globally due to new, more rigid environmental legislation.^{44,45} One of the major demands that is now faced by industry is developing greener methods that are provide environmentally benign and commercially viable routes towards a vast array of functionalised products.

The main heterogeneous oxidation catalysts are typically derived from an active phase such as metal nanoparticles immobilised on a support material such as high surface area or porous metal oxide supports. One of the main classes of materials that is currently used for catalytic oxidation is a large family of titanium silicates that have demonstrated wide applications in epoxide synthesis, hydroxylation and oxidation of alkanes. ^{41,46,47} The heterogeneous titanium (IV) silicate catalysts often use hydrogen peroxide as the source of active oxygen. These catalysts are often hydrophobic molecular sieve structure, and have demonstrated high catalytic performance and selectivity for oxidations of small linear alkenes. Various problems have been encountered when more complex starting materials are used, and issues with the high oxophilicity of the early transition metal system and the use of aqueous hydrogen peroxide as the terminal oxidant. ⁴⁸

The need for improved routes to various products is ever present; the requirements that need to be considered during the design of selective oxidation catalyst are increasing:

- Atom efficiency;
- Waste prevention;
- Energy efficient;
- Hazard prevention;
- Few toxic by-products;
- Recyclability;
- Safe solvent/solventless reaction.

With recent advances in synthetic methods for novel porous, nanostructured supports and also for metal clusters and nanoparticles, there are many tools for chemists to develop new generations of nanocatalysts.

In the last two decades, a gold rush in catalysis has occurred. New gold based catalysts have provided a range of new routes towards selective oxidation of a wide variety of organic substrates which have not been previously explored.

Gold: a surprising catalyst.

Gold has held an important place in human culture for many thousands of years; it has led to the creation and destruction of vast empires and the creation of various gold rushes all over the American continent. Gold, often found as lustrous yellow nuggets, may have been the first metal our ancestors encountered, possibly as far back as 40,000 years ago.⁴⁹ Early societies often associated gold with various deities, gods and their rulers. The chemical symbol of gold (Au) is derived from the latin *aurum* which is related to the goddess of dawn, *Aurora*. The alchemical symbol for gold is also the same pagan symbol used for the sun. Humans, all around the world, intuitively attribute significant value and power to gold. Beyond its industrial and cosmetic uses, gold plays an important function in the economic system as a store of value, and it's an object of speculation. In recent years, speculation has been rampant, with hedge funds, mutual funds, exchange-traded funds (E.T.F.s), and individual investors bidding the price up from six hundred dollars an ounce in 2007 to a peak of US\$1,920.30 in September, 2011, which has recently decreased to around the US\$1400.00 mark. Depending on the source, the gold market is calculated to be worth approximately five trillion dollars a year.

The chemistry of gold

Gold has a rich coordination and organometallic chemistry, but was considered to be catalytically inactive for many years. Gold is a late transition metal belonging to group 11 of the periodic table, it has a doublet $2S$ ($[Xe] 6s^1 4f^{14} 5d^{10}$) atomic ground state. With an atomic mass of 196.97 amu the electronic energy levels of gold are strongly influenced by relativistic effects. The theory of the electronic structure of gold, and other heavy elements for which relativity has a qualitative effect on the chemical properties, have been the subject of several reviews, most notably by Pyykko.^{50,51} The relativistic effect arises from the fast moving electrons that are directly affected in the low lying core states of the atom; which experience the unshielded potential of the nucleus.⁵² The orbital contraction is almost 20 % for gold, which is also the maximum seen for the known, stable elements. Following the same orthogonality argument, the outer p-states also contract but d and f level orbitals expand away from the nucleus. For the valence states of gold the contraction gives stabilisation of the 6s level and destabilisation of the 5d levels. This brings them closer together in energy than would be the case in the absence of relativistic effects and so the gold bonding requiring s-d hybridisation is enhanced.

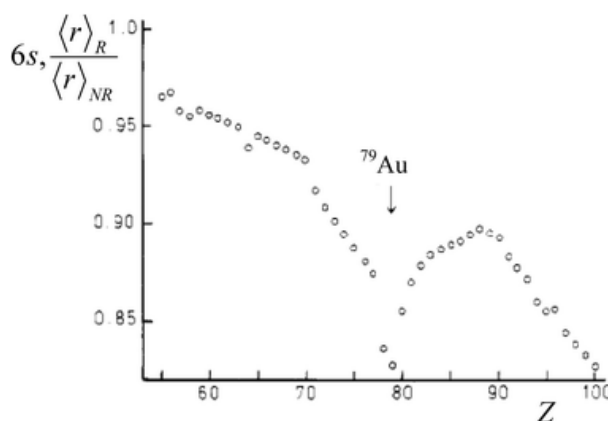


Figure 3: The relativistic contraction of the 6s shell in the elements Cs ($z = 55$) to Fm ($z = 100$) from reference ⁵¹

Earliest reports of gold catalysis

Traditionally, gold has been viewed as a poor catalyst as compared to other noble metals. The earliest recorded studies of gold being used as a catalyst are in the 1906, where gold plates were studied for their potential as for the decomposition of various gases and organic compounds.⁵³ Predictably, the gold (as well as silver) reactions were relatively inactive as compared to the other metals investigated in

the study (iron, copper, platinum). It wasn't until the early 1980s that it was realised that supported gold nanoparticles were active for a range of chemical reactions under relatively mild conditions.

In the late 1980s, Haruta *et al.* showed that small gold nanoparticles supported on a metal oxide support, such as titania, iron oxide, or alumina were active for the oxidation of carbon monoxide, at temperatures as low as 0 °C.⁵⁴⁻⁵⁶ Concurrently, Hutchings independently demonstrated that supported gold on a carbon support was an ideal catalyst for the hydrochlorination of ethyne, forming vinyl chloride as the product.^{57,58} Previously, Bond and his co-workers had observed that gold particles supported over boehmite were active for the hydrogenation of alkynes in the presence of an alkene, and also for the hydrogenation of unsaturated hydrocarbons. The reactivity of these catalysts was relatively poor as compared to other commercially available systems. Since these pioneering catalytic studies, our understanding of the factors that influence activity of gold catalysts has improved significantly.

Supported gold catalysts have now been employed in a wide range of systems, both in the gas- and liquid- phases:

- Low temperature oxidation of carbon monoxide;⁵⁴
- Selective oxidation of propylene to propylene oxide, in the presence of hydrogen;⁵⁹
- Selective oxidation of alkenes and alcohols in the liquid phase;⁶⁰
- Water gas-shift reaction;⁶¹
- Synthesis of hydrogen peroxide.⁶²

Homogeneous gold catalysts had also been ignored; however, in 1998 it was shown that gold (I) complexes could be used to catalyse the addition of alcohols on to alkynes with high turnover frequencies.⁶³ Homogeneous gold catalysis has now developed in to an important tool for the synthesis of a wide range of organic target molecules.⁶⁴ Other examples of homogeneous gold catalysis include selective methane oxidation,⁶⁵ oxidative cross-coupling⁶⁶ and also the room temperature gold(III)-catalysed oxidation of sulfides to sulfoxides with a thirty per cent hydrogen peroxide solution.⁶⁷ Recently, an example of a catalyst in the grey area between homogeneous and heterogeneous catalysts was reported which involved unsupported gold clusters, with only 3-10 atoms of gold, demonstrating turnover numbers of 10⁷ at room temperature for the ester assisted hydration of alkynes and the bromination of arenes.⁶⁸

In the past two decades, gold catalysis has developed rapidly to such an extent that many have viewed it as a *gold rush* in the field of catalysis.⁶⁹⁻⁷¹ Many of the lessons that have been learnt designing

active gold catalysts, such as the need for gold particles of a specific size and the nature of the interaction with the support could lead to more efficient, cost efficient and elegant nanostructured catalysts for the chemical industry.⁷¹

The origin of gold catalysis

In the following section, I will discuss in more detail the two primary factors determining the activity of supported gold nanoparticle catalysts and lead in to the nature of the active site of heterogeneous gold catalysts. The two main factors, that were identified by Haruta and Hutchings, which appear to determine the catalytic activity of heterogeneous gold catalysts are:⁷²

- The size of the gold nanoparticles;
- The nature of the support material.

The early active catalysts, developed by Haruta, comprised of gold nanoparticles with diameters, 5 nm on oxide supports. Further development of these catalysts showed that the most active catalysts required precisely controlled gold particle dimensions between 2–4 nm. Model systems of gold nanoparticles on titania surfaces (110) single-crystal surfaces have linked catalytic activity to the size threshold effect associated with the metal to insulator transition of the gold nanoparticles when their size falls below 3.5 nm. Hence, precise control of the gold particle size is imperative for the development of active catalysts. Recent reports have also highlighted that metallic layers of gold can activate oxygen for further oxidation reactions.⁷³ In contrast, if nitrous oxide is used as the source of active oxygen, larger particles of gold (> 10 nm) have been shown to be more active for the oxidation of styrene than smaller gold nanoparticles (2-5 nm).⁷⁴

Hutchings and his co-workers have identified small 10-15 atom gold clusters supported on an iron oxide support by HAADF-STEM; which they concluded was responsible for the oxidation of carbon monoxide. It is believed that synthetic conditions play an important role in stabilising such small gold clusters.⁷⁵

In recent years, the major developments in gold catalysis have been in the activation of molecular oxygen with atomically precise gold clusters supported on silica, with phosphine or thiol derived ligands.^{76,77} These novel systems have shown that ultra-small gold clusters with particle sizes of around 1.5 nm can activate molecular oxygen, with no additional sacrificial oxidant, for the partial oxidation of styrene and other organic molecules. The origin of the unique activity of such small gold clusters has still

not been experimentally confirmed, but the electronic properties of such small, discreet gold clusters has been proposed as the site for the generation of the active superoxo species from molecular oxygen.⁷⁸ Further developments have shown that thiol stabilised gold clusters on a hydroxyapatite support can also selective oxidise styrene to its' epoxide product with high yields, in the presence of excess tert-butylhydroperoxide.⁷⁹

However, the remarkable catalytic behaviour that is observed might also in part arise from strong electronic interaction between the gold and the metal oxide support. A wide range of metal oxide supports have been shown to be active and influence the reactivity of the supported gold nanoparticles. In particular, titania and iron oxide supports have yielded highly reactivity gold based catalytic systems.⁸⁰⁻⁸² This work will be focused on two supports, titania and silica, which have contrasting electronic properties that should influence the reactivity of the resulting catalysts.

The origin of the catalytic effect of heterogeneous gold catalysts is still under debate, a wide range of factors have all been considered as playing a key role: ⁸³

- Interface of gold nanoparticle with the oxide support;⁸⁴
- Cationic nature of gold Au^{3+} ;⁸⁴
- Metallic nature of gold(Au^0);⁸⁵
- Quantum size effects;⁸⁶
- Defects sites and oxygen vacancies on the oxide support;⁸⁵

Many of these studies in to the origin of gold catalysis (or indeed any heterogeneous system) often involve UHV studies on extended surfaces such as flat substrates of ALD titania or silica with deposited gold nanoparticles. There is often a disconnect between such idealised systems and what is required for understanding industrial catalysis. Often experiments are limited to simple precursors such as carbon monoxide and often what is true for this model system is difficult to apply to other more industrial and environmentally more important reactions.

Characterisation methods

The characterisation methods used in this research project are summarised in the table below and the application of each method is described. At the start of this project, several of these characterisation methods were not available, and only became available at later stage. Several methods, not described below, were also explored for their suitability for characterisation of these materials. Near Edge X-Ray absorption fine structure (NEXAFS) spectroscopy, was briefly used in an attempt to characterise the catalytic materials. The experiments were conducted at the Australian Synchrotron (AS) at the Soft X-Ray (SXR) Beamline. Unfortunately, as the beamline is designed with a thin layer of gold throughout the monochromator; which meant gold NEXAFS could not be conducted. NEXAFS spectroscopy of the support material was conducted in an attempt to ascertain whether the gold affects the electronic structure of the support material proved to be in vain due to the very low loadings of gold on the surface of the support.

Surface Enhanced Raman Spectroscopy (SERS) was briefly conducted on several supported gold clusters, in the hope to observe an enhancement of any species bound to the gold surface. These results yielded little to no information on any surface bound species, possibly due to low concentrations of gold present on the surface and small size of the gold nanoparticles which don't have a plasmon resonance at such small sizes (<2 nm). The aim of these experiments was to determine whether the cluster ligand (triphenylphosphine) was present after the deposition of the cluster on to a support and subsequent catalyst annealing was conducted.

Table 3; Summary of characterisation methods of clusters

| Analytical Method | Information | Advantages | Disadvantage |
|-----------------------------------|---|--------------------------------|---|
| High Resolution TEM | | | Local area characterisation |
| | Particle size | | May not be representative of whole sample. |
| | Particle shape | Direct imaging | Time-consuming. |
| | Size dispersity | | Limits to resolution with metal clusters, especially on non-carbon substrates. |
| NMR | Presence of impurities | Rapid | For large nanoparticles , broad resonances occur from multiple ligand environments and slow exchange on NMR timescale |
| | Cluster identification | Solution phase | |
| | | Bulk Characterisation | |
| Far-IR/Terahertz | Core – ligand bonds | Bulk characterisation | Limited access |
| | Metal- metal bonds | Rapid technique | |
| X-ray Crystallography | Atomic structure of cluster core and ligands | Definitive assignment of atoms | Pure, crystalline samples required Not a bulk technique. |
| Photoelectron spectroscopy | Electronic structure of surface of solid material | Bulk sample analysis | UHV conditions |
| | | Quantitative analysis | Sample charging |
| | | | Contamination |
| | | | Limited access |

Transmission Electron Microscopy

Bright field high resolution TEM is a microscopy method by which a beam of high energy electrons is transmitted through an ultra-thin sample in ultra-high vacuum. The image of the sample is created by the interaction of the electrons that are transmitted through the sample, which is then magnified and focused onto a fluorescent screen or a CCD camera. In figure 4, a lens diagram for imaging and diffraction modes of a HRTEM is shown. HRTEM is one of the primary methods for characterising the structure of metal nanoparticles, where the size and shape of the metal core can be observed.

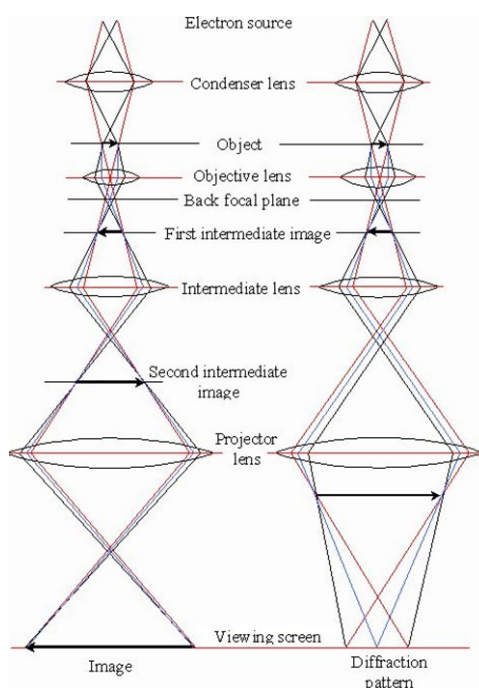


Figure 4: Lens diagram for bright field HRTEM

Due to the small size of the gold clusters on the metal oxide support, it was found that typical 200kV HRTEM was insufficient to image the gold clusters, due to the poor contrast of the gold clusters and the metal oxide supports. High angle annular dark field scanning transmission microscopy (HAADF STEM) was used to image several samples in attempt to observe any of the unsintered gold clusters on the metal oxide supports. High angle annular dark field microscopy excludes the unscattered electron beam from the sample image, which can improve the resolution of the images especially for high Z atoms such as gold. Scanning transmission electron microscope operates by focusing a narrow beam of electrons into a narrow spot which is then scanned over the sample in a raster, a systematic process of covering the sample area gradually one line at a time. Atomic resolution can be achieved in conjunction with a high angle detector (as the image of the MNP is enhanced due to the greater number of electrons scattered to the high angle by the high Z metal atoms) and aberration correction.

Annular dark-field imaging was also employed to observe the sub nanometre gold clusters on the supports. An annular dark-field image is formed only by high angle, incoherently scattered electrons which are sensitive to variations in the atomic number of the atoms in the sample.

During HRTEM, elemental analysis can also be conducted *in-situ* by Energy Dispersive X-Ray spectroscopy (EDS). This technique involves a focused, high energy beam of electrons interacting with a sample. The incident beam of electrons can excite an electron in an inner shell, which is ejected from the shell, creating a hole. An electron from a higher energy, outer shell then fills this hole and the difference in energy of the shells is released in the form of an X-ray, which is measured by an energy-dispersive spectrometer. Each element has characteristic X-rays with energies corresponding to the differences in energy between different shells, facilitating elemental identification. This technique is useful tool to confirm the elements present in a sample that is being studied by TEM. It was noted that in the case of our samples the gold peaks were not observed due to the very low loading (0.17-0.5 wt%) of gold in the samples.

Typically, for a TEM study a sample is deposited on to a substrate that is relatively transparent to electrons; a focused electron beam is passed through the sample which is under ultra-high vacuum. The samples of metal clusters/nanoparticles and supported gold nanoparticles on silica and titania were deposited onto copper TEM grids that are covered with an amorphous carbon film provided by ProSciTech. This thin carbon substrate is designed to minimise the background scattering of electrons; several samples were studied on holey carbon films to observe the sample over the holes with no carbon film background. The electrons are absorbed or diffracted by the sample and pass through the substrate. The transmitted electrons produce an image through the phosphorescence on a screen below the sample or by detection by a CCD camera. Once the image has been optimised for contrast, brightness, the shape and size of the metal core can be quantified with sub-nanometer resolution, and measured by Gatan digital micrograph software. For these experiments, TEM was conducted on Philips CM-200 electron microscope which has a theoretical resolution of 0.45 nm when operated under optimum conditions. Although TEM is an ideal technique for the characterisation of most nanoparticle systems, it becomes difficult to distinguish between different gold cluster species with core sizes below one nanometer. The contrast between the substrate (*i.e.* amorphous carbon film) and the ultra-small gold clusters is significantly lower as compared to the larger gold nanoparticles, which means that larger gold particles are much more visible than the atomically precise sub-nanometre gold clusters. When the gold clusters are deposited onto the titania or silica supports, the observation of gold clusters or nanoparticles

becomes much more difficult as the substrate is now absorbing and diffracting a much higher proportion of the electrons as compared to the gold clusters deposited straight onto the amorphous carbon film. Overall, this method allowed us to quantify the extent to which agglomeration of the small gold clusters was happening.

Nuclear Magnetic Resonance Spectroscopy

NMR spectroscopy can be used for the characterisation of gold clusters and nanoparticles; however, the nature of the core and ligand shell of the system can add complicate the results. ^1H NMR has been used to characterise gold clusters and nanoparticles with metal core diameters of less than one nanometer up to 2 nm, the resultant spectra displays broadened resonance signals as the particle size increases due to the increasing number of magnetic and chemical environments that are experienced by the protons of the ligands.^{87,88} ^{31}P NMR is not particularly applicable to larger gold nanoparticles due significant broadening of the phosphorous peak and may not be detected in the baseline. However, for the atomically precise gold clusters where the proportion of phosphorous to gold is much high as compared to the larger nanoparticles, ^{31}P NMR can provide valuable information on the structure, allowing us to distinguish between particular cluster species present solution by the associated chemical shift of the phosphorous peak from the ligands. Spectra for gold phosphine and thiol clusters are typically much simpler than would be expected from the solid-state structure of these materials due the soft potential energy surfaces for the structural changes in the gold core.⁸⁹ Hence, ^{31}P NMR is an essential characterisation tool for the various gold phosphine clusters studied in this research. ^{90,91} For this research, ^{31}P and ^1H were recorded on a Varian INOVA spectrometer and deuterated solvents were sourced from Cambridge Isotopes.

X-Ray Crystallography

X-Ray Crystallography is an ideal technique when characterising crystalline materials quantitatively, to understand the structure of a material at an atomic level. This method of characterisation requires single crystals of a pure material, which often means that the larger gold nanoparticles are not able to be characterised by this method. Even with the more atomically precise samples, the single crystal sample is often not representative of the bulk sample. For the crystalline samples, single crystal X-ray diffraction experiments were recorded on Bruker APEXII area detector using graphite monochromised Mo $K\alpha$ ($\gamma = 0.71073 \text{ \AA}$) radiation. The crystals of each sample were

mounted on a glass fibre under oil. Intensities were corrected for Lorentzian polarization effects and for absorption effects using multiscan methods. Space groups were determined from systematic absences and checked for higher symmetry. Structures were solved by direct methods using SHELXS-97 and refined with full-matrix least squares on F_2 using SHELXL-97. All non-hydrogen atoms were refined anisotropically.

Photoelectron Spectroscopy

Photoelectron spectroscopy (PES) or X-ray Photoelectron spectroscopy (XPS) is a surface characterisation technique that is used to determine the presence of various elements present on a surface and allowed the chemical shift of various elements can be determined. A more detailed description of this technique is presented in chapter 5. Overall, PES is an ideal technique to characterise nanostructured materials that have unique electronic properties that differ from the bulk form to of the element.⁹² When compared to TEM, PES facilitates the analysis of a much larger area; hence, the information gleaned by PES is representative of the electronic structure as an average of the whole sample rather than as several localised areas. For this research, PES is an ideal technique for the study of the unique properties of the small gold clusters and nanoparticles, including when they are deposited on to various support material. The electronic interaction of the particles with the supports and the extent to which the gold particles have aggregated on the surface can be determined and in conjunction with TEM data can start to help us understand the reactivity of these samples.⁹³ Photoelectron spectroscopy experiments were conducted at the Australian Synchrotron at the Soft X-Ray Beamline under the guidance of Dr. Lars Thompsen.

Scope of this dissertation

Overall, it is hoped that some of the work presented will contribute to a greater understanding of the chemistry of gold based catalysts. The central idea of this dissertation was to study effect of decreasing size of the gold particles supported on silica on the catalytic chemistry. The study was limited to support immobilised materials as these systems are more relevant for industrial applications and have significantly less environmental risk associated with them than with naked metal clusters and other molecular species.

Chapter 2 describes the initial work taken to prepare a range of gold clusters and nanoparticles which were all stabilised by the same organic protecting group or ligand: triphenyl phosphine. The gold clusters and nanoparticles were prepared by the reduction of a gold(I) precursor and further purification, all synthetic procedures were optimised to maximise yields and to ensure the purity of the clusters. The systems chosen for this study were $\text{Au}_8(\text{PPh}_3)_8(\text{NO}_3)_2$, $\text{Au}_9(\text{PPh}_3)_8(\text{NO}_3)_3$, $\text{Au}_{11}(\text{PPh}_3)_8(\text{NO}_3)_3$ and also the much larger 1.5 nm gold phosphine nanoparticle system. Several thiol based systems were also briefly studied but due to the lack of ESI-MS characterisation facilities, it was decided that this project would be focused initially on phosphine stabilised gold clusters. The choice of these clusters ensures that the effect of the addition of a single gold atom on the electronic properties of the cluster can be studied. The detailed characterisation of these clusters by NMR, TEM, ESI-MS, X-ray crystallography, HAADF-STEM, and by EXAFS spectroscopy is described.

In addition to confirming the structure and purity of this range of gold clusters, a series of experiments on the far-infrared properties of these clusters was also conducted in collaboration with Jason Alvino and Dr. Greg Metha from the University of Adelaide at the Far-Infrared Beamline at the Australian Synchrotron. Chapter 3 details the first report on the vibrational structure of pure, ligand stabilised gold clusters, and a comparison between the experimental spectra to simulated spectra that were generated by Jason.

Chapter 4 describes the design and preparation of the catalysts involved in this study. A wide range of factors influencing the reactivity of the catalysts were identified and controlled during the preparation. Evonik P-25 titania and fumed silica supports were chosen as supports for this study. To improve the deposition characteristics of the gold clusters on to the titania support, acid washing of the titania support was also conducted.

One of the main factors that can influence the reactivity of supported metal particles is the loading of the metal on the support material. For this study a relatively low loading of 1 % by weight of gold was chosen in an attempt to minimise particle sintering which contrasts to the standard gold catalysts which vary from 3 -10 % by weight of gold. Post –deposition modification of the supported gold clusters was conducted under a wide range of temperatures and conditions, in an attempt to compare the effect of these various treatments on the electronic structure of the materials. HRTEM was used to characterise these materials; however, due to small size of the gold clusters (~ 1 nm) it often proved difficult to observe these particles on our in-house microscope. Several samples were examined by HAADF-STEM at the Monash University in Australia, which confirmed the presence of gold cluster with

particle sizes < 1 nm. Due to our limited access to such this microscopic technique, we also employed high resolution photoelectron spectroscopy to conduct a more systematic study of the materials prepared in this chapter.

Chapter 5 discusses a large, systematic photoelectron spectroscopy study on the supported gold clusters, which was performed at the Soft X-ray Beamline at the Australian Synchrotron. Due to insulating nature of the support materials, extensive developments on the sample preparation method were required to minimise sample charging. However, the silica samples proved too difficult to characterise under the high intensity of the synchrotron source. The effects of post-deposition treatments were investigated by comparison of untreated samples with analogues that have treated at various temperatures and atmospheres. The final fate of the triphenyl phosphine ligands after post-deposition treatments was also a focus for this chapter.

Chapter 6 reports on the catalytic behaviour of the supported gold phosphine clusters for the oxidation of styrene. A wide range of conditions were examined with differing post-deposition treatments and sources of active oxygen. The chapter describes the initial considerations and development of the catalytic set-up for this lab. The experimental results are then discussed in context of other reports of catalytic oxidation of styrene by supported gold clusters.

In chapter 7, the results from two collaborative projects are discussed, which employed the gold phosphine clusters and supported gold clusters prepared in this work for other applications. $\text{Au}_9(\text{PPh}_3)_8(\text{NO}_3)_3$ clusters were deposited on various tungsten oxide supports and employed as hydrogen gas sensors at RMIT, Australia. Samples of the silica and titania supported samples were also examine for activity in catalytic reduction of alcohols at the University of Auckland, NZ.

References

- (1) Chomksy, N.; Polk, L.: *Nuclear War and Environmental Catastrophe*; Seven Stories Press, **2013**.
- (2) Demeny, P.: Population futures for the next three hundred years: Soft landing or surprises to come? *Population and Development Review* **2004**, *30*, 507-517.
- (3) O'Neill, B. C.; Dalton, M.; Fuchs, R.; Jiang, L.; Pachauri, S.; Zigova, K.: Global demographic trends and future carbon emissions. *Proceedings of the National Academy of Sciences* **2010**, *107*, 17521-17526.
- (4) Gilding, P.: *The great disruption: how the climate crisis will transform the global economy*; Bloomsbury, **2011**.
- (5) Carsen, R.: *Silent spring*. Houghton Mifflin, Boston MA, **1962**.
- (6) Eakin, C.; Lough, J.; Heron, S.: Climate variability and change: monitoring data and evidence for increased coral bleaching stress. In *Coral Bleaching*; Springer, **2009**; pp 41-67.
- (7) Showstack, R.: Carbon dioxide tops 400 ppm at Mauna Loa, Hawaii. *Eos, Transactions American Geophysical Union* **2013**, *94*, 192-192.
- (8) Fearnside, P. M.: Deforestation in the Brazilian Amazon: how fast is it occurring. *Interciencia* **1982**, *7*, 82-88.
- (9) Coe, M. T.; Marthews, T. R.; Costa, M. H.; Galbraith, D. R.; Greenglass, N. L.; Imbuzeiro, H. M.; Levine, N. M.; Malhi, Y.; Moorcroft, P. R.; Muza, M. N.: Deforestation and climate feedbacks threaten the ecological integrity of south–southeastern Amazonia. *Philosophical Transactions of the Royal Society B: Biological Sciences* **2013**, 368.
- (10) Diamond, J.: *Collapse: how societies choose to fail or succeed: revised edition*; Penguin, **2005**.
- (11) Oreskes, N.: The scientific consensus on climate change. *Science* **2004**, *306*, 1686-1686.
- (12) Shapiro, M. A.: Regionalism's challenge to the pollution haven hypothesis: a study of Northeast Asia and China. *The Pacific Review* **2013**, 1-21.
- (13) Michel, H.: Editorial: The nonsense of biofuels. *Angewandte Chemie International Edition* **2012**, *51*, 2516-2518.
- (14) Lapola, D. M.; Schaldach, R.; Alcamo, J.; Bondeau, A.; Koch, J.; Koelking, C.; Priess, J. A.: Indirect land-use changes can overcome carbon savings from biofuels in Brazil. *Proceedings of the national Academy of Sciences* **2010**, *107*, 3388-3393.
- (15) Thomas, J. M.; Raja, R.; Johnson, B. F. G.; O'Connell, T. J.; Sankara, G.; Khimyak, T.: Bimetallic nanocatalysts for the conversion of muconic acid to adipic acid. *Chemical Communications* **2003**, 1126-1127.
- (16) Raja, R.; Thomas, J. M.; Greenhill-Hooper, M.; Ley, S. V.; Paz, F. A. A.: Facile, One-Step Production of Niacin (Vitamin B₃) and Other Nitrogen-Containing Pharmaceutical Chemicals with a Single-Site Heterogeneous Catalyst. *Chemistry : A European Journal* **2008**, *14*, 2340-2348.
- (17) Feynman, R. P.: There's plenty of room at the bottom. *Microelectromechanical Systems, Journal of* **1992**, *1*, 60-66.
- (18) Faraday, M.: The Bakerian Lecture: Experimental Relations of Gold (and Other Metals) to Light. *Philosophical Transactions of the Royal Society of London* **1857**, 147.
- (19) Rao, C. N. R.; Cheetham, A. K.: Science and technology of nanomaterials: current status and future prospects. *Journal Of Materials Chemistry* **2001**, *11*, 2887-2894.

- (20) Brust, M.; W., M.; Bethell, D.; Schiffrin, D. J.; Whyman, R.: Synthesis of Thiol-derivatised Gold Nanoparticles in a Two-phase Liquid-Liquid System. *Journal of the Chemistry Society, Chemical Communications* **1994**, 801-802.
- (21) Puntès, V. F.; Krishnan, K. M.; Alivisatos, A. P.: Colloidal Nanocrystal Shape and Size Control: The Case of Cobalt. *Science* **2001**, *291*, 2115.
- (22) Yin, Y.; Rioux, R. M.; Erdonmez, C. K.; Hughes, S.; Somorjal, G. A.; Alivisatos, A. P.: Formation of Hollow Nanocrystals Through the Nanoscale Kirkendall Effect. *Science* **2004**, *304*, 711-714.
- (23) Ren, J.; Tilley, R. D.: Preparation, Self Assembly and Mechanistic Study of Highly Monodisperse Nanocubes. *Journal of the American Chemical Society* **2007**, *129*, 3287-3291.
- (24) LaMer, V. K.; Dinegar, R. H.: Theory, production and mechanism of formation of monodispersed hydrosols. *Journal of the American Chemical Society* **1950**, *72*, 4847-4854.
- (25) Mingos, D. M. P.; Wales, D. J.: *Introduction to cluster chemistry*; Prentice Hall New York, 1990.
- (26) Jadzinsky, P. D.; Calero, G.; Ackerson, C. J.; Bushnell, D. A.; Kornberg, R. D.: Structure of a Thiol Monolayer-Protected Gold Nanoparticle at 1.1 Å Resolution. *Science* **2008**, *318*, 430-433.
- (27) Levi-Kalisman, Y.; Jadzinsky, P. D.; Kalisman, N.; Tsunoyama, H.; Tsukuda, T.; Bushnell, D. A.; Kornberg, R. D.: Synthesis and Characterization of Au₁₀₂(p-MBA)₄₄ Nanoparticles. *Journal of the American Chemical Society* **2011**, *133*, 2976-2982.
- (28) Billinge, S. J. L.; Levin, I.: The Problem with Determining Atomic Structure at the Nanoscale. *Science* **2007**, *316*, 561-565.
- (29) Robertson, A.: The early history of catalysis. *Platinum Metals Review* **1975**.
- (30) Collins, P.: The pivotal role of platinum in the discovery of catalysis. *Platinum Metals Review* **1986**, *30*, 141-146.
- (31) Roberts, M.: Birth of the catalytic concept (1800-1900). *Catal Lett* **2000**, *67*, 1-4.
- (32) Chen, X.; Engle, K. M.; Wang, D. H.; Yu, J. Q.: Palladium (II)-Catalyzed C-H Activation/C-C Cross-Coupling Reactions: Versatility and Practicality. *Angewandte Chemie International Edition* **2009**, *48*, 5094-5115.
- (33) McMorn, P.; Hutchings, G. J.: Heterogeneous enantioselective catalysts: strategies for the immobilisation of homogeneous catalysts. *Chemical Society Reviews* **2004**, *33*, 108-122.
- (34) Schmid, A.; Dordick, J.; Hauer, B.; Kiener, A.; Wubbolts, M.; Witholt, B.: Industrial biocatalysis today and tomorrow. *Nature* **2001**, *409*, 258-268.
- (35) Corma, A.; Garcia, H.: Crossing the borders between homogeneous and heterogeneous catalysis: developing recoverable and reusable catalytic systems. *Topics in Catalysis* **2008**, *48*, 8-31.
- (36) Zhou, W. P.; Lewera, A.; Larsen, R.; Masel, R. I.; Bagus, P. S.; Wieckowski, A.: Size effects in electronic and catalytic properties of unsupported palladium nanoparticles in electrooxidation of formic acid. *The Journal of Physical Chemistry B* **2006**, *110*, 13393-13398.
- (37) Biswas, P.; Wu, C.-Y.: Nanoparticles and the environment. *Journal of the Air & Waste Management Association* **2005**, *55*, 708-746.
- (38) Grasselli, R. K.: Advances and future trends in selective oxidation and ammoxidation catalysis. *Catalysis Today* **1999**, *49*, 141-153.
- (39) Rafelt, J. S.; Clark, J. H.: Recent advances in the partial oxidation of organic molecules using heterogeneous catalysis. *Catalysis Today* **2000**, *57*, 33-44.
- (40) Spivey, J. J.: Complete catalytic oxidation of volatile organics. *Industrial & Engineering Chemistry Research* **1987**, *26*, 2165-2180.

- (41) Panov, G. I.; Uriarte, A. K.; Rodkin, M. A.; Sobolev, V. I.: Generation of active oxygen species on solid surfaces. Opportunity for novel oxidation technologies over zeolites. *Catalysis Today* **1998**, *41*, 365-385.
- (42) Ozbek, M.; Onal, I.; Van Santen, R.: Why silver is the unique catalyst for ethylene epoxidation. *Journal of Catalysis* **2011**, *284*, 230-235.
- (43) Bäckvall, J.-E.: *Modern oxidation methods*; Wiley-VCH, **2011**.
- (44) Clark, J. H.: Green chemistry: challenges and opportunities. *Green Chem.* **1999**, *1*, 1-8.
- (45) Matus, K. J.; Zimmerman, J. B.; Beach, E.: A Proactive Approach to Toxic Chemicals: Moving Green Chemistry Beyond Alternatives in the “Safe Chemicals Act of 2010”. *Environmental science & technology* **2010**, *44*, 6022-6023.
- (46) Perego, G.; Bellussi, G.; Corno, C.; Taramasso, M.; Buonomo, F.; Esposito, A.: New Developments in Zeolite Science and Technology. *New Developments in Zeolite Science and Technology* **1986**, 129-134.
- (47) Bhan, A.; Iglesia, E.: A Link between Reactivity and Local Structure in Acid Catalysis on Zeolites. *Acc. Chem. Res.* **2008**, *41*, 559-567.
- (48) Notari, B.: Microporous crystalline titanium silicates. *Advances in catalysis* **1996**, *41*, 253-334.
- (49) Bernstein, P. L.: *The power of gold: the history of an obsession*; Wiley, **2012**.
- (50) Pyykkö, P.: Theoretical chemistry of gold. II. *Inorganica Chimica Acta* **2005**, *358*, 4113-4130.
- (51) Pyykko, P.: Relativistic effects in structural chemistry. *Chemical Reviews* **1988**, *88*, 563-594.
- (52) Coquet, R.; Howard, K. L.; Willock, D. J.: Theory and simulation in heterogeneous gold catalysis. *Chemical Society reviews* **2008**, *37*, 2046-2076.
- (53) Bone, W. A.; Wheeler, R. V.: The combination of hydrogen and oxygen in contact with hot surfaces. *Philosophical Transactions of the Royal Society of London. Series A, Containing Papers of a Mathematical or Physical Character* **1906**, *206*, 1-67.
- (54) Haruta, M.; Kobayashi, T.; Sano, H.; Yamada, N.: Novel gold catalysts for the oxidation of carbon monoxide at a temperature far below 0°C. *Chem. Lett. (Jpn)* **1987**, *16*, 405-408.
- (55) Haruta, M.; Yamada, N.; Kobayashi, T.; Iijima, S.: Gold catalysts prepared by coprecipitation for low-temperature oxidation of hydrogen and of carbon monoxide. *Journal of Catalysis* **1989**, *115*, 301-309.
- (56) Haruta, M.: Low-temperature oxidation of CO over gold supported on TiO₂, Fe₂O₃, and Co₃O₄. *Journal of Catalysis* **1993**, *144*, 175-192.
- (57) Hutchings, G.: *Journal of Catalysis* **1985**, *96*, 292-295.
- (58) Hutchings, G. J.: Catalysis : A Golden Future. *Gold Bulletin* **1996**, *29*, 122-130.
- (59) Hayashi, T.; Tanaka, K.; Haruta, M.: Selective vapor-phase epoxidation of propylene over Au/TiO₂ catalysts in the presence of oxygen and hydrogen. *Journal of Catalysis* **1998**, *178*, 566-575.
- (60) Della Pina, C.; Falletta, E.; Rossi, M.: Update on selective oxidation using gold. *Chemical Society reviews* **2012**, *41*, 350-419.
- (61) Ratnasamy, C.; Wagner, J. P.: Water gas shift catalysis. *Catalysis Reviews* **2009**, *51*, 325-440.
- (62) Edwards, J. K.; Carley, A. F.; Herzing, A. A.; Kiely, C. J.; Hutchings, G. J.: Direct synthesis of hydrogen peroxide from H₂ and O₂ using supported Au–Pd catalysts. *Faraday Discussions* **2008**, *138*, 225-239.

- (63) Teles, J. H.; Brode, S.; Chabanas, M.: Cationic gold (I) complexes: Highly efficient catalysts for the addition of alcohols to alkynes. *Angewandte Chemie International Edition* **1998**, *37*, 1415-1418.
- (64) Hashmi, A. S. K.; Rudolph, M.: Gold catalysis in total synthesis. *Chemical Society Reviews* **2008**, *37*, 1766-1775.
- (65) De Vos, D. E.; Sels, B. F.: Gold Redox Catalysis for Selective Oxidation of Methane to Methanol. *Angewandte Chemie International Edition* **2005**, *44*, 30-32.
- (66) Zhang, G.; Peng, Y.; Cui, L.; Zhang, L.: Gold-Catalyzed Homogeneous Oxidative Cross-Coupling Reactions. *Angewandte Chemie International Edition* **2009**, *48*, 3112-3115.
- (67) Yuan, Y.; Bian, Y.: Gold (III) catalyzed oxidation of sulfides to sulfoxides with hydrogen peroxide. *Tetrahedron Letters* **2007**, *48*, 8518-8520.
- (68) Oliver-Meseguer, J.; Cabrero-Antonino, J. R.; Domínguez, I.; Leyva-Pérez, A.; Corma, A.: Small Gold Clusters Formed in Solution Give Reaction Turnover Numbers of 107 at Room Temperature. *Science* **2012**, *338*, 1452-1455.
- (69) Haruta, M.: Catalysis: Gold rush. *Nature* **2005**, *437*, 1098-1099.
- (70) Melchiorre, P.; Marigo, M.; Carlone, A.; Bartoli, G.: Asymmetric aminocatalysis—gold rush in organic chemistry. *Angewandte Chemie International Edition* **2008**, *47*, 6138-6171.
- (71) Grabow, L. C.; Mavrikakis, M.: Nanocatalysis Beyond the Gold-Rush Era. *Angewandte Chemie International Edition* **2008**, *47*, 7390-7392.
- (72) Haruta, M.: Size- and support-dependency in the catalysis of gold. *Catalysis Today* **1997**, *36*, 153-166.
- (73) Baker, T.; Liu, X.; Friend, C.: The mystery of gold's chemical activity: local bonding, morphology and reactivity of atomic oxygen. *Physical chemistry chemical physics : PCCP* **2011**, *13*, 34-80.
- (74) Turner, M.; Vaughan, O. P. H.; Lambert, R.: Partial Oxidations with NO₂ Catalysed by Large Gold Particles. *Chemical Communications* **2008**, 2316.
- (75) Herzing, A.; Kiely, C.; Carley, A.; Landon, P.; Hutchings, G.: Identification of active gold nanoclusters on iron oxide supports for CO oxidation. *Science (New York, N.Y.)* **2008**, *321*, 1331-1336.
- (76) Turner, M.; Golovko, V. B.; Vaughan, O. P. H.; Abdulkin, P.; Berenguer-Murcia, A.; Tikhov, M. S.; Johnson, B. F. G.; Lambert, R. M.: Selective oxidation with dioxygen by gold nanoparticle catalysts derived from 55-atom clusters. *Nature* **2008**, *454*, 981-983.
- (77) Zhu, Y.; Qian, H.; Jin, R.: An atomic-level strategy for unraveling gold nanocatalysis from the perspective of Au(n)(SR)_m nanoclusters. *Chemistry : A European Journal* **2010**, *16*, 11455-11517.
- (78) Pei, Y.; Shao, N.; Gao, Y.; Zeng, X. C.: Investigating active site of gold nanoparticle Au₅₅(PPh₃)₁₂Cl₆ in selective oxidation. *ACS nano* **2010**, *4*, 2009-2020.
- (79) Liu, Y.; Tsunoyama, H.; Akita, T.; Tsukuda, T.: Efficient and selective epoxidation of styrene with TBHP catalyzed by Au₂₅ clusters on hydroxyapatite. *Chemical Communications* **2010**, *46*, 550-552.
- (80) A. Stephen K. Hashmi, G. J. H.: Gold Catalysis. *Angewandte Chemie International Edition* **2006**, *45*, 7896-7936.
- (81) Bond, G. C.: Gold: a relatively new catalyst. *Catalysis Today* **2002**, *72*, 5-9.
- (82) Hutchings, G.: New Directions in Gold Catalysis. *Gold Bulletin* **2004**, *37*.
- (83) Guzman, J.; Gates, B. C.: Catalysis by Supported Gold: Correlation between Catalytic Activity for CO Oxidation and Oxidation States of Gold. *Journal of the American Chemical Society* **2004**, *126*, 2672-2673.

- (84) Bond, G.; Thompson, D. T.: Gold-Catalysed Oxidation of Carbon Monoxide. *Gold Bulletin* **2000**, *33*, 41.
- (85) Wang, J.; Hammer, B.: Oxidation state of oxide supported nanometric gold. *Topics in Catalysis* **2007**, *44*, 49-56.
- (86) Valden, M.; Lai, X.; Goodman, D. W.: Onset of Catalytic Activity of Gold Clusters on Titania with the Appearance of Nonmetallic Properties. *Science* **1998**, *281*, 1647-1650.
- (87) Woehrle, G.; Brown, L.; Hutchison, J.: Thiol-functionalized, 1.5-nm gold nanoparticles through ligand exchange reactions: scope and mechanism of ligand exchange. *Journal of the American Chemical Society* **2005**, *127*, 2172-2183.
- (88) Sharma, R.; Holland, G. P.; Solomon, V. C.; Zimmermann, H.; Schiftenhaus, S.; Amin, S. A.; Buttry, D. A.; Yarger, J. L.: NMR Characterization of Ligand Binding and Exchange Dynamics in Triphenylphosphine-Capped Gold Nanoparticles. *The Journal of Physical Chemistry C* **2009**, *113*, 16387-16393.
- (89) Parker, J. F.; Choi, J.-P.; Wang, W.; Murray, R. W.: Electron Self-exchange Dynamics of the Nanoparticle Couple [Au₂₅(SC₂Ph)₁₈]^{0/1-} By Nuclear Magnetic Resonance Line-Broadening. *The Journal of Physical Chemistry C* **2008**, *112*, 13976-13981.
- (90) Hall, K. P.; Mingos, D. M. P.: Homo- and heteronuclear cluster compounds of gold. *Progress in inorganic chemistry* **1984**, *32*, 237-325.
- (91) Vollenbroek, F.; Van den Berg, J.; Van der Velden, J.; Bour, J.: Phosphorus-31 [proton] nuclear magnetic resonance investigation of gold cluster compounds. *Inorganic Chemistry* **1980**, *19*, 2685-2688.
- (92) Hüfner, S.: *Photoelectron spectroscopy: principles and applications*; Springer, **2003**.
- (93) Van Attekum, P.; Van der Velden, J.; Trooster, J.: X-ray photoelectron spectroscopy study of gold cluster and gold (I) phosphine compounds. *Inorganic Chemistry* **1980**, *19*, 701-1405.

2 Preparation of ligand stabilised gold clusters

Ligand protected metal clusters

A cluster is a class of material that is typically defined as a small aggregation or grouping of a sub-unit. From the view point of a chemist, a cluster is a small array of similar atoms that occupy a niche between a molecule and a bulk material. More recently, the term ‘cluster’ has been used to refer to compounds that contain expressly metal-metal bonds.¹ There are two main classes of metal cluster—naked clusters and ligand stabilised clusters. A naked cluster has no ligand stabilisation and is often generated and studied under high vacuum conditions. In comparison, ligand stabilised clusters are typically prepared by wet chemistry and the metal core is surrounded by a shroud of organic ligands which stabilise the cluster by both steric and electronic means. For metal clusters, common ligands include carbon monoxide, alkenes, isocyanides, halides, and hydrides. For main group clusters, the most common ligand is hydride.

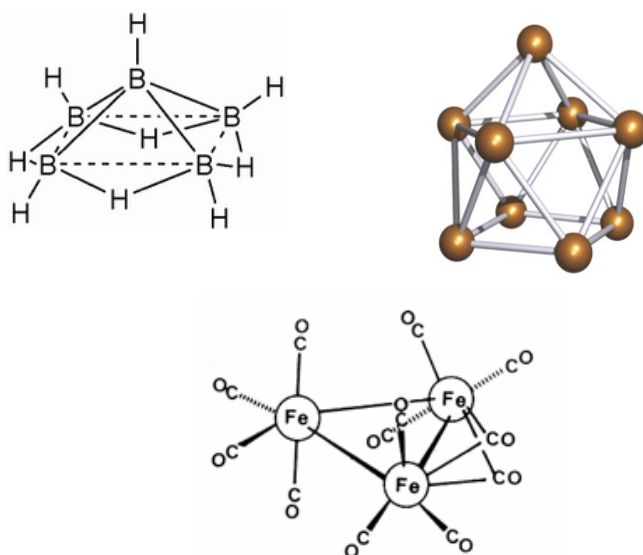


Figure 5; Examples of chemical clusters; A) pentaborane, B) iron carbonyl, and C) $[\text{Ge}_9]^{4-}$

In Figure 5, several examples of chemical clusters are presented, such as pentaborane, iron carbonyl and the zintl ion $[\text{Ge}_9]^{4-}$. Several examples of high nuclearity metal clusters have been well characterised, such as $\text{Au}_{102}(\text{S-pC}_6\text{H}_4\text{COOH})_{44}$, $\text{Au}_{55}(\text{PPh}_3)_{12}\text{Cl}_6$, and $\text{Pd}_{561}\text{BiPy}_{60}\text{OAc}_{180}$.²⁻⁴ Although these giant metal clusters are still molecular in nature, they have properties that are almost metallic in nature *i.e.* embryonic metals. These clusters now have nanometer size dimensions, which means the small clusters are also classified as nanoparticles. At these size dimensions, the difference between the types of metal clusters can become blurred. Some systems have also been classed as metal colloids, which is defined as a stabilised solution of metal nanoparticles.

The properties of ligand stabilised clusters and nanoparticles depend on several distinct structural components;

- The metal core, where the number and type of metal atoms can significantly alter the electronic properties of the metal particles
- The ligand shell, which is bound to the metal core and inhibit particle growth
- The ligand functionalisation, which is regulated by the terminating groups on the ligand which in turn controls interactions with the solvent

From the view point of a chemist, the main distinction between metal nanoparticles and metal clusters is that metal clusters are atomically precise and can be characterised by single crystal X-ray crystallography to determine the exact position of ligands and chirality of the metal core in the solid state. In comparison, metal nanoparticles is a more general term for metal particle systems that have a particle size distribution and this is controlled by the various synthetic conditions and the capping agents used. In recent years, the interplay of size, shape and composition of metal nanoparticle cores has been shown to have an important role in the novel optical, catalytic and electronic properties, leading to potential applications in a wide range of industries.

Phosphine and thiol stabilised gold clusters

Molecular gold clusters have recently been shown to be of significant interest in a wide range of applications due to their size-dependant chemical and physical properties.^{5,6} Gold nanoparticles have been known for their unique optical properties for many years; however, the unique properties of gold clusters in the 1 nm size range have only become apparent in recent years.

Phosphine- and thiol-stabilised gold clusters constitute the two main classes of the chemically synthesised gold clusters. Using chemical tools, a wide range of characteristics of these clusters can be controlled such as the specific number and type of metal atoms in the core (nuclearity and composition), core symmetry, type and number of ligands and type and numbers of counter ions. The optical and electronic behaviour of these clusters has been shown to be sensitive to both the core size and ligand type; increasing size of the cluster leads to increasing metallic behaviour of the cluster.⁷ There have been an extensive number of studies correlating the observed characteristics of the clusters to theoretical models but many of these recent studies have mainly focused on gas-phase systems and ignore the influence or fate of the cluster ligands.

The earliest ligand stabilised gold clusters were prepared by Malatesta *et al.* in 1966 by the reduction of phosphine stabilised gold halide salts with sodium borohydride in ethanol.⁸ Further developments led to the isolation and characterisation of $\text{Au}_{11}(\text{PPH}_3)_7(\text{SCN})_3$ and a wide range of other phosphine-stabilised gold clusters.⁹⁻¹² Gradually, with improved characterisation methods, the structure of these materials was explored more fully using single crystal X-ray crystallography and photoelectron spectroscopy.¹³⁻¹⁶ Due to the unique reactivity of these clusters, ligand exchange in solution is relatively facile, and an undecagold cluster has shown promise for potential applications in cell recognition after ligand exchange reaction with tRNA.^{17,18}

Most of the phosphine clusters prepared by the reduction of gold salts have a general formula of $[\text{Au}_{11}\text{L}_7\text{X}_3]$, with several examples of nonagold and octagold clusters have also been observed.^{19, 20} The undecagold cluster typically has a skeletal structure with C_{3v} structure, which has been observed in many structurally related systems.^{10,15,21,22} The stability of these compounds with this specific structure has been explained by the presence of central icosahedron motif cementing overall structure and by a *noble-gas superatom* analogy.²³ The superatom electronic theory has recently been applied to metal clusters and has successfully predicted the stability and chemistry for

a range of metal clusters and nanoparticles.^{24,25} For metal clusters, the valence electrons of the cluster can delocalise to the ligands, which facilitates the possibility for the cluster to attain the noble-gas electronic configuration; forming the stable maximum valence compound.²⁶ The stability of the phosphine stabilised undecaclusters is attributed to the closing of the eight electron gap between the HOMO and LUMO.²⁶ DFT calculations have shown that the HOMO-LUMO gap is 2.1 eV for the $\text{Au}_{11}(\text{PPh}_3)_8\text{Cl}_3$ cluster have also confirmed the unique stability of these clusters. For the smaller, nonagold and octagold cluster typically prepared by the reduction of a larger gold phosphine precursor, the HOMO-LUMO has been calculated to slightly smaller than the dodecagold cluster, which has been also shown experimentally cyclic voltammetry data^{20,23}

Over the past two decades, thiol stabilised gold nanoparticles and atomically precise thiolate gold clusters have become popular systems due to significant advances in synthetic methodologies and characterisation techniques. Relatively monodisperse gold thiol nanoparticles (~2–5 nm) were prepared by Brust *et al.* in high yield, where a gold precursor is reduced in an aqueous solution and then transferred by phase transfer catalyst to a toluene layer in which an alkane thiol capping group is present to stabilise the gold particles.²⁷ This biphasic method significantly improved the size control of the gold particles and opened new possibilities for the preparation of functionalised gold nanoparticles. Previous methods for gold nanoparticles typically involved preparation of gold citrate nanoparticles, followed by subsequent ligand exchange with the desired capping agent often yielding polydisperse nanoparticles.^{28,29} More recently, preparation of atomically precise gold thiolate clusters, $\text{Au}_n(\text{SR})_m$, has been aided by improvements in characterisation methods such as electro spray ionisation – mass spectrometry and X-ray crystallography. These developments have led to the synthesis, isolation and structural characterisation of the largest ligand stabilised gold cluster $\text{Au}_{102}(\text{S}-p\text{C}_6\text{H}_4\text{COOH})_{44}$ as well as the smaller $\text{Au}_{25}(\text{S}-\text{CH}_2\text{CH}_2\text{Ph})_{18}$ cluster.^{23,30-32} In the case of the larger Au_{102} cluster, the $\text{Au}^1\text{S}-p\text{C}_6\text{H}_4\text{COOH}$ moieties have been shown to hydrogen bond extensively which leads to important intra cluster interactions that lead to the formation of crystals. There has been a range of other gold thiol-protected clusters published that has been characterised by electrospray mass spectroscopy (ESI-MS), which limits the structurally damage done to the cluster, allowing the cluster size and ligand shell to be approximated.³³ The stability of the thiolate gold clusters has been attributed to the unique $\text{Au}^1\text{-SR}$ outer shell which forms a layer around a smaller electron rich gold core.^{23,33}

Synthesis of phosphine stabilised gold clusters

For this study, the focus was on the preparation and use of several phosphine stabilised gold clusters. Some of the early work did initially explore the preparation and crystallisation of several thiolate gold clusters. However, it was found that the yields of these clusters were relatively poor and that without easy access to ESI-MS from the beginning of this project, characterisation of the thiolate clusters proved to be difficult. The first synthesis of $\text{Au}_{102}(\text{S-}p\text{C}_6\text{H}_4\text{COOH})_{44}$ has only recently been published and even then the yields have been poor.³ Recent progress by the Levi-Kalisman on $\text{Au}_{102}(\text{S-}p\text{C}_6\text{H}_4\text{COOH})_{44}$ preparation has significantly improved yields but lies beyond the scope of this project.³⁰

In comparison to the thiolate gold clusters, triphenyl phosphine stabilised clusters have been prepared and structurally characterised often with relatively high yields; ranging from $\text{Au}_2(\text{PPh}_3)_2$ up to the larger $\text{Au}_{13}(\text{PPh}_3)_{10}\text{Cl}_3$ cluster.³⁴ Larger phosphine stabilised gold nanoparticles have been prepared with a core nuclearity greater than 55 gold atoms.⁴ These *embryonic metals*, as they are dubbed by Gunter Schmid, have similar dimensions to $\text{Au}_{102}(\text{S-}p\text{C}_6\text{H}_4\text{COOH})_{44}$ which is known to have significantly metal characteristics.²³ The characterisation of this Au_{55} cluster has been disputed due to several characterisation inconsistencies; investigations by transmission electron microscopy, photoelectron spectroscopy and X-Ray scattering methods have shown that the sample is polydisperse.³⁵ More robust methods for the synthesis of gold phosphine nanoparticles have been developed, which employ a similar biphasic system as the Brust methodology, yielding nanoparticles with a very narrow size distribution (1.4 nm $\sigma = 0.7$ nm).³⁶

The focus of this study was to prepare a small series of atomically precise gold clusters. $\text{Au}_{11}(\text{PPh}_3)_8(\text{Cl})_3$, $\text{Au}_9(\text{PPh}_3)_8(\text{NO}_3)_3$, $\text{Au}_8(\text{PPh}_3)_8(\text{NO}_3)_2$ and the 1.4 nm gold phosphine nanoparticle system were chosen as the target clusters for this study, because each cluster has the same ligand and the cluster size range will hopefully illuminate any size effects during catalysis.

Wet chemical preparations of metal nanoparticles and clusters are prepared by a bottom up approach, where metal salts are reduced in the presence of a ligand or capping agent. The ligand

used for this series of clusters and nanoparticles was always triphenylphosphine and this was not varied throughout this study.

In general, metal nanoparticle preparations employ the reduction of various metal salts in the presence of an appropriate passivating agent, but can lead to low yields of the desired particle size, mainly due to poor control of complex kinetic and thermodynamic controls of the reaction. Recent studies have also shown how the particle size distribution of the product can also be dependent on local concentrations of precursor, reducing agent and capping agent.^{37,38} Other issues can arise due to problems with separation and isolation of the target product with the desired characteristics from either larger particles or excess organic ligands. Common methods of purification of metal nanoparticles involve 1) repeated solvent washes, which selectively remove by-products, inorganic salts, and undesirable particle sizes, 2) centrifugation, 3) crystallisation and 4) size exclusion chromatography. For the larger nanoparticles, solvent washes can be useful for removing unwanted particles sizes through the significant differences in solubility. However with particles with less than 50 atoms, the separation process can be much more difficult due to similar solubility properties of the product and precursors. Detailed description of the synthetic procedures used to make Au-containing precursors used in catalyst fabrication are given below. No modification of the procedures reported earlier was attempted, unless otherwise specified.

H₂AuCl₄

Tetrachloroauric acid was prepared, in house, by dissolving high purity gold (99.999%, 5 g) in a mixture of nitric acid (15 mL) and hydrochloric acid (30 mL), which was stirred for twenty four hours.³⁹ The dissolved gold was then dried under reduced pressure, which resulted in deep orange crystals. The solid was then dissolved in concentrated hydrochloric acid (10 mL). The heated sample volume was reduced to 2 mL, before orange crystals of the pure product formed upon cooling to room temperature.

Au(PPh₃)Cl

The synthesis protocol was adapted from the procedure described by Malatesta *et al.*⁸ Triphenylphosphine (2.65 g, 10.10 mmol) in ethanol (75 mL) was added rapidly to a stirred (500 rpm) solution of tetrachloroauric acid (2.010 g, 5.102 mmol) in ethanol (20 mL). The yellow colour of solution disappeared immediately upon addition of triphenylphosphine and a white precipitate

formed. The resulting solution was stirred vigorously (1000 rpm) for a further 15 minutes to ensure the reaction went to completion. The reaction mixture was centrifuged (5 min, 5000 rpm) to collect the solid white product. The product was washed three times with hot ethanol (3 × 20 mL) on a sintered glass funnel filter (porosity 3). The remaining solid was dissolved in chloroform (30 mL), filtered and the solvent removed under reduced pressure. The crude product was dried in a vacuum desiccator. The product was recrystallized from a mixture of dichloromethane and methanol using vapour diffusion resulting in needle-like white crystals.

Yield: 2.250 g, 90 %. ^{31}P NMR (chloroform, 25 °C); δ 33.5 ppm referenced to H_3PO_4

$\text{Au}(\text{PPh}_3)\text{NO}_3$

$\text{Au}(\text{PPh}_3)\text{NO}_3$ was synthesised according to a protocol described by Mueting *et al.*⁴⁰ A solution of AgNO_3 (3.430 g, 20.191 mmol) in ethanol (130 mL) was added rapidly to a solution of $\text{Au}(\text{PPh}_3)\text{Cl}$ (3.973 g, 8.042 mmol) in chloroform (50 mL). The reaction was left to stir for 1 h in a reaction vessel covered with aluminium foil. The AgCl precipitate was removed by filtration on a sintered glass funnel filter (porosity 3) and the filtrate was dried in a rotary evaporator without heating. The crude product was washed with ethanol (3 × 50 mL). The solid was then dissolved in dichloromethane (50 mL) to which ethanol (150 mL) was later added. The solution was then bubbled thoroughly with a flow of nitrogen for 2 hours to remove the dichloromethane. The resulting white crystals were collected by filtration, washed with cold ethanol (3 × 5 mL) and cold diethyl ether (3 × 5 mL). The product was stored in a freezer in the absence of light.

Yield: 3.648 g, 87 %. ^{31}P NMR (chloroform, 25 °C); δ 25.2 ppm referenced to H_3PO_4

1.5 nm Au nanoparticle

“ Au_{101} ” or $\text{Au}_{101}[\text{P}(\text{C}_6\text{H}_5)_3]_{21}\text{Cl}_5$ stabilized by triphenylphosphine was prepared according to a protocol described by Hutchison *et al.*^{36,41} Tetraoctylammonium bromide (1.40 g, 2.56 mmol) was added to a solution of tetrachloroauric acid (1 g, 2.54 mmol) in ultrapure water (60 mL) and toluene (60 mL). After 5 minutes of vigorous stirring at 1000 rpm, triphenylphosphine (2.3 g, 8.76 mmol) was added to the biphasic system. After 10 minutes of vigorous stirring, a solution of freshly dissolved sodium borohydride (2.0 g, 52.9 mmol) in ultrapure water was rapidly added to the reaction mixture. The reaction mixture was left to stir at 600 rpm for a further 3 hours, at which point the organic layer was separated and washed with saturated solution of NaCl in ultrapure water

(2 × 50 mL) and then ultrapure water (3 × 50 mL). The organic layer was separated, filtered and dried under reduced pressure. The resulting solid was dissolved in chloroform (35 mL) to which pentane (300 mL) was added slowly with gentle swirling and the mixture allowed to stand overnight. The precipitate was collected by filtration on a sintered glass funnel filter (porosity 4) and washed with series of solvent mixtures as follows:

- 2 × 100 mL hexanes followed by 100 mL 2: 3 MeOH: H₂O)
- 2 × 100 mL hexanes followed by 100 mL 1: 1 MeOH: H₂O)
- 2 x 150 mL 3: 1 pentane: chloroform
- 2 x 150 mL 2: 1 pentane: chloroform
- 2 x 150 mL 1: 1 pentane: chloroform

The solvent washes are used to remove by-products, Au(PPh₃)Cl and the phase transfer reagent. The effectiveness of the purification steps was monitored by ¹H NMR. The remaining solid was dissolved in dichloromethane (30 mL) and filtered through to remove any insoluble by-products. Removal of the solvent of the filtrate on a rotary evaporator afforded the pure product as a fine black powder.

Yield: 200 – 250 mg. This cluster was characterised by HR TEM and purity was confirmed by ¹H NMR in CDCl₃

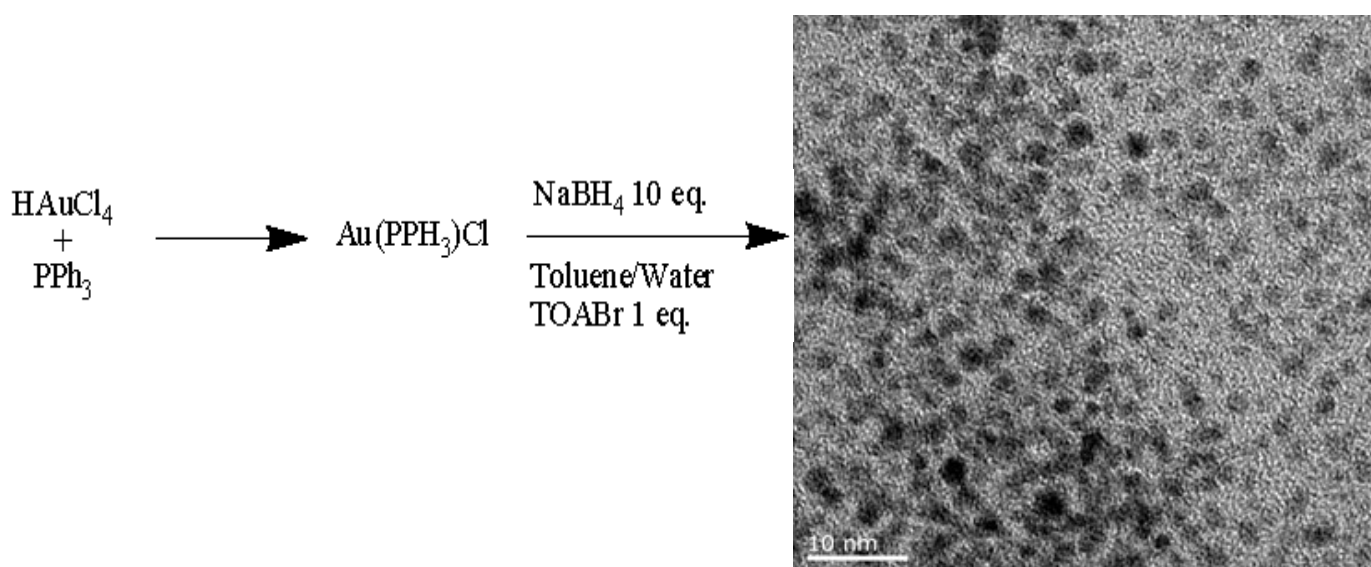


Figure 6; Schematic of 1.5 nm gold nanoparticle preparation

The gold nanoparticles prepared by this method are reproducible; however, yields occasionally varied. The samples were found to be more consistent if the purification steps of these nanoparticles were conducted by centrifugation rather than filtering. The nanoparticles are relatively unstable in solution due to the high lability of the triphenylphosphine in dichloromethane; hence by centrifuging the samples we further minimise the time the nanoparticles are in solution.



$\text{Au}_{11}(\text{PPh}_3)_8\text{Cl}_3$ was synthesised according to a modified protocol described by Hutchison *et al.*⁴² A solution of NaBH_4 (0.075 g, 1.97 mmol) in ethanol (5 mL) was added dropwise to a stirred suspension of $\text{Au}(\text{PPh}_3)\text{Cl}$ (1.0 g, 2.02 mmol) in ethanol (50 mL). The reaction mixture was left to stir for 2 hours, after which time it was poured into hexanes (1 L) and the product was allowed to precipitate overnight. The precipitate was collected using a sintered glass filter funnel (porosity 4). It was then washed with hexanes (4 × 15 mL), 1:1 (v/v) mixture of CH_2Cl_2 : hexanes (4 × 15 mL), and 3:1 (v/v) mixture of CH_2Cl_2 : hexanes (1 × 10 mL). The solid remaining on the filter was dissolved in dichloromethane (20 mL) and filtered through to remove any insoluble by-products. The crude product was obtained upon removal of solvent on a rotary evaporator. It was recrystallized from a mixture of dichloromethane and diethyl ether by vapour diffusion at 4 °C resulting in deep red platelets.

Yield: 155 mg, 17.5% ^{31}P NMR (chloroform, 25 °C); δ 52.2 ppm referenced to H_3PO_4

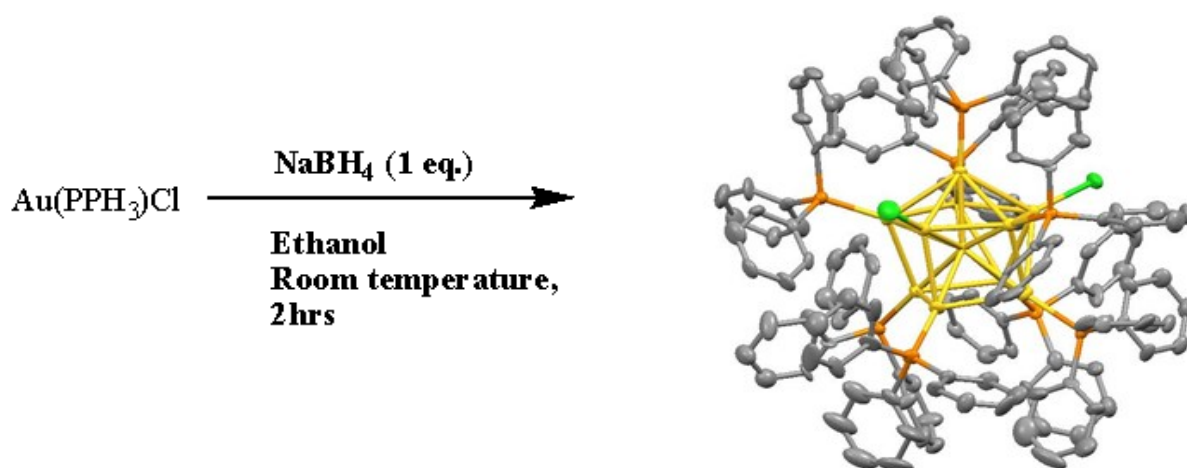
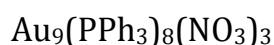


Figure 7: Schematic of the preparation of $\text{Au}_{11}(\text{PPh}_3)_8\text{Cl}_3$

The ligand stabilised undecagold cluster has been investigated in the literature for several decades now due to the unique optical and electronic properties, and more recently the versatile methods for functionalising the ligand shell. The earliest reports of an undecagold cluster come from Maletsta *et al.*, where an undecagold product was identified from the reduction of the monophosphine gold precursor. However, it was not until the works of Mingos and Van der Velden in 1980 that the undecagold cluster was fully characterised and mechanistic insights to the reaction mechanism were discussed. More recently, the potential of undecagold for applications in the targeted labelling of biological structures have been highlighted by the preparation water soluble derivatives of the undecagold cluster by ligand exchange reactions. Many of these early undecagold clusters had a range of derivatized phosphine ligands and counter ions, and employed more exotic reducing reagents (Ti^{IV}), which often limited the reproducibility of the preparations.

Recently, the Hutchison group have shown that the triphenylphosphine stabilised undecagold cluster can be produced in small batches with average yields (20-30%). Recent publications have also highlighted that several polymorphs of the undecagold cluster are also generated. Previously in the literature $\text{Au}_{11}(\text{PR}_3)_7$ and $\text{Au}_{11}(\text{PR}_3)_8$ are often used interchangeably, however the Hutchison *et al.* highlighted that careful tuning of the conditions such as precursor concentration and solvent choice can improve the product selectivity in micro capillary reaction systems.

Structural characterisation of the undecagold cluster shows the cluster stability derives from optimised surface passivation by the triphenyl phosphine ligands. The low yield of the undecagold cluster is due to the formation of much larger colloidal gold nanoparticles, which are removed by solvent washes and subsequent crystallisation.



$\text{Au}_9(\text{PPh}_3)_8(\text{NO}_3)_3$ was synthesised following the protocol described by Wen *et al.*⁴³ A solution of NaBH_4 (0.072 g, 1.92 mmol) in ethanol (92 mL) was added to the magnetically stirred solution of $\text{Au}(\text{PPh}_3)\text{NO}_3$ (4.0 g, 7.6 mmol) in ethanol (160 mL). The solution became deep red within two hours, at which point the solution was filtered to remove insoluble impurities and the solvent removed on a rotary evaporator. The solid so obtained was dissolved in 20 mL CH_2Cl_2 and filtered through a sintered glass filter funnel (porosity 3). Removal of solvent on rotary evaporator yielded the product as a black precipitate, which was washed with 50 mL of THF. Upon washing, the

solid became dark green. The solid was further washed with THF (3×50 mL) and hexanes (3×50 mL). The precipitate was crystallized from methanol by slow diffusion of diethyl ether at 4 °C. Dark green crystals formed within ca. 5 days.

Yield 1.24 g, 36 %. ^{31}P NMR (chloroform, 25 °C); δ 56.8 ppm referenced to H_3PO_4

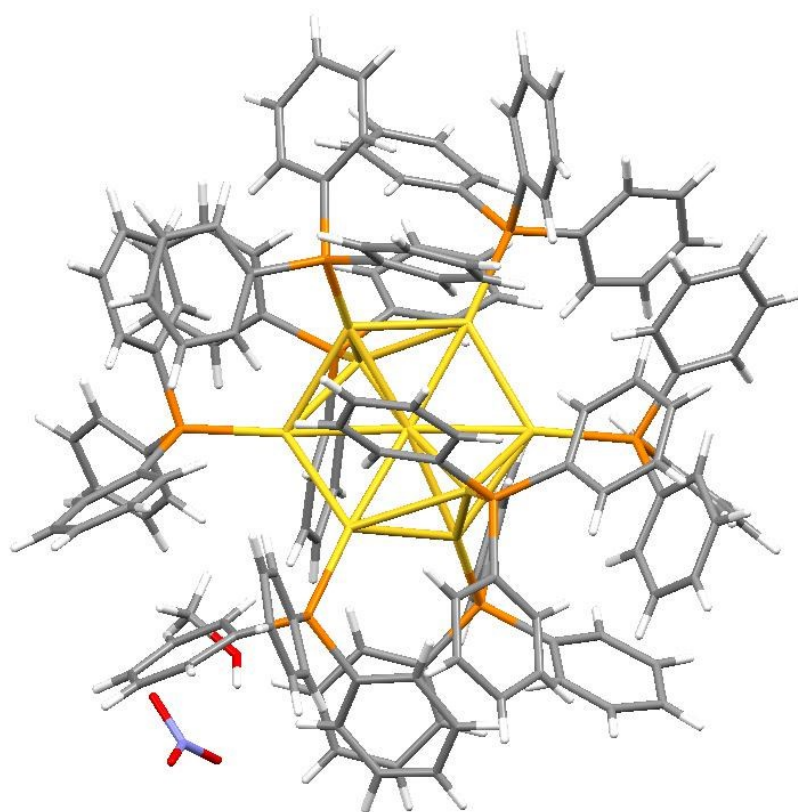
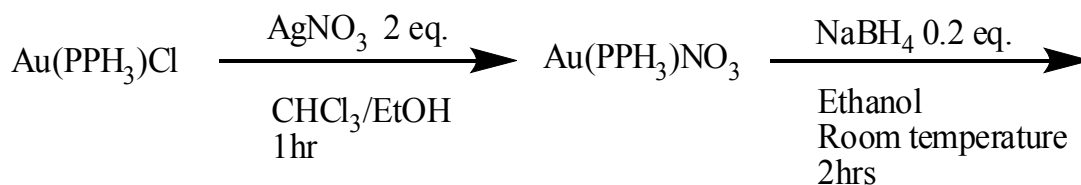


Figure 8: Schematic of $\text{Au}_9(\text{PPh}_3)_8(\text{NO}_3)_3$ preparation

$\text{Au}_8(\text{PPh}_3)_8(\text{NO}_3)_2$

$\text{Au}_8(\text{PPh}_3)_8(\text{NO}_3)_2$ was synthesised following the protocol described by Van der Velden *et al.*

$\text{Au}_9(\text{PPh}_3)_7(\text{NO}_3)_3$ (1.48 g, 0.36 mmol) and PPh_3 (0.96 g, 3.66 mmol, 10-fold excess) were mixed in 20 mL of CH_2Cl_2 . The resulting deep red solution was stirred for a further 30 minutes. The crude product was precipitated by addition of 200 mL of toluene, isolated by filtration on a glass frit (porosity 3), washed alternately with toluene (3×20 mL) and hot hexanes (3×20 mL) and dried. The red product was crystallized from CH_2Cl_2 by slow diffusion of diethyl ether at 4 °C. Deep red crystals formed within ca. 4 days. The crystallization was repeated several times to remove excess triphenylphosphine.

Yield: 1.38 g, 88 %. ^{31}P NMR (chloroform, 25 °C); δ 58.2 ppm referenced to H_3PO_4

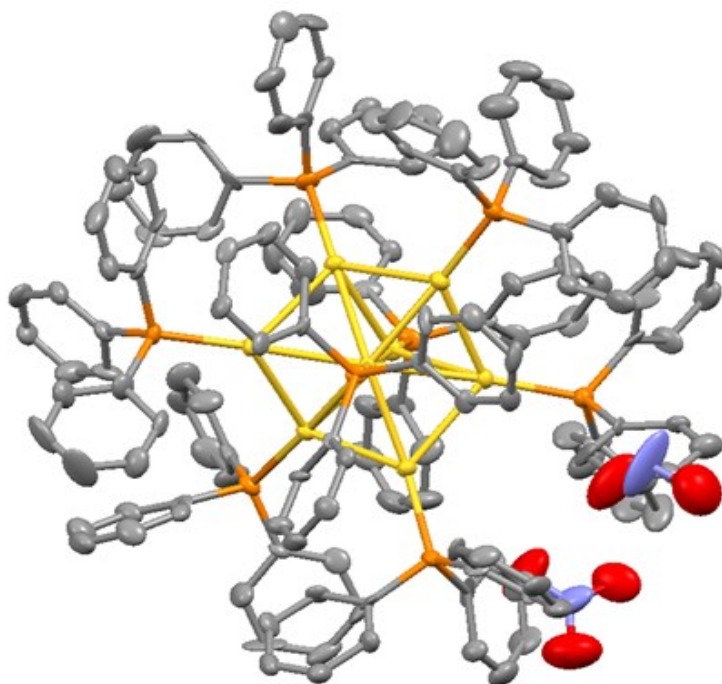
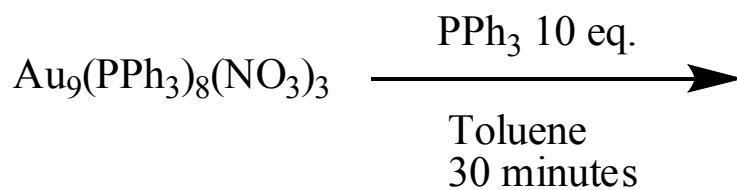


Figure 9: Schematic of $\text{Au}_8(\text{PPh}_3)_8(\text{NO}_3)_2$ preparation

Characterisation of the gold phosphine clusters

All the clusters prepared were high purity and free from unreacted reagents. The presence of larger gold particles will influence chemistry of the clusters in small amounts; hence, further characterisation methods were used to confirm the purity of the clusters prepared for this study.

Electron microscopy of gold clusters

High resolution transmission electron microscopy (HRTEM) was conducted at the Department of mechanical engineering, University of Canterbury on a 200 kV Philips CM-200. HRTEM can provide a range of useful information on the structure of the material of interest using

electron diffraction, however due to the nature of the nanoparticles being investigated in this study; we are only able to discern the particle size from the images. For such small particles, there is no long range order, meaning that electron diffraction yields no information of use.

At 200 kV, the resolution is calculated to be 7 Å, however for measurement of particle size the particle size was limited to 1 nm, due to issues of contrast of the nanoparticles on the carbon film and the quality of the electron beam. The samples of the clusters were typically dissolved in solvent at very low concentrations, typically 0.5 mg in 1 mL of solvent, 10 µL is then dispensed onto an amorphous carbon film supported on a copper grid. For Au₁₀₁, the solution of the cluster was used immediately as the cluster can rapidly agglomerate in solution due to the lability of the triphenylphosphine ligand. For the smaller clusters, methanol was used as the solvent of choice as the cluster was completely soluble and the solvent was easily removed in vacuum. Once the cluster solution was deposited on to the amorphous carbon support, the sample was dried under vacuum for an hour prior to loading into the sample holder of the TEM. Overall, the clusters proved difficult to observe against the amorphous carbon despite the high gold content.

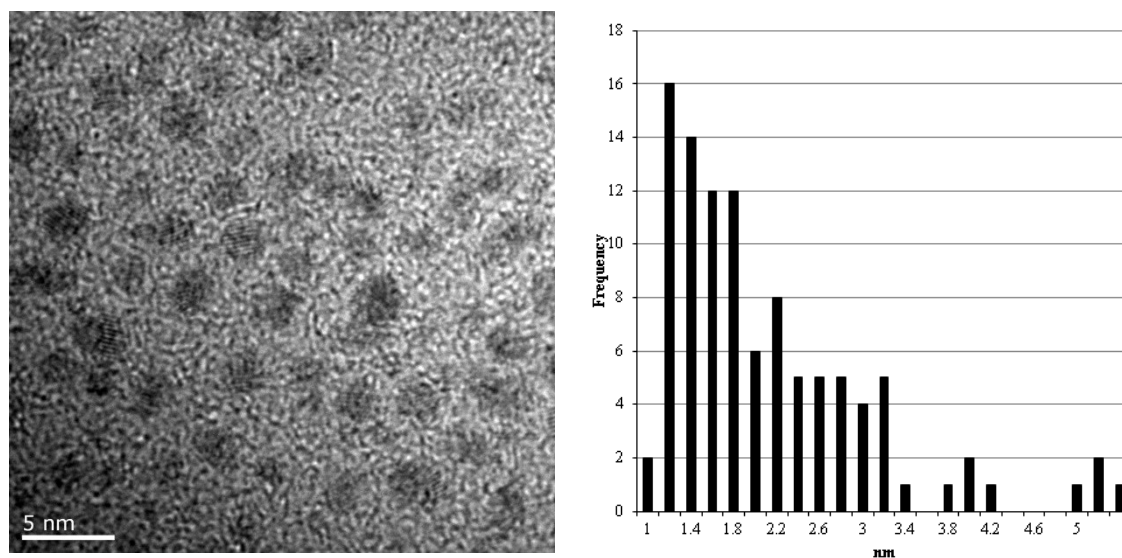


Figure 10; HRTEM of Au₁₀₁ nanoparticles deposited on to amorphous carbon film supported on a 300 mesh cooper grid, and the particle size count of the nanoparticles.

The larger Au₁₀₁ nanoparticles were found to have an average particle size (\bar{X}) of 1.5 nm with a standard deviation (σ) of 0.95 nm. A several batches of Au₁₀₁ were prepared, the particle size was found to vary by 0.4 nm and with a slight increase in σ . If the sample was left in a solution for an hour before depositing on to the carbon film, the population of larger nanoparticles increased

significantly. All manipulations of Au₁₀₁ were carried out rapidly ensuring that the nanoparticles did not aggregate significantly during analysis and deposition on to the support. These results compare well with literature reports of the gold nanoparticles produce by the same method.³⁶

HRTEM of the smaller gold phosphine proved to be much more difficult. The diameter of the gold core of the smaller clusters can be measured from the crystal structure data to be approximately 0.84 nm – 0.9 nm, which is just above the theoretical limit of the Philips C-200 TEM at the Universit of Canterbury. It was not possible to get accurate particle size counts for these clusters for several reasons; dispersion of the clusters on the amorphous carbon, thickness of the amorphous carbon film and also under a prolonged exposure to the electron beam, up to an hour, the gold particles were observed to sinter, forming much larger gold nanoparticles, between 2 – 6 nm in diameter. This agglomeration is assumed to occur due to loss of the triphenylphosphine ligands under the high energy electron beam and the ultra-high vacuum conditions.

For the atomically precise gold phosphine clusters, the measured gold cluster size compares with other literature examples of TEM analysis of such small gold clusters.^{20,44}

Aberration corrected ADF-STEM

A small range of samples was also examined by angular dark field scanning transmission electron microscopy (ADF-STEM), which yielded higher resolution images of the gold clusters. The only cluster examined was $\text{Au}_9(\text{PPh}_3)_8(\text{NO}_3)_3$, to confirm the monodispersity of the phosphine stabilised cluster. The cluster sample was prepared for microscopy and analysed by Sherry Chang, at the University of Monash, Australia, on a Double-corrected FEI Titan 80-300 FEGTEM. The samples were prepared in a similar method to the HRTEM samples above, a small amount of the cluster is dissolved in high purity methanol, of which, a small droplet was deposited on agar holey carbon film, and subsequently dried under nitrogen gas.

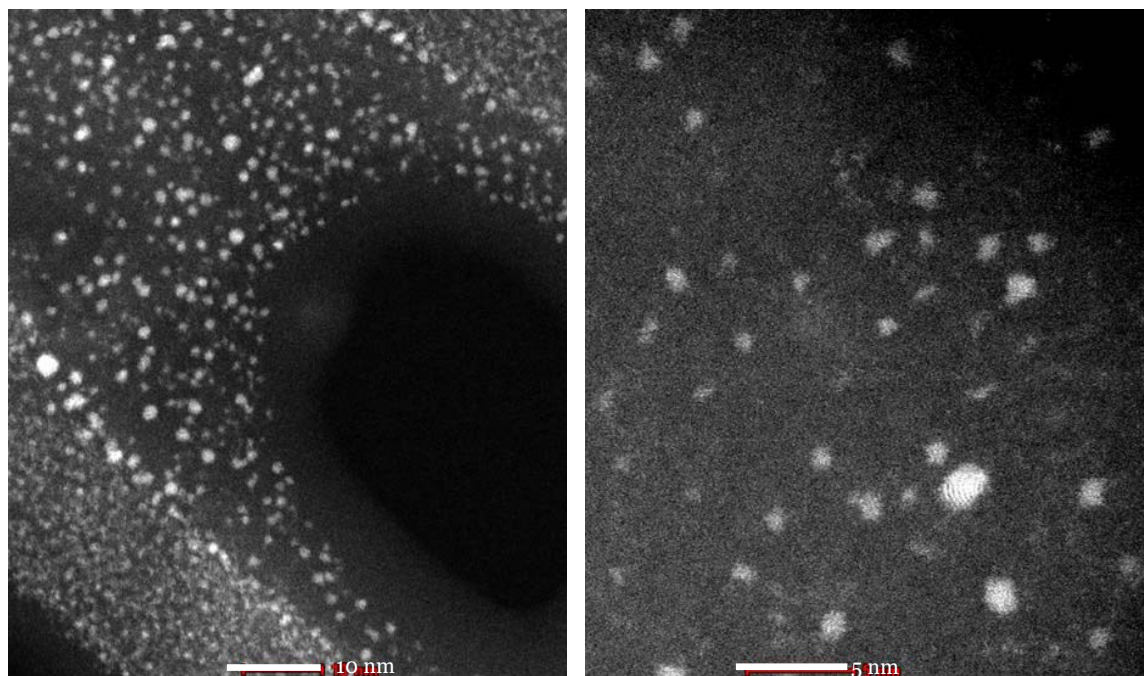


Figure 11; ADF-STEM images of $\text{Au}_9(\text{PPh}_3)_8(\text{NO}_3)_3$ on an amorphous carbon film.

At first, the samples were prepared at similar concentrations to the HRTEM samples, which resulted in the carbon film being completely covered with small gold clusters. At cluster concentrations seen in Figure 8 (1 mg per 10 ml), the sample appears to be polydisperse, where the smallest particles are $\sim 0.8/0.9$ nm, whilst there does appear to be larger particles of up to ~ 2 nm. Initially, this was an indication that there may be issues of contamination from by-products of the reaction. However, as the ^{31}P NMR data show only one peak present, which was assigned to the phosphorous bound to the cluster, other possible explanations were explored. Under these experimental conditions, the 300 kV electron beam under high vacuum can induce desorption of the triphenyl phosphine ligands; this could then lead to the aggregation of the clusters, forming the

larger gold nanoparticles. Alternatively, this concentration the gold cluster may include small, soluble crystallites, which give the observed bimodal distribution in the particle size.

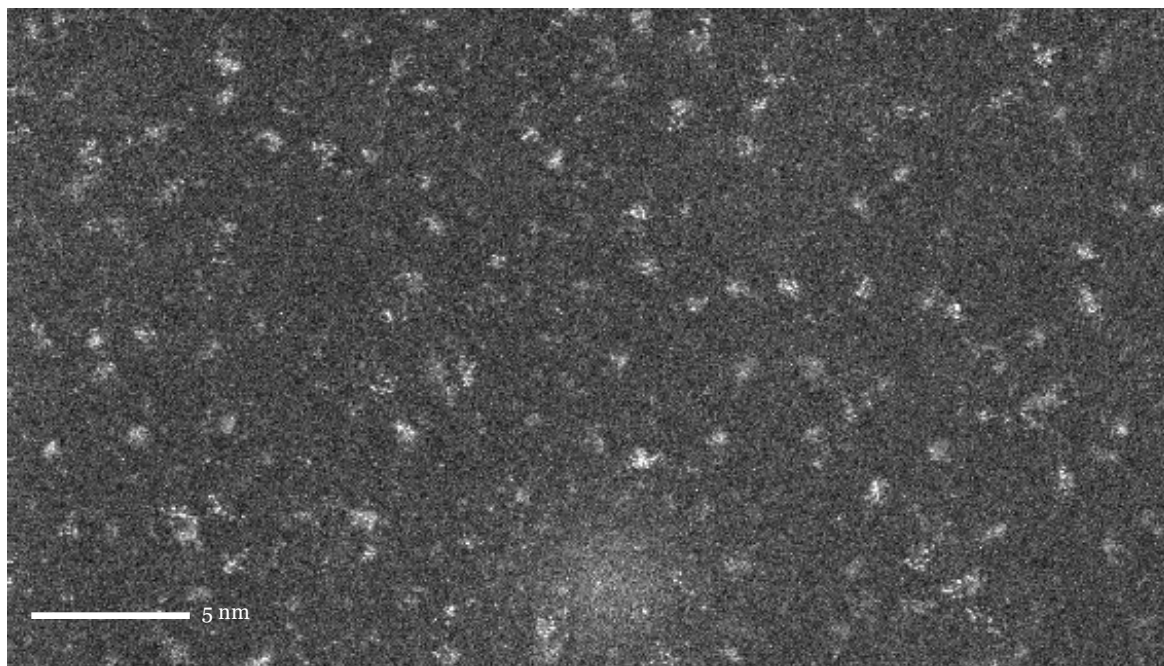


Figure 12; ADF-STEM of lower concentration of $\text{Au}_9(\text{PPh}_3)_8(\text{NO}_3)_3$ cluster on an amorphous carbon film

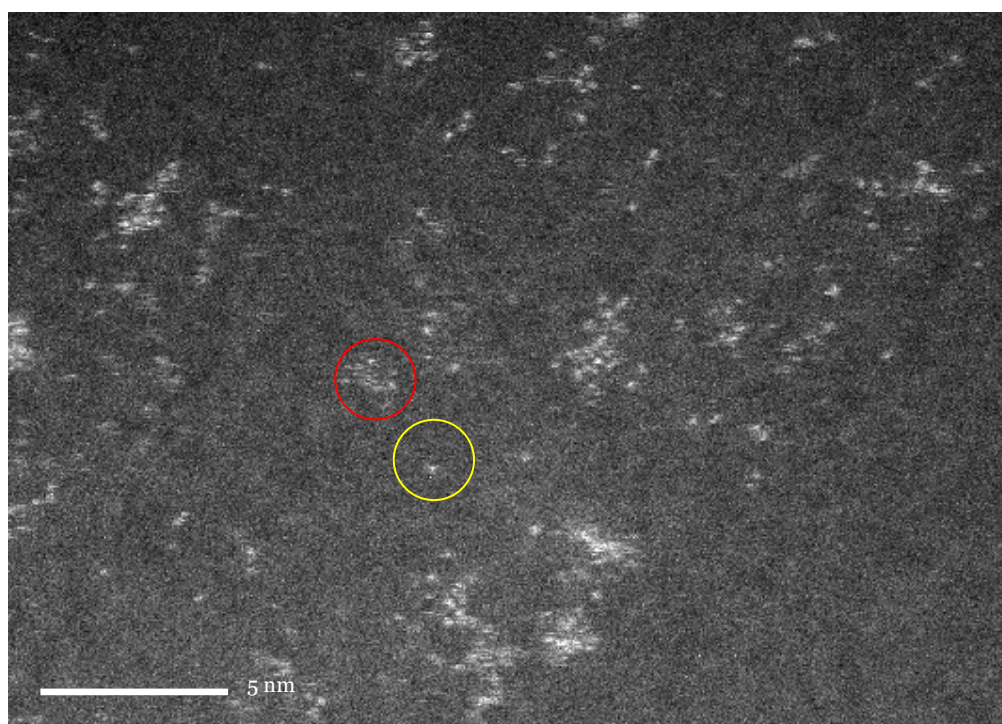


Figure 13; Higher resolution image of $\text{Au}_9(\text{PPh}_3)_8(\text{NO}_3)_3$, showing the presence of single gold atoms (Yellow circle) along with the gold cluster (Red circle)

A sample with a significantly lower concentration of the cluster (1 grain per 6 mL of MeOH) was examined, where the gold clusters was mono-disperse, with a typical size of ~ 0.8 nm (Figure 14). However, there appears to be a small proportion of single gold atoms present on the surface, which was attributed to beam induce damage from the incident electrons. At these concentrations, the beam damaged results in the formation of single gold atoms at the surface; whilst at the higher concentrations of gold cluster, it results in the formation of larger gold nanoparticles.

Alternatively, the single gold atoms could be derived from the mono gold phosphine starting material which was reduced controllably to form the cluster. However, ^{31}P NMR does not give any indication that the mono-nuclear species are present in the any of the purified batches of $\text{Au}_9(\text{PPh}_3)_8(\text{NO}_3)_3$ that were prepared during this work. From both the 200 kV HRTEM and 300 kV AFD-STEM experiments, we did observe the growth of the gold clusters forming slightly larger nanoparticles, which we attributed to damage from the incident electrons that removed the stabilising triphenylphosphine ligands and resulted in the agglomeration of the cluster, possibly by a Ostwald ripening mechanism due to the presence of single gold atoms on the surface.

EXAFS of the phosphine stabilised gold clusters

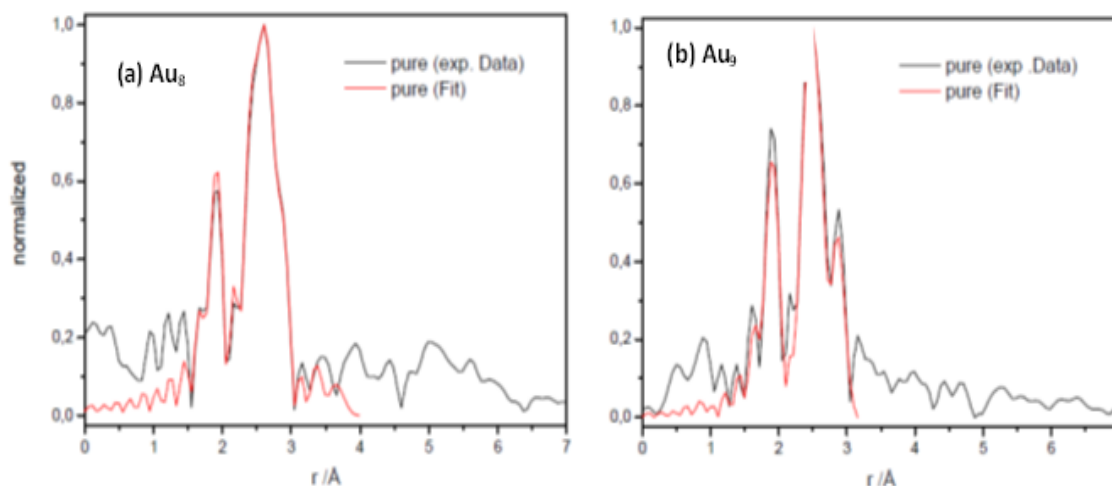


Figure 15; Experimental EXAFS data (black) and the XFit fit (red) for the (a) $\text{Au}_8(\text{PPh}_3)_8(\text{NO}_3)_2$ cluster and the (b) $\text{Au}_9(\text{PPh}_3)_8(\text{NO}_3)_3$ cluster. The fit window was limited to 3Å .

In Figure 15, the results from an EXAFS study of the pure unsupported gold clusters (Au_8 and Au_9) is displayed with a simulation of the expected results also overlaid. The data were collected by Dr. Greg Metha and co-workers at the ANBF Beamline in March 2012, while the same samples were concurrently being investigated at the soft X-Ray Beamline at the Australian

synchrotron. The clusters were modeled using the Xfit software program, based upon the DFT-optimised structures from the X-ray crystal structure. The number of fitting parameters was reduced to simplify the calculations, meaning only the gold and phosphorous atoms were modeled, based on the assumption that only the heavy atoms significantly scatter the electrons. $\text{Au}_8(\text{PPh}_3)_7(\text{NO}_3)_2$ and $\text{Au}_9(\text{PPh}_3)_8(\text{NO}_3)_3$ were analysed in detail, whilst for investigations on the Au_{11} cluster was not conducted due to issues in the separation of ($\text{Au}_{11}(\text{PPh}_3)_8\text{Cl}_3$ and $\text{Au}_{11}(\text{PPh}_3)_7\text{Cl}_3$) at the time of the experiment. Previous EXAFS studies on these gold clusters are similar to the results that were attained in this study.⁴⁵ Overall, the two clusters that were studied had peaks between 1.6–2.1 Å, which were attributed to the Au–P bonds and the other major peaks between 2.5–3.0 Å were attributed Au–Au bonds. The two clusters have similar spectra both differ slightly. The model of the DFT optimized cluster is in good agreement with data, which is shown in Figure 16.

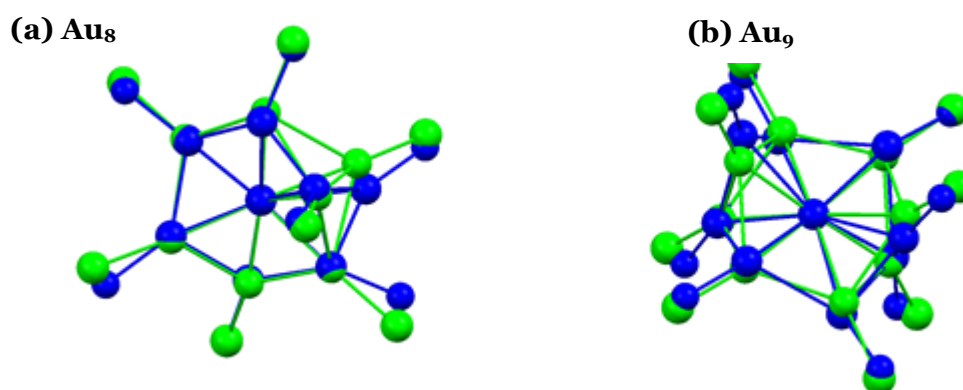


Figure 16; Overlay of the DFT optimized crystal structure (green) and the XFit structure (blue) for (a) $\text{Au}_8(\text{PPh}_3)_8(\text{NO}_3)_2$ and (b) $\text{Au}_9(\text{PPh}_3)_8(\text{NO}_3)_3$.

Summary

Overall, a selected range of ligand stabilised gold clusters have been prepared and characterised in detail, ensuring the atomic precision for each of the clusters. These studies have focused on the preparation of the phosphine stabilised gold clusters as opposed the more recent thiolate gold clusters. This reason for this focus was to allow characterization by single crystal X-ray crystallography. There are very few thiolate clusters that have been successfully analysed by crystallography. The combination of crystallography and the surface chemistry of phosphine stabilised gold clusters has been the primary focus of this project.

Bridge

In the following chapter, this series of gold clusters, prepared in this chapter, were characterised by far-infrared spectroscopy (Far-IR) to further understand their vibrational structure; in attempt to elucidate the origin of the catalytic activity of small gold clusters. There are very few far-IR studies on ligand-stabilised metal clusters due to limited availability of far-IR photon sources. The following chapter describes the initial steps towards the studying phosphine stabilised gold clusters at the far-IR spectroscopy Beamline at the Australian Synchrotron.

References

- (1) Mingos, D. M. P.; Wales, D. J.: *Introduction to cluster chemistry*; Prentice Hall New York, **1990**.
- (2) Vargaftik, M. N.; Zagorodnikov, V. P.; Stolyarov, I. P.; Moiseev, I. I.; Likholobov, V. A.; Kochubey, D. I.; Chuvilin, A. L.; Zaikovskiy, V. I.; Zamaraev, K. I.; Timofeeva, G. I.: A novel giant palladium cluster. *Journal of the Chemical Society, Chemical Communications* **1985**, 937-939.
- (3) Jadzinsky, P. D.; Calero, G.; Ackerson, C. J.; Bushnell, D. A.; Kornberg, R. D.: Structure of a Thiol Monolayer-Protected Gold Nanoparticle at 1.1 Å Resolution. *Science* **2008**, *318*, 430-433.
- (4) Schmid, G.; Pfeil, R.; Boese, R.; Bandermann, F.; Meyer, S.; Calis, G.; van der Velden, J. W.: Au₅₅ [PPH₃]₁₂Cl₆—ein Goldcluster ungewöhnlicher Größe. *Chemische Berichte* **1981**, *114*, 3634-3642.
- (5) Schmid, G.: *Nanoparticles: From Theory to Applications*; Wiley-VCH, **2010**.
- (6) Sardar, R.; Funston, A. M.; Mulvaney, P.; Murray, R. W.: Gold Nanoparticles: Past, Present, and Future[†]. *Langmuir* **2009**, *25*, 13840-13851.
- (7) Vollmer, M.; Kreibitz, U.: Optical properties of metal clusters. *Springer Ser. Mat. Sci* **1995**, *25*.
- (8) Malatesta, L.; Naldini, L.; Simonetta, G.; Cariati, F.: Triphenylphosphine-gold(0)/gold(I) compounds. *Coordination Chemistry Reviews* **1966**, *1*, 255-262.
- (9) McPartlin, M.; Mason, R.; Malatesta, L.: Novel cluster complexes of gold (0)–gold (I). *Journal of the Chemical Society D: Chemical Communications* **1969**, 334-334.
- (10) Cariati, F.; Naldini, L.: Trianionoeptakis (triarylphosphine) undecagold cluster compounds. *Inorganica Chimica Acta* **1971**, *5*, 172-174.
- (11) Cariati, F.; Naldini, L.: Preparation and properties of gold atom cluster compounds: octakis-(triarylphosphine)enneagold trianion. *Journal of the Chemical Society, Dalton Transactions* **1972**, 2286.
- (12) Vollenbroek, F. A.; Bour, J. J.; Trooster, J. M.; van der Velden, J. W.: Reactions of gold–phosphine cluster compounds. *J. Chem. Soc., Chem. Commun.* **1978**, 907-909.
- (13) Jones, P. G.: X-ray structural investigations of gold compounds. *Gold Bulletin* **1983**, *16*, 114-124.
- (14) Van Attekum, P.; Van der Velden, J.; Trooster, J.: X-ray photoelectron spectroscopy study of gold cluster and gold (I) phosphine compounds. *Inorganic Chemistry* **1980**, *19*, 701-1405.
- (15) Smits, J. M.; Bour, J. J.; Vollenbroek, F. A.; Beurskens, P. T.: Preparation and X-ray structure determination of [pentakis {1, 3-bis (diphenylphosphino) propane}] undecagoldtris (thiocyanate), Au₁₁(PPh₂C₃H₆PPh₂)₅(SCN)₃. *Journal of crystallographic and spectroscopic research* **1983**, *13*, 355-363.
- (16) Bellon, P.; Manassero, M.; Sansoni, M.: Crystal and molecular structure of triiodoheptakis (tri-p-fluorophenylphosphine) undecagold. *J. Chem. Soc., Dalton Trans.* **1972**, 1481-1487.
- (17) Blechschmidt, B.; Shirokov, V.; Sprinzl, M.: Undecagold cluster modified tRNAPhe from Escherichia coli and its activity in the protein elongation cycle. *European Journal of Biochemistry* **1994**, *219*, 65-71.
- (18) Caragheorghopol, A.; Chechik, V.: Mechanistic aspects of ligand exchange in Au nanoparticles. *Physical Chemistry Chemical Physics* **2008**, *10*, 5029-5041.

- (19) Van der Velden, J. W. A.; Bour, J. J.; Bosman, W. P.; Noordik, J. H.: Reactions of cationic gold clusters with Lewis bases. Preparation and x-ray structure investigation of $[\text{Au}_8(\text{PPh}_3)_7](\text{NO}_3)_2 \cdot 2\text{CH}_2\text{Cl}_2$ and $\text{Au}_6(\text{PPh}_3)_4[\text{Co}(\text{CO})_4]_2$. *Inorganic Chemistry* **1983**, *22*, 1913-1918.
- (20) Fei Wen; Ulli Englert; Benjamin Gutrath; Ulrich Simon: Crystal Structure, Electrochemical and Optical Properties of $\text{Au}_9(\text{PPh}_3)_8(\text{NO}_3)_3$. *European Journal of Inorganic Chemistry* **2008**, *2008*, 106-111.
- (21) McKenzie, L. C.: Mechanistic insights on nanoparticle formation: Investigation of reaction pathways and development of controlled syntheses for triphenylphosphine-stabilized undecagold. University of Oregon, **2009**.
- (22) Malatesta, L.: Cluster compounds of gold. *Gold Bulletin* **1975**, *8*, 48-52.
- (23) Walter, M.; Akola, J.; Lopez-Acevedo, O.; Jadzinsky, P. D.; Calero, G.; Ackerson, C. J.; Whetten, R. L.; GrÅnbeck, H.; HÅkkinen, H.: A unified view of ligand-protected gold clusters as superatom complexes. *Proceedings of the National Academy of Sciences* **2008**, *105*, 9157-9162.
- (24) Khanna, S.; Jena, P.: Assembling crystals from clusters. *Physical review letters* **1992**, *69*, 1664-1667.
- (25) HÅkkinen, H.: Atomic and electronic structure of gold clusters: understanding flakes, cages and superatoms from simple concepts. *Chemical Society Reviews* **2008**, *37*, 1847-1859.
- (26) Pauling, L.: *The nature of the chemical bond and the structure of molecules and crystals*; Cornell University Press, **1967**.
- (27) Brust, M.; Fink, J.; Bethell, D.; Schiffrin, D. J.; Kiely, C.: Synthesis and reactions of functionalised gold nanoparticles. *Journal of the Chemical Society, Chemical Communications* **1995**, 1655-1656.
- (28) Turkevich, J.; C.Stevenson, P.; Hillier, J.: A Study of the Nucleation and Growth Processes in the Synthesis of Colloidal Gold. *Journal of Discussions of the Faraday Society* **1951**, *11*, 55.
- (29) Kimling, J.; Maier, M.; Okenve, B.; Kotaidis, V.; Ballot, H.; Plech, A.: Turkevich Method for Gold Nanoparticle Synthesis Revisited. *J. Phys. Chem. B* **2006**, *110*, 15700-15707.
- (30) Levi-Kalisman, Y.; Jadzinsky, P. D.; Kalisman, N.; Tsunoyama, H.; Tsukuda, T.; Bushnell, D. A.; Kornberg, R. D.: Synthesis and Characterization of $\text{Au}_{102}(\text{p-MBA})_{44}$ Nanoparticles. *Journal of the American Chemical Society* **2011**, *133*, 2976-2982.
- (31) Shichibu, Y.; Negishi, Y.; Watanabe, T.; Chaki, N. K.; Kawaguchi, H.; Tsukuda, T.: Biicosahedral Gold Clusters $[\text{Au}_{25}(\text{PPh}_3)_{10}(\text{SCnH}_{2n+1})_5\text{Cl}_2]^{2+}$ ($n = 2$ −18); A Stepping Stone to Cluster-Assembled Materials. *The Journal of Physical Chemistry C* **2007**, *111*, 7845-7847.
- (32) Akola, J.; Walter, M.; Whetten, R. L.; Hakkinen, H.; Gronbeck, H.: On the Structure of Thiolate-Protected Au_{25} . *Journal of the American Chemical Society* **2008**, *130*, 3756-3757.
- (33) Jin, R.: Quantum sized, thiolate-protected gold nanoclusters. *Nanoscale* **2010**, *2*, 343-362.
- (34) Schmid, G.: Large clusters and colloids. Metals in the embryonic state. *Chemical Reviews* **1992**, *92*, 1709-1727.
- (35) Rapoport, D. H.; Vogel, W.; Cölfen, H.; Schlögl, R.: Ligand-Stabilized Metal Clusters: Reinvestigation of the Structure of “ $\text{Au}_{55}[\text{P}(\text{C}_6\text{H}_5)_3]_{12}\text{Cl}_6$ ”. *The Journal of Physical Chemistry B* **1997**, *101*, 4175-4183.
- (36) Weare, W. W.; Reed, S. M.; Warner, M. G.; Hutchison, J. E.: Improved synthesis of small (d core 1.5 nm) phosphine-stabilized gold nanoparticles. *Journal of the American Chemical Society* **2000**, *122*, 12890-25781.

- (37) Li, C.; Zhong, Z.; Leong, W. K.: Organometallic Clusters As Precursors for Metallic Nanoparticles: Effect of Cluster Size, Ligand Set, and Decomposition Method. *Langmuir* **2008**, *24*, 10427-10431.
- (38) Hyeon, T.: Chemical synthesis of magnetic nanoparticles. *Chemical Communications* **2003**, 927-934.
- (39) *Handbook of Preparative Inorganic Chemistry* Brauer, G., Ed.; Academic Press: NY., **1963**; Vol. 1.
- (40) Mueting, A. M.; Alexander, B. D.; Boyle, P. D.; Ito, L. N.; Johnson, B. J.; Pignolet, L. H.: *Inorganic Syntheses*; John Wiley and Sons, Inc, **1992**; Vol. 29.
- (41) Hutchison, J. E.: *Inorganic Syntheses*. Macmillan Publishers Limited, 2004; pp 228-232.
- (42) Woehrle, G. H.; Warner, M. G.; Hutchison, J. E.: Ligand Exchange Reactions Yield Subnanometer, Thiol-Stabilized Gold Particles with Defined Optical Transitions. *The Journal of Physical Chemistry B* **2002**, *106*, 9979-9981.
- (43) Wen, F.; Englert, U.; Gutrath, B.; Simon, U.: Crystal structure, electrochemical and optical properties of [Au₉ (PPh₃)₈](NO₃)₃. *European Journal of Inorganic Chemistry* **2008**, *2008*, 106-217.
- (44) McKenzie, L.; Haben, P.; Kevan..., S.: Determining Nanoparticle Size in Real Time by Small-Angle X-ray Scattering in a Microscale Flow System. *The Journal of ...* **2010**.
- (45) Yuan, Y.; Asakura, K.; Wan, H.; Tsai, K.; Iwasawa, Y.: Preparation of supported gold catalysts from gold complexes and their catalytic activities for CO oxidation. *Catal Lett* **1996**, *42*, 15-20.

3

Far-infrared studies of gold clusters

Objectives

This chapter will describe the far-infrared spectroscopy of atomically-precise gold phosphine clusters and a comparison will be made with calculated spectra that were conducted by Jason Alvino and Dr. Gregory Metha at the University of Adelaide. Despite our extensive search through the literature, we have been unable to identify far-infrared studies of these small chemically-prepared gold clusters stabilised by ligands. It is hoped that the understanding of the catalytic properties of small gold clusters may be further improved by undertaking these far-IR studies, which should illuminate the nature of the metal–core vibrations and metal–ligand vibrations.

Introduction

Vibrational spectroscopy has been used for the characterisation of materials and chemical compounds for many decades, such as infrared (IR) and Raman spectroscopy, which can easily study the vibrational frequency range of 350–3500 cm^{-1} . In the region of the mid-IR, we can garner a range of information on the vibrational structure and the key functional groups present in a wide range of inorganic and organic compounds that are produced by chemical synthesis. However, this region of electromagnetic spectrum is known to be insensitive to the structure and bonding of the metal–metal bonds in the core of metal clusters and nanoparticles, and also insensitive to the nature of the metal–ligand interactions. In the context of the study of metal clusters, the important vibrational modes of metal–metal and metal–ligands interactions actually appear in the far-IR (10–400 cm^{-1}). Up until recently, access to the far-IR region has been limited due a lack of adequate photon sources that can achieve the required wavelength, particularly below 100 cm^{-1} .¹ Recent

advances in terahertz spectroscopy have facilitated a renaissance in far-IR spectroscopy, particularly in the field of nanoparticles.

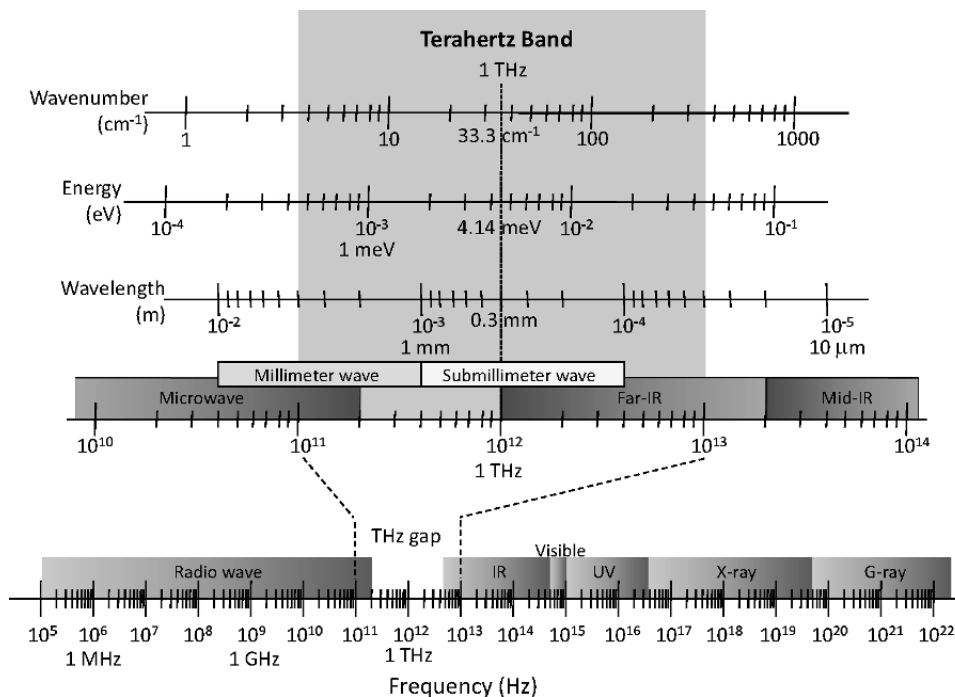


Figure 17: Terahertz band in the electromagnetic spectrum

Structural determination of isolated metal clusters often involves the use of vibrational spectroscopy, especially when other techniques may not be suitable for structure determination such as NMR, XPS, EELS or XANES.² Over the last two decades, isolated gas-phase metal clusters have been generated in molecular beams or special ion traps and subsequently characterised by far-IR spectroscopy; however, the synthetic control of particle size and shape of these metal clusters was limited.³ In recent years, there have been significant improvements in mass selected gas-phase clusters, which are monodisperse. These clusters are typically embedded in a rare gas matrix and various Raman/far-IR spectra can be obtained in situ and compared with simulated spectra.³ In the last decade, Fielicke and his co-workers have conducted a range of pioneering studies into the far-IR properties of isolated metal clusters in the gas-phase.²⁻⁵ A wide range of different metal clusters have been generated and studied such as silicon,⁶ vanadium,⁷ rhodium,⁵ niobium⁸ and gold.⁴ The far-IR spectrum of the metal cluster is dependent on the number of metal atoms in the metal core, the charge of the cluster and also the 3-dimensional shape of the cluster in the gas phase.

Prior to Fielicke's work on the vibrational spectroscopy of gas-phase gold clusters, there have been very few studies on the vibrational structure of small gold clusters. Many studies on gas-phase

gold clusters have focused on elucidating their electronic structure using EELS, XPS, and XANES.^{9,10} Fielicke *et al.* studied the far-IR spectra of size-specific gold clusters prepared in the gas-phase by laser ablation, using the FELIX tunable IR-free electron laser to elucidate the low-frequency gold-gold vibrations. The metal clusters were detected by time-of-flight mass spectrometry, and in conjunction with DFT calculations, the IR-active cluster vibrational modes were identified. A wide range of gas-phase gold clusters were experimentally identified and modelled such as the neutral tetrahedral Au₂₀ cluster, the neutral Au₁₉ and Au₇ clusters.⁴ The gold-gold core vibrations were observed between 60 and 180 cm⁻¹. This study highlighted that vibrational spectra of small neutral gold clusters is dependent on size and shape of the clusters. In parallel, several mixed gold cluster systems were also explored such as yttrium-doped gold clusters in the gas-phase, which displayed different behaviour to the pure gold clusters. For the Au_nY clusters, it was noted that the clusters demonstrated a 3-D shape rather than a 2-D shape that was observed for the pure gold systems.¹¹ The authors concluded that the presence of a dopant metal in the gold cluster possibly enhanced the thermodynamic stability of the gold clusters, stabilising previously unstable 3-D shapes of pure gold clusters.¹¹ How the presence of dopants affects gold nanoparticle based catalysts has still not been fully studied in depth. Although, the presence of bismuth has been previously shown to improve the reactivity and the lifetime of supported gold nanoparticles on carbon.¹² Gold-palladium mixed metal nanoparticles have also shown promise as commercially viable oxidation catalysts.¹³

Although ligand-stabilised gold clusters and nanoparticles have been prepared for many years, there have been very few far-IR studies conducted on these materials. The absence of detailed far-IR studies on these and other analogous materials could largely be due to the limited availability of high-quality spectrometers that can readily access the necessary range of frequencies required. In the literature, far-IR spectroscopy has often been employed to confirm the presence or absence of the desired ligands or capping agents. Brust *et al.* prepared a wide range of thiol stabilised gold nanoparticles (> 2 nm) with a narrow particle size distribution.¹⁴ FTIR spectroscopy was used to investigate the effect of different capping agents that were used.¹⁴ The absence of the S-H vibrational mode was used as spectroscopic evidence for attachment of the thiol capping groups, such *p*-mercaptophenol via the thiol functionality. More recently, Creutz *et al.* investigated the nature of the gold-thiolate bond and the adsorption of thiol-containing capping groups on both two dimensional self-assembled monolayers and three dimensional monolayer-protected nanoparticles.¹⁵ By using far infrared spectroscopy rather than mid-infrared region, Creutz *et al.* attempted to elucidate the

chemistry of the nanoparticle and thiolate ligand interaction. Various gold nanoparticle assemblies were prepared by the reduction HAuCl_4 with sodium borohydride under biphasic conditions as described by Brust,¹⁴ using a variety of different capping agents with different alkane chain lengths, which were deposited on to polyethylene films for spectroscopic studies.

Vibrational modes were observed in the range of 170 cm^{-1} – 270 cm^{-1} were attributed to the Au-S stretch; this observation was consistent with the proposed Au(I)-bridged thiolate structure that has been proposed for the much smaller thiolate clusters.^{16,17} The gold–gold vibrations were not detected for many of the samples in this study except for the C_{12} and C_{18} alkane thiol stabilised nanoparticles. The gold–gold vibration modes were observed at 88 cm^{-1} and 89 cm^{-1} respectively, which was consistent with the author’s predictions for the 2 nm gold thiol nanoparticles. The discussion of this gold peak was limited as the peak did not occur in all the nanoparticle samples studied. There have also been a few reports on chemically synthesised, atomically precise gold phosphine clusters which demonstrated a strong metal-ligand vibration appearing at 450 cm^{-1} . However, more detailed study of the weaker, low frequency vibrations has been largely focused on the highly symmetrical metal carbonyl clusters ($\text{Ru}_3(\text{CO})_{12}$).

More recently, gold-thiolate clusters have been shown to be active for several catalytic reactions, which have precisely known gold core nuclearity from ESI-MS data. To date, there have been no known far-IR studies on chemically-prepared gold-thiolate clusters. Although in recent months a density functional theory study of the vibrational modes of small thiolate-gold clusters (Au_n , $n = 4, 12, 18, 19, 20, 24$) has been published.¹⁸ The calculated IR spectra for each cluster were shown to be characteristic for each cluster, akin to fingerprint. The dominant peak that was observed in the far-IR arose due to the gold-sulfur vibrational mode typically around 250 cm^{-1} . The gold-gold core vibrations were found between 60 cm^{-1} up to 200 cm^{-1} , but were relatively small as compared to dominant gold–sulfur vibrational modes. The position of the gold core vibrations was dependent on the size and charge of the cluster.

The work described in this chapter was initially focused on obtaining reliable and reproducible far-IR spectra of several gold-phosphine clusters as prepared in chapter 2 and then identifying the low frequency vibrational modes by comparison with DFT calculations, which were conducted by Jason Alvino and Dr. Gregory Metha at the University of Adelaide. The spectra of each cluster were obtained over multiple visits to the Far-IR beamline at the Australian Synchrotron,

under the guidance Dr. Dominique Appadoo between Novemebr 2010 and June 2012. The optimised methodology for acquiring spectra of phosphine-stabilised gold clusters (Au_8 , Au_9) will be described and the resulting spectra were comapred with DFT vibrational frequency calculations of the whole cluster with phosphine ligands, which allowed key features of the far-IR spectra to be assiged specific vibrational modes. It is hoped that this work can be the foundation for a range of further studies in to mixed gold clusters, also lead in to a comparative study with thiol/thiolate stabilised gold clusters and also for studies in gas-phase catalysis of gold clusters.

Experimental

Spectra were collected at the high resolution Far-Infrared Beamline at the Australian Synchrotron, where measurements were conducted on a Brüker IFS 125/HR Fourier Transform (FT) spectrometer between the wavelengths of 5 cm^{-1} to 650 cm^{-1} , at 1 cm^{-1} resolution utilising the synchrotron light source (200 mA in top-up mode), a 6 micron thick multilayer Mylar beamsplitter, in combination with a Si bolometer detector; the bolometer was equipped with a 800 cm^{-1} far-IR cut-on cold-filter consisting of a 13 micron PE film overlaid with 6 micron diamond scatter layer. Samples were recorded at room temperature and also at 77 K. Samples were prepared by pressing 50 mg of pure powdered cluster material into a pellet.



Figure 18; The Far-IR beamline at the Australian Synchrotron, and the Brüker IFS 125/HR FT spectrometer

Samples of the relevant pure gold clusters and precursors were prepared according to the descriptions in Chapter 2. Previous studies have used small metal nanoparticles prepared by gas-evaporation methods or laser ablation, were typically deposited in to a Teflon, polyethylene or alkali halides matrix.^{19,20} Kin and Schmid have reported on the far-IR of the ligand stabilised cluster $\text{Au}_{55}(\text{PPh}_3)_{12}\text{Cl}_6$, which was prepared for Far-IR measurements by dispersion of the gold cluster in a cesium iodide (CsI) medium. The $\text{Au}_{55}/\text{CsI}$ mixture was ground repeatedly, ensuring uniform particle distribution and then compressed to form a 10mm pellet.

Initially, the samples were prepared by adding 5 mgs of the pure dried cluster to 50 mgs of powdered INDUCOS polyethylene powder, which was maintained in dry cabinet. However, it was found that pellet of the pure clusters alone were required to attain high quality spectra. The sample of pure clusters were ground into a fine homogeneous powder and then pressed into a 10 mm disk. A nitrogen cooled cryostat was used to mount the sample, which was able to load three samples concurrently. The pressed disc of the pure clusters were placed over the sampling hole and fixed in to position gently, ensuring the sample disk is not broken and to prevent cross-contamination between the different samples. The cryostat sample holder was allowed to warm up to room temperature under dry instrument grade air before samples were removed to prevent condensation of water on to the samples.



Figure 19; Samples were prepared with a pellet press and subsequently loaded on to the LN_2 cryostat sample holder

The mono gold compound, $\text{Au}(\text{PPh}_3)\text{Cl}$, was initially used to confirm the accuracy of the spectrometer and to validate the sample preparation methodology. The early experiments involved preparing the samples in a polyethylene support; however, several issues came to light with regards to small peaks and variable backgrounds. The variation of the polyethylene background was attributed to slight variation in thickness of the press pellet sample and also absorption of ambient moisture. Hence, comparison of the spectra of phosphine stabilised gold clusters proved difficult. Pressed pellets of the pure gold compounds (50 mg) were prepared, with no polyethylene background, which was found to solve these issues. Although the samples were delicate, spectra could easily be measured. The spectra of monogold sample were also measured at 77 K rather than a room temperature, and very little observable differences were noted between the two temperatures. The spectra of $\text{Au}(\text{PPh}_3)\text{Cl}$ in Figure 20 was also found to be in agreement with earlier reported data.²¹

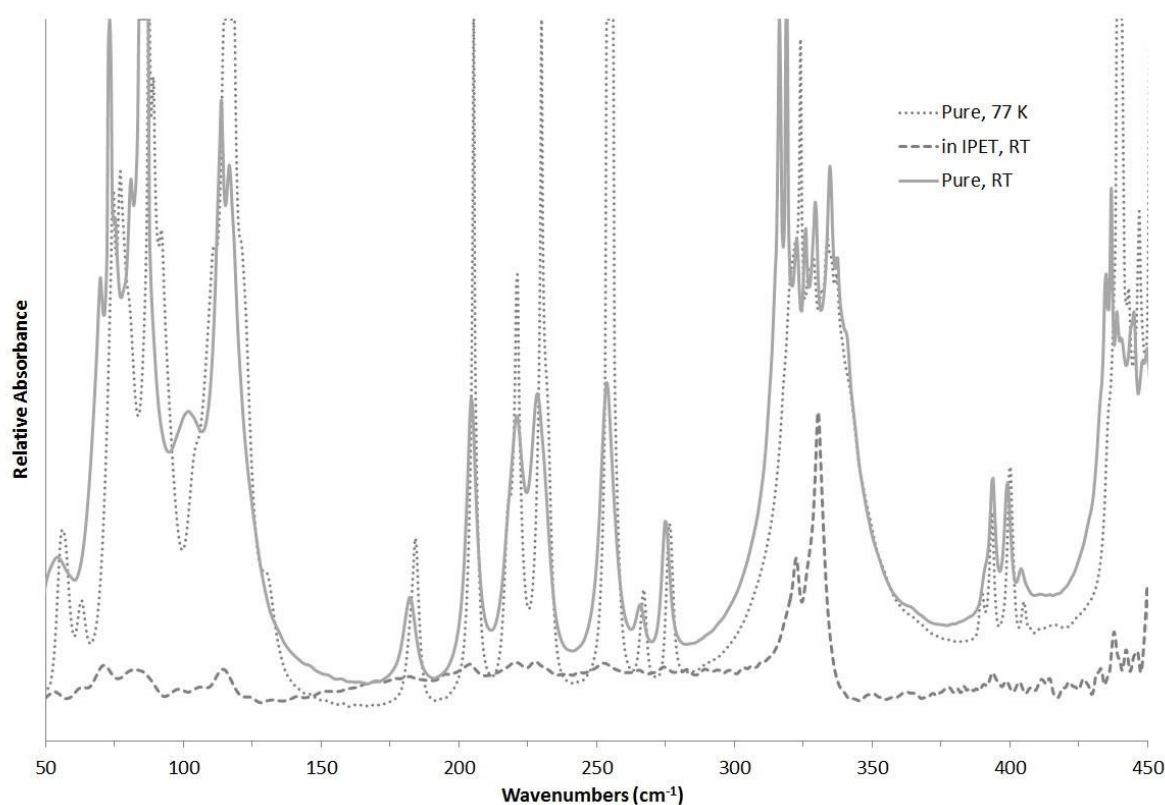


Figure 20: Absorption spectra of $\text{Au}(\text{PPh}_3)\text{Cl}$ at room temperature, and 77K , as well as a 5 % loaded sample in Inducos polyethylene at room temperature.

The simulation of the spectra for the $\text{Au}_9(\text{PPh}_3)_8(\text{NO}_3)_2$ and the $\text{Au}_8(\text{PPh}_3)_8(\text{NO}_3)_2$ clusters was conducted by Jason Alvino and Dr. Gregory Metha at the University of Adelaide, Australia. The geometry optimisation and harmonic vibrational frequency calculations of the gold cluster compounds, included all phosphine ligands, were undertaken using the MO6 density functional in the Gaussian 09 suite of programs.^{22,23} The starting geometries of the gold clusters were taken from crystal structures obtained from X-ray diffraction patterns of the synthesised clusters. All counter ions were removed, with the appropriate number of electrons removed from the calculations to balance the charge. All atoms were treated using the LanL2DZ basis set and related Effective Core Potentials (ECP).²⁴ All optimisations were performed with no symmetry constraints, *i.e.* in the C_1 point group. For the Au_9 cluster, the optimised geometry was followed by a harmonic frequency calculation to confirm that the geometry was a true minimum with no imaginary frequencies. For the Au_8 cluster, the geometry was optimised to a stationary point with three low-frequency imaginary frequencies (42.6, 30.8, and 26.1 cm^{-1}). Inspection of the imaginary modes reveal that they correspond to slight rotations of phenyl groups and despite numerous attempts at re-optimisation using finer grid sizes and alternative minimization algorithms we were unable to eliminate them. In light of the small magnitude and local nature of these vibrations, it was concluded that they do not adversely impact on our assessment of the core cluster vibrations, which are of primary interest here. To obtain the predicted IR spectra, each stick spectrum is convoluted with a Gaussian line shape function with 8 cm full width at half maximum using the GaussView 5 program.

Results and discussion

The experimental far-IR spectra for Au₁₁, Au₉, and Au₈ is shown in Figure 21; where they all demonstrate a strong absorbance above 430 cm⁻¹ and another broad absorption with little or no features below 140 cm⁻¹. In the case of the Au₈ and Au₉ clusters, the spectra display distinct, sharp peaks around 180 cm⁻¹ and 260 cm⁻¹. The large absorbance at 430 cm⁻¹ was attributed to the P–Ph₃ stretching frequencies, which was also observed in the spectrum of the pure triphenyl phosphine ligand that was also conducted in parallel as a control sample. Above 440 cm⁻¹, it was observed that 100 % absorption was reached in many samples. As the spectra were taken on pressed pure cluster sample pellets, there was no easy solution to this issue without adding issues with background subtraction and moisture contamination. By using the pure cluster, we maximised the intensity of the gold core and gold-phosphine stretches, which were of primary interest in this study.

In the case of the Au₁₁, the spectrum does not have the distinct sharp peaks as the other two clusters. The broad absorbance at 185 cm⁻¹ can be attributed to the gold cluster core. We attributed the broadening of the gold core peak to possible presence of multiple Au₁₁ by-products from the preparation. Although NMR had confirmed the high purity of the Au₁₁(PPh₃)₈(Cl₃) cluster; however, recent reports have highlighted that other ennagold cluster products are also generated that are difficult to distinguish from our target cluster, such as Au₁₁(PPh₃)₇(Cl₂), possibly leading to the observed broadening of the gold core peak(s). During the synthesis of the ennagold cluster, it has been shown to be difficult to separate the two different products.²⁵ Other larger metal nanoparticle products are also generated during the preparation of this compound, which would result in a large broad absorbance.

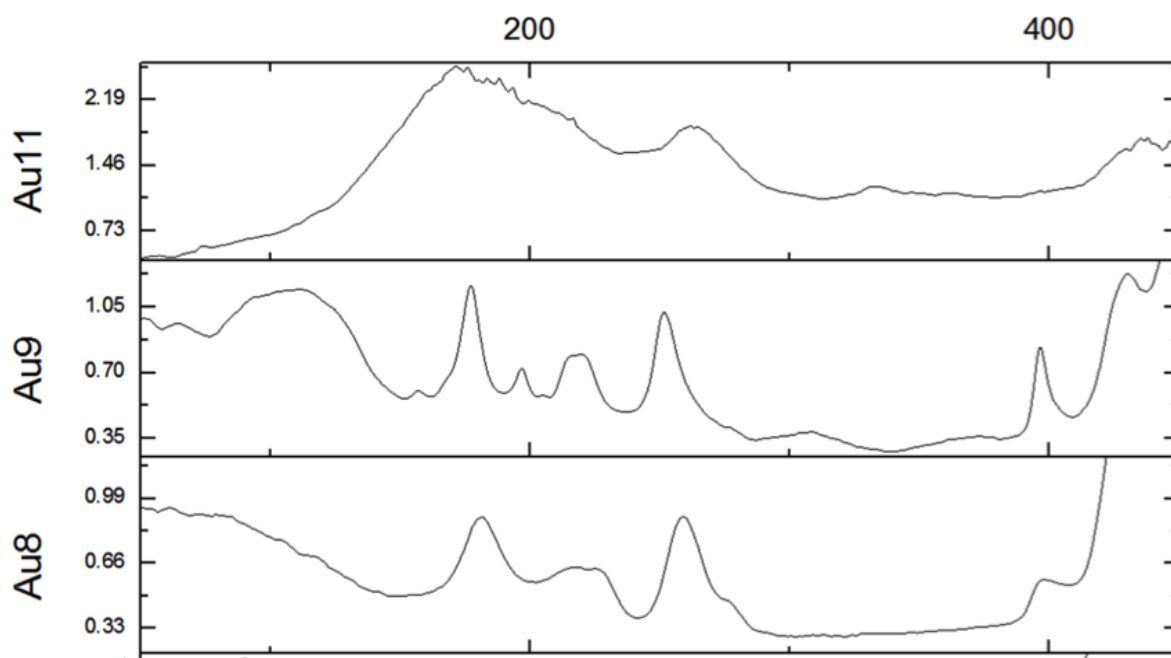


Figure 21: Comparison of the far-IR spectra for Au₁₁, Au₉, and Au₈ collected at the Infrared Beamline at the Australian Synchrotron.

Comparison of experimental and simulated spectra

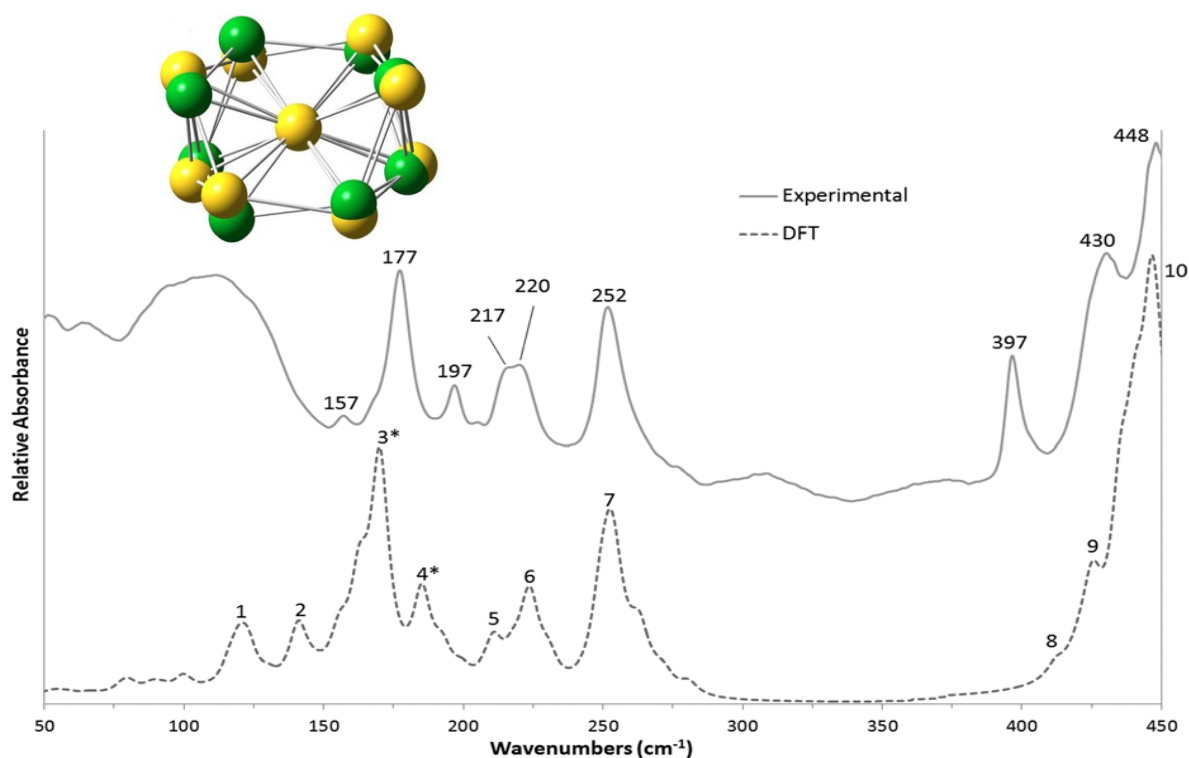


Figure 22: A comparison of the simulated (dotted line) and the experimental (solid line) far-IR spectrum of the Au₉(PPh₃)₈(NO₃)₃; inset, X-ray crystal structures and DFT optimised structures of the Au₉(PPh₃)₈(NO₃)₃ with the ligands omitted for clarity.

Table 4: Summary table of all calculated contributing transitions for the Au₉(PPh₃)₈ cluster, and the assignment to their predicted spectral shifts.

| # | Peak (cm ⁻¹) | Contributing vibrations (cm ⁻¹) | IR intensity (km mol ⁻¹) | % Au motion | % P motion | Assigned (cm ⁻¹) | Mode Description |
|----|--------------------------|---|--------------------------------------|-------------|------------|------------------------------|-----------------------------|
| 1 | 121 | 116.0 | 2.1 | 1.9 | 1.7 | | |
| | | 119.3 | 2.7 | 6.0 | 2.4 | | |
| | | 120.0 | 2.0 | 5.6 | 2.3 | | |
| | | 122.9 | 4.6 | 3.6 | 1.7 | | |
| 2 | 141 | 140.9 | 7.2 | 8.3 | 5.8 | 157.2 | Au core distortion |
| 3 | 170 | 162.8 | 11.2 | 8.1 | 4.6 | 177.4 | Au core distortion |
| | | 170.1 | 28.0 | 17.7 | 3.3 | | |
| 4 | 185 | 185.2 | 11.2 | 17.7 | 1.7 | 196.7 | Au core distortion |
| 5 | 211 | 210.7 | 2.0 | 0 | 1.1 | 216.5 | Ph Rock |
| | | 211.0 | 3.2 | 0 | 0.8 | | |
| 6 | 224 | 217.6 | 2.7 | 0 | 1.2 | 219.8 | Ph Rock |
| | | 222.2 | 2.3 | 0 | 0.7 | | |
| | | 223.7 | 5.6 | 0 | 0.7 | | |
| | | 224.2 | 3.1 | 0 | 1.4 | | |
| 7 | 253 | 248.9 | 6.6 | 0 | 1.0 | 251.7 | PPh ₃ Distortion |
| | | 251.6 | 6.2 | 0 | 0.8 | | |
| | | 252.2 | 3.2 | 0 | 0.6 | | |
| | | 253.9 | 9.9 | 0 | 0.9 | | |
| 8 | 411 (shoulder) | 411.8 | 0.9 | 0 | 1.0 | 396.8 | Ph Twist |
| | | 412.2 | 0.7 | 0 | 1.0 | | |
| 9 | 426 | 424.5 | 1.5 | 0 | 3.2 | 430.0 | Ph Twist |
| | | 424.6 | 1.9 | 0 | 3.0 | | |
| | | 425.4 | 3.6 | 0 | 4.7 | | |
| | | 425.5 | 1.9 | 0 | 2.5 | | |
| 10 | 447 | 435.2-448.8 | Avg. 8.1 | Avg. 0 | Avg. 13.0 | 447.9 | PPh ₃ Distortion |

In Figure 22, a comparison of the experimental and calculated spectra for the Au₉ cluster is shown. The optimised structure for the gold cluster is superimposed on the corresponding crystal structure, with the organic phenyl ligands omitted to improve the clarity of the structure. The superimposed structures are shown to be very similar, highlighting the likeness of the crystal structure bond geometries to the isolated “gas-phase” structure that was modelled. In Table 4, a list of the calculated vibrational modes up to 450 cm⁻¹ is presented, which have passed two selection criteria; To distinguish between the normal vibrational modes of the gold cluster vibrations from other low frequency modes, the normal coordinate motions that involve motion of the gold and phosphorous atoms have been identified, which appear as a percentage of the total non-mass-weighted atomic motion (i.e. % Au and % P). In addition, the list of peaks include any normal mode that has significant infrared intensity of >1 km mol⁻¹. These modes are listed individually or as a group of peaks and numbered accordingly. The peaks are numbered from sequentially at low energy and are the relevant peaks are labelled in Figure 22.

As previously discussed, the intense peak (# 10) at 440 cm⁻¹ corresponds to the P-Ph₃ vibrations. The high number of ligands bound to the core which each have three similar P-Ph bonds, accounts for the high intensity of the peak. In addition, a small shoulder at 430 cm⁻¹ (#9) is also observed which is attributed to a group of four similar transitions resulting from Ph-twisting distortions. At 396.8 cm⁻¹, a strong absorbance is observed; however, the calculations predicted a much weaker feature at a similar energy. The higher intensity of this peak is attributed to a combination of two normal modes in the Au₉ cluster, involving phenyl groups twisting vibrations. In the calculated spectrum of the Au₉ cluster, peaks found at 253 cm⁻¹ (#7), 224 cm⁻¹ (#6), 211 cm⁻¹ (#5) are all caused by PPh₃ distortions such as PPh₃ rocking. The experimental spectrum matches this series of peaks well with the observed absorbances at 251 cm⁻¹, 219.8 cm⁻¹, 216.5 cm⁻¹. The experimentally observed peaks at 196.7 cm⁻¹ and 177.4 cm⁻¹ are matched by the predicted peaks at 185 cm⁻¹ (#4) and 170 cm⁻¹ (#3). These absorbances are due to the gold core vibrations, which is confirmed by the % gold motion. The smaller absorbance at 157.2 cm⁻¹ is also due to vibrations of the central atom of the gold core, which is also predicted by the model (#2). The calculated transitions at 121 cm⁻¹ (#1) are not experimentally observed, which are predicted occur due to large amplitude motions spanning multiple ligands, but have very low intensities. Due to the nature of the samples, pressed pellets of crystalline Au₉ cluster, these modes are difficult to observe due to their low intensity.

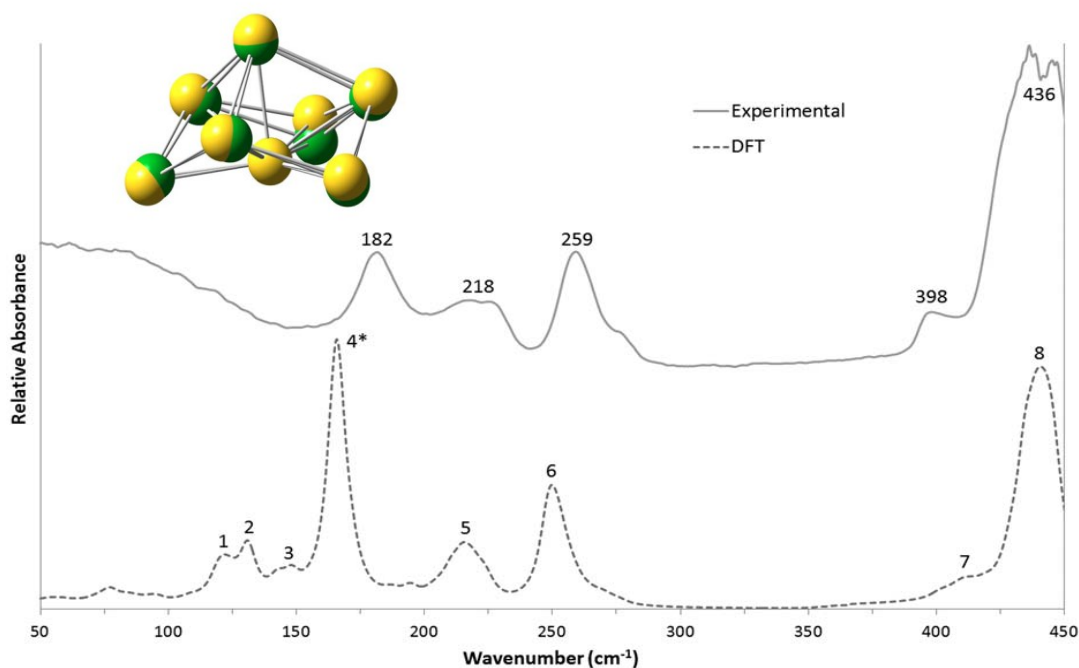


Figure 23: A comparison of the simulated (dotted line) and the experimental (solid line) far-IR spectrum of the $\text{Au}_8(\text{PPh}_3)_8(\text{NO}_3)_2$; inset, X-ray crystal structures and DFT optimised structures of the $\text{Au}_8(\text{PPh}_3)_8(\text{NO}_3)_2$ with the ligands omitted for clarity.

In Figure 23, the simulated and experimental spectra for the $\text{Au}_8(\text{PPh}_3)_8(\text{NO}_3)_2$ cluster is presented and

Table 5 summarises the calculated vibrational modes. As with the Au_9 cluster, the large absorbance found 436.7 cm^{-1} , which is also found in the simulated spectrum (#8), is attributed to ligand P-Ph vibrations. Distinct peak at 398.2 cm^{-1} due to phenyl group twisting. Although the intensity is found to be larger for the observed experimental spectrum which is similar to Au_9 . The observed Au_8 spectrum has strong absorbances at 258.9 cm^{-1} and at 181.9 cm^{-1} , as well as a weaker and broader transition at 217.8 cm^{-1} . The simulated peaks found at 250 cm^{-1} (#5), 166 cm^{-1} (#3) and 216 cm^{-1} (#4) are found fit well with both relative intensity and energy. The origin of these peaks is due to the rocking of the phenyl groups. At lower energy, the intense gold core vibrations are found. The calculated peak is found at 166 cm^{-1} , which was assigned to the experimental observed peak at 182 cm^{-1} . From the normal calculated mode analysis conducted by Jason Alvino and co-workers, the predicted transitions of the Au_8 cluster, found at 165 cm^{-1} and 166 cm^{-1} , involve the largest combined motion of the metal core atoms (approximately 20 % gold motion). When comparing this set of data with the gas-phase work conducted on $\text{Au}_7\text{--Kr}$ clusters reported by Fielicke *et al.*, similar frequencies for the bare Au_7 cluster are observed.⁴ The authors observed three peaks at 165 cm^{-1} , 186

cm^{-1} , and 201 cm^{-1} which were attributed to the cluster core having C_s -planar structure made of five equilateral triangle and the three vibrational peaks were associated to the various delocalised motions of all the gold atoms in the cluster. The similarity in the observed absorbance peaks could indicate that the two types of cluster systems have similar bond strengths despite having different geometric structures.

Table 5: Summary table of all calculated contributing transitions for the $\text{Au}_8(\text{PPH}_3)_8$ cluster, and the assignment to the predicted spectral shifts.

| # | Peak (cm^{-1}) | Contributing vibrations (cm^{-1}) | IR intensity (km mol^{-1}) | % Au motion | % P motion | Assigned (cm^{-1}) | Mode Description |
|---|------------------------------|--|--|----------------|---------------|----------------------------------|---------------------------|
| 1 | 122 | 119.1 | 3.4 | 5.2 | 4.6 | | |
| | | 121.1 | 1.7 | 3.8 | 3.9 | | |
| | | 122.2 | 2.0 | 3.2 | 3.5 | | |
| | | 124.4 | 1.9 | 4.8 | 4.3 | | |
| 2 | 131 | 131.1 | 9.3 | 7.5 | 5.6 | | |
| 3 | 148 | 142.6 | 2.9 | 10.7 | 5.2 | | |
| | | 147.4 | 1.7 | 12.7 | 5.0 | | |
| | | 148.7 | 1.9 | 12.6 | 4.8 | | |
| 4 | 166 | 165.1 | 23.9 | 20.3 | 2.7 | 181.8 | Au core distortion |
| | | 166.4 | 23.9 | 20.2 | 2.9 | | |
| | | 171.6 | 3.2 | 16.7 | 1.6 | | |
| 5 | 216 | 210.3 | 1.5 | 0 | 0.8 | 217.9 | Ph Rock |
| | | 210.9 | 1.7 | 0 | 1.4 | | |
| | | 214.5 | 2.8 | 0 | 1.2 | | |
| | | 215.8 | 1.2 | 0 | 1.3 | | |
| | | 217.0 | 1.6 | 0 | 1.5 | | |
| | | 219.1 | 1.8 | 0 | 1.3 | | |
| 6 | 250 | 247.4 | 4.1 | 0 | 1.1 | 258.9 | Ph Rock |
| | | 248.3 | 3.8 | 0 | 0.9 | | |
| | | 249.4 | 4.1 | 0 | 1.2 | | |
| | | 249.9 | 3.3 | 0 | 1.3 | | |
| | | 250.2 | 1.7 | 0 | 1.4 | | |
| | | 251.7 | 3.1 | 0 | 1.0 | | |
| | | 253.1 | 3.9 | 0 | 1.3 | | |
| 7 | 411 (shoulder) | 410.5 | 0.5 | 0 | 1.9 | 398.2 | Ph Twist |
| | | 411.5 | 0.4 | 0 | 0.7 | | |
| 8 | 441 | 428.9-445.8 | Avg. 3.9 | Avg. 0 | Avg.13% | 436.3 | PPh_3 Distortion |

Summary

In this brief chapter, the first detailed synchrotron study of the far-IR spectra of chemically synthesised phosphine stabilised gold clusters is presented. Metal core and metal–ligand transitions were identified and compared to DFT simulated spectra that were conducted at the University of Adelaide. The difference in spectra was attributed to the fact that the simulation of the clusters was conducted on an isolated, gas-phase cluster, whilst the spectra were collected from a pressed pellet of a crystalline cluster sample. There were no obvious size-dependent changes in the observed vibrational modes of the gold core and the gold phosphine ligands. The gold core vibrations presented as broad peaks between 80 cm^{-1} to 180 cm^{-1} for the Au_8 and Au_9 samples; whilst the gold-phosphine vibrations were observed at around 150 cm^{-1} to 440 cm^{-1} . The larger Au_{11} sample proved difficult to acquire a clear spectrum, possibly due to the presence of two Au_{11} products with slightly different structures or due to contamination with larger gold nanoparticles. Investigations on the larger Au_{101} nanoparticle samples were attempted but issues with preparing a pure pressed pellet of such nanoparticles prevented any further studies from being carried out. Overall, it was demonstrated that far-IR spectra of ligand stabilised gold clusters could be acquired and that each cluster had a unique spectrum.

These initial steps have provided a platform for further investigations into the effect of adding heteroatoms to the metal core and the subsequent changes to the structure of the system. As this thesis has been limited to using triphenyl phosphine as the ligand of all the clusters, the interplay of the ligand with the metal core should be studied in much more detail, particularly as recent reports have highlighted the importance of the ligand during catalysis. Other less sterically demanding phosphine and thiols ligands would provide a fruitful avenue for further research. As this study was focused with pressed pellets of sample, other sample preparation methods should also be investigated such liquid-phase and grazing incident methods, in attempt to study the possible catalytic intermediates found at the gold cluster surface.

References

- (1) Mantsch, H. H.; Naumann, D.: Terahertz spectroscopy: The renaissance of far infrared spectroscopy. *Journal of Molecular Structure* **2010**, *964*, 1-4.
- (2) Fielicke, A.; von Helden, G.; Meijer, G.: Far-Infrared spectroscopy of isolated transition metal clusters. *The European Physical Journal D - Atomic, Molecular, Optical and Plasma Physics* **2005**, *34*, 83-88.
- (3) Fielicke, A.; Kirilyuk, A.; Ratsch, C.; Behler, J.; Scheffler, M.; von Helden, G.; Meijer, G.: Structure Determination of Isolated Metal Clusters via Far-Infrared Spectroscopy. *Physical review letters* **2004**, *93*, 023401.
- (4) Gruene, P.; Rayner, D. M.; Redlich, B.; van der Meer, A. F. G.; Lyon, J. T.; Meijer, G.; Fielicke, A.: Structures of Neutral Au₇, Au₁₉, and Au₂₀ Clusters in the Gas Phase. *Science* **2008**, *321*, 674-676.
- (5) Harding, D. J.; Gruene, P.; Haertelt, M.; Meijer, G.; Fielicke, A.; Hamilton, S. M.; Hopkins, W. S.; Mackenzie, S. R.; Neville, S. P.; Walsh, T. R.: Probing the structures of gas-phase rhodium cluster cations by far-infrared spectroscopy. *The Journal of Chemical Physics* **2010**, *133*, 214304-9.
- (6) Fielicke, A.; Lyon, J. T.; Haertelt, M.; Meijer, G.; Claes, P.; De Haeck, J.; Lievens, P.: Vibrational spectroscopy of neutral silicon clusters via far-IR-VUV two color ionization. *The Journal of chemical physics* **2009**, *131*, 171105.
- (7) Ratsch, C.; Fielicke, A.; Kirilyuk, A.; Behler, J.; Von Helden, G.; Meijer, G.; Scheffler, M.: Structure determination of small vanadium clusters by density-functional theory in comparison with experimental far-infrared spectra. *The Journal of chemical physics* **2005**, *122*, 124302.
- (8) Fielicke, A.; Ratsch, C.; von Helden, G.; Meijer, G.: The far-infrared spectra of neutral and cationic niobium clusters: Nb to Nb. *The Journal of chemical physics* **2007**, *127*, 234306.
- (9) Wertheim, G.: Electronic structure of metal clusters. *Zeitschrift für Physik D Atoms, Molecules and Clusters* **1989**, *12*, 319-326.
- (10) Rao, C. N. R.; Vijayakrishnan, V.; Aiyer, H. N.; Kulkarni, G. U.; Subbanna, G. N.: An investigation of well-characterized small gold clusters by photoelectron spectroscopy, tunneling spectroscopy, and cognate techniques. *The Journal of Physical Chemistry* **1993**, *97*, 11157-11160.
- (11) Lin, L.; Claes, P.; Gruene, P.; Meijer, G.; Fielicke, A.; Nguyen, M. T.; Lievens, P.: Far - Infrared Spectra of Yttrium - Doped Gold Clusters Au_nY (n= 1–9). *ChemPhysChem* **2010**, *11*, 1932-1943.
- (12) Hughes, M. D.: Tunable gold catalysts for selective hydrocarbon oxidation under mild conditions. *Nature* **2005**, *437*, 1132-1135.
- (13) Meenakshisundaram, S.; Nowicka, E.; Miedziak, P. J.; Brett, G. L.; Jenkins, R. L.; Dimitratos, N.; Taylor, S. H.; Knight, D. W.; Bethell, D.; Hutchings, G. J.: Oxidation of alcohols using supported gold and gold–palladium nanoparticles. *Faraday Discussions* **2010**, *145*, 341-356.
- (14) Brust, M.; Walker, M.; Bethell, D.; Schiffrin, D. J.; Whyman, R.: Synthesis of thiol-derivatised gold nanoparticles in a two-phase Liquid-Liquid system. *Journal of the Chemical Society, Chemical Communications* **1994**, 801-802.

- (15) Petroski, J.; Chou, M.; Creutz, C.: The coordination chemistry of gold surfaces: Formation and far-infrared spectra of alkanethiolate-capped gold nanoparticles. *Journal of Organometallic Chemistry* **2009**, *694*, 1138-1143.
- (16) Jadzinsky, P. D.; Calero, G.; Ackerson, C. J.; Bushnell, D. A.; Kornberg, R. D.: Structure of a Thiol Monolayer-Protected Gold Nanoparticle at 1.1 Å Resolution. *Science* **2008**, *318*, 430-433.
- (17) Jin, R.: Quantum sized, thiolate-protected gold nanoclusters. *Nanoscale* **2010**, *2*, 343-362.
- (18) Tlahuice-Flores, A.; Whetten, R. L.; Jose-Yacamán, M.: Vibrational Normal Modes of Small Thiolate-Protected Gold Clusters. *The Journal of Physical Chemistry C* **2013**, *117*(23), 12191-12198
- (19) Plyukhin, A. V.; Sarychev, A. K.; Dykhne, A. M.: Far-infrared absorption in small metal particles. *Physical Review B* **1999**, *59*, 1685-1688.
- (20) Kim, Y. H.; Tanner, D. B.: Far-infrared absorption by aluminum small particles. *Physical Review B* **1989**, *39*, 3585-3589.
- (21) Jones, A.; Powell, D.: Low-frequency vibrational spectra of triphenylphosphine and triphenylarsine complexes of gold and Nickel. *Spectrochimica Acta Part A: Molecular Spectroscopy* **1974**, *30*, 563-570.
- (22) Zhao, Y.; Truhlar, D. G.: The M06 suite of density functionals for main group thermochemistry, thermochemical kinetics, noncovalent interactions, excited states, and transition elements: two new functionals and systematic testing of four M06-class functionals and 12 other functionals. *Theoretical Chemistry Accounts* **2008**, *120*, 215-241.
- (23) Frisch, M. J.; Trucks, G. W.; Schlegel, H. B.; G. E. Scuseria; Robb, M. A.; Cheeseman, J. R.; Scalmani, G.; V. Barone; Mennucci, B.; Petersson, G. A.; Nakatsuji, H.; M. Caricato; Li, X.; Hratchian, H. P.; Izmaylov, A. F.; J. Bloino, G. Z.; Sonnenberg, J. L.; Hada, M.; Ehara, M.; Toyota, K.; Fukuda, R.; Hasegawa, J.; Ishida, M.; Nakajima, T.; Honda, Y.; Kitao, O.; Nakai, H.; Vreven, T.; Montgomery, J. A.; Peralta, J. E.; Ogliaro, F.; Bearpark, M.; Heyd, J. J.; Brothers, E.; Kudin, K. N.; Staroverov, V. N.; R. Kobayashi; Normand, J.; Raghavachari, K.; Rendell, A.; . C. Burant; Iyengar, S. S.; Tomasi, J.; Cossi, M.; Rega, N.; N. J. Millam; Klene, M.; Knox, J. E.; Cross, J. B.; Bakken, V.; C. Adamo; Jaramillo, J.; Gomperts, R.; Stratmann, R. E.; O. Yazyev; Austin, A. J.; Cammi, R.; Pomelli, C.; J. W. Ochterski; Martin, R. L.; Morokuma, K.; Zakrzewski, V. G.; G. A. Voth; Salvador, P.; Dannenberg, J. J.; Dapprich, S.; A. D. Daniels; Farkas, O.; Foresman, J. B.; Ortiz, J. V.; Cioslowski, J.; Fox, D. J.: Gaussian, Inc., Wallingford CT. **2009**.
- (24) Hay, P. J.; Wadt, W. R.: Ab initio effective core potentials for molecular calculations. Potentials for K to Au including the outermost core orbitals. *The Journal of Chemical Physics* **1985**, *82*, 299.
- (25) McKenzie, L.; Haben, P.; Kevan, James E. Hutchison: Determining Nanoparticle Size in Real Time by Small-Angle X-ray Scattering in a Microscale Flow System. *The Journal of Physical Chemistry, C* **2010** *114*, 22055-22063.

4

Preparation of supported gold phosphine clusters

Objectives

In this chapter, the preparation of gold catalysts based upon gold phosphine clusters is described. There are several important factors that contribute toward the design of these active, nanostructured catalysts. The goal of the work described in this chapter is to design a range of model active catalysts that can help discern the effect of gold cluster and nanoparticle size on the reactivity and structure of the resultant catalytic material. Many studies have been reported of small gold nanoparticles on flat substrates, such as anatase (111) and silica (110), which are ideal as model catalytic studies on extended surfaces and for elucidating the origins of the catalytic behaviour. This chapter will describe the preparation of gold catalysts derived from powders of silica and titania rather than flat substrates. These model catalysts are more suited towards catalytic studies in the liquid phase.

Preparation of active heterogeneous catalysts

In the chemical industry, a typical heterogeneous catalytic reaction occurs at the surface of a solid interphase with either the liquid or gas phase. The catalytically active material rapidly forms and breaks a range of bonds with the various precursors and intermediates to form the eventual target product(s). The importance of catalysts to our present global economy cannot be understated: world demand for catalysts is approximately US\$15 billion per annum which is predicted to rise by 6 % annually due increased demand from South American and Asian economies. These materials are the backbone of the chemical products industry which is worth upwards of US\$10 trillion; many of

these products would not be possible or economically viable without the variety of catalytic materials currently available.¹

These catalytic materials are often very high surface area materials, which helps increase the total area of the active components of the catalyst. Metal nanoparticles dispersed on a metal oxide support are one of the most common types of heterogeneous catalysts for oxidation reactions.² Due to the complex nature of metal oxide surfaces and their interaction with metal nanoparticles, it is often very difficult to identify the active site(s) of the reaction. For gold based catalysts, the activity increases significantly as the gold particle size falls below three nanometres.³ It is believed that a combination of the unique electronic properties of gold particles below two nanometres and high surface area of such small gold particles contributes to the observed activity in various modal catalytic systems. For gold – titania systems, the formation of the active oxygen species is believed to occur at the interface of the gold particles and the titania support material.⁴ Experimental evidence for these intermediate species is hard to come by because of the transient nature of the intermediates. In contrast, gold – silica systems have not been studied as extensively as gold titania; however, recent studies have shown that very small gold clusters supported on silica or hydroxyapatite can activate molecular oxygen with no radical initiators.^{5,6} This difference in reactivity between the two support types has not been explained; mainly due to the difficulty in obtaining in situ experimental data on the active species present in solution.

It has been observed that unsupported, naked metal nanoparticles in solution will precipitate from the solvent under ambient conditions, such as the Au₁₀₁ nanoparticles prepared in Chapter 2. Supported metal nanoparticles are much more resilient to particle agglomeration due to their interaction with the support material.² Metal oxide materials are also known to be catalytically active for a wide range of oxidation reactions (*i.e.* titanium silicates, zeolites); therefore they can be viewed as co-catalysts in their own right.⁷ The addition of metal nanoparticles can significantly increase the reactivity of the catalyst and influence the selectivity of the final products.⁸

The formation of small metal nanoparticles is thermodynamically unfavourable due significantly higher surface energies that increase as the particle size decreases. There is a large thermodynamic driving force to decrease the surface energy of the system, through the sintering of these small particles to form larger more stable particles which have a much smaller surface areas. Many heterogeneous catalytic reactions are conducted at high temperatures (<100 °C), which

promotes the sintering of the small metal particles on the surface of the substrate, decreasing the activity of the catalyst. This sintering process can occur through several mechanisms, such as particle – particle agglomeration and also by a form of Ostwald ripening, where sparingly soluble atomic gold species are preferentially transferred to larger particles. Understanding the factors that influence particle sintering on various substrates is an important aspect to designing active catalysts, especially for gold based systems; which have a very narrow particle size window within which they are active.⁹ It is also important to note that not all heterogeneously catalysed chemical reactions are dependent on the particle size; recently various cross coupling reactions catalysed by supported gold particles have been shown to be more active with larger gold nanoparticles (≈ 20 nm).¹⁰

The main factors that control the susceptibility of the metal nanoparticles towards agglomeration are:

Nature of the support

There are a wide range of metal oxide materials that can be employed as a support such as alumina, silica, titania, ceria, magnesium oxide and titanium silicates. In recent years, nanostructured, porous materials have become increasingly popular, due to the possibilities of site isolation of individual metal nanoparticles in a single pore, preventing particle agglomeration. The support can interact electronically with the metal nanoparticles, with the strength of the interaction dependent upon various factors such as molecular orbital considerations, surface charges, presence of organic capping reagents and preparation conditions. Silica is considered to be a relatively electronically inert support material for gold nanoparticles as opposed to titania supports which interact significantly with the gold nanoparticles. This effect can be experimentally observed by photoelectron spectroscopy, by the chemical shifts of the elemental peaks. Various polymorphs of the metal oxides materials exist which can impact on the catalytic performance. At elevated temperatures ($> 500^\circ\text{C}$), a phase change between the various polymorphs can be induced in the support material. The two primary phases of titania, anatase and rutile, have been shown to have very different surface chemistries, which means that the metal nanoparticles sinter at different temperatures depending on the phase initially present during deposition at ambient conditions. The interaction between the metal nanoparticle (or metal salts) and the support is dominated by the interaction with species present at the surface of the support.

Surface functionalisation

There are many examples of functionalisation of supports with various thiols, silanes or other organic groups in an attempt to influence the agglomeration of metal nanoparticles on the surface. The functionalisation of the support is intended to form a favourable interaction with the metal nanoparticles and hence prevent particle sintering. The functionalisation of the support can affect the interaction of the support with the solvent and activation of other reagents during the reaction. There are several examples of silica functionalised with $\text{Au}[\text{N}-(\text{SiMe}_3)_2]_4$ moieties, upon treatment under hydrogen at 300°C led to the formation of small, well dispersed gold nanoparticles (2.0 nm) supported on SiMe_3 . The modified support resulted in a catalyst that was active for the selective oxidation of stilbene, which was more resistant to particle agglomeration when compared to the non-functionalised control silica support samples with deposited gold nanoparticles of comparable sizes.¹¹

There is also interest growing in the functionalisation of the catalyst, after deposition and activation of the catalyst has been conducted. The post-functionalisation of the catalyst, by treatment with acids/base, or various silanes or organic groups, has been shown to significantly influence the reactivity of the systems as well as product selectivity.^{12,13}

Activation conditions

The preparation of heterogeneous catalyst from metal oxides or zeolites often involves an activation step which often involves high temperature treatment, which can significantly influence the extent to which the metal particles sinter, and consequently, influence the activity of the resultant catalysts. The high temperature treatment is designed to anneal the active metal nanoparticles to the support. The activation atmosphere has also been shown to exert a major influence on the stability of metal nanoparticles on the surface.^{14,15} Reducing (H_2) and oxidising (air, O_2) atmospheres have all been employed; the choice of which depends on the target reaction. Often organic stabilising groups need to be removed; which require high temperature treatment under air or oxygen to decompose the organic groups.¹⁶

The primary methods, by which supported metal nanoparticle catalysts are fabricated, are termed impregnation, co-precipitation, adsorption and deposition. These preparative methods involve the reduction of the metal precursors, which have been deposited on the support material, followed by the formation of metal nanoparticles on the surface. These methods are relatively inexpensive and effective routes towards preparing active supported metal nanoparticle catalysts. A wide range of synthetic conditions can be used to control the metal particle size distribution, electronic and surface properties of the final product. A brief outline of the main synthetic procedures will now be presented and then a comparison between the use of preformed metal clusters and nanoparticles as precursors will be discussed. The discussion will be concluded with an overview of some common methods for the synthesising heterogeneous gold catalysts.

Impregnation

Impregnation is the synthetic method which consists of the porous support material being saturated in a solution of the metal salt precursor of the active phase (*i.e.* cobalt chloride, tetrachloroauric acid). This preparative method is dependent on the interaction of the surface of the support and the precursor species. Ion exchange with the acidic hydrogen ions of the surface hydroxyl groups or the relative concentration of the precursor on the surface to the concentration of the surface functional groups can influence the resultant catalytic material.

Two distinct impregnation methodologies exist;

- Dry impregnation: Also known as pore-volume impregnation, involves introducing a volume of the precursor solution that is equal to or less than the volume of the pores of the support material. This method is dependent on the retention of the precursor species within the pores prior to annealing. The main advantage of this method is that metal loading can be easily controlled, but the resultant catalyst may not be entirely uniform. Regions of the support material that have larger pores will absorb larger volumes of the precursor solution, which can lead to increased metal particle size.
- Wet impregnation: In contrast, when the volume of metal precursor solution is in excess of that required to fill the pores of the support, the technique is known as wet impregnation. The specific interactions of the precursor and the support play a much more important role for the formation of the active catalyst. The solute concentration is typically much less than

during the dry impregnation process which can cause significantly inhomogeneity of the resultant material.

Several factors are important during the impregnation process:

- Transportation of the soluble precursors to the surface of support material;
- If the support is porous, diffusion of the solutes in to the pores needs to occur;
- Interaction of the solute with the surface of the surface.

The drying process can also significantly affect the activity of the resultant catalytic material. Certain conditions can lead to the formation of metal nanoparticles with a wide particle size distribution or a porous material in which the catalytically active material has become concentrated at the mouth of the pores. During the drying process, the solvent is removed under elevated temperature or under reduced pressure, leading to a decrease in the volume of the solvent on the surface or in the pores. As the volume decreases, this makes the precursor oversaturated and precipitation occurs. Rapid evaporation is generally preferred as it favours rapid supersaturation, causing the rapid formation of well-dispersed nuclei of metal nanoparticles analogous to the formation of monodisperse solution phase metal nanoparticles. Other factors that influence resultant catalyst:

- Nature of the solvent (boiling point, dielectric charge, viscosity etc.)
- Nature of the precursor (solubility etc.)

Once the desired dried material has been attained, further activation steps may be required. These additional activation steps involve annealing the metal crystallites to the surface at high temperature, calcination under air or oxygen, removal of moisture or any decomposition products (nitrates) or reduction the metal salt to achieve the desired metal nanoparticles particle. These steps can induce sintering of the metal nanoparticles due to the high temperatures and presence of either hydrogen or oxygen gas.

Adsorption

Adsorption is defined as the selective removal of metal salts or metal ion species from their solution by a process of either physisorption or chemical bonding with sites on the support.¹⁷ Depending upon the strength of adsorption of the adsorbing species, the concentration of the active

material through the catalyst particle may be varied and controlled. This technique has been widely used in the preparation of industrial catalysts as it permits a greater degree of control over the dispersion and distribution of the active species on the support. In some systems, however, the weight of the active component that can be incorporated into the support is limited.

Co-precipitation

The preparation of supported catalysts by the co-precipitation of metal ions with the support ions usually produces an intimate mixing of catalysts and support.¹⁷ An example of this technique is the co-precipitation of metal ions with aluminium ions to produce a precipitated alumina gel containing the metal hydroxide.² This precipitate when calcined produces a refractory support with active component dispersed throughout the bulk as well as at the surface. However, in the preparation of multi-component catalysts, it is possible under improper conditions to obtain a heterogeneous product because of the different solubility products of the constituents. Variants of this methodology can involve deposition-precipitation routes, than often require accurate control of pH and other conditions to yield highly loaded active catalysts.

Deposition of preformed metal nanoparticles

For the study of model catalytic systems, it is often beneficial to pre-form the active metal nanoparticles or metal clusters; which are then deposited on to the chosen support. In recent years, metal clusters have grown in popularity due to their unique size dependent properties.¹⁸ Metal clusters have previously proven difficult to fully exploit as high performance catalysts, but in recent years, with the advent of site-isolated porous zeolites as supports for metal clusters, the research into catalysis by ligand stabilised clusters has grown. Deposition of preformed metal nanoparticles or clusters typically on to the desired support occurs in solution, where a solution of the preformed particles is added to a suspension of the support and stirred for a certain time.¹⁹⁻²¹ The active metal particles can have a strong bonding interaction with the support or the sample volume is decreased under reduced pressure to supersaturate the metal particles and deposit them onto the surface. Activation of these supported metal particle systems requires the removal of the stabilising organic group that surrounds the metal nanoparticle. Common capping agents for metal nanoparticles include polyvinylpyrrolidone and polymeric species or carbonyl ligands in the case of the smaller metal clusters.²² Catalyst derived from carbonyl stabilised transition metal clusters are easily

activated under mild temperatures (150- 250 °C) in a vacuum, whilst many organic ligands are calcined under oxygen at temperatures greater than 300 °C, to burn the carbon material.²³⁻²⁵ As the activation procedures involve high temperatures, metal particle sintering is again an issue; hence site isolating supports have become an important development in the heterogeneous catalysis due to their ability to physically prevent agglomeration of metal cluster or nanoparticles.²⁶ Heterogeneous catalysts derived from such small metal clusters, with carbonyl or other ligands could truly be classed as nanostructured catalysts; however there is a whole range of challenges ahead that need to be solved before such catalysts used in common use in industrial processes.^{27,28}

Preparation of active heterogeneous gold catalysts

The earliest examples of gold catalysis did not show remarkable conversions or selectivities using gold-silica catalysts prepared via the precipitation method. In recent years, the remarkable attention that gold-titania heterogeneous catalysts have received due to their excellent reactivities for the oxidation of carbon monoxide and direct selective epoxidation of propylene with hydrogen can be traced to the unique chemistry of the –OH moiety on the titania surface.^{4,29-31} Gold-based catalysts have also been shown to be effective for low temperature carbon monoxide oxidation, down to 75 K, the water gas shift reaction and also for various photocatalytic reactions.³²⁻³⁴ The gold catalyst preparation favoured by Haruta is a deposition-precipitation method performed at a fixed pH buffered with ammonia or sodium carbonate.^{35,36} Tetrachloroauric acid precursor is used, but due to the high chloride content, subsequent washes with a solution of ammonia are required. This method typically produces gold particles with relatively narrow size distribution, where the gold particle size is influenced by the pH of solution.^{37,38}

Since the first report by Haruta of gold-titania catalysts which were active for heterogeneous catalysis, a range of other synthetic methodologies have been developed with various degrees of success.³⁹ Many these methods offer a degree of control of the gold particle size, but there are other variables influencing their relative susceptibility to particle sintering and catalytic activity.

Impregnation method: Using tetrachloroauric acid as the gold precursor, a wide range of supports can be impregnated and calcined to form active gold catalysts. However, the high concentration of chloride ions present on the surface from the precursor causes a range of complications. The presence of the chloride ions on the surface of the support increases the

susceptibility of the gold nanoparticles towards sintering and decreases the lifetime of the catalysts. Under optimised conditions, relatively small gold nanoparticles (3-5 nm) can be produced.⁴⁰

The cation/anion adsorption method involves the adsorption of gold cations (from $[\text{Au}(\text{en})_2]^{3+}$) at a fixed pH (typically pH = 9) at 80 °C. With increasing adsorption time, the gold loading gradually increases along with the average gold particle size (2-5 nm). This relatively simple method of preparation does not control the gold particle size as the gold loading is increased.⁴¹

Deposition-precipitation with urea: Deposition–precipitation with urea is a method that was developed first to deposit high metal loadings of supported nickel and copper catalysts by Geus.⁴² This method involves the gradual decomposition of urea in solution, due to the reaction temperature being at 80 °C, which results in the production of hydroxide ions which gradually increase the pH of the solution. The progressive change of the pH facilitates the gradual precipitation of the gold precursor onto the support, rather than variable local increases in pH, which affects the heterogeneity of the resultant catalyst. The major benefit of this urea method is that significantly higher loadings of gold can be achieved (up to ~ 8%); other methods struggle to achieve more than 3 % by weight of gold. Small gold particles with very narrow size distributions can be achieved.⁴³

One of the main issues that have arisen with gold catalysts is that it can be difficult to reproduce results from different groups and that the systems are very sensitive to the synthetic conditions. It has been noted by Hutchings that two gold-iron oxide catalysts prepared under identical conditions except for which oven was used for calcining the catalysts lead to two catalysts with remarkably different activities. One sample prepared under a static air atmosphere was completely inactive whilst the sample prepared in a convection oven was active for carbon monoxide oxidation.⁴⁴ HRTEM studies on both samples indicated that the inactive sample actually had smaller gold nanoparticles (7.4 nm) present than the active sample (8.3 nm). The difference in reactivities was attributed to the presence of small gold clusters, consisting of less than twelve atoms of gold which could only be observed by HAADF-STEM which provided atomic resolution.⁴⁴

Experimental

For this research project, the focus will be on understanding the nature of small gold phosphine clusters and nanoparticles on two distinct supports, fumed silica and titania. Several unexplored novel methods for the activation of these nanostructured gold catalysts were also developed and their resulting electronic properties will be studied by photoelectron spectroscopy in detail.

Materials

All basic laboratory chemicals (solvents *etc.*, AR grade) have been purchased from established suppliers, such as Sigma-Aldrich, and used without further purification. Evonik TiO₂ P-25 aeroxide (CAS-No 13463-67-7) was purchased from Chemiplas NZ. P-25 aeroxide is a titania photocatalyst that is widely used due to its very high reactivity in a wide range of photocatalytic reactions, in recent years it has become the de-facto reference titania support material for a wide range of systems. P-25 consists of a mixture of anatase and rutile crystallites with particle sizes between 20–50 nm, with a typical ratio of 70:30 or 80:20, the exact ratio is known to vary slightly between different batches.⁴⁵ Recent reports have also shown that a small amount of amorphous titania can also be present. Individual samples of rutile and anatase support materials were also purchased for our final photoelectron spectroscopy studies, in an attempt to determine whether there is any detectable difference in the electronic structure of supported gold clusters on rutile or anatase. The individual anatase and rutile samples were prepared in similar method to the Evonik P-25, but have slightly higher specific surface areas.

Fumed silica was used also used as a support material and was purchased from Sigma Aldrich (99.99%). Fumed silica is typically prepared by flame pyrolysis of silicon tetrachloride in electric arc at 3000 °C, which results in the formation of amorphous silica particles with branched chain-like clusters of particles. Fumed silica is an ideal support material for applications in heterogeneous catalysis due to its high surface area relative to other commercial sources of silica. Particle sizes for fumed silica are reported to be approximately between 7–10 nm, however the particles form branched chain like structures that have dimensions between 50–100 nm. The

specific surface area of the fumed silica is reported as 395 m²/g, which is much greater than 50 m²/g for the Evonik P-25.

These two metal oxide support materials were chosen as the initial support materials for this research project as they have been previously shown to be active in a wide range of catalytic reactions. The difference in electronic properties of the support materials and their subsequent electronic interaction with nanoparticles of gold has been shown to be important for the reactivity of the subsequent catalysts.

Deposition of clusters onto the support

The synthesis of the Au_n clusters (n = 8, 9, 11, 101) has been described in the previous chapter. The target gold loading for this experiment was 0.5 % by weight of gold, which is significantly less than the reported values for the gold reference catalyst. This low loading was chosen to minimise the effect of cluster sintering on the surface of the support during the activation process and also during the reaction. It was also calculated that at these loadings that the coverage of the support by the cluster is just under one monolayer. Lower levels of gold loadings were also prepared for study, with 0.05 % by weight of gold; however, due to such small amounts of gold present it proved too difficult to study the catalytic activity and the photoelectron spectra at the Australian Synchrotron of these samples. At such low levels of gold, the gold 4f peaks proved to be very difficult to distinguish from the background even after extending the data collection time.

Previous preparations of gold based catalysts have involved much higher loadings of gold due to the differing surface areas of the support materials, variation of gold nanoparticle size and the need for high levels of gold during the synthetic process. Several more recent studies have also moved towards using much less gold on the support, mainly to minimise the effect of nanoparticle sintering.

The support materials (SiO₂ and TiO₂) were pre-treated prior to deposition by heating under vacuum at 200°C, stirred, in a Schlenk tube connected to a vacuum manifold line for two hours. Two grams of each support was then weighed and loaded into an acid cleaned Schlenk tube. Each batch of catalyst was limited to two grams, due to difficulties in stirring larger amounts of the supports in the Schlenk tubes. The samples were put under vacuum whilst the cluster solutions were prepared to ensure the supports were dry.

For each of the Au_n clusters (n = 8, 9, 11), the amounts required to achieve the 0.5 % loading of gold were accurately calculated according to the molecular formula of the crystal structure of each cluster. A solution of the cluster (20 mg) in methanol (30 mL) was prepared and allowed to stir for thirty minutes, ensuring that the cluster had fully dissolved. Such a dilute solution was used for deposition to guarantee that as few nanocrystals of the cluster as possible remained in the solution. Whilst the cluster was being stirred, a suspension of the support was prepared by adding methanol (50 mL) and stirring under nitrogen. The cluster solution was then rapidly added to the stirred support suspension. The stirred mixture was briefly purged by alternating between vacuum and nitrogen three times; finally the suspension was left stirring under nitrogen. The titania samples were wrapped with aluminium foil to minimise exposure to ambient light. For the silica samples, it was observed that after several hours of stirring, the solution was much less coloured and the previously white silica support material was a yellow/orange colour, indicating the cluster was now bound to the support material. In the case of the titania samples, the solution was still significantly coloured, indicating that the cluster was present in solution rather than on the support. The contrasting observations are possibly due to the slightly more acidic nature of the silica support material as compared to the titania. The suspensions were left to stir overnight.

For the silica samples, the suspension was allowed to settle for thirty minutes, and the clear methanol solvent was removed by syringe, leaving the wet, unactivated, supported cluster. The samples were then dried under vacuum for 4 hours, resulting in a fine yellow/orange powder, which were stored under nitrogen at - 20°C in the absence of light. Whilst the solvent was removed under vacuum, care was taken to avoid contamination of the Schlenk line with the resulting dry powder.

After stirring the titania samples overnight, the methanol solvent was still coloured from the dissolved cluster, which indicated that the cluster was not fully deposited on to the titania. In contrast to the silica samples, the titania suspensions were dried under vacuum via a Schlenk line without removing the methanol via syringe. In this way, any unsupported gold cluster was forced on to the titania as the solvent volume was decreased and cluster concentration in the methanol increased. The samples were kept under vacuum for four hours to ensure the samples were dried, resulting in light, pale, orange powders which were stored under nitrogen at - 20°C in the absence of light.

For the Au₁₀₁ cluster, the method for deposition of this cluster differed slightly such that dichloromethane was used as the solvent and the cluster was stirred for only 10 minutes prior to addition to the stirred suspension of the support in dichloromethane. This was due to the instability of the larger gold phosphine cluster in the dichloromethane solvent because of the lability of the phosphine ligand. For the silica supported samples, the cluster was found to stick to the silica very well and then sample was dried in a similar fashion to the other cluster. However, in the case of the titania samples, the mixture of support and cluster was only stirred for two hours before the mixture was dried under vacuum. These differences in the deposition procedure were designed to minimise any possible agglomeration of the Au₁₀₁ clusters in solution. Due to the increase in particle size of the Au₁₀₁ cluster as compared to the smaller (< 1 nm), more atomically precise clusters, the colour of the resulting powders differed significantly. The silica sample is a deep pink colour, whilst the titania sample was a darker violet colour.

When compared to the standard gold titania reference catalysts, which consists of gold nanoparticles generated on P-25 titania via a deposition-precipitation method, the colour of the supported gold phosphine cluster on P-25 (pale orange) differs significantly from the intense purple colour of the reference sample. The contrasting colours was initially attributed to the lower loading in the systems used in this study; however, upon exposure to ambient light conditions for 24 hours, the titania supported gold phosphine cluster sample changed from the initial orange colour to a pale, purple colour. The silica supported samples appeared to be much less sensitive to ambient light, as no colour change was observed. Previous studies have shown that gold based catalysts to be sensitive to their storage conditions such as light, air and moisture. For this study as all samples were stored under nitrogen at - 20°C, samples were equilibrated to the ambient temperature prior to manipulations too minimise condensation. Exposure to light was minimised as much as possible, particularly for the titania supported samples, a known photocatalyst.

Activation of supported gold clusters

The activation step for preparing heterogeneous catalyst is an essential step in the process of making active catalysts. The activation protocols can vary significantly between different researchers and laboratories and often involve high temperature treatment (300 – 900 °C) of the pre-catalyst under a specific atmosphere of either hydrogen, oxygen or air. Gold catalysts have even been shown

to be very sensitive to the flow of the atmosphere, which can affect the presence of sub 1 nm particles on the surface of the iron oxide surface.

For this project, a range of activation methods were studied that hopefully allowed us to improve the activity or at the very least begin to understand the nature of the catalytic behaviour of the supported small gold clusters. Due to the nature of the small clusters, high temperature methods would cause significant agglomeration of the clusters on the surface, whilst a low temperature regime was predicted to result in an inactive catalyst. A moderate temperature of 200 °C was chosen and was found to yield catalytically active species for this study.

Heat treatment, follows the protocol described by M. Turner *et al.*⁶ Typically, the supported cluster on SiO₂ or TiO₂ (ca. 500 mg) in a Schlenk tube was stirred (1000 rpm) and heated at 200 °C (oil bath) under vacuum for 2 hours. The sample was then removed from the oil bath and allowed to cool to room temperature under reduced pressure. The material obtained in this way was stored in a refrigerated Schlenk tube under N₂ and in the absence of light.

Calcination, a common method for activation supported metal nanoparticle catalysts, is a method whereby the pre-catalyst is treated with either air or oxygen at elevated temperatures. Typically, the supported cluster on SiO₂ or TiO₂ (ca. 500 mg) in a Schlenk tube was stirred (1000 rpm) under vacuum, and then filled with dried air (BOC gases, instrument grade). The sample was stirred at 200 °C for 2 hours. The sample was allowed to cool to room temperature, and was then stored in a refrigerated Schlenk tube under N₂ and in the absence of light. Extended calcination of some samples was also conducted to ascertain the fate of the gold cluster after exposure to the calcination conditions at 200 °C for an extended amount of time. Under similar conditions as described above, a sample of the precatalyst was calcined at 200 °C for twelve hours and stored under in a refrigerated Schlenk tube under N₂ and in the absence of light. Milder calcination temperatures were also explored at 100 °C briefly as a comparison to this temperature for photoelectron studies.

Calcination at 400 °C was also conducted in a tube furnace. The supported cluster on SiO₂ or TiO₂ (ca. 500 mg) was loaded into a quartz boat and loaded into dual zone tube furnace, which was set to heat the sample at 400 °C under static atmospheric oxygen for two hours. The higher temperature was expected remove much more of the triphenylphosphine ligand but lead to more gold particle sintering.

A selection of novel activation methods were also investigated for their potential in preparing nanostructured gold catalysts.

Refluxing or Washing the precatalyst in a suitable solvent that will preferentially remove the organic ligand, but leave the metal nanoparticle attached to the surface of the support. This solvent treatment (washing) was first undertaken by J. A. Lopez-Sanchez et al.⁴⁶ where PVP stabilised gold particles were deposited on to acid washed titania, heated in ethanol solvent at 80 °C to remove the PVP polymer, leaving the naked metal nanoparticles on the surface of the titania support. In this system, very little aggregation of the gold particles occurred, and the catalysts were active for the oxidation of carbon monoxide and benzyl alcohol. For this research, toluene was used as the solvent to remove the triphenyl phosphine ligands. The gold clusters are sparingly soluble in toluene whilst the phosphine ligand is soluble. The larger Au₁₀₁ system is more soluble in toluene, but the triphenyl phosphine is very labile in solution. Typically, the magnetically stirred (1000 rpm) suspension of the supported cluster on TiO₂ (ca. 500 mg) in toluene (50 mL) was heated to 100 °C for 2 hours. The solid was then recovered using centrifugation (10 min, 5000 rpm). The solid was then washed three times with toluene (50 mL) by forming a suspension using a Vortex agitator followed by centrifugation (10 min, 5000 rpm) to recover the solid, which was then dried under reduced pressure. The material obtained in this way was stored in a refrigerated Schlenk tube under nitrogen and in the absence of light. Some calcined (mild) samples were also treated by washing of the samples in toluene at 100 °C in an attempt to understand the effect of such treatments and the effect of such catalytic-like conditions on the samples.

Ozone treatment of the precatalysts was briefly investigated due to the possibility of oxidatively removing any organic residues from the surface at room temperature.^{47,48} A pre-dried sample (ca. 300 mg) was loaded in to a Schlenk tube attached to an ozone generator at the glass tap with a tube connector at the top of flask to facilitate the flow of gas. A gentle flow of ozone was introduced, whilst the powder sample was stirred gently at 600 rpm for two hours. For both silica and titania samples, the observed colour of samples changed rapidly under exposure to the ozone, which was attributed to the formation of gold (III) oxide on the surface. The first titania supported samples treated by ozone demonstrated sensitivity to light due to the return of the light purple colour which was attributed to gold clusters and nanoparticles on the surface. This reversal could be

attributed to photoreduction of the gold oxide species back to Au⁰. Subsequent samples were protected from light and stored in a refrigerated Schlenk tube under nitrogen.

Characterisation of the supported gold clusters

HRTEM of the supported gold clusters on various support materials showed that the gold nanoparticles were present, with a particle size distribution between 2 nm and 5 nm, with several systems showing a greater degree of gold cluster sintering. Gold particles below 1.5 nm proved difficult to observe as the crystalline nature of the support materials hindered identification of the smaller particles, unlike the unsupported gold clusters on amorphous carbon. The low loading of the supported clusters (0.5 %) as compared to common literature catalysts (1–8 %) meant the population of gold nanoparticles was relatively low. The most robust method for depositing the samples on to the copper grids, supplied by Pro-Sci-tech, was to suspend a small amount of the powder sample (< 1 mg) in diethyl ether (2 mL) and swirl the sample vigorously. Using a micropipette, 20 µL of the suspension was deposited onto a copper grid. The samples were initially dried under a gentle flow of nitrogen, and then dried under vacuum in a small glass vial with a rubber septum. Early work used methanol, acetone and occasionally toluene to form a suspension to deposit the catalysts on to the grid; however, it was observed in several instances that the gold clusters were deposited on the amorphous carbon rather than on the support material. This occurred in the case of the titania supported gold phosphine clusters where methanol was used to deposit the untreated supported clusters. To deal with this issue, toluene was employed for the preparation of the TEM samples; however, due to its higher boiling point it proved difficult to dry the samples. Finally, diethyl ether was settled upon as the solvent to suspend the sample in, as it results in well dispersed samples and solubility issues are avoided for the untreated samples. Significant delays were also encountered due to the damage that was incurred to the Philips CM-200 TEM during the Canterbury earthquakes, and once repairs were complete, effect of the constant seismic activity reduced the resolution that could be achieved.

A small selection of samples were also studied by aberration corrected HAADF STEM, which further highlighted that the titania and silica supports had a significantly greater coverage of the sub 1 nm phosphine clusters than was initially observed by HRTEM at the University of Canterbury. Due

to the limits of HRTEM, such smaller gold clusters were not observed; however, the extent of cluster sintering can be gauged by HRTEM.

Table 6: Summary of HRTEM particle counts for supported gold clusters

| Cluster | Activation method | Fumed SiO ₂ | | P-25 TiO ₂ | |
|---|-------------------------|------------------------|-----|-----------------------|-----|
| | | nm | σ | nm | σ |
| Au ₁₀₁ | Untreated | 1.8 | 0.8 | 2.3 | 0.8 |
| | Heated treated @ 200 °C | 2.3 | 1.3 | 3.2 | 1.7 |
| | Calcined @ 200 °C | 3.4 | 1.5 | 3.8 | 2.3 |
| | Calcined @ 400 °C | 4.7 | 2.6 | 5.3 | 3.5 |
| Au ₉ (PPh ₃) ₈ (NO ₃) ₃ | Untreated | — | — | — | — |
| | Heated treated @ 200 °C | 1.8 | 1.0 | 2.4 | 1.7 |
| | Calcined @ 200 °C | 2.6 | 1.6 | 3.1 | 2.1 |
| | Calcined @ 400 °C | 3.5 | 2.2 | 4.8 | 2.8 |
| Au ₈ (PPh ₃) ₈ (NO ₃) ₂ | Untreated | — | — | — | — |
| | Heated treated @ 200 °C | 1.9 | 0.9 | 2.2 | 1.4 |
| | Calcined @ 200 °C | 2.7 | 1.9 | 3.6 | 2.7 |
| | Calcined @ 400 °C | 4.1 | 2.1 | 5.2 | 3.4 |
| Au ₁₁ (PPh ₃) ₈ (NO ₃) ₃ | Untreated | — | — | — | — |
| | Heated treated @ 200 °C | 2.1 | 0.8 | 2.7 | 1.4 |

Supported Au₁₀₁ nanoparticles

The untreated, as deposited samples, proved difficult to confirm the presence of the gold phosphine clusters which have a gold core diameter of approximately 0.8 nm; however, the Au₁₀₁ nanoparticles which had a larger particle diameter, proved to be much easier to observe and measure. The P-25 titania samples were shown to be sensitive to photo induced gold reduction, which resulted in significant sintering of the gold clusters on the titania support upon prolonged exposure to ambient light. In contrast to the titania support, the silica supported clusters proved to be very stable under ambient light conditions. The samples were stored under nitrogen in a Schlenk

tube at $-20\text{ }^{\circ}\text{C}$, and wrapped in aluminium foil to ensure that the samples were not significantly affected by light.

The untreated Au_{101} samples had a similar gold nanoparticle size as compared to the unsupported gold nanoparticle samples, although there does appear to be slight increase in particle size for P-25 titania sample, which could be attributed to small amounts of photoinduced reduction of the gold.

Upon heat treatment at $200\text{ }^{\circ}\text{C}$ under vacuum, particle agglomeration due to the elevated temperature was observed on both silica and titania supports. An analogous system using Au_{101} on fumed silica under similar conditions reported particles sizes of approximately 1.5 nm , which is slightly lower than our observations. The differences may have their origin in slightly different manipulations of the materials, or the superior resolution of the HRTEM used in that study improved the detection of the smaller ($< 1.5\text{ nm}$) particles which we struggled to detect for the reasons reported above. The titania supported sample appeared to have significantly higher population of larger ($> 2\text{ nm}$) particles present than the silica samples. The reason for the larger particles present on the titania support when compared to the silica support was due to the poor interaction of these small cationic gold phosphine clusters with the titania.

Under these conditions, it is expected that the metal core will anneal to the surface of the support material. Under an oxygen atmosphere, the organic capping groups are expected to decompose. In recent years, there have been several reports on the effect of the differing atmospheric conditions could have on the catalyst. Under oxygen, it was shown that the gold nanoparticles are more susceptible to sintering even at relatively mild conditions. Behm *et al.* showed that gold catalysts could be active after treatment at moderate temperatures under hydrogen, where sintering of the gold particles was less than under an oxygen atmosphere.

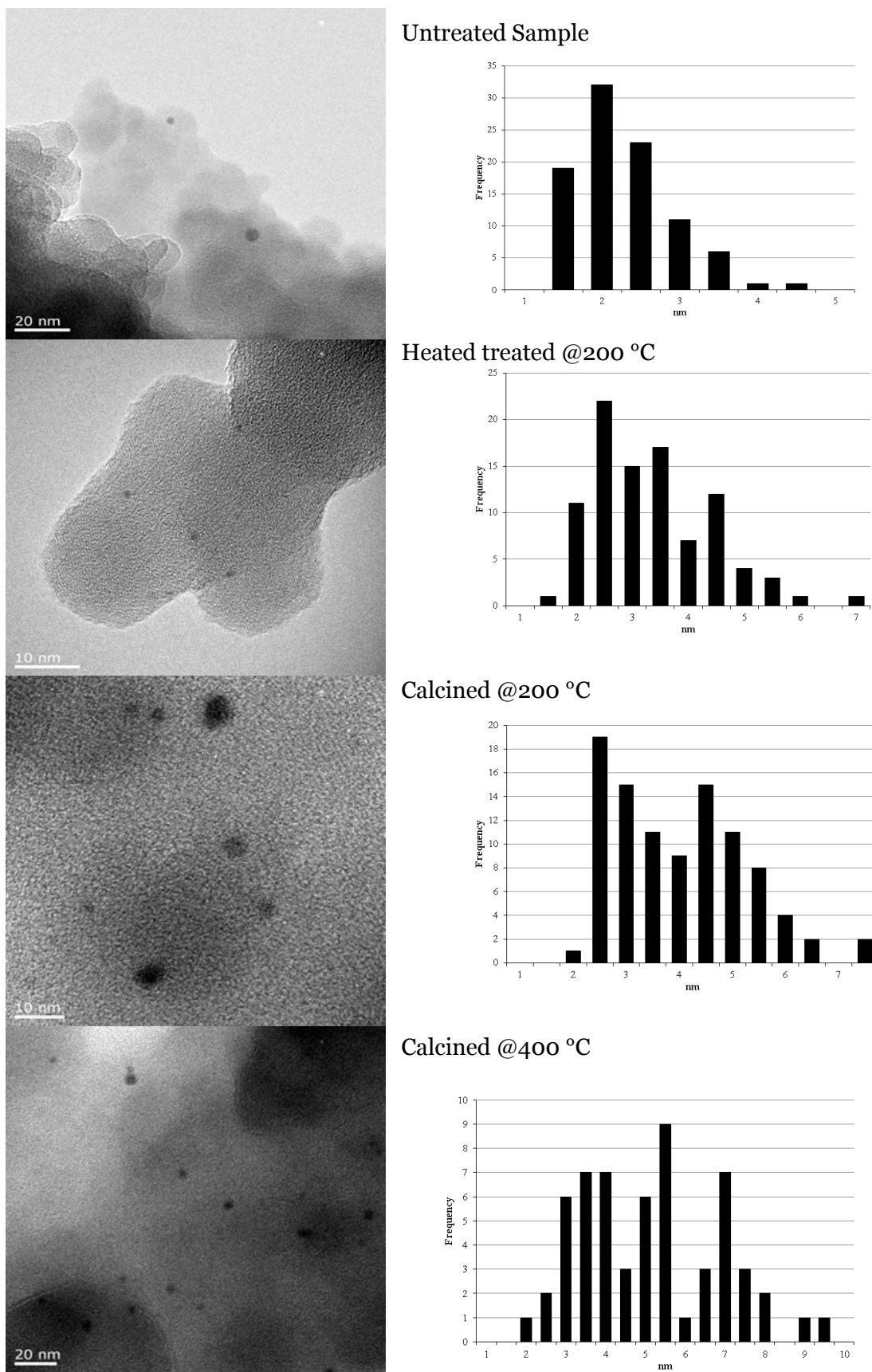


Figure 24; Representative TEM images (1) and the corresponding particle size distribution (2) for Au₁₀₁ supported on fumed silica

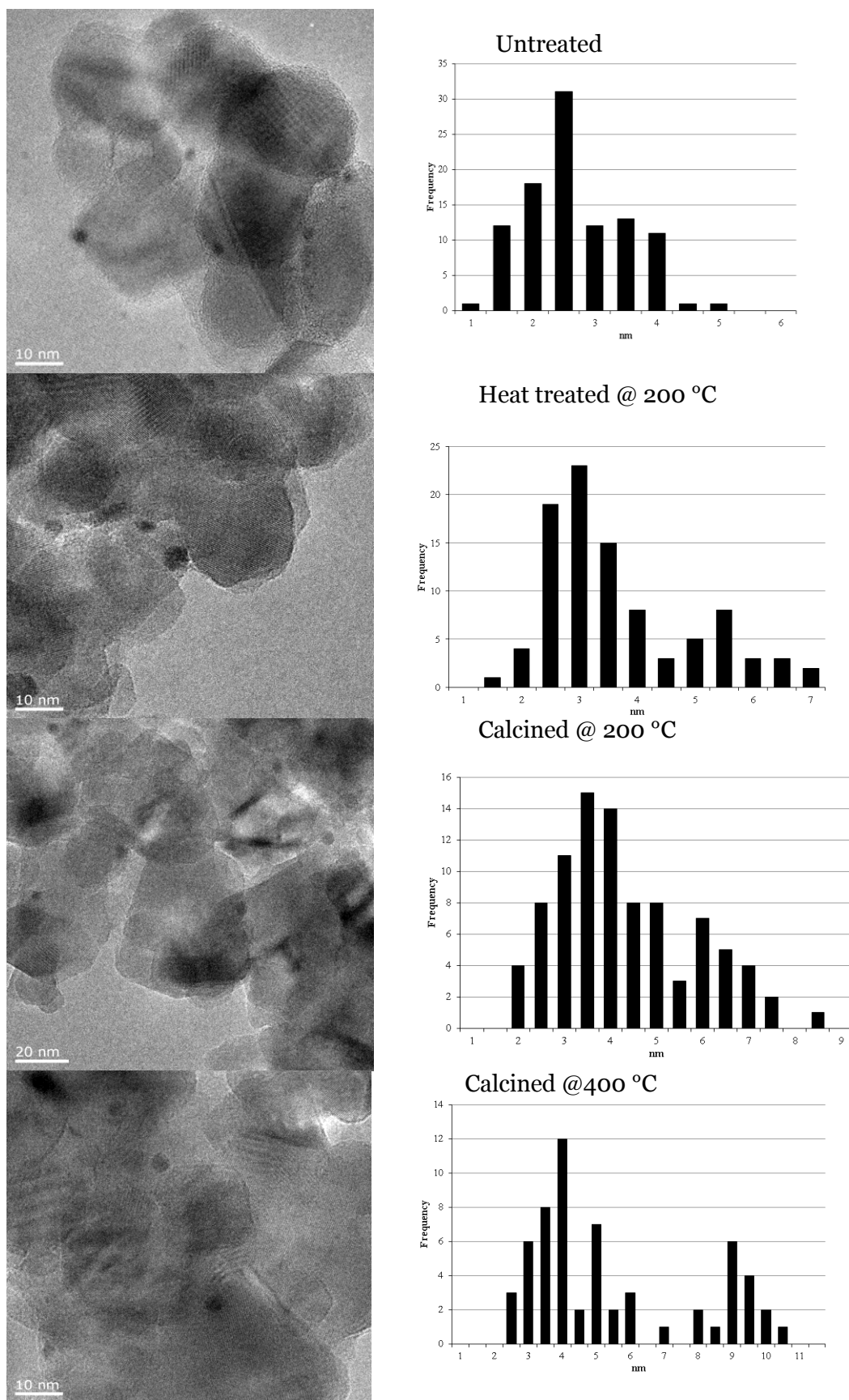


Figure 25: Representative TEM images and the corresponding particle size distribution for Au₁₀₁ supported on P-25 titania.

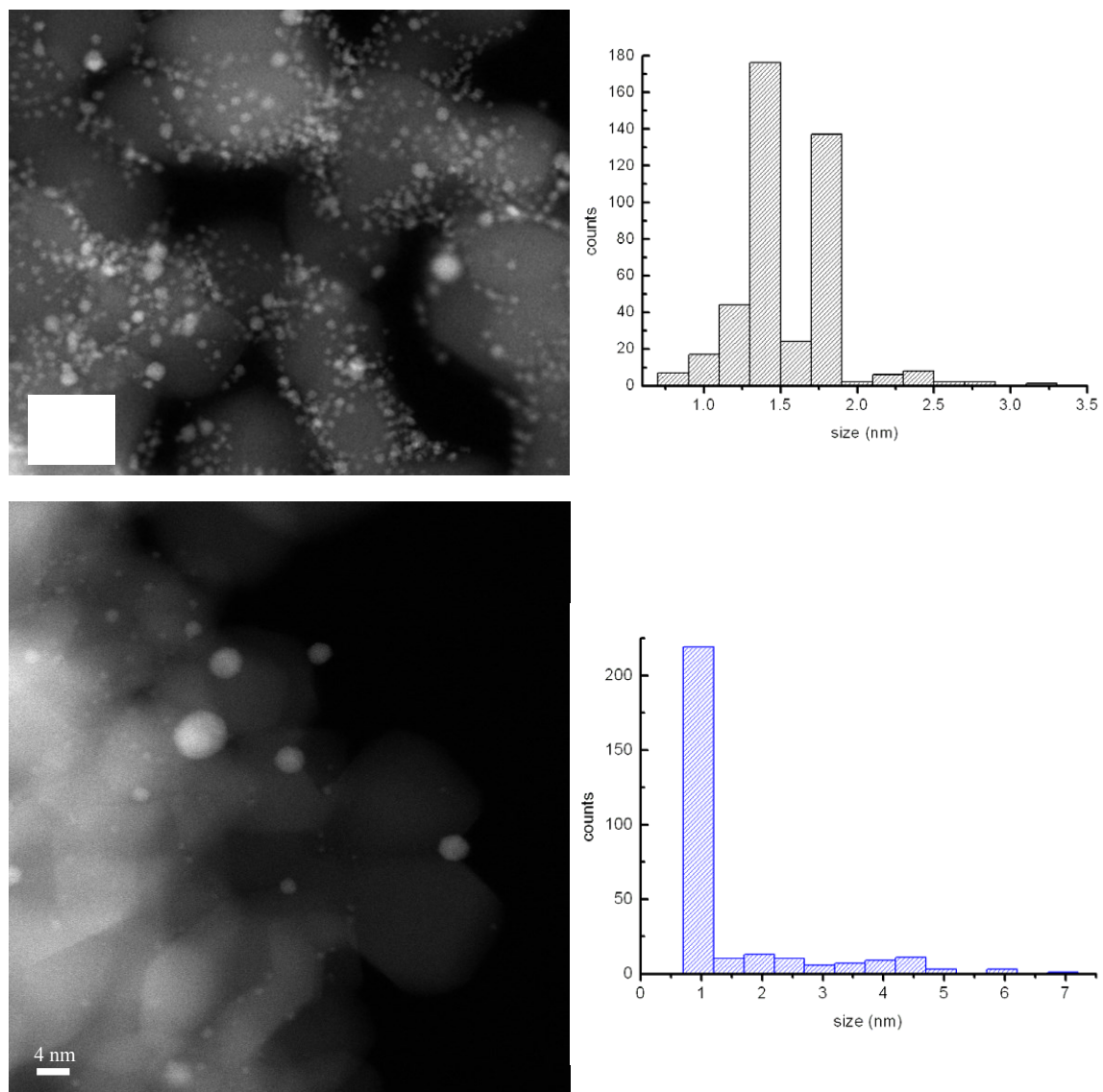


Figure 26: Aberration corrected STEM of Au₁₀₁ on TiO₂, (A) Untreated, (B) Heat treated at 200 °C for two hours.

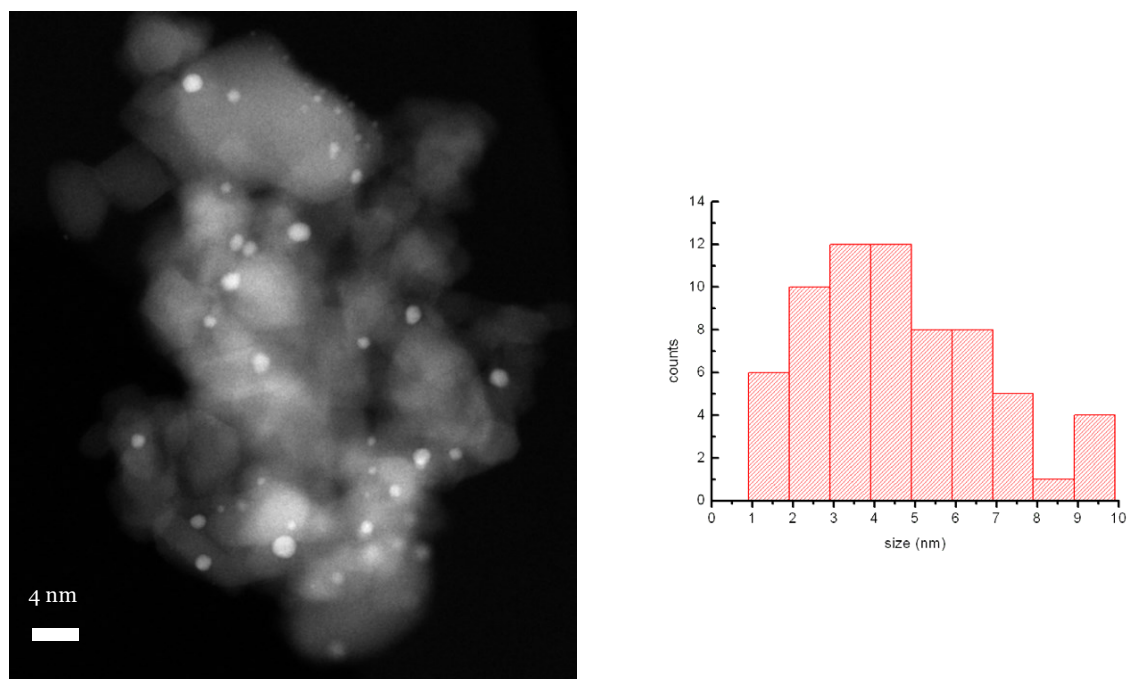
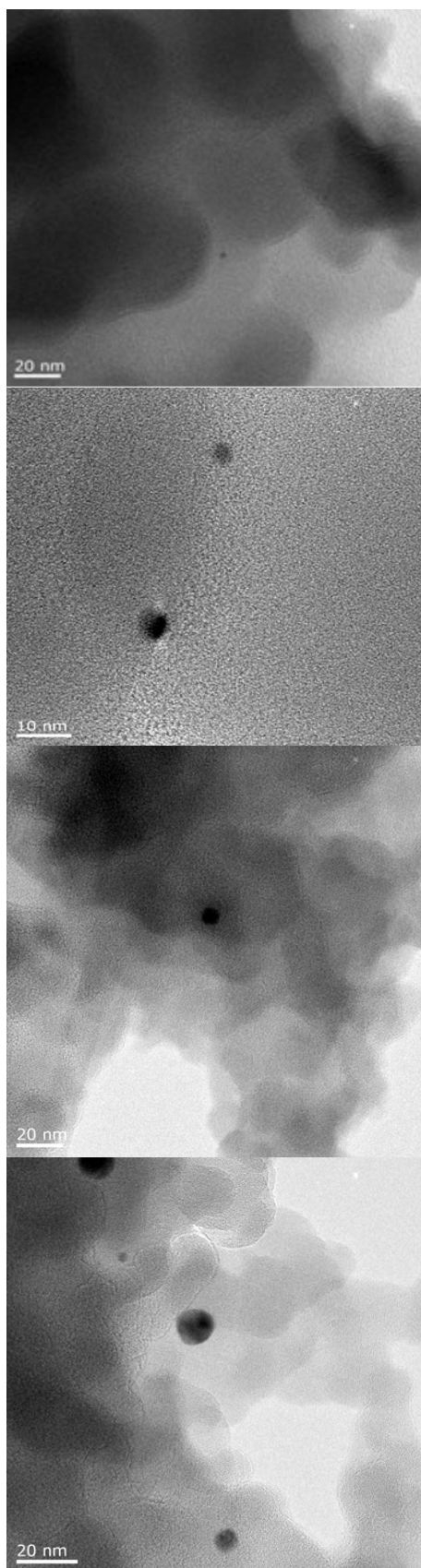


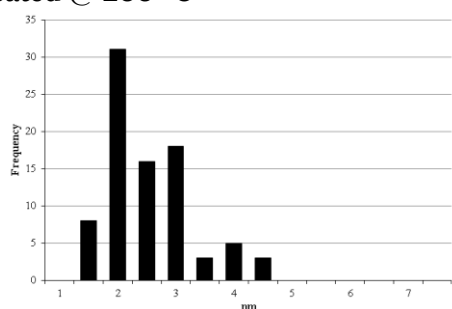
Figure 27: Aberration corrected STEM of Au₁₀₁ on acid-washed TiO₂, treated by refluxing in toluene at 100 °C for two hours

Supported $\text{Au}_9(\text{PPh}_3)_8(\text{NO}_3)_3$

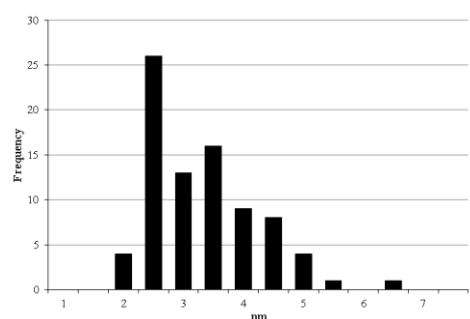


Untreated

Heat treated @ 200 °C



Calcined @ 200 °C



Calcined @ 400 °C

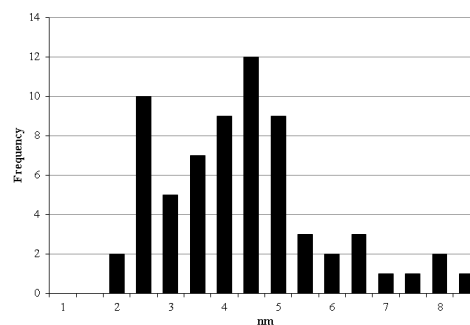


Figure 28: Representative TEM images (1) and the corresponding particle size distribution for A) Au_9 on fumed silica

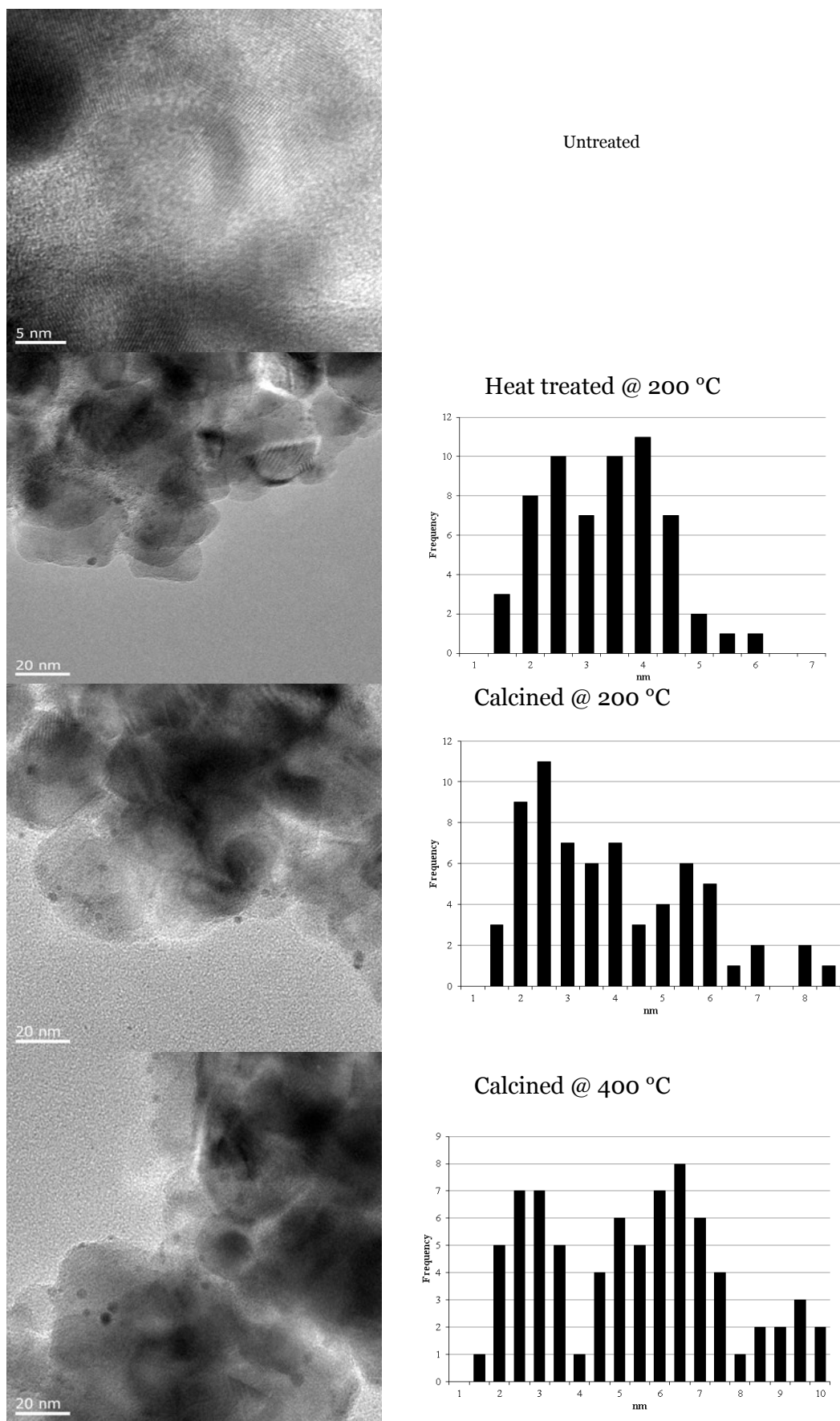


Figure 29: Representative TEM images and the corresponding particle size distribution for Au₉ on P-25 titania

Supported $\text{Au}_8(\text{PPh}_3)_8(\text{NO}_3)_2$

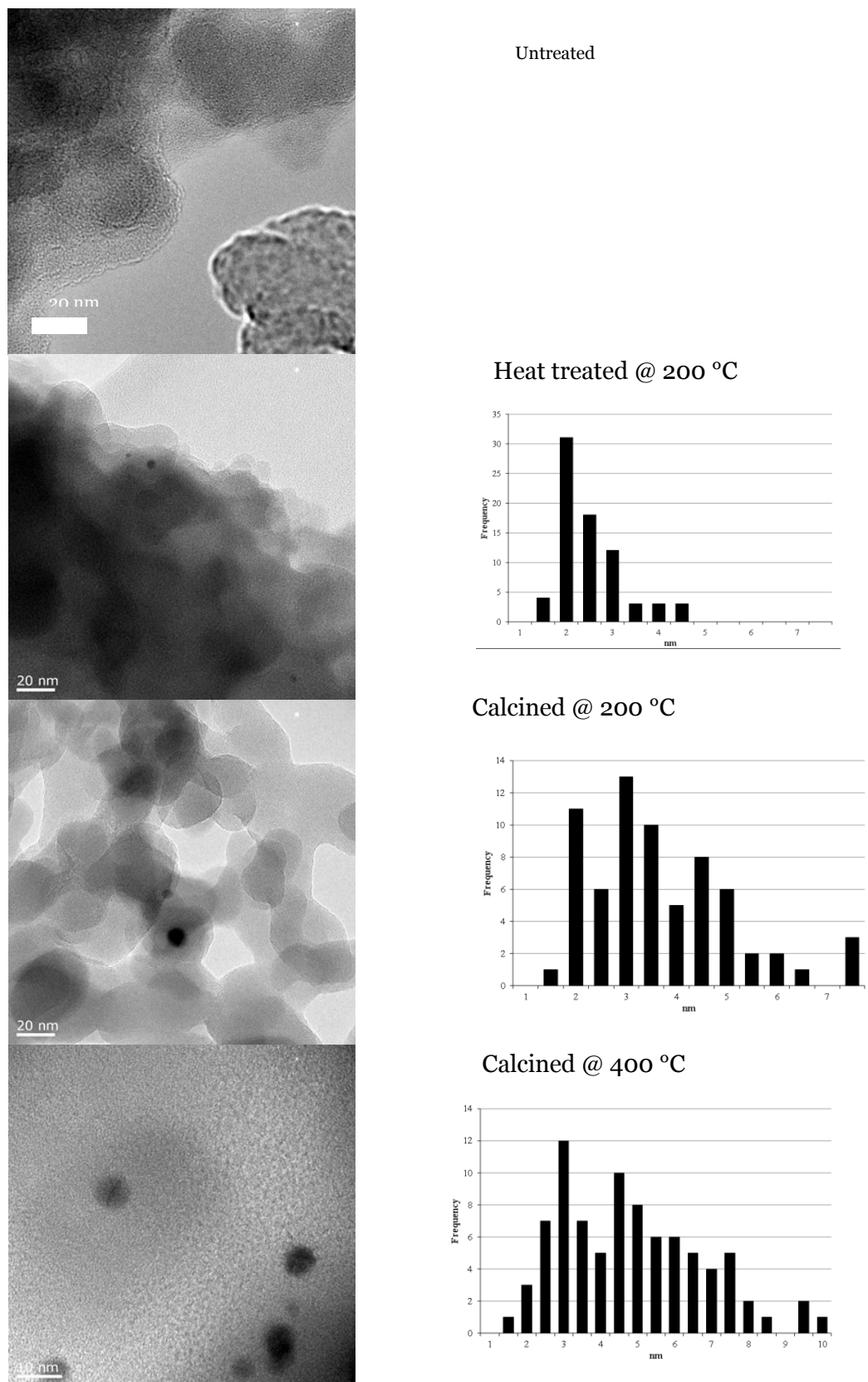


Figure 30: Representative TEM images (1) and the corresponding particle size distribution for A) Au_8 on fumed silica

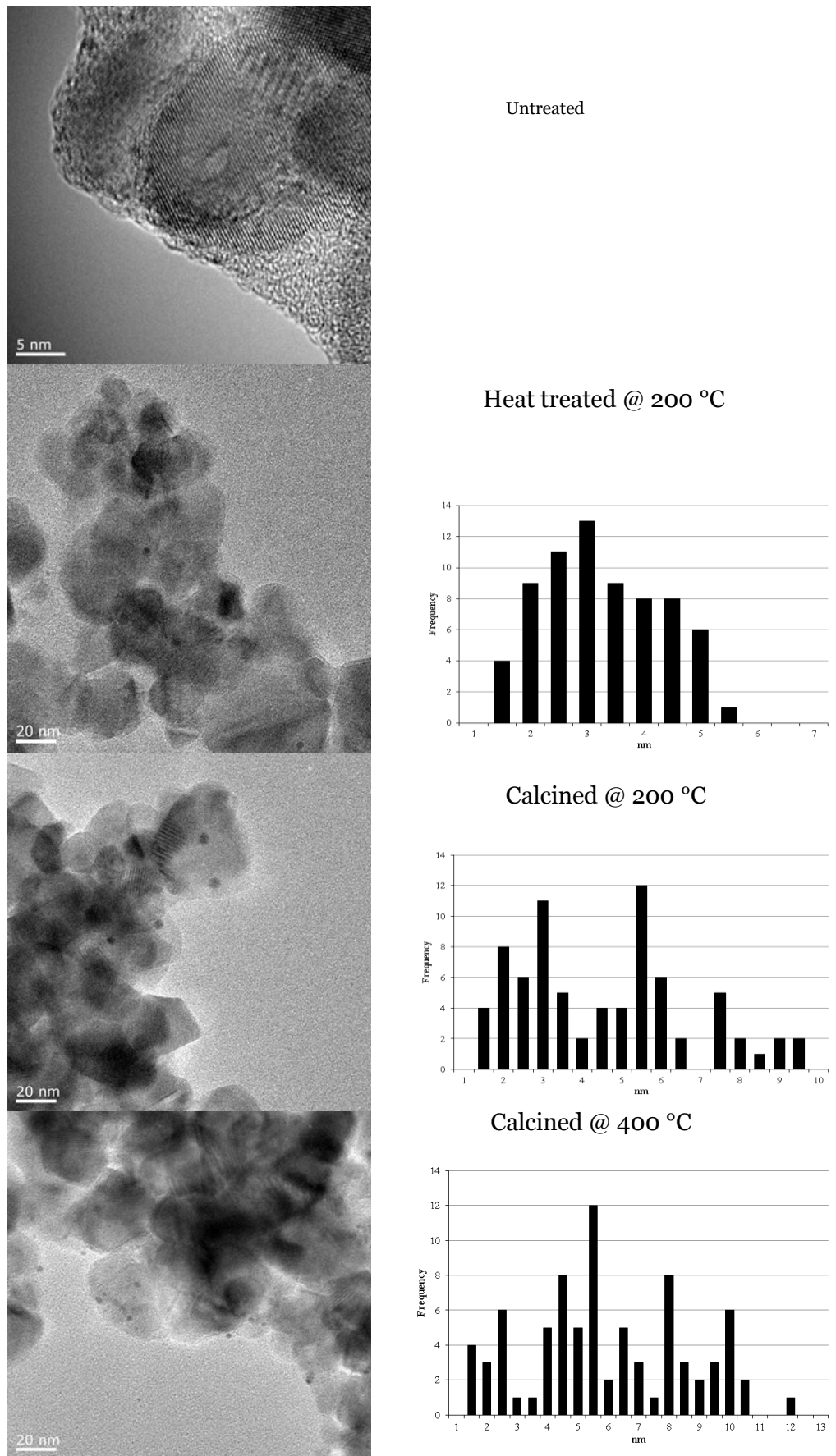


Figure 31: Representative TEM images (1) and the corresponding particle size distribution for A) Au₈ on P25 titania

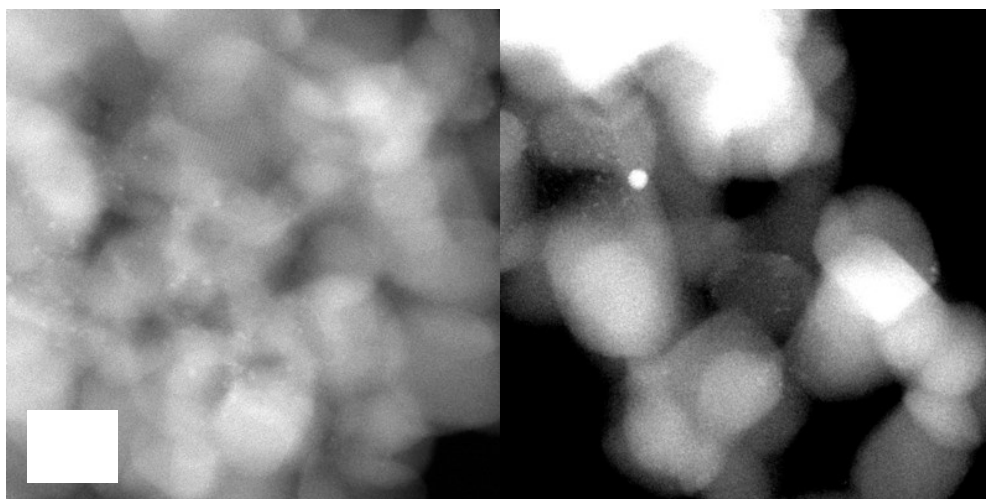


Figure 32: Aberration corrected STEM of heat treated Au₈ supported on P-25 titania

Summary

Overall, a large range of nanostructured gold based catalysts were produced, which have gold particle sizes down to < 1 nm. The gold particles were shown to agglomerate differently depending on the type of activation procedure employed. A selection of atomically precise gold phosphine clusters and nanoparticles were deposited on two supports, fumed silica and P-25 titania. The identification of the small gold clusters (< 1 nm) on the support material by high resolution transmission electron microscope was difficult, due to the small size of the gold particles, and due to the greater diffraction of the electron beam by the support material as compared to the flat amorphous carbon thin film. Gold particles supported on titania were also observed to be sensitive to ambient light, leading to photoinduced sintering of the gold particles. Acid washing of the titania was also used in an attempt to control the photosensitivity of these catalysts. Typically, the silica supported samples were characterised as a light yellow material, changing to slight mauve colour after activation, whilst the titania supported gold nanoparticles resulted in a light purple material that deepened in colour after activation.

A range of activation procedures were investigated and briefly characterised by electron microscopy but due to the limited ability to identify the ultra-small gold clusters (< 1.4 nm), a more systematic analysis by HRTEM could not be achieved. The primary conditions that were investigated were conducted at a relatively low temperature of 200 °C under various atmospheric

conditions. The presence of oxygen during the activation steps as compared to activation under a vacuum was also studied, which showed that the supported gold particles sinter readily on both silica and titania. Solvent induced removal of the phosphine ligands was also investigated, but this appeared to produce inactive catalysts which demonstrated significant particle agglomeration. Several higher temperature procedures were also studied at 400 °C, which led to greater particle agglomeration on both silica and titania supports. A range of novel, mild activation conditions were also prepared for further study by photoelectron spectroscopy.

EXFAS experiments were also conducted by Jason Alvino on a handful of samples prepared at the University of Canterbury. These experiments confirmed that aggregation of the gold particles on the surface was occurring. Several samples were studied by HAADF-STEM, which showed that the atomically precise clusters were well dispersed on the surfaces of both titania and silica supports. STEM highlighted that in many samples in which aggregation had occurred, there was still significant proportion of the atomically precise gold clusters present; hence, HRTEM experiments were only able to confirm the extent of particle agglomeration.

Further work is warranted on correlating the observed colour changes of the silica based catalysts to the increase in particle size.

Bridge

Overall, electron microscope characterisation of these nanostructured materials proved to be difficult. Observation of the larger, agglomerated gold particles (> 1.5 nm) was possible by TEM but confirmation of the presence of smaller gold particles was elusive. Although the HAADF-STEM data on several samples illustrated the presence or even complete absence of the gold clusters, we were unable to complete a comprehensive survey of these nanocatalysts by HAADF-STEM. In an attempt to further understand these results, detailed photoelectron spectroscopy experiments were conducted on a wide range of these materials. Photoelectron spectroscopy experiments were mainly conducted at the Soft X-Ray Beamline at the Australian Synchrotron, but several preliminary experiments were conducted on a lab based XPS machine. Photoelectron spectroscopy is a technique that can provide detailed electronic data on a wide range of samples, and is also very important for understanding the nature of the gold catalysts. A detailed electronic study on gold

based catalysts, supported on titania and silica powders rather than flat substrates, derived from such small gold clusters has not been previously conducted. The following chapter discusses many of the trials and tribulations of studying these materials by photoelectron spectroscopy.

References

- (1) Riegel, E. R.; Kent, J. A.: *Handbook of Industrial Chemistry*; Kluwer Academic/Plenum Publishers, **2003**.
- (2) Ertl, G.; Knözinger, H.: *Handbook of heterogeneous catalysis*; Wiley-VCH, **2008**.
- (3) Bond, G. C.: Gold: a relatively new catalyst. *Catalysis Today* **2002**, *72*, 5-9.
- (4) Bond, G.; Thompson, D. T.: Gold-Catalysed Oxidation of Carbon Monoxide. *Gold Bulletin* **2000**, *33*, 41.
- (5) Liu, Y.; Tsunoyama, H.; Akita, T.; Tsukuda, T.: Efficient and selective epoxidation of styrene with TBHP catalyzed by Au₂₅ clusters on hydroxyapatite. *Chemical Communications* **2010**, *46*, 550-552.
- (6) Turner, M.; Golovko, V. B.; Vaughan, O. P. H.; Abdulkin, P.; Berenguer-Murcia, A.; Tikhov, M. S.; Johnson, B. F. G.; Lambert, R. M.: Selective oxidation with dioxygen by gold nanoparticle catalysts derived from 55-atom clusters. *Nature* **2008**, *454*, 981-983.
- (7) Thomas, J. M.; Raja, R.; Sankar, G.; Bell, R. G.: Molecular Sieve Catalysts for the Regioselective and Shape Selective Oxyfunctionalization of Alkanes in Air. *Accounts of Chemical Research* **2001**, *34*, 191-200.
- (8) Robert Raja; Tetyana Khimiyak; John Meurig Thomas; Sophie Hermans; Johnson, B. F. G.: Single-Step, Highly Active, and Highly Selective Nanoparticle Catalysts for the Hydrogenation of Key Organic Compounds. *Angewandte Chemie International Education* **2001**, *40*, 4638.
- (9) Parker, S.: Reactivity and sintering kinetics of Au/TiO₂ (110) model catalysts: particle size effects. *Topics in Catalysis*. **2007**, *44*, Issue 1-2, 3-13
- (10) Kyriakou, G.; Beaumont, S. K.; Humphrey, S. M.; Antonetti, C.; Lambert, R. M.: Sonogashira Coupling Catalyzed by Gold Nanoparticles: Does Homogeneous or Heterogeneous Catalysis Dominate? *ChemCatChem* **2010**, *2*, 1444-1449.
- (11) Gajan, D.; Guillois, K.; Delichère, P.; Basset, J.-M.; Candy, J.-P.; Caps, V.; Copéret, C.; Lesage, A.; Emsley, L.: Gold nanoparticles supported on passivated silica: access to an efficient aerobic epoxidation catalyst and the intrinsic oxidation activity of gold. *Journal of the American Chemical Society* **2009**, *131*, 14667-14669.
- (12) Yang, J.; Li, P.; Wang, L.: Postsynthetic modification of metal-organic framework as a highly efficient and recyclable catalyst for three-component (aldehyde–alkyne–amine) coupling reaction. *Catalysis Communications* **2012**, *27*, 58-62
- (13) Proust, A.; Matt, B.; Villanneau, R.; Guillemot, G.; Gouzerh, P.; Izzet, G.: Functionalization and post-functionalization: a step towards polyoxometalate-based materials. *Chemical Society Reviews* **2012**, *41*, 7605-7622.
- (14) Kielbassa, S.; Kinne, M.; Behm, R.: Thermal Stability of Au Nanoparticles in O₂ and Air on Fully Oxidized TiO₂ (110) Substrates at Elevated Pressures. An AFM/XPS Study of Au/TiO₂ Model Systems. *The Journal of Physical Chemistry B* **2004**, *108*, 19184-38374.
- (15) Kielbassa, S.; Häbich, A.; Schnaidt, J.; Bansmann, J.; Weigl, F.; Boyen, H.-G.; Ziemann, P.; Behm, R.: On the morphology and stability of Au nanoparticles on TiO₂(110) prepared from micelle-stabilized precursors. *Langmuir*, **2006**, *22*, 7873-7953.
- (16) Zheng, N.; Stucky, G.: A general synthetic strategy for oxide-supported metal nanoparticle catalysts. *Journal of the American Chemical Society* **2006**, *128*, 14278-14358.
- (17) Pinna, F.: Supported metal catalysts preparation. *Catalysis Today* **1998**, *41*, 129-137.

- (18) Kulkarni, A.; Lobo-Lapidus, R.; Gates, B.: Metal clusters on supports: synthesis, structure, reactivity, and catalytic properties. *Chemical Communications* **2010**, 46, 5997-12012.
- (19) Raja, R.; Thomas, J. M.; Greenhill-Hooper, M.; Ley, S. V.; Paz, F. A. A.: Facile, One-Step Production of Niacin (Vitamin B3) and Other Nitrogen-Containing Pharmaceutical Chemicals with a Single-Site Heterogeneous Catalyst. *Chemistry : A European Journal* **2008**, 14, 2340-2348.
- (20) Hungria, A. B.; Raja, R.; Adams, R. D.; Captain, B.; Thomas, J. M.; Midgley, P. A.; Golovko, V.; Johnson, B. F. G.: Single-Step Conversion of Dimethyl Terephthalate into Cyclohexanedimethanol with Ru₅PtSn, a Trimetallic Nanoparticle Catalyst. *Angewandte Chemie International Edition*, **2006**, 45, 4782-4785.
- (21) Thomas, J. M.; Raja, R.: Exploiting Nanospace for Asymmetric Catalysis: Confinement of Immobilized, Single-Site Chiral Catalysts Enhances Enantioselectivity. *Acc. Chem. Res.* **2008**, 41 (6), 708-720
- (22) Lu, P.; Teranishi, T.; Asakura, K.; Miyake, M.; Toshima, N.: Polymer-Protected Ni/Pd Bimetallic Nano-Clusters: Preparation Characterisation and Catalysis for hydrogenation of Nitrobenzene *Journal of Physical Chemistry B* **1999**, 103, 9673-9682.
- (23) Shephard, D. S.; Maschmeyer, T.; Sankar, G.; Thomas, J. M.; Ozkaya, D.; Johnson, B. F. G.; Raja, R.; Oldroyd, R. D.; Bell, R. G.: Preparation, Characterisation and Performance of Encapsulated Copper –Ruthenium Bimetallic Catalysts Derived from Molecular Cluster Carbonyl Precursors. *Chemistry : A European Journal* **1998**, 4, 1214-1224.
- (24) Femoni, C.; Iapalucci, M. C.; Kaswalder, F.; Longoni, G.; Zacchini, S.: The possible role of metal carbonyl clusters in nanoscience and nanotechnologies. *Coordination Chemistry Reviews* **2006**, 250, 1580-1604.
- (25) Tsunoyama, H.; Ichikuni, N.; Sakurai, H.; Tsukuda, T.: Effect of electronic structures of Au clusters stabilized by poly(N-vinyl-2-pyrrolidone) on aerobic oxidation catalysis. *Journal of the American Chemical Society* **2009**, 131, 7086-7179.
- (26) Thomas, J. M.; Raja, R.; Johnson, B. F. G.; O'Connell, T. J.; Sankara, G.; Khimyak, T.: Bimetallic nanocatalysts for the conversion of muconic acid to adipic acid. *Chemical Communications* **2003**, 1126-1127.
- (27) Thomas, J. M.: Heterogenous Catalysis: Enigmas, Illusions, Challenges, Realities and Emergent Strategies of Design. *The Journal of Chemical Physics* **2008**, 128, 182502.
- (28) Yuan, D.; Ding, L.; Chu, H.; Feng, Y.; McNicholas, T. P.; Liu, J.: Horizontally Aligned Single-Walled Carbon Nanotube on Quartz from a Large Variety of Metal Catalysts. *Nano Letters* **2008**, 8 (8), pp 2576-2579
- (29) Haruta, M.; Yamada, N.; Kobayashi, T.; Iijima, S.: Gold catalysts prepared by coprecipitation for low-temperature oxidation of hydrogen and of carbon monoxide. *Journal of Catalysis* **1989**, 115, 301-309.
- (30) Hayashi, T.; Tanaka, K.; Haruta, M.: Selective vapor-phase epoxidation of propylene over Au/TiO₂ catalysts in the presence of oxygen and hydrogen. *Journal of Catalysis* **1998**, 178, 566-575.
- (31) Haruta, M.; Kawahara, J.: Epoxidation of Propylene with Oxygen-Hydrogen Mixtures. *Mechanisms in Homogeneous and Heterogeneous Epoxidation Catalysis* **2011**, 297.
- (32) Schumacher, B.; Plzak, V.; Kinne, M.; Behm, R.: Highly Active Au/TiO₂ Catalysts for Low-Temperature CO Oxidation: Preparation, Conditioning and Stability. *Catal Lett* **2003**, 89, 109-223.
- (33) Primo, A.; Corma, A.; García, H.: Titania supported gold nanoparticles as photocatalyst. *Physical Chemistry Chemical Physics* **2011**, 13, 886-910.
- (34) Ratnasamy, C.; Wagner, J. P.: Water gas shift catalysis. *Catalysis Reviews* **2009**, 51, 325-440.

- (35) Tsubota, S.; Cunningham, D.; Bando, Y.; Haruta, M.: CO oxidation over gold supported on TiO₂. In *Studies in Surface Science and Catalysis*; T. Inui, K. F. T. U., Masai, M., Eds.; Elsevier, **1993**; Vol. Volume 77; pp 325-328.
- (36) Haruta, M.: Gold as a low-temperature oxidation catalyst: factors controlling activity and selectivity. In *Studies in Surface Science and Catalysis*; R.K. Grasselli, S. T. O. A. M. G., Lyons, J. E., Eds.; Elsevier, **1997**; Vol. Volume 110; pp 123-134.
- (37) Moreau, F.; Bond, G. C.; Taylor, A. O.: Gold on titania catalysts for the oxidation of carbon monoxide: control of pH during preparation with various gold contents. *Journal of Catalysis* **2005**, *231*, 105-114.
- (38) Moreau, F.; Bond, G.: Preservation of the Activity of Supported Gold Catalysts for CO Oxidation. *Topics in Catalysis* **2007**, *44*, 95-101.
- (39) Hugon, A.; Kolli, N. E.; Louis, C.: Advances in the preparation of supported gold catalysts: Mechanism of deposition, simplification of the procedures and relevance of the elimination of chlorine. *Journal of Catalysis* **2010**, *274*, 239-250.
- (40) Delannoy, L.; El Hassan, N.; Musi, A.; Le To, N. N.; Krafft, J.-M.; Louis, C.: Preparation of supported gold nanoparticles by a modified incipient wetness impregnation method. *The Journal of Physical Chemistry B* **2006**, *110*, 22471-22478.
- (41) Zanella, R.; Giorgio, S.; Henry, C. R.; Louis, C.: Alternative methods for the preparation of gold nanoparticles supported on TiO₂. *Journal of Physical Chemistry B* **2002**, *106*, 7634-7642.
- (42) Geus, J. W.: Production and Thermal Pretreatment of Supported Catalysts. **1983**; Vol. 16; pp 1-33.
- (43) Zanella, R.; Delannoy, L.; Louis, C.: Mechanism of deposition of gold precursors onto TiO₂ during the preparation by cation adsorption and deposition-precipitation with NaOH and urea. *Applied Catalysis A: General* **2005**, *291*, 62-72.
- (44) Herzing, A.; Kiely, C.; Carley, A.; Landon, P.; Hutchings, G.: Identification of active gold nanoclusters on iron oxide supports for CO oxidation. *Science (New York, N.Y.)* **2008**, *321*, 1331-1336.
- (45) Hurum, D. C.; Agrios, A. G.; Gray, K. A.; Rajh, T.; Thurnauer, M. C.: Explaining the enhanced photocatalytic activity of Degussa P25 mixed-phase TiO₂ using EPR. *The Journal of Physical Chemistry B* **2003**, *107*, 4545-4549.
- (46) Lopez-Sanchez, J. A.; Dimitratos, N.; Hammond, C.; Brett, G. L.; Kesavan, L.; White, S.; Miedziak, P.; Tiruvalam, R.; Jenkins, R. L.; Carley, A. F.; Knight, D.; Kiely, C. J.; Hutchings, G. J.: Facile removal of stabilizer-ligands from supported gold nanoparticles. *Nat Chem* **2011**, *3*, 551-556.
- (47) Ho, K. Y.; Yeung, K. L.: Effects of ozone pretreatment on the performance of Au/TiO₂ catalyst for CO oxidation reaction. *Journal of Catalysis* **2006**, *242*, 131-141.
- (48) Crespo-Quesada, M.; Andanson, J.-M.; Yarulin, A.; Lim, B.; Xia, Y.; Kiwi-Minsker, L.: UV-Ozone Cleaning of Supported Poly (vinylpyrrolidone)-Stabilized Palladium Nanocubes: Effect of Stabilizer Removal on Morphology and Catalytic Behavior. *Langmuir* **2011**, *27*, 7909-7916.

5 Photoelectron spectroscopy of supported gold phosphine clusters

Objectives

Supported metal nanoparticles play an indispensable role in the chemical industry acting as catalysts during the production of target compounds. Understanding the electronic properties of supported metal nanoparticles is essential for improving the selectivity, reactivity and lifetime of a catalyst; which in turn will improve the efficiency of many industrial processes.

The chemistry of gold is still in its infancy, and there is a lot of potential for supported gold nanoparticles to provide novel routes to commercially important products, and as catalysts for the conversion of hazardous waste into more environmentally benign products. Studies into the nature of gold particles on various substrates were first conducted in earnest in the 1980s by Wertheim *et al.*, who focused on the ultrahigh vacuum (UHV) deposition of gold particles onto various carbonaceous substrates. Over the last twenty years, there has been significant interest in the nature of gold nanoparticles on a wide range of metal-oxide and carbonaceous supports and discussion about their contrasting natures. Photoelectron spectroscopy is an important tool for the exploration of the chemistry of the surface of such material.

In this chapter, I will highlight the electronic nature of precisely controlled gold clusters deposited on various support materials. Previously reported studies of supported gold nanoparticles typically have looked at particles with dimensions of between 2–5 nm in diameter with a polydispersity around 1–4 nm depending on the synthetic procedure used. By using a range of gold clusters with precisely known nuclearity and ligand shell, we can develop a bottom-up picture of how the electronic properties of gold particles change with increasing size on various support materials and conditioning procedures. The objectives of this chapter are to investigate:

- The surface chemistry of gold clusters on titania, silica and carbon
- The effect of cluster core size
- The effect of cluster loading on the support
- Compare and contrast gold clusters supported on flat substrates and powdered substrates
- The effect of activation process on the electronic properties of the supported gold clusters
- The various oxygen and titania electronic environments

Introduction

Technique

The first detailed studies into the electronic nature of gold began in the early 1920s. However, it was not until the development of X-ray photoelectron spectroscopy (XPS) during the 1950s by Kai Siegbahn that the electronic properties of metals were probed in a systematic way.¹ Metal clusters had to wait until the late 1970s and early 1980s for their physical and electronic properties to be explored in earnest. During these years, there was a flurry of publications on metal and metal-oxide clusters on various substrates, typically generated under UHV conditions. An overview of this vast area was provided by Egelhoff, who presented the main theoretical principals and origins for the binding energy shifts seen for many systems, including metal clusters.²

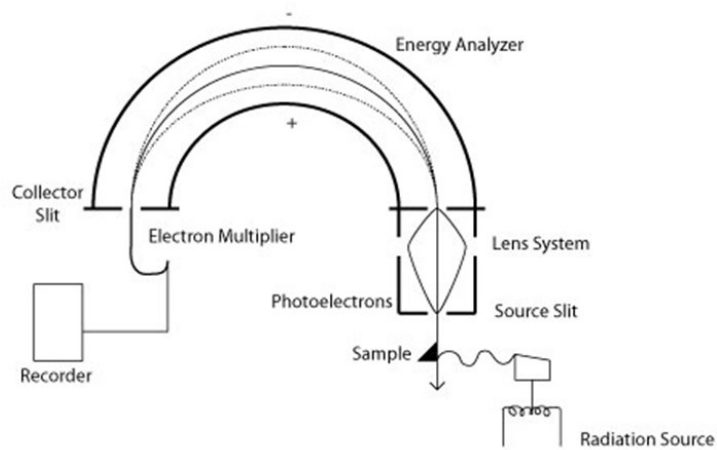
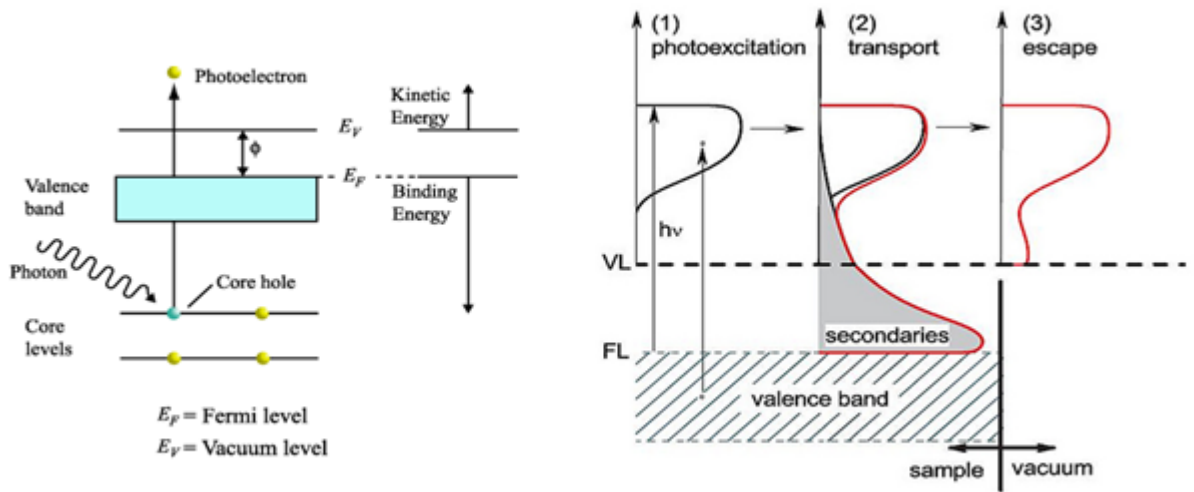
Photoelectron spectroscopy (PES) is a technique that is used extensively to study the elemental composition of a surface, and which yields quantitative data about elements on the surface. Furthermore, a small shift in the photoelectron peak conveys information about the chemical environment of an element. The technique is based on the principle of the photoelectron effect; that an electron can be emitted from a solid due to the absorption of sufficient energy from electromagnetic radiation with short wavelengths. The first observations of the photoelectron effect were reported by H. Hertz in 1887,³ however his observations were not fully explained until Albert Einstein described the quantisation of electromagnetic radiation in 1905, for which he received the Nobel prize in 1921.⁴ The photoelectron effect was not truly exploited for spectroscopy until the late fifties, when Kai Siegbahn developed a high-resolution photoemission spectrometer. Throughout the sixties and seventies, the technique and methodology were improved to such an extent that the technique is now an indispensable tool for probing the surface and electronic properties of a wide variety of materials. Early work by Siegbahn used an X-ray tube as a source of photons (XPS), but subsequent variations on this set-up using extreme ultra-violet (UV) and synchrotron sources have also been developed.

PES measures the kinetic energy of an electron after it has been ejected by an incident photon of known energy under UHV conditions. The binding energies of the electrons can then be determined from the relationship between the incident photon and photoelectron, as described by;

$$E_k = \hbar\omega - E_b - \Phi$$

Equation 1: Relationship between the incident photon and the photoelectron

where E_k is the kinetic energy of the photoelectron, $\hbar\omega$ is the energy of the incident photon; E_b is the energy by which the photoelectron is bound to the parent atom and Φ is the work-function of the solid. This relationship was first described by Rutherford in 1914.⁵



A typical PES experiment is illustrated in Figure 34A. There are three distinct phases as illustrated in Figure 35B; 1) photoexcitation of the electron, 2) transport of the electron to the surface and 3) penetration the photoelectron through the surface into the vacuum.

During each step, there are a number of factors that influence the final kinetic energy of the photoelectron.

- The initial photon energy dictates the penetration depth from which electrons are liberated.
- Electrons have a small escape depth, which means that the photoelectron is representative of the surface characteristics of the material, not the bulk properties. However, the initial photon energy also dictates the surface sensitivity of the experiment.
- As the electron escapes, there may be several elastic or inelastic scattering events, which contribute to the background signal.
- Once the photoelectron has been lost to the vacuum, an electron hole remains. This means the material is now different from its initial state. The final state of the material can make it difficult to infer the electronic properties of a material.

During PES experiments, the loss of photoelectrons results in a residual positive charge being generated on the surface of the sample. If the sample is a good electrical conductor, and in contact with an electron source (such as the body of the spectrometer) the charge is easily neutralised due to a flow of electrons to the sample. In contrast, for samples that are electrically insulating, neutralisation does not occur fast enough and the sample acquires a positive charge.⁶ The equilibrium potential on the surface of samples is also dependent on secondary electrons which are emitted from the samples as well as from the surroundings.

This build-up of positive charge on the sample surface can be seen in changes in the position and shapes of the peaks in the spectra. By ensuring that the sample does not accumulate charge, the peak width is narrower and experiment resolution is maximised. PES resolution is a direct function of peak width (expressed as FWHM), narrower lines generally mean higher spectral resolution.⁷ To counteract the effects, a flood gun can be employed to bombard the sample with secondary electrons that neutralise the sample.⁸ By removing the effects of charging, the spectral shifts are diminished significantly (typically < 10 eV) and peak distortion is minimised. However, the use of a flood gun can also cause some issues that should be considered prior to analysis. It has been shown that the use of flood gun can induce significant changes in samples morphology and electronics. A more recent study by Goodman have also used a flood gun to induce the removal of the organic ligands from gold phosphine cluster deposited onto TiO₂.⁹

In addition to using a flood gun, a reference is also required to calibrate the spectra. The reference peak must be one that is recognisably distinct and originates from a species that is commonly present and is in electrical equilibrium with the sample; typically adventitious carbon is used.¹⁰ Many organic components of samples may undergo rapid irreversible changes under the conditions of a PES experiment.

These changes can be caused by the need to reduce the interfacial energy of a system.⁷ When choosing a reference it is imperative that the peak is stable under experimental conditions.

The core level binding energy (BE) is defined as a difference in total energies between the ground state and the excited state of the system of interest. Core level binding energy shift is then defined as a secondary contribution to this energy of the peak. This second contribution can be broken in to two parts; the initial and final state contributions to the BE shift. This theoretical approach is used to model BE shifts as it is computationally more efficient than a total energy approach.² Binding energy shifts can also be viewed as a shift from the elemental binding energy of the element of interest.¹¹ Binding-energy shifts of core-level electrons were first detected by XPS in 1958, where copper (I) oxide was observed and distinguished from elemental form of copper.¹² It is now possible today to use core-level binding-energy shifts to identify a wide range of chemical species present on surfaces, which have important applications in polymer science, catalysis, nanomaterials and biotechnology. The BE shift in photoelectron spectroscopy can be viewed as analogous chemical shift seen in nuclear magnetic resonance (NMR), which allows fine details in the electronic structure of a molecular structure to be distinguished due to small chemical shifts associated with different magnetic environment for spin $\frac{1}{2}$ nuclei in a system.⁷ XPS is a powerful tool that can be used to identify not only the elements present in the upper surface layers of a material, but is also an important tool for exploring the chemistry at the surface. Recent advances in ambient pressure PES promise a range of new applications of XPS under more relevant conditions

For photoelectron experiments, there are several sources of photons which used such as Al $K\alpha$ X-ray source (1486.7 eV), Mg X-ray source (1253 eV) and also synchrotron radiation (0-2500 eV). From this early work with a lab based Mg source, it became apparent that resolution and signal to noise ratio would need to be improved and that the use of a flood gun should be minimised to ensure that beam-induced sample damage is limited. By using a synchrotron source of photons, many of these problems can be overcome. Synchrotron radiation is generated when electrons moving at relativistic speeds are accelerated by a magnetic field. Modern-day (third-generation) synchrotrons are typically composed of multiple linear sections interspersed with various magnetic structures that are used to control the light being generated: bending magnets, undulators and wigglers. As synchrotron radiation is a continuous source (between 100 – 2500 eV at the Australian Synchrotron), it is possible to tune the wavelength to match the cross-section of the elements of interest and thereby improve the surface sensitivity of the experiment. The response factor of an element is dependent on the energy of the incident photon energy; in the case of phosphorous the response factor increases significantly with decreasing photon energy (Figure 36). Hence, by choosing a

lower photon energy, the surface sensitivity and specific element sensitivity can be significantly improved for the elements of interest in this study.

These photoelectron experiments were conducted at the Soft X-ray Beamline at the Australian Synchrotron, in collaboration with Dr. Lars Thomsen (Australian Synchrotron), Dr. Greg Metha (University of Adelaide) and Dr. Gunther Anderson (Flinders University)

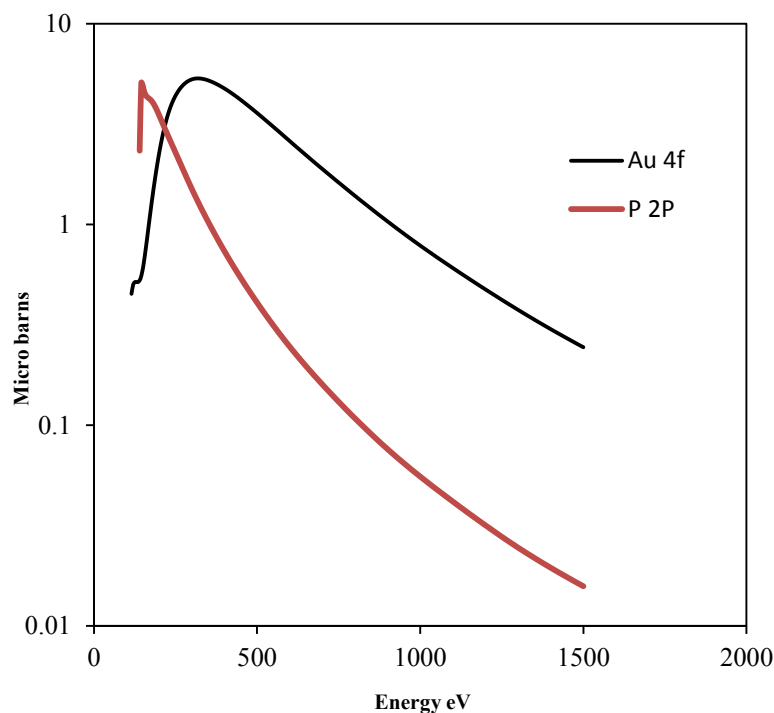


Figure 36: Elemental cross section for gold 4f and phosphorous 2p orbitals from reference ¹³

Photoelectron properties of supported gold particles

Early studies on gold

Although the pioneering work on gold catalysis was undertaken by Haruta and Hutchings in the late 1980s, it was the work of Wertheim that was focused on the electronic properties and binding energies shifts of gold clusters and nanoparticles during the early part of the eighties.¹⁴ These experiments typically consisted of the synthesis of polydisperse gold nanoparticles under UHV conditions by vaporising a gold source and depositing onto various types of amorphous carbon *in situ* i.e. the gold clusters were generated under UHV conditions and deposited on to various carbon substrates for analysis by PES rather than prepared by wet chemical methods. A shift to higher binding energies was usually observed for small clusters with poor electronic interaction with the carbon substrates.¹⁴⁻¹⁶

Whilst there is general agreement that the size and the electronic structure of the active components of the nanoparticles plays a critical role in catalytic processes, systematic studies revealing the electronic structure of chemically synthesized gold clusters for use as catalysts are still scarce. For this reason, PES is an important tool in identifying the electronic effects at play.¹⁷ For various gold systems, many studies have focussed on the $4f_{7/2}$ spin orbital of gold, since it provides a convenient and sensitive measure of the electronic state of gold. The valence orbitals, where the binding energy is between .1 eV to 15 eV, can be very difficult to study when multiple elements are present in a sample such as titanium, silicon, oxygen and carbon, due to the difficulty in the definitive assignment of the peaks.

The oxidation state of an element is a significant factor in determining the positions of its PES peaks. The position of the gold $4f_{7/2}$ peak is used to calibrate the energy scale for PES experiments. The literal gold standard is bulk gold (*i.e.* Au⁰), in which the $4f_{7/2}$ peak is defined as having an energy of 84.0 eV with a 3.67 eV separation to the $4f_{5/2}$ peak. Upon oxidation to Au₂O₃, the $4f_{7/2}$ peak shifts into the range 85.8 – 86.2 eV, depending upon the substrate.^{18,19} The thickness of the gold oxide layer have been estimated to be between 0.75 nm¹⁸ and 3.3 nm,¹⁹ providing the $4f_{7/2}$ peak position values for the macroscopic layer of gold oxide surface (*cf.* nanoparticles of Au₂O₃). Additionally, initial- and final-state effects determine the peak position and the full-width-at-half-maximum (FWHM) of the peaks, both of which depend on the element forming the cluster, its size and its interaction with the substrate.²⁰ Changes in the electronic structure associated with reducing the size of the nanoparticle (*cf.* the bulk metal) and changes to the interaction with the substrate contribute to the initial state effects.²⁰ After excitation, the metal nanoparticles stay in a charged state for a certain period of time, the length of which depends on the size of the cluster and the conductivity of the substrate. This is typically referred to as a final-state effect.²⁰ Therefore, the peak position and FWHM can provide information that is of fundamental importance for understanding the electronic structure of metal nanoparticles, whether they are prepared via gas-phase deposition or by wet-chemical methods. However, interpreting these changes in the peak positions as initial- or final-state effects based on experimental evidence can be difficult, as it is in the case of gold.^{20,21} In the present work, only changes in peak positions and shapes will be considered and they will not be interpreted as initial- or final-state effects.

Studies on small ligand-stabilised gold clusters

As the importance of the catalytic properties of gold became more apparent since these early experiments on the electronics of gold clusters, studies into the origin on this new catalytic ability of gold particles were conducted.²²⁻²⁵ A significant proportion of these studies have focused on the deposition of gold particles onto flat substrates under UHV conditions, which, at that time, offered limited size control of

the particles. Some studies had limited direct evidence of the particles size. More recently, with improved methodologies and technologies, mass-selected clusters have been deposited directly onto substrates and analysed by XPS and by Ultra-violet photoelectron spectroscopy (UPS), which allows the study of the valence orbitals.²⁶ These improvements have led to detailed studies on the effect of cluster charge and nuclearity on the activity of gold clusters for the activation of oxygen and carbon monoxide.^{27,28}

As previously discussed in chapter 2, ligand-stabilised metal clusters occupy a niche position in both catalysis and nanoparticle research areas due to their unique electronic and catalytic properties that are dependent on the number and type of metal atoms. Some of the larger clusters can have properties that are almost metallic in nature, could viewed as embryonic metals.²⁹ It has only been during the last 20 years that ligand-stabilised clusters have been used as heterogeneous catalysts.³⁰ These systems have typically been used as models for molecular catalysts, which provide important insights for further developments in the selectivity and reactivity of industrial catalysts. The main disadvantage to supported clusters as catalysts is the issue of particle agglomeration on the surface during the activation of the catalyst during the reaction.³¹ Although metal clusters are still viewed as model systems, there has been much progress with systems that involve site-isolation of the metal clusters, which inhibits sintering of the catalyst during the activation procedure and during the catalytic runs.^{32,33} These systems typically involve highly porous silicate or zeolite-type supports that prevent sintering by segregating the individual clusters inside the pores of the support.^{31,34}

Carbonyl-stabilised clusters have been used as precursors for a wide range of catalysts. Metal carbonyl chemistry has now been well established for many decades, and methodologies for the preparation of metal carbonyls is well documented in the literature.³¹ The carbonyl group is a very labile ligand that can be removed under vacuum at slightly elevated temperatures as compared to higher-temperature methods for removing an organic periphery. The reactivity of the catalyst, derived from a metal carbonyl cluster precursor, can often depend on how effective the decarbonylation was, the temperature at which the activation was conducted, the presence of hydrogen or oxygen and the strength of the interaction with the support material. Although carbonyl-type systems have proven useful for the preparation of model molecular catalysts, there is a wide range of clusters with a vast array of differing organic ligands. The ligands are often phosphines, thiols and even arsines.³¹ These strongly bound ligands can often remain intact once the cluster is adsorbed on to the support material and then require treatment to activate the systems. Reports on these activation conditions vary significantly on the effectiveness of each procedure for activation. The ultimate fate of the ligands is also rarely considered.³¹ Examination of the resultant catalysts by photoelectron spectroscopy can not only yield information on the metal oxidation state, but also reveal

what became of the ligands and other stabilised reagents. Due to issues with sensitivity and charging of the sample, it can often prove difficult to distinguish between small amounts of ligand from the background. Hence, by using synchrotron radiation, it may be possible to uncover whether small amounts of ligands remain on surface of the activated catalyst.

Recent studies on the electronic properties of supported small gold particles

Over the last decade there have been a number of studies of sub-monolayer gold films *i.e.* gold clusters deposited onto various substrates and of chemically synthesised clusters in various matrices. A large variety of results has been reported. The difficulty with finding a unifying thread between these studies is the uncertainty in particle size, particularly below 1 nm, where exact size determination is difficult. Over the next few pages, a succinct summary of the literature on PES studies on supported organometallic gold clusters will be presented with several comparisons to UHV studies of sub-monolayer gold films. Several reports from the early 1980s on the PES of organometallic clusters are only briefly discussed as experimental methodologies and techniques have advanced significantly.

The earliest PES study of supported organometallic gold clusters was reported by Goodman *et al.*, where the $[\text{Au}_6(\text{PPh}_3)_6][\text{BF}_4]_2$ cluster was used as the gold source.⁹ The cluster was deposited by a solution deposition method on to a flat surface of a titania (110) crystal. Electron-stimulated desorption (ESD) was performed to remove the organic ligands, which involves bombarding the sample with electrons to remove the phosphine ligands and clean the surface of the sample. Cluster agglomeration on the surface was prevented by pre-treatment of the surface by sonication in acetone. XPS results revealed that the Au $4f_{7/2}$ peak shifted from 83.9 eV to 84.3 eV after treatment with ESD. This shift is believed to be caused by increased screening of electrons due to the removal of the ligands.⁹ It should be noted that these XPS studies were conducted using a lab based Mg $K\alpha$ source with $h\nu = 1253.6\text{eV}$; the elemental cross-section is quite low for gold and phosphorous at this photon energy. As a result, it proved difficult to confirm what the ultimate fate of the phosphorous was as a result of ESD treatment. By using a synchrotron source, the photon energy for the experiment can be chosen to significantly improve the elemental response. The experiments also relied on repetitive scans on the same spot (up to 475 sweeps) to gain improved signal to noise ratio, which could have induced significant beam damage. The report does not say whether scanning tunnelling microscopy (STM) was conducted after the XPS experiments, which would confirm whether any beam-induced particle sintering occurred. The Au $4f$ peaks were fitted with a Gaussian line shape and the background subtraction was conducted using a cumulative function. Recently, more rigorous background correction methodologies and curve-fitting procedures have become more accessible, such as the improved Shirley background correction,³⁵ Tougaard background correction³⁶ and Voigt function based peak fitting.³⁷

It should also be noted that, from a visual inspection of the XPS spectra presented, that the gold 4f peak has shifted by +0.4eV upon treatment by ESD, and the FWHM also increases, as does the peak asymmetry.

Goodman *et al.* have also demonstrated how the catalytic activity of gold is strongly dependent upon the particle size and the appearance of non-metallic properties of the gold particles.²³ This early study focused on using STM to probe the reactivity of gold particles (1 nm – 6 nm) on cleaned titania (110) surfaces and the effect of catalytic conditions. Preliminary XPS studies were also conducted on the samples with a lab-based photon source. The main peak reported was the Ti 2p, which highlighted that the small shoulder peak attributed to Ti³⁺ (458 eV) disappeared due to exposure to carbon monoxide and oxygen, whilst the area of the Ti⁴⁺ (460 eV) peak increased. This subtle shift in peak intensities highlighted the electronic interaction between the titania support and the support gold particles.

The thermal stability of gold nanoparticles on a cleaned flat titania (110) was investigated in detail by Behm *et al.*,²⁴ where the stability of gold nanoparticles with sizes ranging from 2.5 – 4 nm in diameter under various conditions (oxygen, air and UHV) were characterised by XPS and AFM.^{24,38} It was found that under UHV conditions the particles were stable to annealing at 400°C. In the presence of 50 mbar of oxygen, the nanoparticles were stable at room temperature; however, after annealing at 400°C, the particles were found to have sintered significantly. It is believed that gold nanoparticles sinter by an atomic mechanism (or Ostwald ripening) as proposed by Campbell.³⁹ In contrast, annealing under a hydrogen atmosphere at 200°C had little or no effect on the structure of the gold nanoparticles on titania surface. It was surmised that oxygen has a significant influence on the stability of gold based catalysts, and that this effect becomes more significant at elevated temperatures. It was also demonstrated that gold nanoparticle sintering increases substantially under UHV conditions at 500°C. The gold nanoparticles were shown to have a binding energy of approximately 84.3 – 84.4 eV, and a second peak appears at 85.7 eV, which can tentatively attributed to gold hydroxide species forming on the surface.⁴⁰

These recent studies by Behm³⁸ and Campbell^{39,41} have been aimed at understanding the driving force behind the sintering of gold particles on oxidised titania surfaces and developing improved methodologies to activate gold-based catalysts under mild conditions. Behm has shown the potential of activating gold based systems under a reducing atmosphere using gold nanoparticles generated by a modified deposition-precipitation procedure.²⁵ In this system a gold salt was added to a suspension of titania (20 – 25 nm particles) and then reduced to form gold nanoparticles. Two contrasting conditioning procedures were compared;

- calcination at 400°C under a 10% O₂/N₂ for 30 minutes
- annealing at 200 °C under H₂/N₂

The reactivity of the resultant catalysts was shown to be significantly greater for the system that was annealed under hydrogen rather than oxygen.

Büttner *et al.* evaporated gold onto pristine highly ordered pyrolytic graphite (HOPG) and defect-rich HOPG, to form sub-monolayer layers of surface gold, which was bombarded with argon ions to removed organic impurities. No peak shifts were found on the ordered surface, whereas gold on the defect-rich HOPG showed peak shifts of up to +1.5 eV, with appearance of multiple peaks and peak broadening.⁴² The authors attribute the peak shift and broadening to the preferential formation of gold particles at the defect sites, which occur in a much higher number on the HOPG exposed to argon bombardment. Kitsudo *et al.* evaporated gold onto graphite and various metal oxides.⁴³ The gold peaks did not shift on the graphite and nickel oxide (001) substrates. However, peak shifts of up to +0.4 eV were observed on SrTiO₃, Al₂O_x/NiAl (110), titania and nickel oxide (111) at sub-monolayer gold coverage. Importantly, on both SrTiO₃ and graphite the FWHM of the gold peak decreased slightly with increasing particle size. Lykhach *et al.* evaporated gold on Nb₂O₅/Nb, Nb₂O₅/W and NbO/Nb surfaces.⁴⁴ They found shifts in the gold peak position of up to +0.7 eV, with the largest shifts observed for the smallest Au coverage *i.e.* the smallest gold nanoparticles. Lim *et al.* evaporated gold on SiO₂/Si and observed shifts of the gold peak of up to +1 eV. Again, the largest shift corresponded to the smallest amount of gold evaporated. Exposure to atomic oxygen leads to the appearance of a second peak at about 86 eV, attributed to the formation of Au₂O₃.⁴⁵

Methods for depositing size-selected clusters, produced under gas-phase conditions, have been known for over a decade. Di Cenzo *et al.* collected the photoelectron spectra for gas-phase size-selected Au_{*n*} clusters, deposited on amorphous carbon. For clusters with *n* = 5, 7, 27 and 33 they observed shifts of +0.7, +0.6, +0.5 and +0.5 eV, respectively for the Au 4f_{7/2} peak, with FWHM being broader for the smaller clusters.⁴⁶ Cox *et al.* reported Au 4f_{7/2} XPS data for gas-phase, size-selected, positively charged clusters deposited on silica (natural oxide layer on Si (100)-wafers). They observed shifts of +0.8-1.0 eV for Au_{*n*} (*n* = 1-7).⁴⁷ More recently, Lim *et al.* have published a series of papers where mass-selected Au cluster anions of up to 20 atoms were deposited onto SiO₂/Si surfaces and the samples were subsequently exposed to atomic oxygen.^{45,48-50} Although peak widths of 1.5 eV were observed, in addition to Au⁰ peaks, the clusters also exhibited features attributed to Au^{III}, which were shifted by +1.5 eV with respect to bulk gold. Interestingly, an even-odd effect was observed, whereby the odd-numbered clusters appeared inert towards oxidation and exhibited small Au^{III} peaks, particularly so for Au₅, Au₇ and Au₁₃ clusters. These workers also deposited the same gold clusters on sputter-damaged HOPG, which increased the number of defects present on the surface. In this case, only Au₈ showed any ability to act as catalytic oxidant after oxygen treatment. Small gold peak shifts of +0.1 eV to +0.2 eV were observed relative to bulk gold.

XPS studies have also been performed on chemically synthesised, ligand-protected gold species; from monoatomic Au compounds (*e.g.* Au(PPh₃)(NO₃)), to atomically precise Au clusters (*e.g.* Au₈(PPh₃)₈(NO₃)₃), to larger, less precise, nanoparticles spanning the size range from *ca.* 1.5 nm (“Au₁₀₁”)⁵¹ and above. Yuan *et al.* have deposited Au(PPh₃)(NO₃) on Ti(OH)₄ and titania and observed a gold 4f_{7/2} peak with a binding energy of 85.5 eV in the first case and 84.8 eV in the latter case, attributing the difference to interactions of the clusters with the substrate.⁵² Very early XPS studies by Battistoni *et al.* investigated Au₁, Au₄, Au₈, Au₉ and Au₁₁ clusters stabilised by triphenylphosphine ligands.^{53,54} Samples deposited from alcohol solutions onto a polished steel sample plate showed Au binding energies that were 0.7 to 1.7 eV higher than for bulk gold, which depended upon the number of ligands and the counter ions. By analysing the different peak shapes, it was concluded that Au₉ and Au₁₁ cluster possess centred polyhedral geometries with a central metal atom involved only in metal-metal bonds. Van Attekum and co-workers similarly published an XPS analyses of chemically synthesised Au₈, Au₉ and Au₁₁ clusters stabilised by triarylphosphine ligands.⁵⁵ The clusters were evaporated onto graphite substrates from solutions in dichloromethane. All clusters exhibited a single Au 4f_{7/2} peaks with widths of 1.5 eV. Only kinetic energy values were presented and calibrated relative to the phosphorous peak; however, the phosphorous peak could be subject to a chemical shift so the peak positions may not be reliable. Boyen *et al.* used XPS to investigate a series of gold nanoparticles made using polymers as stabilizing agents, with metal core sizes ranging from 2.9 down to 0.8 nm deposited on silicon. Following removal of stabilizers by treatment, first with oxygen and subsequently with hydrogen plasma, the authors found peak shifts of up to +0.5 eV at their smallest cluster size.⁵⁶ The same authors found that phosphine stabilized 1.4-nm (similar size as Au₁₀₁)⁵¹ nanoparticles show an Au 4f_{7/2} peak at 84.2 eV after oxygen/hydrogen plasma treatment. Ono *et al.* reported results for polymer-stabilised gold particles with peak positions of about 85 eV for 1.5-nm gold and about 87 eV for oxidised 1.5 nm gold-clusters on both titania and silica substrates following treatment at 150 K with oxygen plasma only.⁵⁷ Upon heating, they observed very fast decomposition of gold oxide species (within 6 min at 350 K) for the nanoparticles supported on titania, which was in stark contrast to much greater stability in the case of silica-supported gold oxide species. More recently, Turner *et al.* found the Au 4f_{7/2} peak of 1.5-nm gold clusters deposited on boron nitride at a binding energy of 85.1 eV.⁵⁸ The electronic influence of the ligands stabilising the clusters was highlighted by Tsukuda *et al.*⁵⁹ In their work, these PVP-40 stabilised gold nanoparticles had a binding energy of 82.7 eV for the 4f_{7/2} peak, which contrasts with the thiol stabilised Au₃₆ cluster, which has a 4f_{7/2} binding energy of 84.6 eV. This significant drop is attributed to the electronic donation from the carbonyl moiety of the pyrrolidine monomer. It should be noted that the cationic nature of the PVP-stabilised gold nanoparticles could also be the result of final-state effects due excess amount of polymer being present.

In summary, smaller clusters tend to exhibit higher binding energy shifts, with the binding energy converging to the bulk value of 84.0 eV for larger sizes.^{43,46,56,60,61} In many cases the FWHM also shows an increase with decreasing cluster size.⁶² The shift, however, also strongly depends on the substrate. For “inert” substrates such as HOPG and pure Si, only small shifts, <0.1 eV, are typically observed. SiO₂ surfaces tend to shift the peaks by ~0.2 eV to higher energy. Highly interacting surfaces such as CeO₂, TiO₂, SrTiO₃, Al₂O₃ and NiO (111) can induce shifts up to 1.5 eV.

Experimental

I. Preliminary XPS experiments

Our first PES experiments of supported gold phosphine clusters were conducted by Dimitri Murzin at the University of Turku in Finland. XPS measurements were carried out in a PHI Quantum 2000 Scanning ESCA Microprobe spectrometer with Al K α X-ray source with a photon energy of 1486.7 eV. Samples were analysed as powders deposited on double-sided carbon tape which was purchased from 3M and sample charging was compensated by using a flood gun. From this early work, it became apparent that resolution and signal to noise ratio would need to be improved and that the use of a flood gun should be minimised to ensure that beam-induced sample damage is limited.

II. Photoelectron experiments at the Soft X-Ray Beamline

Our first experiments at the SXR facility were hampered due to issues of sample charging, which were overcome in subsequent visits by depositing the titania samples thinly on P-doped silica wafers that were then attached on to the backing plate of the sample holder with carbon tape. Sample preparation was found to be an important factor for acquiring quality data. In the case of the silica samples, sample charging was unable to be overcome by several sample preparation techniques. Modified experimental set-ups were used with the expectation that the lower intensity of photon beam would decrease the magnitude of the sample charging; however, suitable resolution of the small gold peak proved difficult to achieve. The focus of the PES experiments detailed in the results section will be on the titania supported samples

These early experiments were conducted at a photon energy of 700 eV. For a typical catalyst sample, 1 mg of sample was suspended in methanol (5 mL) and sonicated briefly to ensure a homogenous suspension. For the unconditioned samples it was necessary to use a solvent that would not remove the

cluster from the substrate (typically hexane or toluene). One drop ($\sim 20 \mu\text{L}$) of each sample was deposited onto a cleaned $6 \text{ mm} \times 6 \text{ mm}$ silicon (Si) wafer and air dried. Up to 10 samples were then affixed by double-sided copper tape onto a gold-plated backing plate and the XPS spectra were recorded using a SPECS Phoibos 150 hemispherical electron analyser with the photon energy set to 650 eV. The photon energy was modified from 700 eV, in order to shift the silicon and oxygen Auger peaks to positions that did not interfere with the photoelectron peaks of interest for our study. No sample cleaning with Ar^+ sputtering or sample annealing under UHV conditions were undertaken as this can lead to significantly different results.^{23,63} This is believed to be due to partially reduced surface regions, which can alter binding energy shifts and the chemical reactivity of the surface. The beam was adjusted to yield an irradiation spot size of $600 \mu\text{m}$, yielding an X-ray photon flux of approximately $10^{12} \text{ photons mm}^{-2} \text{ s}^{-1}$, conditions that have recently been shown to not induce thermal damage to samples of NaAuCl_4 .⁶⁴ XPS spectra were recorded by scanning the electron analyzer in 0.05 eV increments from 200 to 70 eV to observe signals from C, O, Si, P, Ti and Au. The electron analyzer pass energy was set to 10 eV, yielding an instrumental kinetic energy resolution of 295 meV.⁶⁵ Scans were repeated several times to ensure that no photon-induced changes were occurring to the samples. Spectra were calibrated using the Au $4f_{7/2}$ peak (84.0 eV) of the gold reference bar, which was located permanently in the analyser chamber. The sample sensitivity to the intense source photons was tested by designing a scan protocol that involved seventeen high resolution short scans of the peak of interest enabling detection of any shift in peak position due to beam damage. The raw data were then summed together for analysis.

III. Preparation of the reference samples and recording of the reference spectra

Samples for measuring photoelectron reference spectra of the gold cluster were prepared by drop casting two droplets of a 1 mg/cm^3 isopropanol solution of the Au_n cluster on a silicon wafer covered with 10 nm of atomic layer deposited (ALD) titania. The solution was left drying in air. The photoelectron spectra of the reference samples were recorded using a non-monochromatic Mg- $K\alpha$ radiation and a Phoibos 100 electron energy analyser from SPECS in a vacuum chamber with a base pressure of $\sim 10^{-10}$ mbar.

IV Data analysis I: Background correction

The photoelectron peaks are superimposed on a rather high and strongly structured background, so to produce the background-free line shape, one has to remove the assumed contribution due to inelastic scattering.³⁵ Inelastic scattering occurs when the kinetic energy of incident particle (electron in this case) is altered by the scattering process. The main contribution to this background is due to energy loss processes, roughly categorized as extrinsic (occurring away from the emitting atomic centre, through the response of

the loosely bound electrons to the probing electron) and intrinsic (occurring in the close vicinity of the emitting atomic centre through the response of the core).

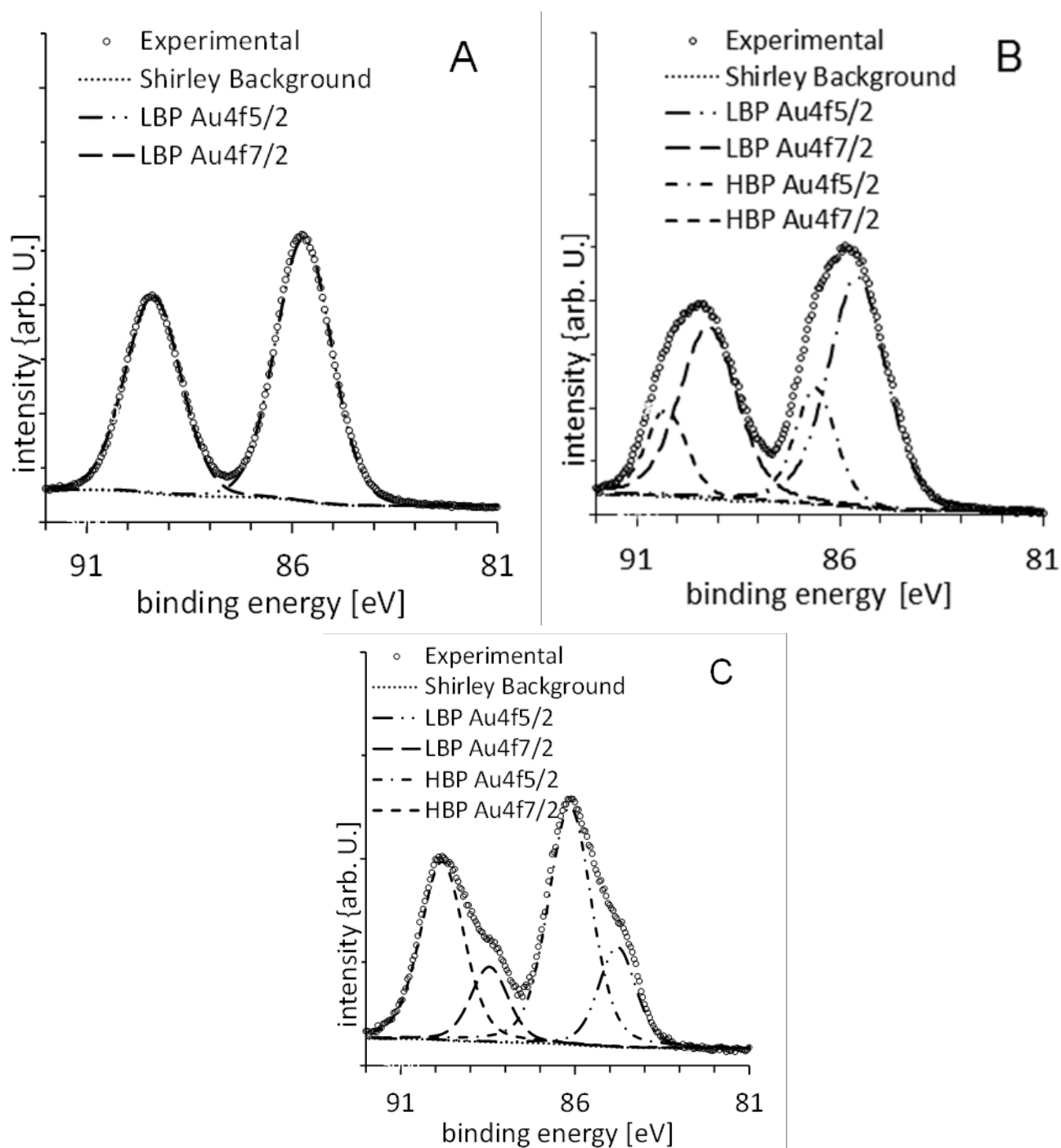


Figure 37: An example of the fitted gold 4f peaks of the supported Au₉ spectra: A) the untreated cluster, B) the washed and C) the calcined cluster. High Binding Energy peak (HBP) and Low Binding Energy peak (LBP)

It is generally accepted that a linear background underestimates significantly the “true background” at the high-energy side of a peak while the opposite is true at lower binding energy. The Shirley method assumes that the background at any energy to be due to inelastic scattering of electrons of higher kinetic energy and is thus proportional to the integrated photoelectron current intensity for higher kinetic energy electrons.³⁶ Another aspect is the criterion of the goodness of fit of the background. Originally Shirley said:

“In making the correction it was observed that the spectrum returned to a constant level at kinetic energies below those of the valence bands.”⁶⁶ The classic Shirley background assumes two background regions with constant intensity on both sides of the peak. It has also been argued that the plasmon losses and asymmetric broadening may be misinterpreted as part of the inelastic background, which may affect the curve fitting process.⁶⁷ An improved Shirley background was applied to remove the electron-scattering background and maintain the inherent line shape from the raw data as described Vegh.^{36,68}

V Data Analysis II: Curve fitting

All XPS spectra were fitted in the following manner after the background was corrected. A pseudo-Voigt function composed of the sum of Gaussian (30%) and Lorentzian (70%) components was used and all peak positions were allowed to vary using nonlinear least-squares minimization.⁶⁹ For the Au 4f spin-orbit peaks (*i.e.* 4f_{7/2} and 4f_{5/2}), energy splitting was fixed at 3.67 eV, while for the P 2p doublet a splitting of 0.84 eV was used. The energy difference between the high binding energy peaks (HBP) to the lower binding energy peak (LBP) is fixed due to spin-orbit coupling. All spectra were fitted with the least number of peaks allowing a variation of the FWHM. The FWHMs of the bands associated with a single species however were kept constant. This means that a gold spectrum was fitted with two sets of 4f_{7/2} and 4f_{5/2} doublets, the FWHM within a single doublet was kept constant but was allowed to differ between the doublets.^{36,68,69}

$$fpv(x) = (1 - \eta)fg(x; \gamma g) + \eta fl(x; \gamma l)$$

$$fg(x; \gamma g) = \left(1/\pi^{1/2} \gamma g\right) \exp\left(-\frac{x^2}{\gamma^2 g}\right)$$

$$fl(x; \gamma l) = (1/\pi \gamma l) \left(1 + \frac{x^2}{\gamma^2 l}\right)^{-1}$$

Equation 2: Pseudo-Voigt function (*fpv*) consisting of the sum of Gaussian (*fg*) (30%) and Lorentzian (*fl*) (70%) components, η is the parameter which mixes the two functions.

Cross sections were calculated according to Yeh and Lindau using the photoionization cross section and the asymmetry parameter.¹³ The angle between the direction of the incident synchrotron radiation and the emission of the electrons (direction from the target to the detector) was 125°. The angle between the emission of the electrons and the plane span of the polarisation vector of the X-ray and the direction of the synchrotron radiation was 0°.

VI. Data Analysis III: Normalisation of the gold intensity

The gold signal needed to be normalised against the silicon dioxide of signal, as the prepared sample was inhomogeneous, according to

Equation 3: Calculation for normalisation of gold intensity

$$I_{\text{Au}}^{\text{norm}} = I_{\text{Au}} / \left(1 - \left(I_{\text{Si,Si}} + I_{\text{Si,SiO}_2} + I_{\text{O,SiO}_2} \right) \right)$$

where $I_{\text{Au}}^{\text{norm}}$ is the normalised gold intensity, I_{Au} is the relative gold intensity, $I_{\text{Si,Si}}$ the relative intensity of silicon in the silicon substrate, $I_{\text{Si,SiO}_2}$ the relative intensity of silicon in the native SiO_2 layer at the surface of the Si wafers and $I_{\text{O,SiO}_2}$ the relative intensity of the oxygen of the silicon dioxide layer covering the silicon substrate. Relative intensity means that the intensity element is normalised by its photo-ionisation cross section and divided by the sum of the intensities of all elements detected. Thus $\left(I_{\text{Si,Si}} + I_{\text{Si,SiO}_2} + I_{\text{O,SiO}_2} \right)$ and $\left(1 - \left(I_{\text{Si,Si}} + I_{\text{Si,SiO}_2} + I_{\text{O,SiO}_2} \right) \right)$, respectively, represent the fractions of the surface not covered or covered by titania particles. The uncertainty of the normalisation procedure is the largest contribution to the error bar of the gold intensity in Figure 54B

VII. Data analysis IV: Relative intensity of the phosphorous spectra

For the quantitative analysis of the phosphorous intensity only the phosphorous-to-gold ratio has been considered. The ratio is calculated as

Equation 4: Calculation for the relative intensity of the phosphorous spectra

$$I_{\text{P-Au}}^{\text{ratio}} = I_{\text{P}} / I_{\text{Au}}$$

where I_{P} is the phosphorous intensity and I_{Au} the gold intensity.

VIII. Survey Scan

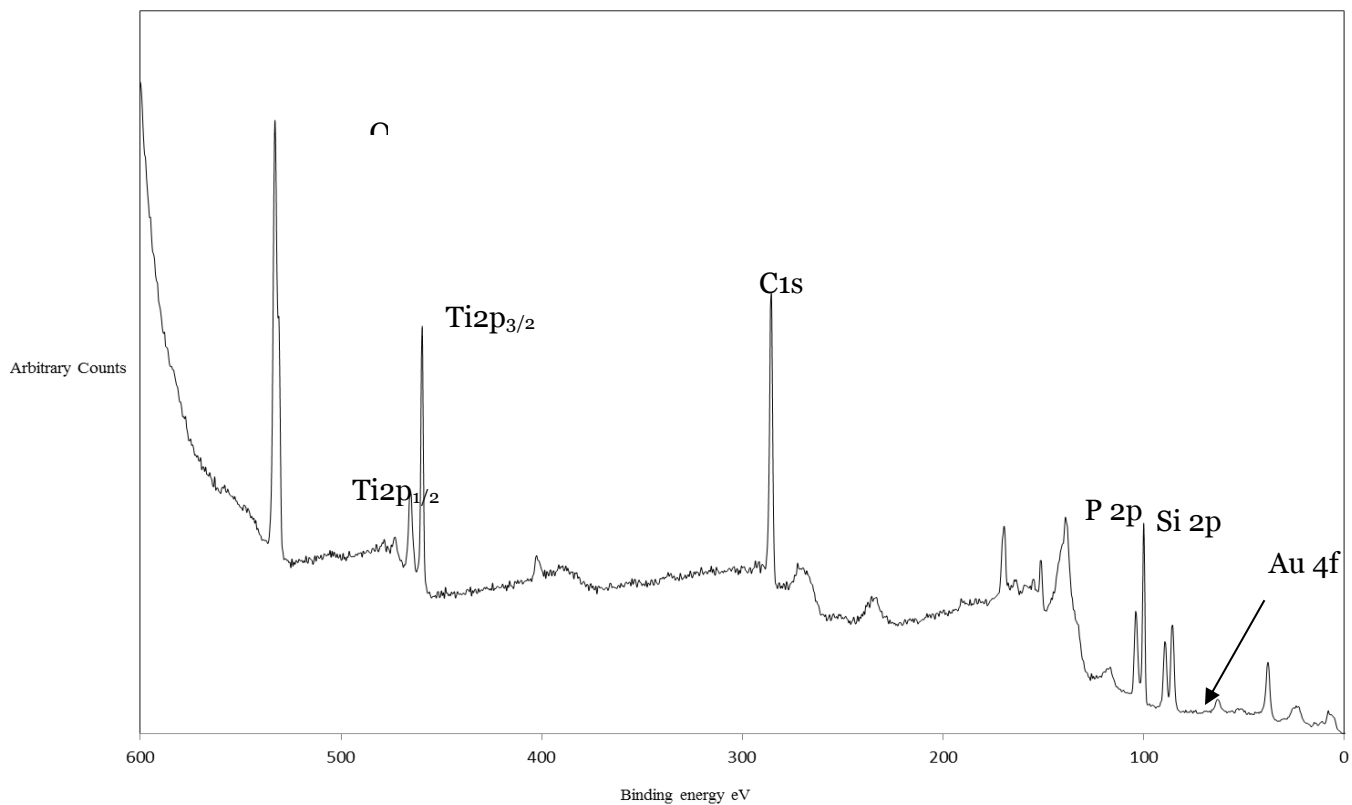


Figure 38: Survey scan of a supported Au₉ cluster supported on acid washed titania. The peaks of interest have been identified, of which high resolution scans were conducted after a survey scan was conducted.

Results and Discussion

Preliminary experiments

Preliminary XPS experiments were conducted on a lab-based machine (PHI Quantum 2000 Scanning ESCA). Spectra were taken of the gold 4f, silicon 2p, titanium 2p, oxygen 1s and carbon 1s regions for a few select samples. The carbon signal is attributed primarily to the carbon tape that the samples were deposited upon. For the gold clusters on silica samples, the gold 4f signal is derived from the gold phosphine cluster. The gold loading on average for most of these early samples was 0.5 %; for several lower-loaded samples (0.1 % loading) a gold peak was not detected. The silicon signal is mainly attributed to the amorphous silicon support and is found at 103.43 eV (Si^{4+} 2p_{1/2}). For the silicon-supported samples, the oxygen peak at 532.73 eV (O 1s) is mainly due to the oxygen bound to the silicon, whilst for the titania-supported samples the oxygen peaks were at 530.95 eV (adsorbed H₂O) and at 529.79 eV, the latter being attributed to oxygen from the titania support. There was no detectable signal for phosphorous which was assumed to be bound to the cluster. There are several possible reasons for the absence of the phosphorous signal, the most likely of which is that the amount of phosphorous present was below the detection limits of the instrument. Another significant experimental factor that may explain the absence of a phosphorous peak was the use of an electron flood gun, which can induce significant loss of organic ligands as shown by Goodman and workers.⁹ Figure 39 shows a typical survey scan of each of the peaks of interest for sample of 0.5 % Au₀/SiO₂, heat treated at 200 °C under vacuum for 2 hours.

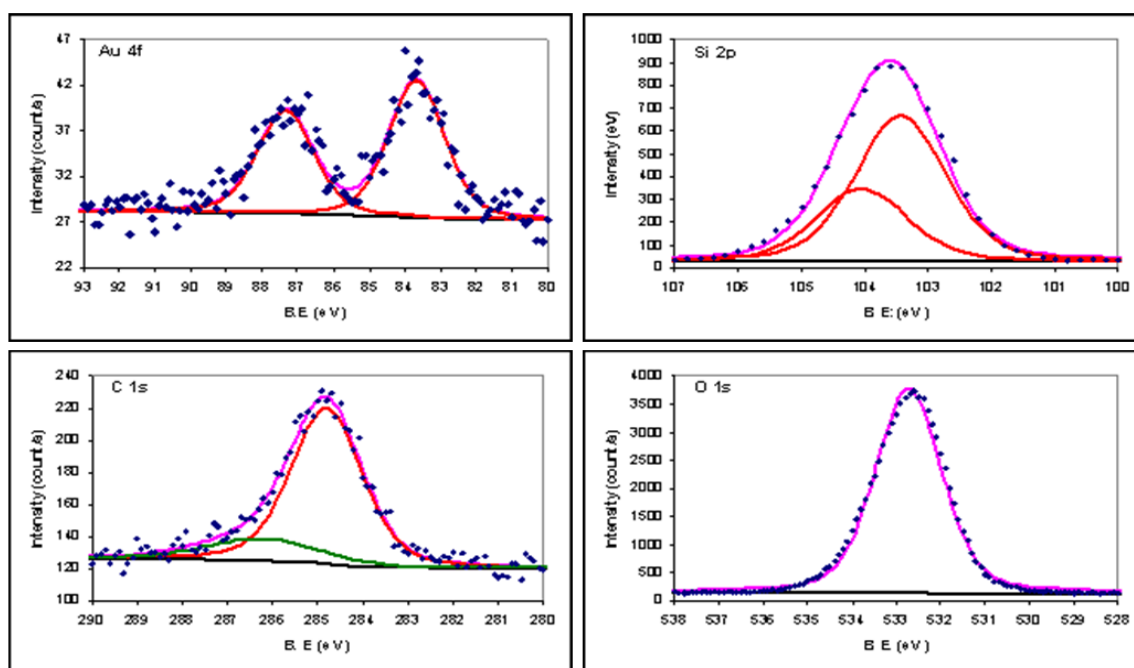


Figure 40: XPS survey scans of the elements present, performed with a photon energy of 1486.7 eV, of Au₀/SiO₂ heat treated at 200°C under vacuum

Figure 41A suggests that there is only one gold species present with a $4f_{7/2}$ binding energy of 83.7 eV, which is slightly lower than bulk gold (84.0 eV) indicating slight anionic ($\text{Au}^{\delta-}$) character of the gold present on the surface. A BE shift to lower binding energy can be attributed to particles with dimension smaller than 2 nm, due the larger electron density localised on the surface on the cluster and the poor electronic interaction between the support and the cluster. In Figure 42B, the sample 0.5 % $\text{Au}_{11}/\text{SiO}_2$ (untreated, as deposited) indicates a cationic contribution to the gold signal of 85.6 eV, which is lower than the binding energy corresponding to Au^{3+} . In this sample the FWHM of the peak at 83.8 eV is 2.18 eV, which is larger than that observed in samples where only one gold peak is required for curve fitting (e.g. 1.86 eV observed the 0.5 % Au_9/SiO_2). However, the resolution limit of this lab-based spectrometer is 0.55 eV in high resolution mode. When two or more species are identified the peaks become broader than is observed in samples with only one contribution.

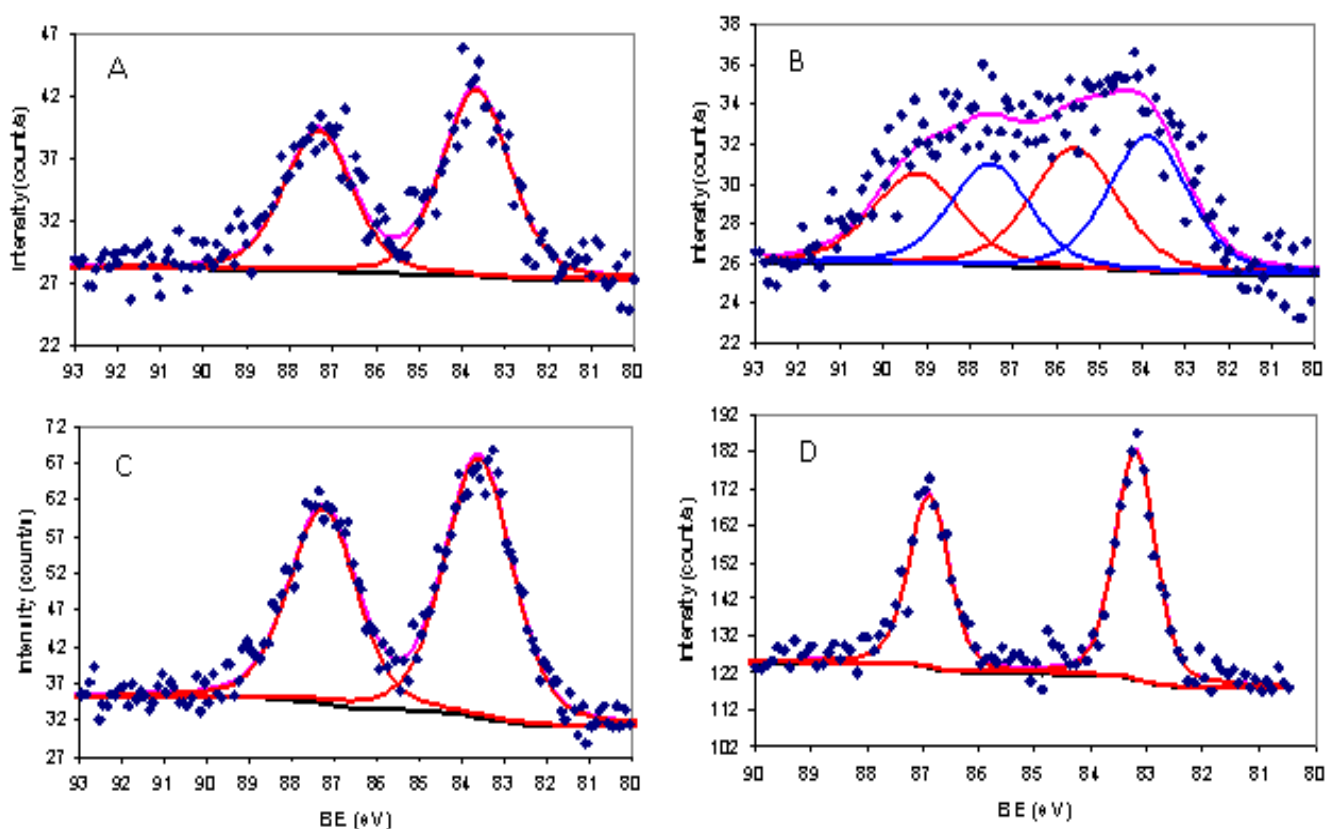


Figure 43: A comparison of the photoelectron gold 4f peak of A) Au_9/SiO_2 0.5% B) $\text{Au}_{11}/\text{SiO}_2$ 0.5% C) $\text{Au}_{55}/\text{SiO}_2$ 0.5% D) $\text{Au}_{55}/\text{TiO}_2$ 0.5%, conducted on lab based XPS machine. All samples were heated at 200°C under vacuum for two hours.

In Figure 44C, for the sample 0.5 % Au₅₅/SiO₂, heat treated @ 200°C under vacuum, there is only one gold species detected with a binding energy of 83.6 eV. For these silica-supported gold cluster samples, the gold 4f peak shows the presence of anionic gold (Au^{δ-}) with a binding energy lower than that of metallic gold (84.0 eV). A BE shift to lower binding energy can be attributed to particles with dimension smaller than 2 nm, due the larger electron density localised on the surface on the cluster and the poor electronic interaction between the support and the cluster. In Figure 45D, the sample 0.5 % Au₅₅/TiO₂, the gold 4f_{7/2} peak is shifted to a binding energy of 83.21eV which indicates a much more anionic nature than for Au/SiO₂ samples, and is assumed to be caused by increased electronic interaction with the support and due to small size of the gold particles on the surface.

Overall, these preliminary studies of this small selection of nanostructured gold catalysts highlighted a number of issues. The low gold loadings of these samples ($\approx 0.5\%$), as compared to many other supported metal nanoparticle catalysts ($> 1\%$), can make data collection difficult due issues with detection limits of a lab based machine. Increasing the amount of sample can lead to significant sample charging; hence the balance between sample charging and getting a signal for the gold peak can be difficult to achieve. In addition, the small amount of charging, due to the electrically insulating nature of silica, required a flood gun to neutralise the charge. From these experiments it is not clear if the presence of the anionic gold species is an initial- or final- state effect.

Samples were studied on the SXR at the Australian Synchrotron, in an attempt to deal with issues of sensitivity.

High resolution studies at 650 eV

Spectra have been taken at the gold 4f, phosphorous 2p, silicon 2p, titanium 2p, carbon 2s and oxygen 1s regions for Au_n clusters deposited on titania nanoparticles and from a gold reference sample at the SXR beamline at the Australian Synchrotron. The majority of carbon on the samples is either from the triphenylphosphine ligands of the gold cluster or adventitious hydrocarbons. In either case, we assigned the C 1s peak to 285.0 eV and used it for calibrating the peak positions of other elements. This is justified because adventitious hydrocarbons display very stable C 1s peak position and are present in all samples exposed to air (and not cleaned by sputtering *etc.* prior to XPS measurements).⁷⁰ The titanium signal is exclusively due to the titania nanoparticles and is found at 459.0 ± 0.1 eV. The silicon signals are due to the silicon wafer substrate and found at 99.2 ± 0.1 eV (Si) and 103.1 ± 0.1 eV (SiO₂). The oxygen signals are mostly due to titanium dioxide (530.3 ± 0.1 eV) and silicon dioxide (532.4 ± 0.1 eV). Gold signals due to clusters are found between 83.7 and 86.1 eV. Phosphorous signals, from the ligands, are found at 131.8 ± 0.1

eV and 133.0 ± 0.2 eV. The Au and P signals are used for quantitative analysis. At the energy calibration used here, Au $4f_{7/2}$ signal of bulk gold is usually found at within a range of ± 0.2 eV 84.0 eV,⁷⁰⁻⁷³ and this value is used here to determine the shift between the Au $4f_{7/2}$ signal of the gold clusters and the bulk gold binding energy. The invariance of the titanium and silicon signals relative to the gold reference is less than 0.05 eV, indicating that there is no charging of the samples or instability in the beam, which meant that no flood gun was required during the measurements.

The Au $4f$ spectra for the Au₈, Au₉, Au₁₁ and Au₁₀₁ clusters supported on acid-washed Evonik P-25 titania are shown in Figure 46 for untreated (*i.e.* as deposited) clusters (Figure 46A), samples washed after deposition (Figure 51A) and calcined samples (Figure 54)

Untreated samples on acid washed titania

In the spectra of the untreated samples, the gold peaks shift towards higher binding energies with decreasing number of atoms in the metal cluster. All four spectra can be fitted with two peaks, one each for the Au $4f_{7/2}$ and Au $4f_{5/2}$ components. The Au $4f_{7/2}$ peak positions and FWHMs are shown in Figure 46B (which will be discussed below, these peaks are referred to as the gold low binding peak, Au-LBP). The positions of all peaks except for Au₁₀₁ are at a higher binding energy than that of metallic gold.

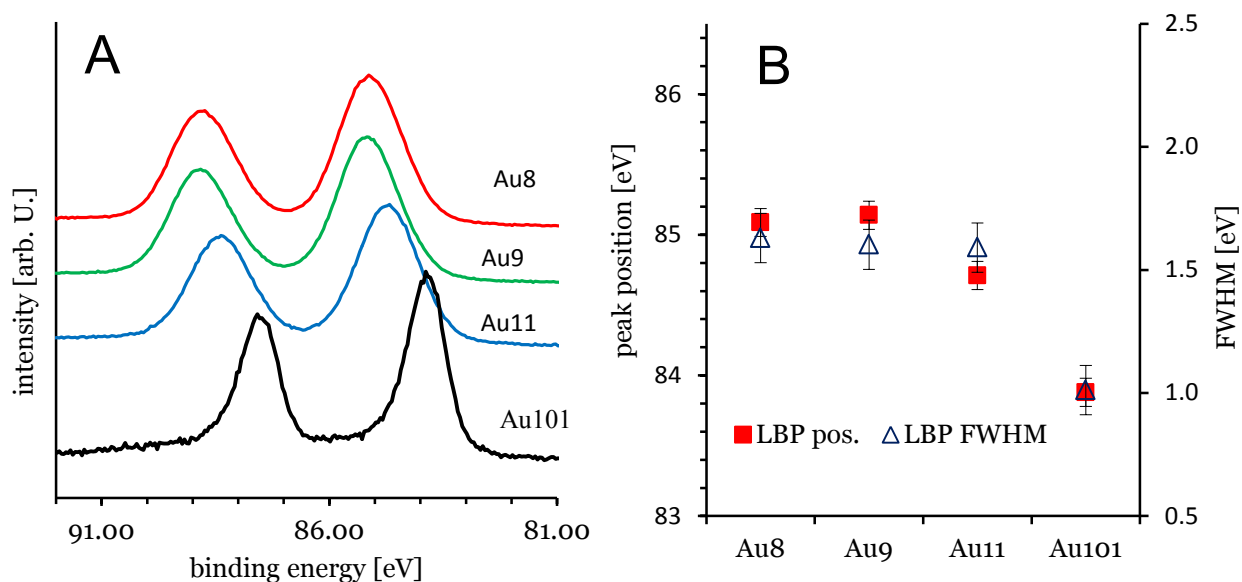


Figure 46: A) XPS spectra of untreated Au_n and B) $4f_{7/2}$ binding position of the Au LBP and FWHM of the peaks

The FWHMs of Au₈, Au₉ and Au₁₁ are the same within experimental error but all are larger than that for Au₁₀₁. Shifts in the peak position and an increase in the FWHM of the XPS signal of particles consisting of a small number of metal atoms have been attributed, in a number of cases, to finite-size effects and

depend on the element constituting the nano-sized object, as well as the substrate on which they are deposited.^{43,74} In the case of gold, peak shifts up to +1.5 eV,⁷⁵ +0.7 eV,^{14,76} and +1.1 eV have been previously reported. In all cases, an increase of the FWHM relative to that of bulk gold signal has also been reported. Thus, we attribute the shift of the gold peak position to the decrease in size of the gold cluster. The peak positions relative to the bulk gold Au4f_{7/2} found here are +1.1 eV for Au₈ and Au₉, +0.7 eV for Au₁₁ and -0.1 eV for Au₁₀₁.

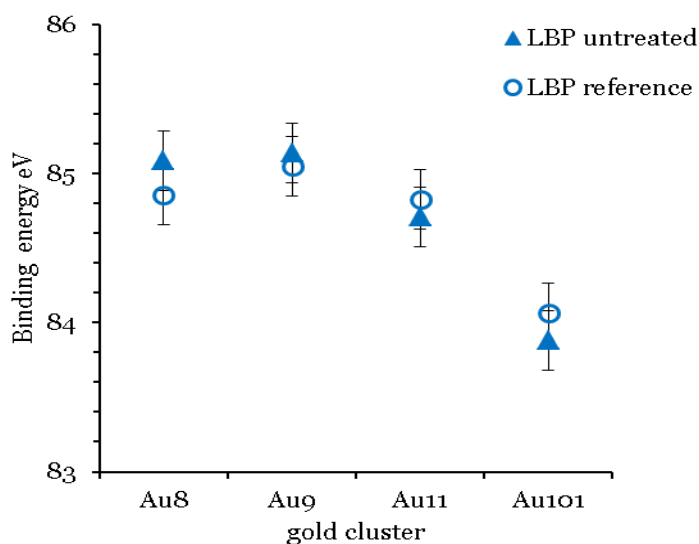


Figure 47: the peak position of the gold clusters in the reference spectra are shown

The positions of Au 4f_{7/2} peaks of the untreated samples are very close to the peak positions of the reference spectra, within 0.2 eV, as shown in Figure 47. Thus it can be concluded that the clusters, as deposited, are not affected by the titania substrate. The position of the Au 4f_{7/2} peaks both of the untreated gold clusters and the reference samples are in the range of the Au 4f_{7/2} position reported for nanosized gold. For example, Battistoni *et al.* using the same approach to energy calibration, reported that for Au₉(PPh₃)₈(NO₃)₃ deposited on titania substrate the Au 4f_{7/2} was at 85.2 eV.⁷⁷ The position of the gold peak is shown as a function $N^{1/3}$, where N is the number of gold atoms in Figure 48A. $N^{1/3}$ is intended as a proxy of the cluster diameter although for very small values of N , this approximation is only rough). The graph has similarities to the $1/d$ relation found for gold nanoparticles by Boyen *et al.*⁷⁸ To the best of our knowledge, there is only one previous gold XPS study of a chemically prepared, atomically precise gold cluster deposited on titania. Chusuei *et al.* using a similar binding energy calibration as used here, observed a binding energy of 83.9 eV for Au₆(PPh₃)₆(BF₄)₂ deposited onto a TiO₂ (110) surface, which is significantly lower than the values we observed.⁹

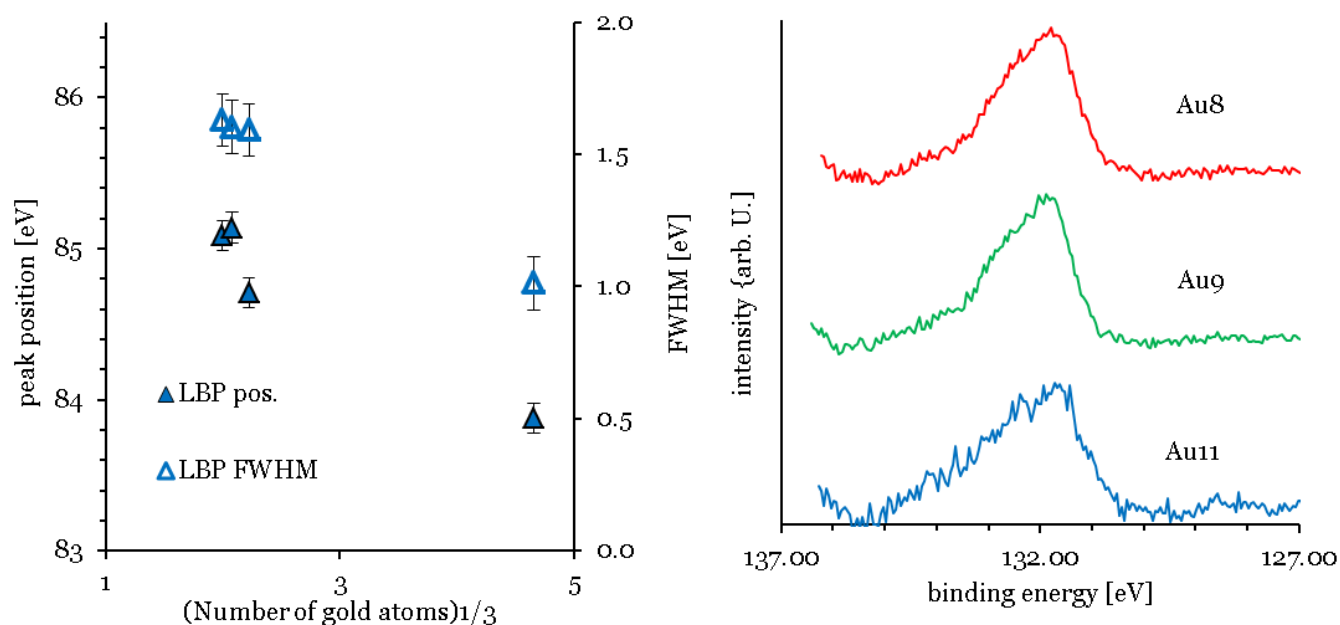


Figure 48: A) the Au-LBP position and FWHM of the untreated clusters are shown as a function of the diameter

and B) P 1S spectra of the untreated clusters

In Figure 48, the phosphorous spectra of the untreated Au₈, Au₉ and Au₁₁ cluster samples are shown. The phosphorous spectra from the Au₁₀₁ samples were too weak to reliably separate the spectrum from the background and hence are not shown. The spectra are fitted with two peaks, one at 131.8 eV, which is referred to as the phosphorous low binding energy peak (P-LBP), and another at 133.1 (± 0.2) eV, which is referred to as the phosphorous high binding energy peak (P-HBP). The position of the P-LBP is the same as that found in the reference samples and as reported by Battistoni *et al.*⁷⁷ We can attribute the P-HBP to oxidised phosphorous which will be justified below.

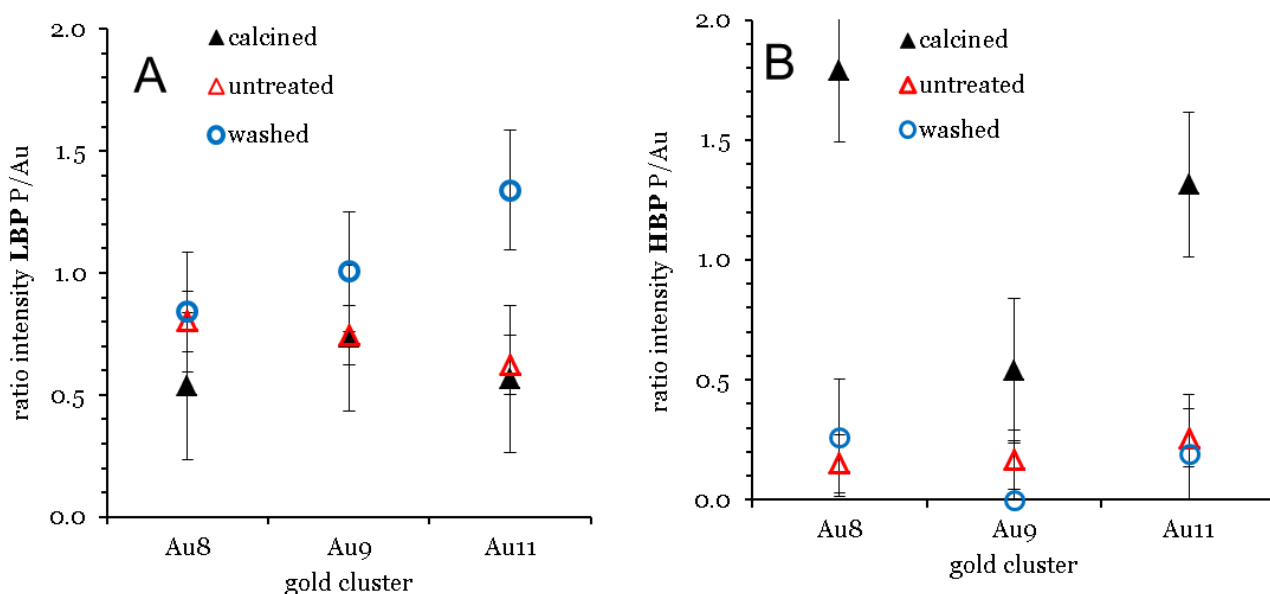


Figure 49: Ratio of the intensity of A) the P-LBP and B) the P-HBP

Figure 49A and Figure 49B show the ratios of the P-LBP and P-HBP, relative to the sum of the Au $4f_{7/2}$ signal. It can be seen that the P-LBP in the untreated samples is the dominant peak (*i.e.* intensity in 5A > 5B for all untreated clusters) but also that the sum of both ratios (Figure 50) is close to unity. In the spectrum of AuPPh₃Cl, only the P-LBP is observed with an intensity ratio between phosphorous and gold very close to 1:1. Hence, the P-LBP in Figure 48 is attributed to phosphorous of the ligands bound to gold. Higher binding energies of phosphorous (similar to that of P-HBP) are found for compounds with phosphorous bound to oxygen.⁷⁹ Hence, it is concluded that in the case of the untreated support-immobilised clusters, there is about one ligand per gold atom and that the nature of the bond between the phosphorous of the ligand and the gold is very similar to that in AuPPh₃Cl

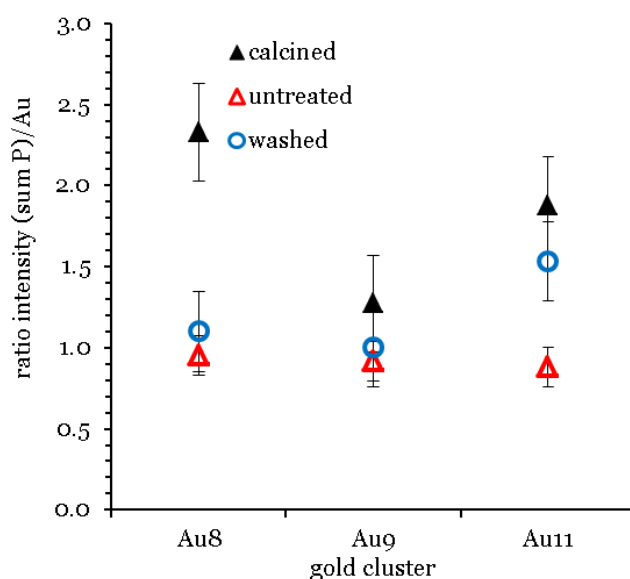


Figure 50: The P-HBP and P-LBP relative to the sum of the intensity of the respective Au peaks (*i.e.* both Au-LBP and Au-HBP).

Refluxed/Washed samples

As previously described, this method of activation involves stirring a suspension of the supported cluster in toluene for two hours at 100 °C which is then followed by centrifugation and drying. This method is hoped to selectively remove the ligands that are bound to the cluster whilst leaving the naked metal core on the surface of the acid washed titania. In the Au 4f spectra of the washed samples (Figure 51A) it is necessary to fit a second, higher energy, gold doublet for Au₈, Au₉ and Au₁₁ (hereafter referred to as Au-HBP). Figure 51B shows that the Au-LBP peak positions relative to bulk Au $4f_{7/2}$ are +0.8 eV for Au₈ and Au₉, +1.0 eV for Au₁₁ and -0.1 eV for Au₁₀₁ and only marginally different to those of the untreated samples. The FWHMs are the same within the experimental error as those for the Au-LBP in the untreated samples. The Au-HBP is found at +1.6 eV for Au₈, at +1.9 eV for Au₉, +2.1 eV for Au₁₁. No Au-HBP peak is found for Au₁₀₁. This binding energy is very similar to that of Au₂O₃ thin films which shows a shift in binding energy of

1.8 to 2.1 eV.⁸⁰⁻⁸² Ono *et al.* have reported shifts in binding energies from about 85 eV to about 87 eV, when exposing 1.5 nm sized gold clusters supported on TiO₂ and on SiO₂ to oxygen plasma (*i.e.* about 3 eV higher binding energy than bulk gold).⁸³ It is worth noting that Au₁₀₁ also has a size of about 1.5 nm. Lim *et al.* reported that gold peaks from gas-phase deposited Au_n (n= 3-20) clusters on silica after exposure to atomic oxygen are found at about 86 eV with a shift of about 2 eV relative to the unexposed sample, which was attributed to the formation of gold oxide.⁸²

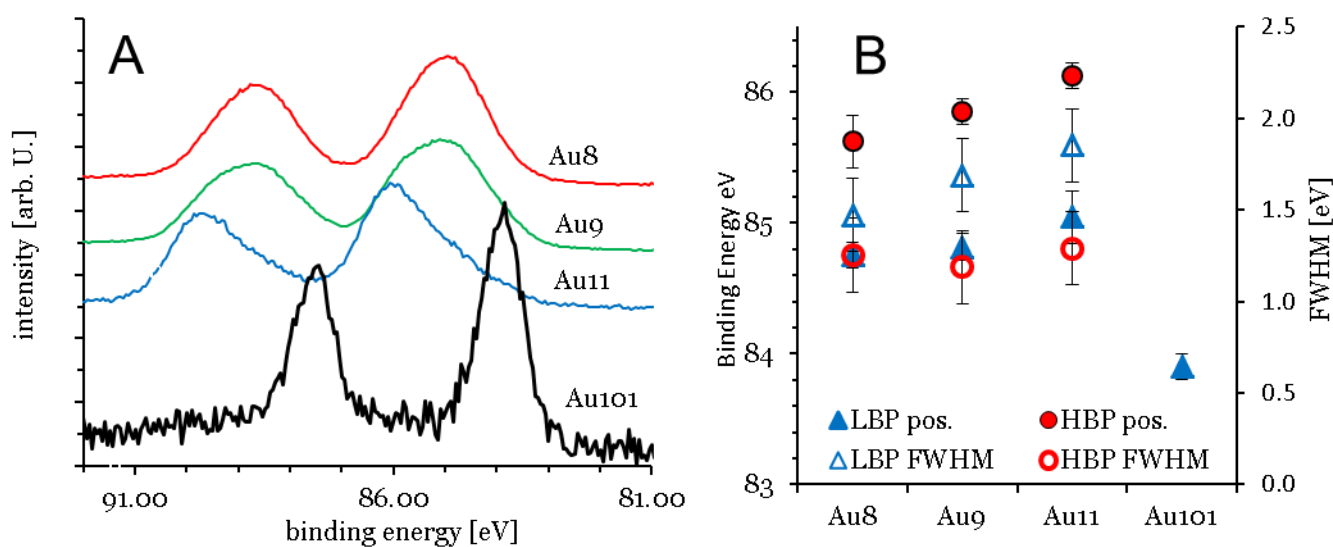


Figure 51: A) washed Au_n spectra and B) position of the Au LBP and FWHM of the peaks

Figure 51 shows the intensity of both the Au-LBP and Au-HBP. The intensities have been normalised as outlined above and then divided by the intensity of the untreated samples (*i.e.* ratio < 1). In general, the total intensity of the peaks is lower than that of the untreated samples (*i.e.* ratio < 1). Furthermore, it can be seen that in case of Au₈ and Au₉ the intensity of the Au-LBP is larger than that of the Au-HBP, while this is reversed for Au₁₁.

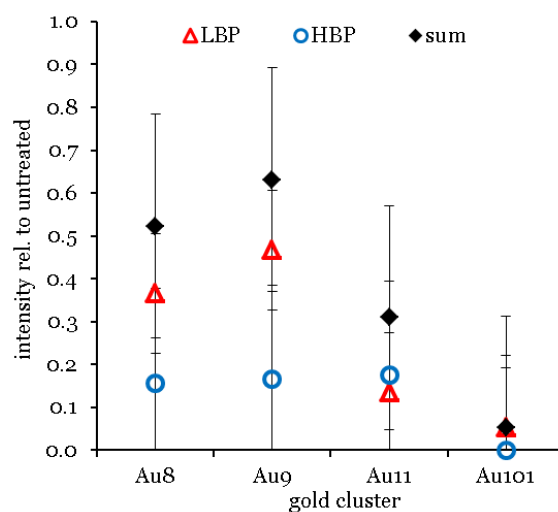


Figure 52: Ratio of the intensity of the Au-LBP and Au-HBP of the washed cluster relative to the intensity of the Au peak of the untreated cluster.

As both the position and the FWHM of the Au-LBP are similar to that of the untreated clusters, it can be concluded that a significant portion of the gold clusters is not significantly altered in its size and chemical state by the treatment. We attribute the appearance of the Au-HBP to the formation of Au-O bonds involving the gold atoms of the cluster cores as the chemical shifts are significantly larger than that of the untreated clusters. We do not attribute it to fully oxidised gold clusters as the shift in peak position relative to the untreated samples is +0.8 to +1.1 eV and, thus, significantly less than the +2 eV shifts reported by others.^{83,84} Whether the shift is due to the formation of partially oxidised gold clusters or due to a strong interaction of the flat (2D), “raft-like” gold cluster core with the TiO₂ support cannot be distinguished. Earlier reports suggest that XPS spectra of the ultra-small “raft-like” metal clusters can be strongly affected due to metal-support interactions.⁸⁵ However, it has to be noted that previously oxidation of gold clusters has only been achieved by using a strong oxidising agent.⁸⁰⁻⁸² In contrast, we have heated the samples to 100 °C in toluene which is not a strong oxidising environment for the clusters. Hence, the oxidation of the gold with oxygen due to the traces of air dissolved in the liquid phase seems to be less likely than the formation of Au-O bonds with oxygen of the titania surface. For the latter, some of the ligands of the gold cluster have to be removed to allow for the formation of Au-O bonds. Removal of the ligands is considered as being required in the activation of the clusters for catalysis.³¹ To the best of our knowledge, this report provides the first ever evidence of the formation of Au-O bonds between metal cores of chemically synthesised atomically precise clusters and material of oxide support due to the removal of ligands induced by mild treatment. The removal of ligands also assists in shift to higher binding energy as ligands are electron donors.

Alternatively, it could be argued that the Au-HBP is due to the formation of bulk gold oxide after agglomeration of the gold clusters. We consider this option as unlikely for the same reason as before, that the applied treatment is not a strong enough oxidising treatment to form an oxide layer on bulk gold. Therefore, the overall reduction in gold intensity has to be interpreted as removal of clusters from the surface through the washing procedure.

The Au₁₀₁ clusters show a peak at the same position and with the same FWHM as the untreated sample but with a very significant reduction in intensity. Therefore, it seems that the washing process removes Au₁₀₁ clusters from the sample but does not change the chemical state of the Au₁₀₁ cluster core. It has to be noted that Au₁₀₁ clusters are easiest to remove by washing.

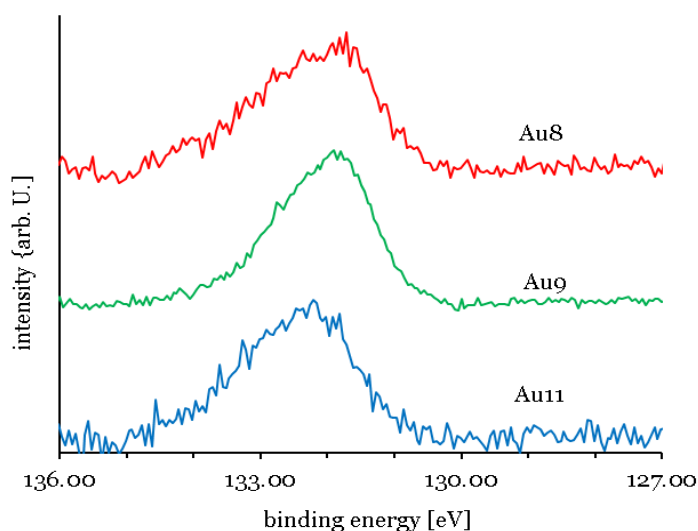


Figure 53: P 1S spectra of the washed clusters

In Figure 53, the P spectra of the washed Au₈, Au₉ and Au₁₁ cluster samples are shown. The spectra show peaks with the same position and FWHM as the untreated samples. Figure 49A and B show the ratio of the P-LBP and P-HBP, respectively, relative to the sum of the Au 4f_{7/2} signal. It can be seen that in the washed samples the P-LBP is the dominant form, which is similar to the spectra of the untreated samples as can be seen in Figure 50. The sum of both ratios is close to unity for the Au₈ and Au₉ clusters but is around 1.3 for the Au₁₁ cluster. In the latter case, however, we ascribe this to relatively large uncertainty in peak area.

It could be argued that for the formation of Au-O bonds some ligands have to be removed and hence the P/Au intensity should decrease which is not observed in the data. However, the uncertainty of the phosphorous signal is too large to allow for the conclusion that this is a contradiction.

Heat treated samples at 200 °C under vacuum

The Au 4f spectra of the heat treated samples are shown in Figure 54A. Again, it is clear that two doublets are required to fit the experimental spectra. Figure 54B shows that the positions of the Au-LBP found here relative to bulk Au4f_{7/2} are 0.0 eV for Au₈, +0.2 eV for Au₉ and Au₁₁ and -0.1 eV for Au₁₀₁ and thus are only marginally different to that of bulk gold. The FWHM for these peaks is ca. 1.2 eV, which is smaller than those of the untreated and the washed samples.

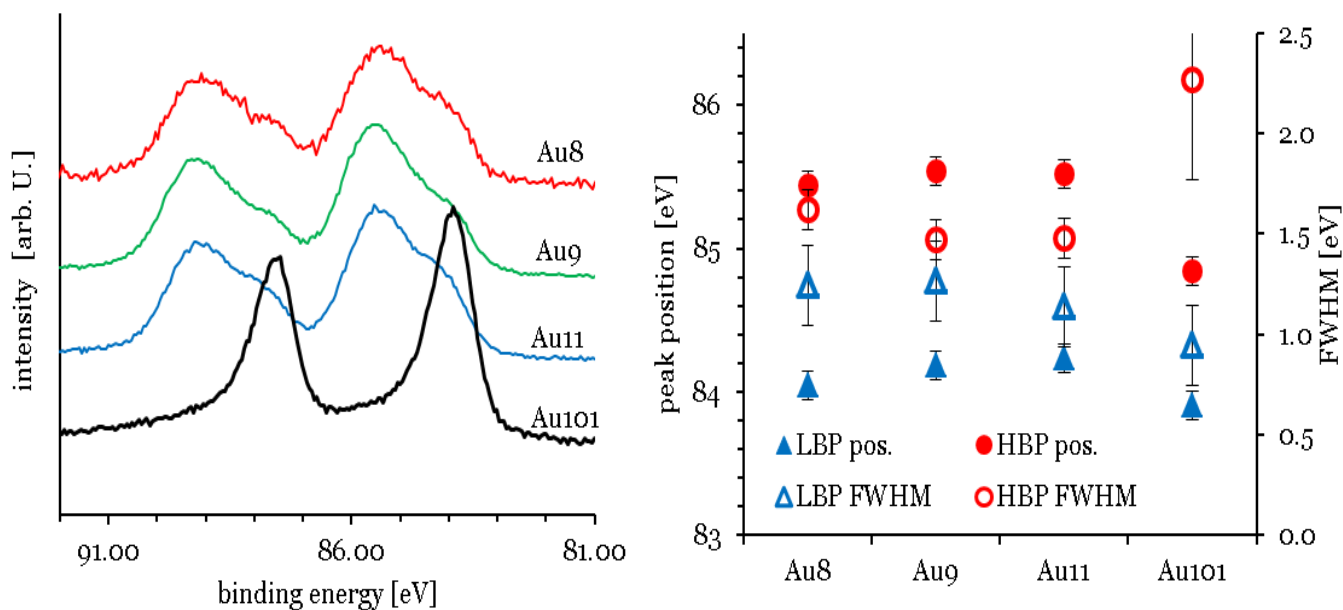


Figure 54: A) Heat treated Au_n spectra and B) position of the Au LBP and FWHM of the peaks

Based on the trend of the untreated samples (Figure 46B and Figure 54B), we attribute the decrease in binding energy of the Au-LBP after heat treatment to agglomeration of the clusters. The change in the gold binding energy allows us to conclude that the size of the agglomerated clusters is only marginally smaller than that of untreated Au_{101} , which is also reflected in the FWHMs as they are only little larger than that of Au_{101} . The Au-HBP relative to bulk $Au_{4f_{7/2}}$ is found at +1.4 eV for Au_8 , +1.5 eV for Au_9 and Au_{11} and +0.8 eV for Au_{101} . The FWHM of these peaks is 1.5 to 1.6 eV and is similar to that of ultra-small untreated support-immobilised clusters. In the same way as for the washed samples, we attribute the Au-HBP to the formation of Au-O bonds involving the gold atoms of the cluster cores as the chemical shift is similar to, but slightly (0.2 to 0.6 eV) smaller than, that of the washed samples. In this case, the peak positions are too low in binding energy for assigning these peaks to either fully oxidised gold clusters or oxidised bulk gold. Here again, we cannot pinpoint whether the shift is due to the formation of partially oxidised gold clusters or due to a strong interaction of the flat (2D), “raft-like” gold cluster cores with the TiO_2 support. Heating at 200 °C in low vacuum is a somewhat harsher environment than the washing procedure, but still cannot be considered as a strong oxidising treatment comparable to oxygen plasma. Also, gold oxide has been found to be unstable at temperatures applied here. Hence, also in this case the oxidation of the gold with oxygen from the gas phase is unlikely and the formation of Au-O bonds with oxygen of the titania surface has to be considered as being much more likely. The shifts are slightly reduced relative to the washed samples. The reason could be some degree of agglomeration of the clusters that have formed Au-O bonds under higher temperature conditions.

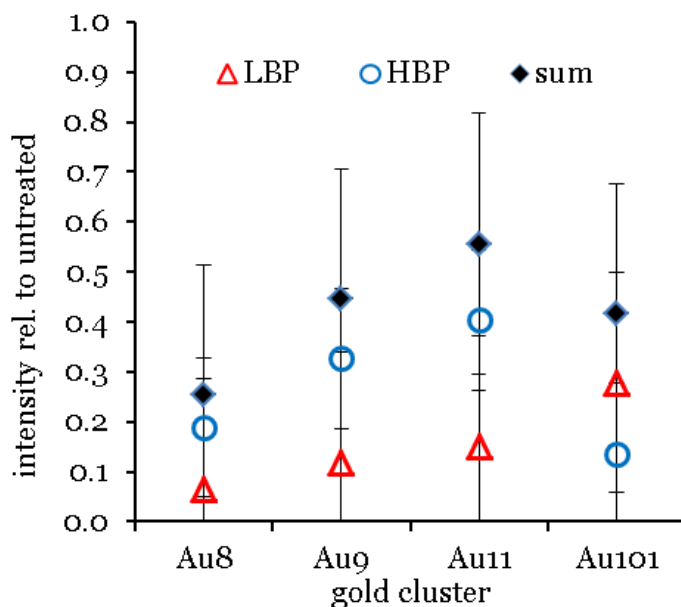


Figure 55: Ratio of the intensity of the Au-LBP and Au-HBP of the heat treated cluster relative to the intensity of the Au peak of the untreated cluster

The total intensity of gold is significantly reduced compared to the untreated sample as can be seen in Figure 46B, with the Au-HBP being more intense than the Au-LBP. Different to washing, heat treatment could not remove clusters from the support; hence, the amount of gold in the sample must be the same as for the untreated samples. Thus, the decrease in gold intensity can only be attributed to agglomeration of the gold cores of the clusters. An increase in gold particle size means that the signal of the gold from the side of the cluster closer to the substrate is attenuated due to the limited mean free path of the photoelectrons. As the amount of gold on the sample is constant, the total gold intensity decreases. This interpretation is supported by the fact that the position of the Au-LBP is close to 84eV.

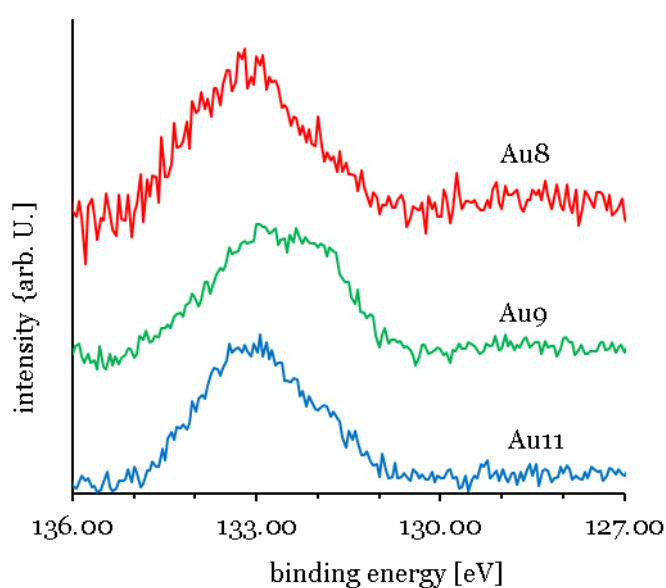


Figure 56: P 1S spectra of the calcined clusters

Figure 56 shows the phosphorous spectra of the calcined Au₈, Au₉ and Au₁₁ cluster samples. The spectra clearly illustrate a shift in the peak position compared to the spectra of the untreated samples from the P-LBP to the P-HBP position. A similar shift of the phosphorous peak has been reported earlier after heat treatment of Au(PPh₃)(NO₃) on TiO₂.⁵² Based on XPS results and ³¹P-NMR by Yuan *et al.* assigned the change of their sample to either the formation of species where phosphine is bound to a larger metal particle, *i.e.* the formation of gold clusters surrounded by triphenylphosphine ligands, or the oxidation of phosphorous. Based on our results presented here, we can rule out the first possibility as the untreated Au_n clusters show a lower binding energy of the phosphorous. Hence, we ascribe the P-HBP to oxidised phosphorous species which is also supported by the peak position of phosphorous in phosphorous doped titania.^{85,86} Noteworthy, the ratio of the P-LBP and the P-HBP to the sum of the gold 4f signal (Figure 50) has almost entirely shifted to the P-HBP peak for the Au₈ and Au₁₁ clusters and to some extent for the Au₉ cluster. The sum of both ratios is larger than unity for the Au₈ and Au₁₁ clusters. This finding can be explained by gold clusters agglomerating into larger particles during heat treatment, consistent with the Au-LBP signal shifting to lower binding energy and the overall decrease in total gold peak intensity. The extraneous ligand P moves elsewhere onto the surface and becomes oxidised or bound to the titania surface resulting in an increase in the P-HBP signal (Figure 49B). The formation of larger gold particles should reduce the gold signal due to the limited electron mean free path leading to an increase in the total P: Au ratio (see Figure 50C) and also to an increase in the P-HBP signal (see Figure 49B). The amount of “ligand-like” phosphine species (P-LBP) is reduced by *ca.* 50 % due to the maintained presence of a fraction of the non-agglomerated clusters even in calcined samples (see Figure 5A). This interpretation is supported for Au₈ and Au₁₁ by the changes in the phosphorous signal shown in Figure 50: The P-HBP and P-LBP relative to the sum of the intensity of the respective Au peaks (*i.e.* both Au-LBP and Au-HBP). To a lesser degree the interpretation is also supported for Au₉. However, the removal of the ligands from the cluster and their oxidation seems to be less efficient for the Au₉ compared to Au₈ and Au₁₁ as the P-LBP is stronger in the case of Au₉ compared to Au₈ and Au₁₁. In summary, it can be concluded that the phosphorous of the ligands oxidises during heat treatment and, thus, most likely is removed from the clusters but remains in an oxidised form on the surface as triphenyl phosphine oxide.

Detailed study of titania

Although, gold clusters supported on acid-washed Evonik P-25 titania are resistant to particle sintering, catalytic investigations showed that these samples were ineffective for the oxidation of alkenes. To understand the chemistry of gold clusters supported on untreated titania, it was decided to attempt this distinguish the difference between gold cluster supported on anatase or rutile. P-25 titania comprises a

mixture of anatase ($\approx 70\%$), rutile ($\approx 25\%$) and also an amorphous phase ($\approx 5\%$).⁸⁷ The individual supports were ordered with similar particle sizes, but with a slightly higher measured surface area ($\approx 150\text{ m}^2/\text{g}$). Therefore, the gold loading was decreased to make the surface coverage of these samples comparable to the Evonik P-25 samples that were used for catalysis, rather than 0.5% by weight of gold, 0.17% loading was used. The study was limited to the Au_8 , Au_9 and Au_{101} clusters as yields of the Au_{11} were relatively low. Unfortunately, photoelectron samples of the rutile samples yielded small contamination of zinc in these samples. The zinc 2p overlapped with the gold 4f peak, which prevented any detailed analysis of the gold present on these samples. In the case of anatase samples, samples also proved to be sensitive to ambient light conditions; hence exposure was minimised as much as possible. Photoelectron studies were conducted under the same conditions as the acid-washed samples. Further spectra were also collected at 400 eV , in the hope of increasing the response of the phosphorous peak. Overall, the contrast to the acid washed P-25 samples was stark; the gold clusters appear to readily sinter on the surface of the untreated anatase surface to form slightly larger particles.

Untreated anatase

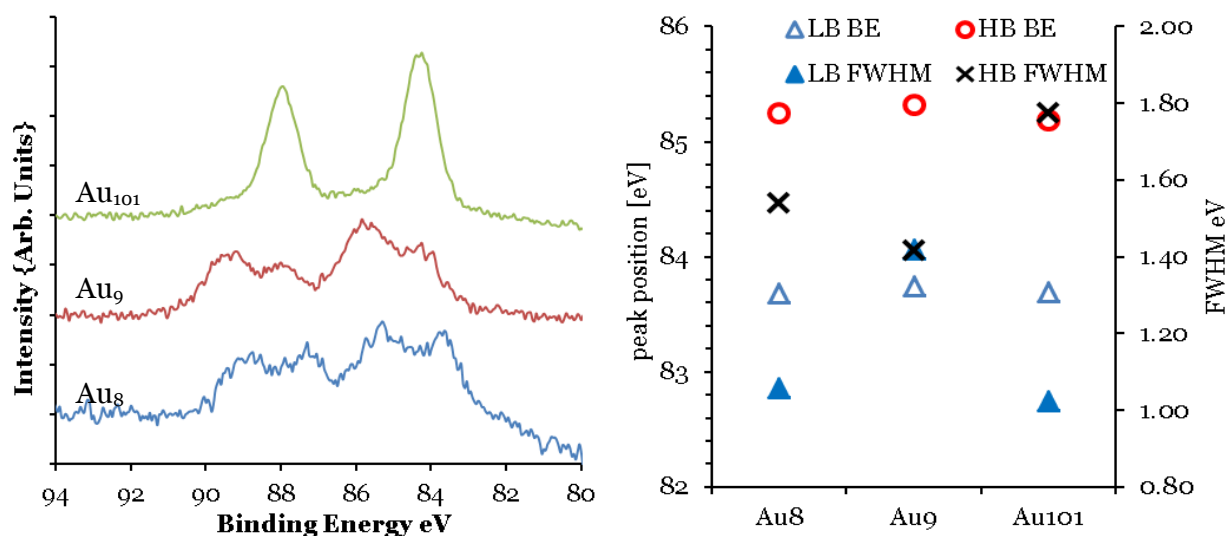


Figure 57; Summary of gold 4f peak of untreated gold clusters deposited on anatase

The untreated clusters supported on anatase appear to show the presence of multiple contributions to the gold peak. In comparison to the acid-washed system, the gold 4f peak was fitted with two peaks for the atomically precise Au_8 and Au_9 samples whilst in the case of the larger Au_{101} only one main peak with a small shoulder was fitted. In Figure 58B, it is apparent that the peak positions for the higher energy binding peak are at 85.25 eV (Au_8), 85.31 eV (Au_9) and 85.15 eV (Au_{101}), whilst for the lower energy binding energy peak is at 83.7 for all of these clusters. The lower binding energy peak is slightly lower than that of metallic gold (84.0 eV) which indicates slight anionic characteristic of the small particles ($< 3\text{ nm}$) on the anatase

surface. The increasing metallic nature of the gold peak is apparent as the gold cluster size is increased. The two small clusters demonstrate significantly more agglomeration of the small cluster forming slightly larger nanoparticles, which contrasts starkly with acid washed system that has only one main peak between 85.1 and 85.4 eV for the same clusters.

The relative ratio of the HBP to the LBP deviates significantly from expected values based on the atomically precise molecular clusters to the colloidal Au₁₀₁ which is made apparent in Figure 59. It is apparent that the HB peak accounts for approximately 60 % of the total intensity of the gold 4f peak in the case of the atomically precise clusters. In contrast to these ultra-small, atomically precise clusters in the case of the colloidal Au₁₀₁ the HB peak only contributes 15 % to the total Au 4f peak intensity. The presence of the HB peak in the latter case could be attributed to the small amount of sub 1 nm particles which may be detected under STEM. Alternatively, this peak can be attributed to the small proportion of Au₁₀₁ colloid metal cores interacting with the anatase support.

Another possible explanation for the variation of HB/LB peak intensity ratio is due to the portion of atoms that are interacting with the support. For the atomically precise clusters which have a proportionally greater number of surface gold atoms, the HB peak contribution to the intensity of the gold 4f peak is greater.

The samples in Figure 60 were prepared with a gold loading of 0.17% by weight of gold, in addition samples with half loading(0.7 %) was also prepared in attempt to see if a lower loading will prevent gold cluster agglomeration. However, the results show very similar results for lower loadings samples which were also untreated.

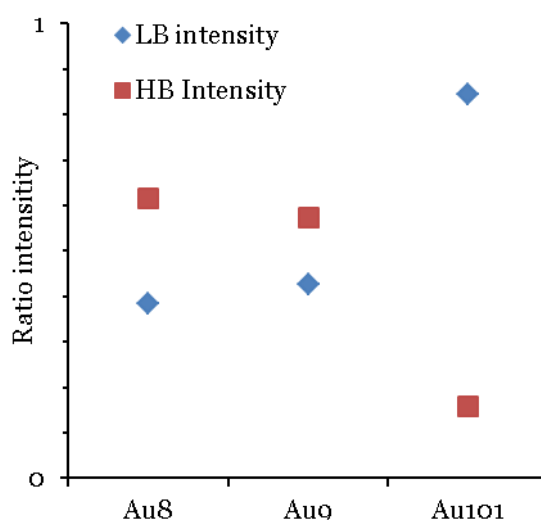


Figure 61; Relative intensity ratio of HB and LB peak for each cluster untreated on anatase

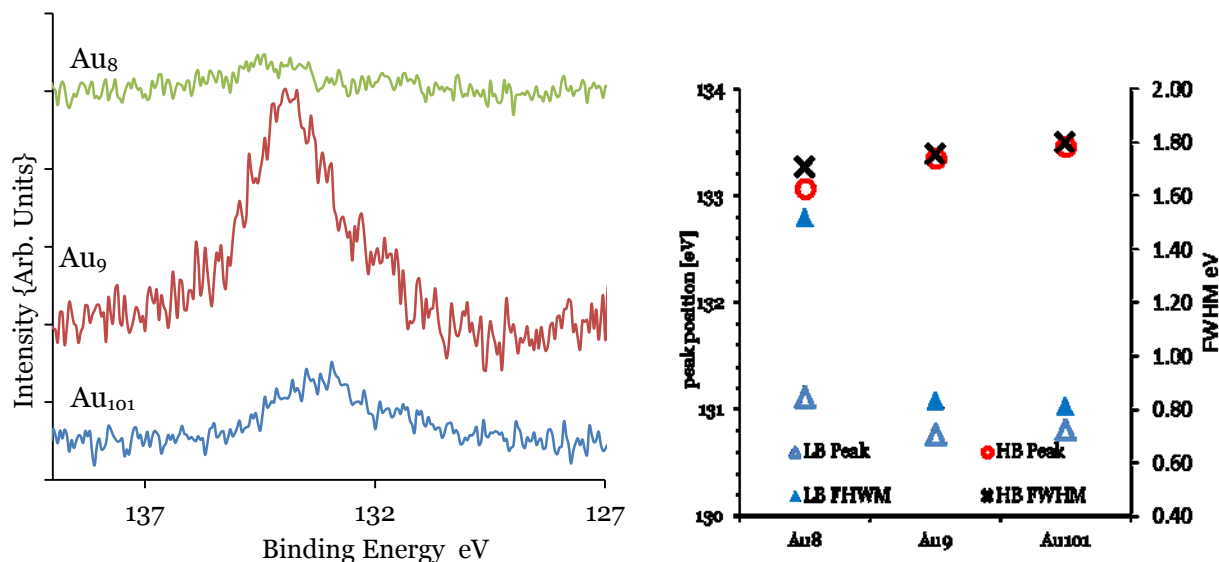


Figure 62; Phosphorous 1s Spectra for untreated samples A) Spectra and B) peak positions and FWHM

The phosphorous peak for the untreated samples was more difficult to attain. Multiple samples spots were used to achieve the best signal; however, the response was much less than expected especially when compared to the untreated acid-washed samples. For the Au₉ sample, a relatively well defined phosphorous peak was observed at 133.2 eV, and a slight peak at around 131 eV. In the case of Au₈ and Au₁₀₁ sample, the HBP was also observed at 133.1 and 133.4 eV respectively. The LB peak for these samples was fitted at 132.8 eV for Au₈ and 130.8 eV Au₁₀₁. The fitting of the small LB peak proved to be difficult and may be an artefact of the fitting process rather than represent the physical presence of phosphorous at this binding energy. The LB Peak was previously attributed to gold cluster bound phosphorous in the untreated samples on acid-washed titania, due to the “intact-like” cluster. The LB FWHM of Au₈ sample is much broader than that of the other two clusters, which may arise due to issues with the peak fitting process and such low amounts of phosphorous present in these samples. If these spectra are representative of the electronic structure of these samples, the sintering of the clusters may be caused by a photoinduced reaction of the phosphorous ligands with the support, which may be more reactive with smaller gold clusters. The reaction may lead to oxidation of the triphenylphosphine ligand to triphenylphosphine oxide which would easily dissociate from the gold cluster.

Calcined under Oxygen

The gold clusters on anatase were treated at 200°C under an oxygen atmosphere, which resulted in significant changes in the electronic structure of the gold 4f peaks for each sample as compared with the untreated samples on anatase (Figure 63). For the Au₈ cluster supported on anatase, the Au 4f_{7/5} peak was again fitted with two curves, however there are some differences with the peak positioning and FWHM. The HB peak is positioned at 85.38 eV as opposed to 85.25 eV for the untreated sample, and the FWHM has

also increased from 1.54 eV to 2.2 eV. The LB peak is positioned at 83.74 eV with a FWHM of 0.96 eV, although the peak position has not changed when compared to the untreated sample, the FWHM has narrowed significantly from 1.43 eV for the untreated sample. In the case of the supported Au₉ cluster, the higher binding peak is positioned at 85.40 eV with a FWHM of 2.0 eV. As with the smaller Au₈ cluster, there is a slight shift of the HB peak to higher binding energies (~ 85.40 eV). The FWHM maximum of the HB peak has increased from 1.4 eV in the case of the untreated sample. The LB peak is positioned at 83.74 eV with a FWHM of 1.0 eV where a decrease in the FWHM from 1.4 eV is observed, which is similar to both Au₈ and Au₁₀₁ cases. The HB peak for Au₁₀₁ is found at 85.42 eV with FWHM of 2.5 eV after the oxygen treatment. The HB peak has shifted slightly by 0.27 eV and the FWHM has increased from 1.8 eV. The LB peak is found at 83.8 eV with a FWHM of 0.96 eV, which is 0.1 eV higher than both Au₈ and Au₉, which illustrates the increased metallic character of the larger Au₁₀₁ particles.

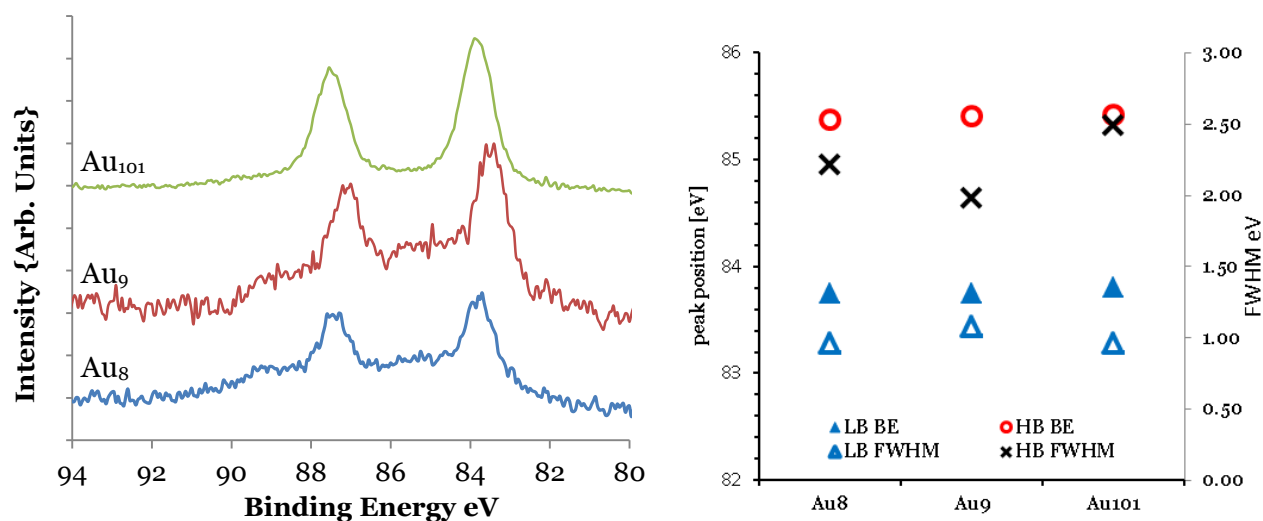


Figure 64; Summary of gold 4f peak of calcined under 200°C under oxygen gold clusters deposited on anatase

The relative intensities of the HB peak and LB peak change significantly after treatment with oxygen at 200°C as shown in Figure 65 especially for the atomically precise Au₈ and Au₉ supported samples. This increase in relative intensity of the HB peak as compared to LB peak may be indicative of oxidation of the gold clusters rather than just simple aggregation of the clusters on the surface. After annealing, the samples appear less susceptible to photoinduced aggregation of the clusters. The Au₁₀₁ seems to undergo little change as far as intensities are concerned, but there is a slight shift in HB - peak and -FWHM which may be caused by oxidation of some of the smaller particles on the surface.

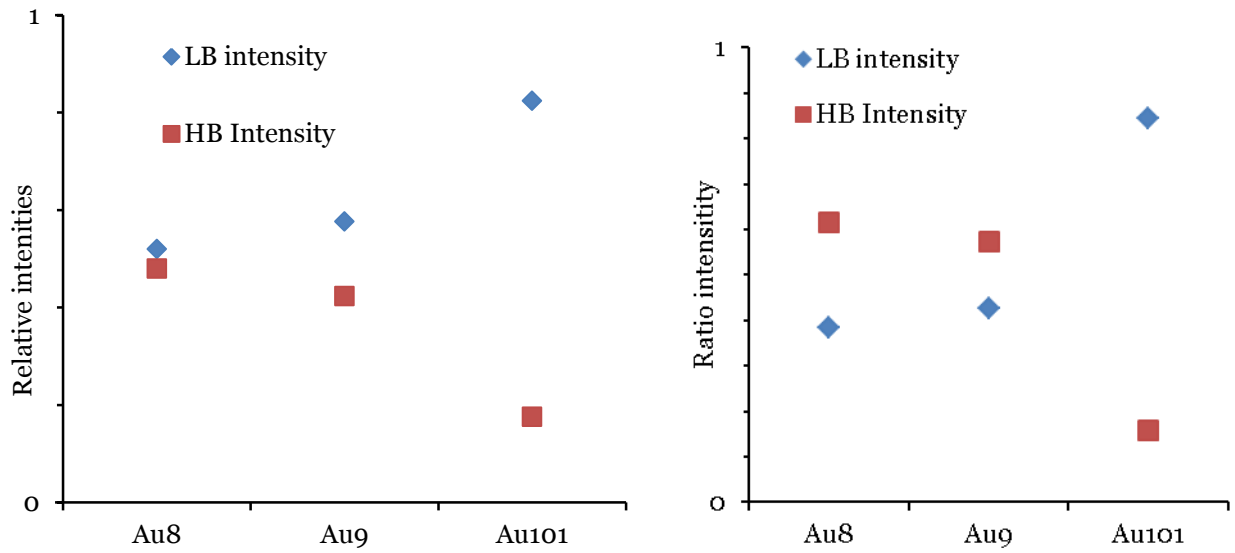


Figure 66: Relative Au 4f_{7/2} intensity ratio of HB and LB peak for each cluster oxygen treated on anatase (left) and untreated samples (right)

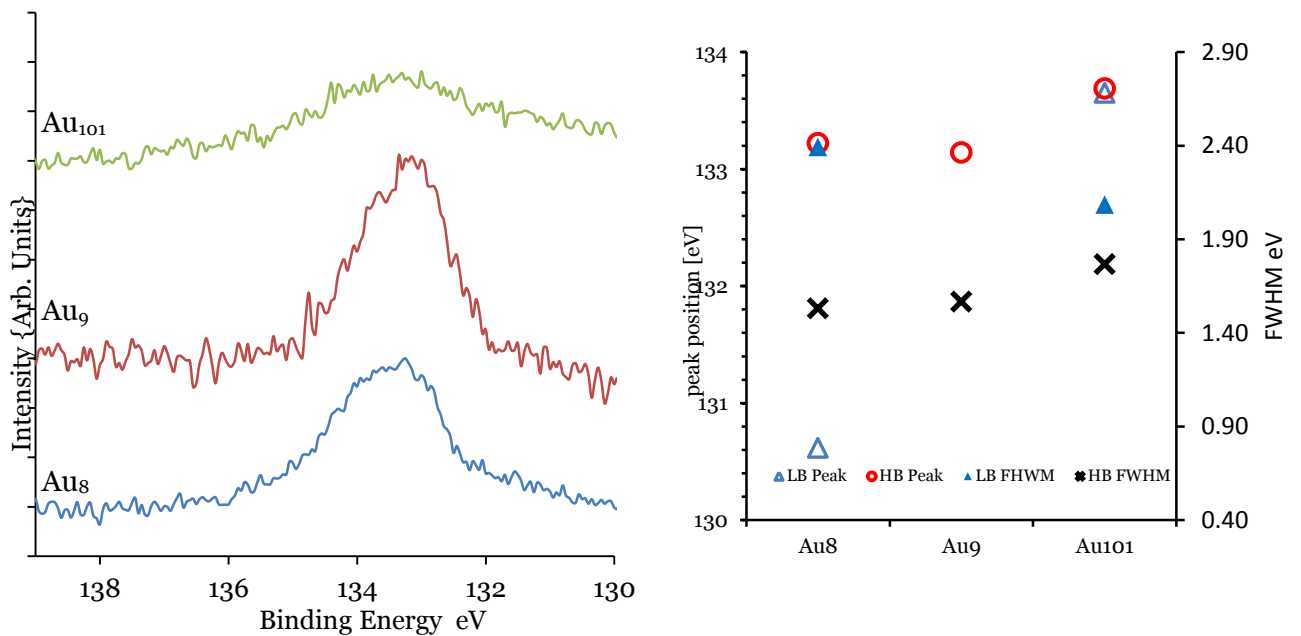


Figure 67: Phosphorous 1s Spectra for calcined at 200°C under oxygen samples A) Spectra and B) peak positions and FWHM

The phosphorous peak for each of the calcined samples was detected for each cluster, even for the low loaded samples (0.08%), which contrast significantly with the untreated samples. Overall the phosphorous samples for the calcined samples had a main HB peak, detected at 133.29 eV (Au_8), 133.25 eV (Au_9) and 133.35 eV (Au_{101}), when treated at 200 °C under oxygen which was attributed to the oxidised phosphorous bound to the surface of the sample. This compares well with the heat treated samples on acid washed titania, in that the triphenyl phosphine ligand is now fully oxidised to triphenyl phosphine oxide and remains on the surface. The issue that remains is why the phosphorous signal was so difficult to observe for the untreated anatase samples; physical sample issues, data collection issues such as charging or peak fitting issues may be the cause.

Calcined with oxygen and hydrogen

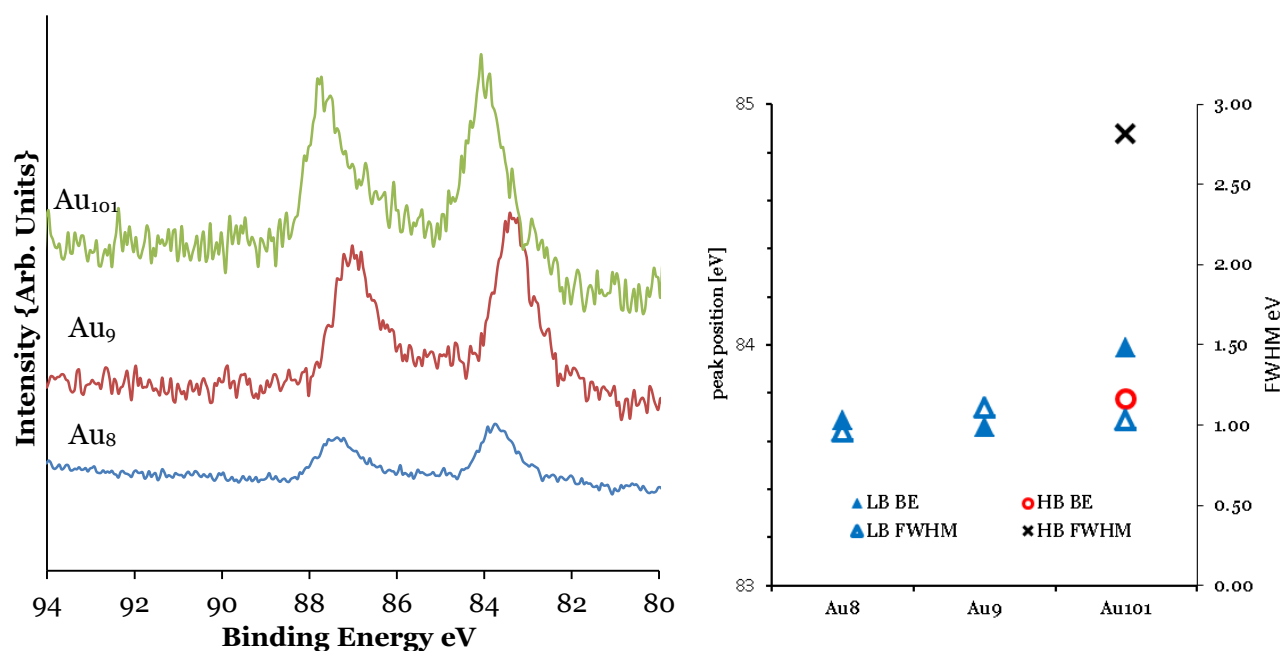


Figure 68: Summary of gold 4f peak of calcined at 200°C under oxygen/hydrogen gold clusters deposited on anatase

Following the oxygen treatment at 200°C, the samples were heated further under a reducing atmosphere of hydrogen for two hours at 200°C in a similar method to Behm.²⁴ This resulted in further changes in the electronic structure of the gold peak. Overall, only one peak was required for peak fitting in contrast to the untreated and oxygen treatment, which required two peaks. For the Au_8 and Au_9 samples, the peak was located at 83.69 eV and 83.65 eV respectively with FWHMs of 0.96 eV and 1.1 eV. If compared with the LB-peak of the oxygen treated samples, there is a shift of around 0.5eV- 0.7 eV to a lower binding energy in the case of the Au_8 and Au_9 cluster, which is within the experimental error of 0.1 eV. These small

values for the gold peak indicates that the gold clusters have agglomerate but that the gold present on the surface is not fully metallic in nature. In contrast, the $Au_{4f_{7/5}}$ peak of the supported Au_{101} differs in that the peak position increases from 83.98 eV, which is akin to that of metallic gold (84.00 eV). Overall, it is difficult to ascertain whether the sintering of the cluster is purely due to the increased time at elevated temperatures alone or due the reducing atmosphere of the hydrogen.

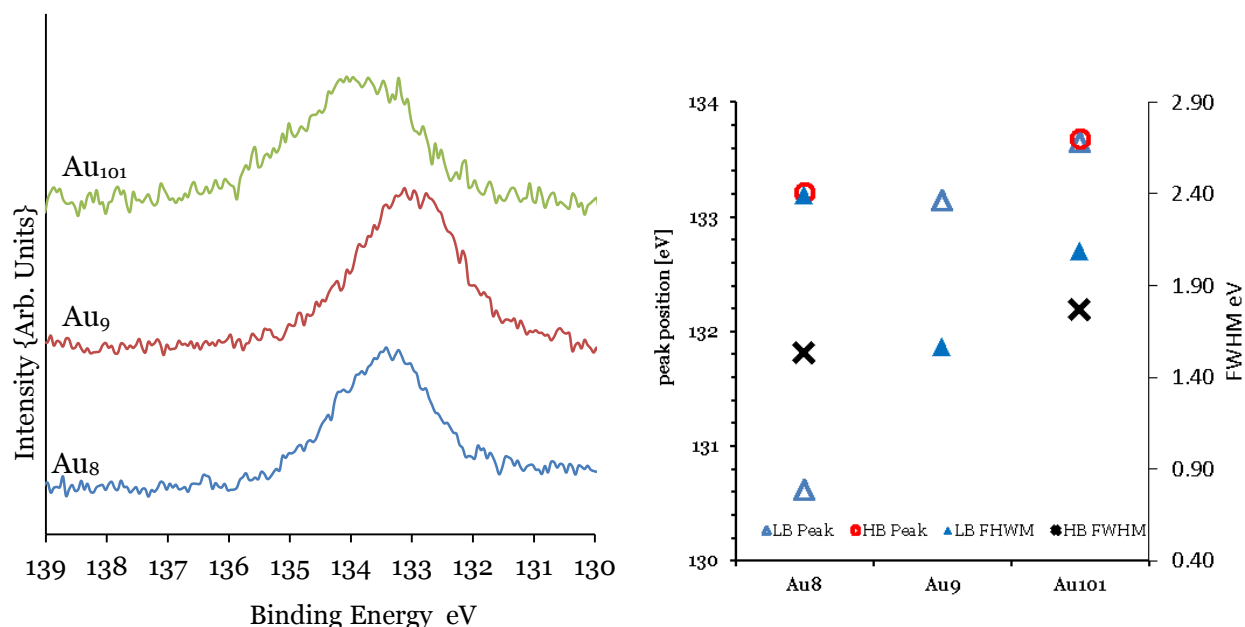


Figure 69: Phosphorous 1s Spectra for calcined at 200°C under oxygen/hydrogen samples A) Spectra and B) peak positions and FWHM

The phosphorus peak which has been treated under O_2/H_2 show for each sample was fitted with two peaks except in the case of Au_9 . From visual inspection of the Au_8 and Au_{101} , the LB peak is just an artefact of the fitting procedure and the low amounts of phosphorous present on the surface. The main, HB peak (HB peak for Au_8 and Au_{101} was found at 133.3 eV and at 133.7 eV for Au_{101}) is representative of the oxidised form of the triphenylphosphine ligand present on the support material. It may have expected that there would have been a change in the peak position; however, as samples were not stored under Ar/N_2 during the trip to the Australian Synchrotron the phosphine may have re-oxidised under ambient conditions. In the case of Au_8 , it is apparent that a low intensity LB peak is detected at a lower binding energy, which may be indicative that some of the phosphorous has been reduced back to the triphenyl phosphine.

Preliminary comparison of other possible modes of activation

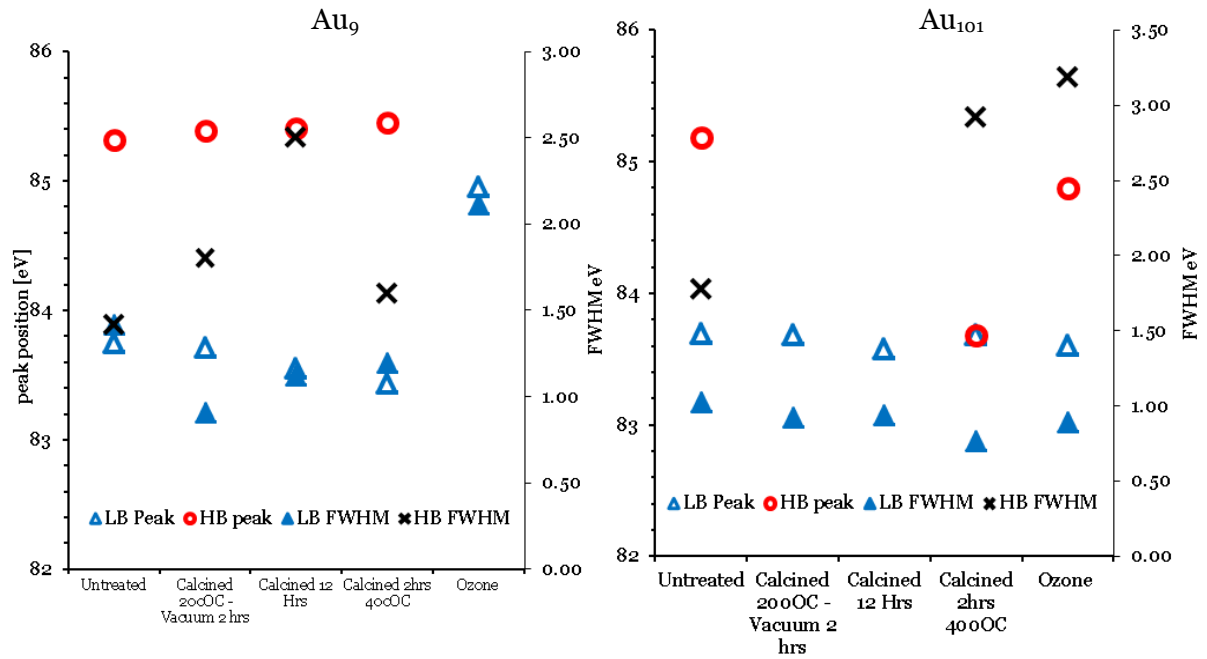


Figure 70: Plot of peak positions and FWHM for A) Au₉ on anatase treated under a selection of modified treatment conditions and B) Au₁₀₁ on anatase treated under a selection of modified treatment conditions

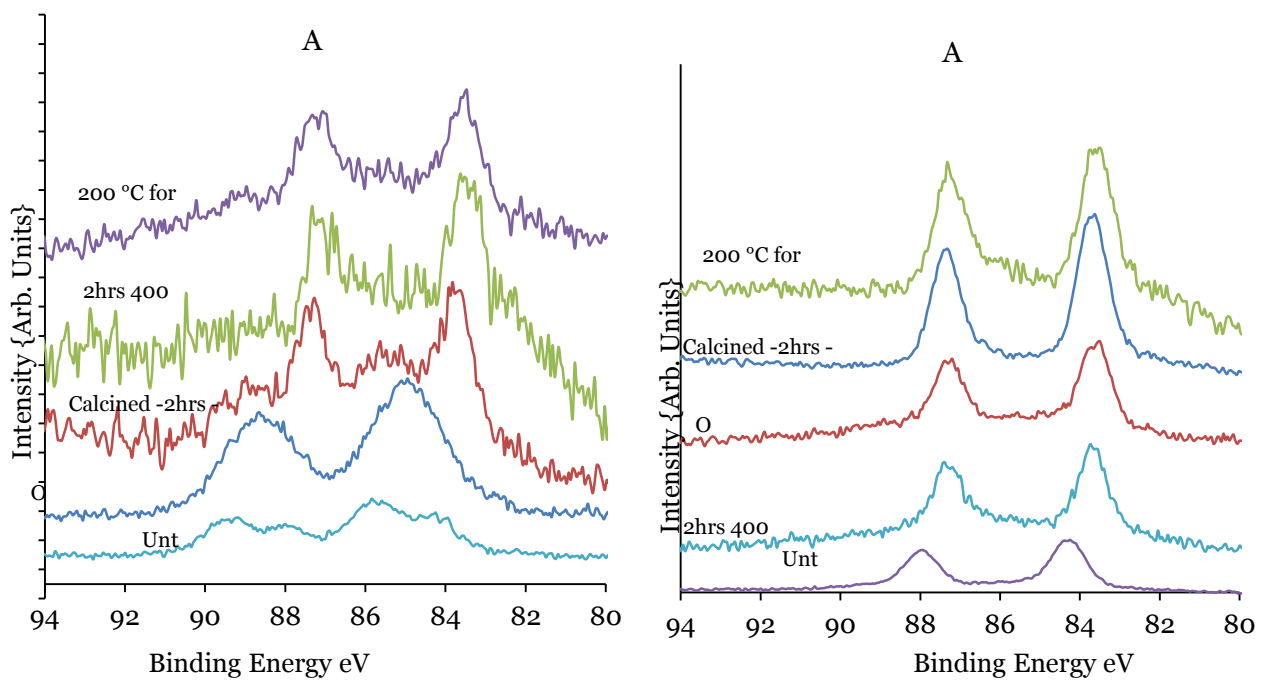


Figure 71: Spectra of gold clusters on anatase treated under a selection of high temperature treatment conditions

In an effort to investigate other novel routes towards activating supported gold cluster towards catalysis, a range of alternative routes of activating these systems were investigated.

Figure 72 and Figure 73 shows the photoelectron results of a series of treatments on 0.17 % Au₉ and Au₁₀₁ on anatase;

- 2 hours at 400 °C
- 12 hours at 200 °C
- 2 hours under a flow of ozone
- Heat treatment under 200 °C

These routes are designed to examine how increases in time and temperature can influence the electronic structure of the system. Ozone treatment was aimed at oxidatively removing the ligands, which has only recently been used for catalyst activation.⁸⁸

In the case of the Au₁₀₁, sintering of the gold particles occurs under treatments at 400 °C, 12 hours and also under heat treatment. This is evidenced by the presence of only a single peak at 83.7 eV; the presence of the second peak at 83.7 eV is an artefact of the fitting program for calcination under 400 °C. In the case of the ozone, the broadening HB peak at 84.8 eV indicates the formation of gold oxide on the surface.⁸⁹ In comparison, the supported Au₉ cluster on anatase under this range of treatments has a more varied electronic structure than Au₁₀₁. Under milder treatments of 200 °C, the HB peak present at 85.3 eV indicates the presence of small clusters on the surface. The LB peak further indicates that a certain degree of cluster agglomeration has occurred, possibly due to exposure to light. Ozone treatment again results in the formation of gold oxide on the surface with a similar broad peak at 84.9 eV, although there is only one peak fitted to the Au₉ spectrum as opposed to the Au₁₀₁ treated by ozone which has a second LB peak at 83.7 eV, indicating the presence of larger gold nanoparticles.

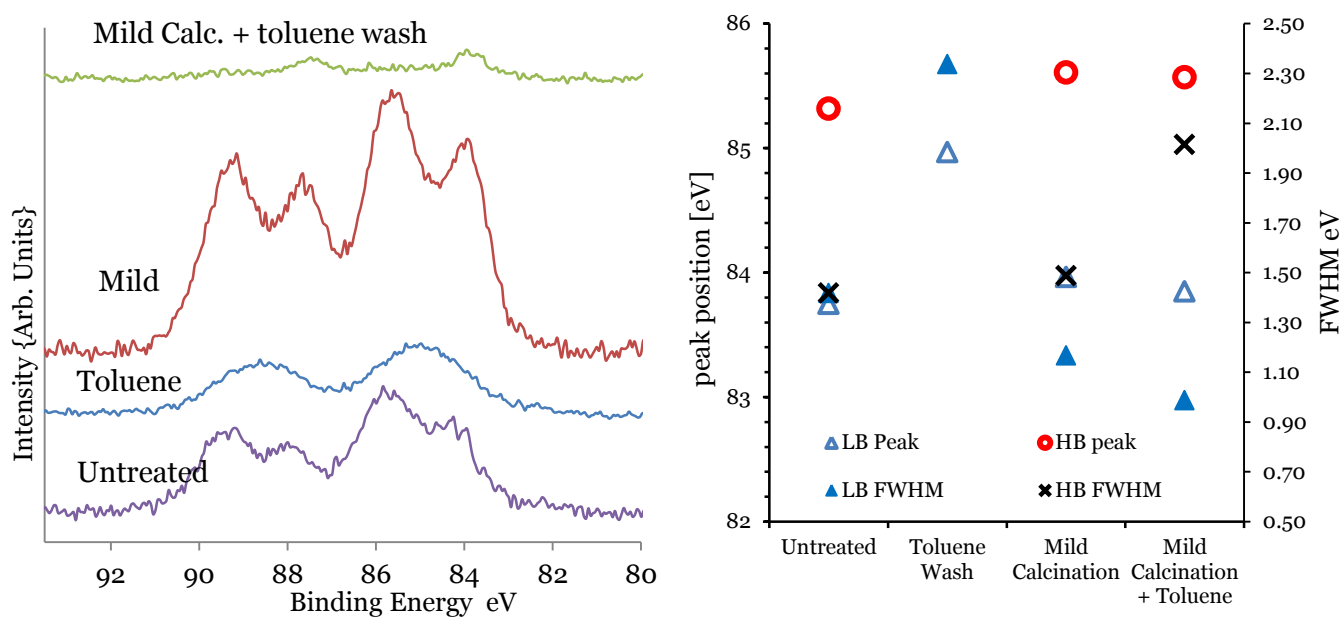


Figure 74: Au₉ on anatase treated under a selection of mild conditions A) Spectra and B) plot of peak positions and FWHM

In Figure 75, the photoelectron spectra of Au9 on anatase (0.17 %) conditioned under a range of mild treatments that are intended to perturb the ligand sphere are shown. The toluene washed sample, which was refluxed in toluene for two hours, filtered and dried under reduced pressure, is done under similar conditions as the previously described toluene-wash on the acid washed titania. The spectrum is fitted with a single peak with a binding energy of 84.96 eV and FWHM of 2.34 eV, which indicates the possible formation of gold oxide, similar to the acid washed samples.⁸⁰⁻⁸² Compared to the untreated sample there is significant peak broadening occurring.

In the case of the mild calcination procedure, where the untreated sample was heated under vacuum at 100 °C for two hours under air, there is a slight shift of the HB peak from 85.2 eV (untreated) to 85.6 eV. There is also an increase of the FWHM to 1.42 eV for the HB peak. The second LB peak has increased to 83.9 eV, which may indicate increased metallic nature of gold nanoparticles on the surface. This low temperature regime indicates again that the gold oxide particles are forming. Gold (III) oxide readily decomposes at approximately 160 °C; these mild treatments which don't come close to this temperature. Washing the calcined samples with toluene results in a significantly smaller gold 4f peak, which indicates gold has been physically removed from the surface of the anatase to the solvent. The main peak present in this sample is at 83.8 eV, indicating that the only gold present on the surface is agglomerated to form metallic gold nanoparticles.

Conclusions

Investigations were conducted into chemically synthesised atomically precise gold clusters deposited on titania supports using photoelectron spectroscopy. Subsequent to their deposition onto titania support, the gold clusters have been treated with washing and calcination to remove the phosphine ligands from the gold cluster core. Photoelectron spectroscopy has been used as a tool to determine changes in the chemical nature, composition, and to estimate changes in the size of the gold clusters.

On acid-treated titania supports, it was observed that the as deposited, untreated clusters remain virtually unchanged and can be described as ultra-small clusters with decreasing size from Au_{101} to Au_8 , as indicated by positions and widths of the gold and phosphorus peaks in photoelectron spectroscopy spectra. The peak positions in the gold photoelectron spectroscopy spectra shift systematically in agreement with the size of the clusters determined by x-ray diffraction immediately after their synthesis.

Washing of the support-immobilised cluster with toluene at 100°C leads to the removal of a fraction of the clusters from the titania surface. Of those clusters left on the titania surface some remain virtually unchanged. The other fraction shows formation of Au-O bonds, most likely to the oxygen of the titania surface or the formation of gold oxide particles on the surface. No significant agglomeration or successful complete removal of phosphine ligands from the clusters could be inferred from observed photoelectron spectroscopy spectra.

Heat treatment of the support-immobilised clusters has two effects. First, the ultra-small clusters aggregate forming slightly larger gold particles still protected by phosphine ligands. The average size of the aggregated clusters can be estimated to be marginally smaller than that of the untreated Au_{101} . Second, a fraction of gold clusters forms Au-O bonds, most likely to the oxygen of the titania surface, which coincides with the loss of phosphine ligands and formation of oxidised phosphorous species.

Immobilised gold clusters on non-acid treated anatase support results gold clusters that are more susceptible to agglomeration than the acid-washed titania supported samples as evidenced to the photoelectron peak similar to metallic gold. The peak positions in the gold photoelectron peak do not appear to be dependent on the cluster precursor as observed for the acid-washed titania samples. It was concluded that the samples are susceptible to photoinduced particle sintering; possible due to support induced oxidation of the triphenyl phosphine ligands.

Calcination under oxygen and subsequent treatment under hydrogen at 200°C leads to the gold photoelectron peaks that are more metallic gold in nature than was observed with the acid-washed

treatment under oxygen. In the case of the atomically precise gold clusters, a slightly less pronounced HB peak indicating a small amount of un-sintered gold cluster is present.

A small range of alternative catalyst activation treatments were also investigated for the potential for decreasing the extent of cluster sintering. Further investigation with STEM would give a better idea about the presence of smaller sub nanometer clusters. HRTEM, as discussed previously, could only indicate the extent to which the small gold clusters have aggregated.

Silica supported gold clusters were also studied but due to the extent of sample charging that could not be avoided, studies on this support proved fruitless. A range of sample preparation routes were discussed that decreased sample charging; however, charging was unable to be avoided. As silica supported gold clusters have been shown to be of interest for oxygen-only oxidation of alkenes, solving the issue of sample charging is imperative. Other experimental routes such as NEXAFS/XANES should also be explored for their potential as tools to explore the electronic structure of silica supported gold clusters.

Bridge

Following this systematic electronic study of supported gold clusters and nanoparticles on titania supports, a series of catalytic studies will be detailed on the wide range of silica and titania catalysts.

References

- (1) Siegbahn, K. M.: Electron Spectroscopy for Atoms, Molecules and Condensed Matter. In *The Nobel Lecture*, **1981**.
- (2) Egelhoff Jr, W. F.: Core-level binding-energy shifts at surfaces and in solids. *Surface Science Reports* **1987**, 6, 253-415.
- (3) Hertz, H.: Ueber einen Einfluss des ultravioletten Lichtes auf die elektrische Entladung. *Annalen der Physik* **1887**, 267, 983-1000.
- (4) Einstein, A.: On a Heuristic Viewpoint Concerning the Production and Transformation of Light. *Annalen der Physik* **1905**, 17, 132.
- (5) Rutherford, E.; Robinson, H.: Analysis of the Gamma Rays of the Thorium and Actinium Products. *Phil. Mag. VI* **1914**, 26, 937.
- (6) Lewis, R. T.; Kelly, M. A.: Binding-energy reference in X-ray photoelectron spectroscopy of insulators. *Journal of Electron Spectroscopy and Related Phenomena* **1980**, 20, 105-115.
- (7) Ratner, B. D.; Castner, D. G.: Advances in X-ray photoelectron spectroscopy instrumentation and methodology: instrument evaluation and new techniques with special reference to biomedical studies. *Colloids and Surfaces B: Biointerfaces* **1994**, 2, 333-346.
- (8) Huchital, D. A.: Use of an Electron Flood Gun to Reduce Surface Charging in X-Ray Photoelectron Spectroscopy. *Applied Physics Letters* **1972**, 20.
- (9) Chusuei, C.; Lai, X.; Davis, K.; Bowers, E.; Fackler, J.; Goodman, D.: A nanoscale model catalyst preparation: Solution deposition of phosphine-stabilized gold clusters onto a planar TiO₂ (110) support. *Langmuir* **2001**, 17, 4113-8230.
- (10) Anthony, M.; Seah, M.: XPS: Energy calibration of electron spectrometers. 1—An absolute, traceable energy calibration and the provision of atomic reference line energies. *Surface and interface analysis* **1984**, 6, 95-106.
- (11) Kim, K. S.; Winograd, N.: X-ray photoelectron spectroscopic binding energy shifts due to matrix in alloys and small supported metal particles. *Chemical Physics Letters* **1975**, 30, 91-95.
- (12) Sokolowski, E.; Nordling, C.; Siegbahn, K.: Chemical shift effect in inner electronic levels of Cu due to oxidation. *Physical Review* **1958**, 110, 776-1552.
- (13) Yeh, J. J.; Lindau, I.: Atomic Subshell Photoionization cross sections and asymmetry parameters : $1 < Z < 103$. *Atomic Data and Nuclear Data* **1985**, 32, 1-155.
- (14) Wertheim, G. K.; DiCenzo, S. B.: Cluster growth and core-electron binding energies in supported metal clusters. *Physical Review B* **1988**, 37, 844.
- (15) Wertheim, G.: Electronic structure of metal clusters. *Zeitschrift für Physik D Atoms, Molecules and Clusters* **1989**, 12, 319-326.
- (16) Wertheim, G.; DiCenzo, S.; Youngquist, S.: Unit charge on supported gold clusters in photoemission final state. *Physical review letters* **1983**, 51, 2310-2313.
- (17) Porsgaard, S.; Jiang, P.; Borondics, F.; Wendt, S.; Liu, Z.; Bluhm, H.; Besenbacher, F.; Salmeron, M.: *Angewandte Chemie International Edition* **2011**, 50, 2266-2269.
- (18) Juodkazis, K.; Juodkazytė, J.; Jasulaitienė, V.; Lukinskas, A.; Šebeka, B.: XPS studies on the gold oxide surface layer formation. *Electrochemistry Communications* **2000**, 2, 503-507.

- (19) Koslowski, B.; Boyen, H. G.; Wilderotter, C.; Kästle, G.; Ziemann, P.; Wahrenberg, R.; Oelhafen, P.: Oxidation of preferentially (111)-oriented Au films in an oxygen plasma investigated by scanning tunneling microscopy and photoelectron spectroscopy. *Surface Science* **2001**, *475*, 1-10.
- (20) Borman, V.; Pushkin, M.; Tronin, V.; Troyan, V.: Evolution of the electronic properties of transition metal nanoclusters on graphite surface. *Journal of Experimental and Theoretical Physics* **2010**, *110*, 1005-1025.
- (21) Zafeiratos, S.; Kennou, S.: A study of gold ultrathin film growth on yttria-stabilized ZrO₂(100). *Surface Science* **1999**, *443*, 238-244.
- (22) Kolmakov, A.; Goodman, D.: Scanning tunneling microscopy of gold clusters on TiO₂(110): CO oxidation at elevated pressures. *Surface Science* **2001**, *490*.
- (23) Valden, M.; Lai, X.; Goodman, D. W.: Onset of catalytic activity of gold clusters on titania with the appearance of nonmetallic properties. *Science* **1998**, *281*, 1647-1650.
- (24) Kielbassa, S.; Kinne, M.; Behm, R.: Thermal Stability of Au Nanoparticles in O₂ and Air on Fully Oxidized TiO₂ (110) Substrates at Elevated Pressures. An AFM/XPS Study of Au/TiO₂ Model Systems. *The Journal of Physical Chemistry B* **2004**, *108*, 19184-38374.
- (25) Schumacher, B.; Plzak, V.; Kinne, M.; Behm, R.: Highly Active Au/TiO₂ Catalysts for Low-Temperature CO Oxidation: Preparation, Conditioning and Stability. *Catal Lett* **2003**, *89*, 109-223.
- (26) Johnson, G.; Wang, C.; Priest, T.; Laskin, J.: Monodisperse Au₁₁ clusters prepared by soft landing of mass selected ions. *Analytical chemistry* **2011**, *83*, 8069-8072.
- (27) Lim, D.-C.; Hwang, C.-C.; Ganteför, G.; Kim, Y.: Model catalysts of supported Au nanoparticles and mass-selected clusters. *Physical chemistry chemical physics : PCCP* **2010**, *12*, 15172-15180.
- (28) Kunz, S.; Hartl, K.; Nesselberger, M.; Schweinberger, F.; Kwon, G.; Hanzlik, M.; Mayrhofer, K. J.; Heiz, U.; Arenz, M.: Size-selected clusters as heterogeneous model catalysts under applied reaction conditions. *Physical chemistry chemical physics : PCCP* **2010**, *12*, 10288-10291.
- (29) Jadzinsky, P. D.; Calero, G.; Ackerson, C. J.; Bushnell, D. A.; Kornberg, R. D.: Structure of a Thiol Monolayer-Protected Gold Nanoparticle at 1.1 Å Resolution. *Science* **2008**, *318*, 430-433.
- (30) Thomas, J. M.; Johnson, B. F. G.; Raja, R.; Sankar, G.; Midgley, P. A.: High-Performance Nanocatalysts for Single-Step Hydrogenations. *Accounts of Chemical Research* **2003**, *36*, 20-30.
- (31) Kulkarni, A.; Lobo-Lapidus, R. J.; Gates, B. C.: Metal clusters on supports: synthesis, structure, reactivity, and catalytic properties. *Chemical Communications* **2010**, *46*, 5997-6015.
- (32) Thomas, J. M.; Raja, R.: Exploiting Nanospace for Asymmetric Catalysis: Confinement of Immobilized, Single-Site Chiral Catalysts Enhances Enantioselectivity. *Acc. Chem. Res.* **2008**.
- (33) Raja, R.; Sankar, G.; Thomas, J. M.: Powerful Redox Molecular Sieve Catalysts for the Selective Oxidation of Cyclohexane in Air. *Journal Of the American Chemical Society* **1999**, *121*, 11926-11927.
- (34) Hungria, A. B.; Raja, R.; Adams, R. D.; Captain, B.; Thomas, J. M.; Midgley, P. A.; Golovko, V.; Johnson, B. F. G.: Single-Step Conversion of Dimethyl Terephthalate into Cyclohexanedimethanol with Ru₅PtSn, a Trimetallic Nanoparticle Catalyst. *Angewandte Chemie International Edition* **2006**, *45*, 4782-4785.
- (35) Vegh, J.: On analyzing the intrinsic processes through the Shirley background correction procedure. *Surface Science* **2005**.
- (36) Vegh, J.: The Shirley background revised. *Journal of Electron Spectroscopy and Related Phenomena* **2006**, *151*.

- (37) Hesse, R.; Streubel, P.; Szargan, R.: Product or sum: comparative tests of Voigt, and product or sum of Gaussian and Lorentzian functions in the fitting of synthetic Voigt based X ray photoelectron spectra. *Surface and interface analysis* **2007**, *39*, 381-772.
- (38) Kielbassa, S.; Häbich, A.; Schnaidt, J.; Bansmann, J.; Weigl, F.; Boyen, H.-G.; Ziemann, P.; Behm, R.: On the morphology and stability of Au nanoparticles on TiO₂(110) prepared from micelle-stabilized precursors. *Langmuir* **2006**, *22*, 7873-7953.
- (39) Stephen, C. P.; Charles, T. C.: Reactivity and sintering kinetics of Au/TiO₂(110) model catalysts: particle size effects. *Topics in Catalysis* **2007**, *44*.
- (40) Pireaux, J.; Liehr, M.; Thiry, P.; Delrue, J.; Caudano, R.: Electron spectroscopic characterization of oxygen adsorption on gold surfaces:: II. Production of gold oxide in oxygen DC reactive sputtering. *Surface Science* **1984**, *141*, 221-453.
- (41) Campbell, C. T.; Parker, S. C.; Starr, D. E.: The effect of size-dependent nanoparticle energetics on catalyst sintering. *Science* **2002**, *298*, 811-814.
- (42) Büttner, M.; Oelhafen, P.: XPS study on the evaporation of gold submonolayers on carbon surfaces. *Surface Science* **2006**, *600*, 1170-1177.
- (43) Kitsudo, Y.; Iwamoto, A.; Matsumoto, H.; Mitsuhara, K.; Nishimura, T.; Takizawa, M.; Akita, T.; Maeda, Y.; Kido, Y.: Final state effect for Au 4f line from gold-nano-particles grown on oxides and HOPG supports. *Surface Science* **2009**, *603*, 2108-4222.
- (44) Lykhach, Y.; Plšek, J.; Spirovová, I.; Bastl, Z.: Thermal Stability of Au/NbO_x/Nb and Au/Nb₂O₅/W Model Catalysts Studied by Angle-Resolved X-Ray Photoelectron Spectroscopy. *Collection of the Czechoslovak Chemical Communication* **2003**, *68*, 1791-1804.
- (45) Lim, D.-C.; Hwang, C.-C.; Gantefor, G.; Kim, Y. D.: Model catalysts of supported Au nanoparticles and mass-selected clusters. *Physical Chemistry Chemical Physics* **2010**, *12*, 15172-15180.
- (46) DiCenzo, S. B.; Berry, S. D.; Hartford, E. H., Jr.: Photoelectron spectroscopy of single-size Au clusters collected on a substrate. *Physical Review B* **1988**, *38*, 8465-8468.
- (47) Cox, D. M.; Eberhardt, W.; Fayet, P.; Fu, Z.; Kessler, B.; Sherwood, R. D.; Sondericker, D.; Kaldor, A.: Electronic structure of deposited monosized metal-clusters. *Zeitschrift für Physik D Atoms, Molecules and Clusters* **1991**, *20*, 385-386.
- (48) Lim, D. C.; Dietsche, R.; Ganteför, G.; Kim, Y. D.: Chemical properties of size-selected Au clusters treated under ambient conditions. *Chemical Physics Letters* **2008**, *457*, 391-395.
- (49) Lim, D. C.; Dietsche, R.; Ganteför, G.; Kim, Y. D.: Oxidation of deposited Au_n (n=2-13) on SiO₂/Si: Influence of the NaOH(aq) treatment. *Chemical Physics* **2009**, *359*, 161-165.
- (50) Lim, D. C.; Dietsche, R.; Ganteför, G.; Kim, Y. D.: Size-selected Au clusters deposited on SiO₂/Si: Stability of clusters under ambient pressure and elevated temperatures. *Applied Surface Science* **2009**, *256*, 1148-1151.
- (51) Weare, W. W.; Reed, S. M.; Warner, M. G.; Hutchison, J. E.: Improved Synthesis of Small (dCORE ≈ 1.5 nm) Phosphine-Stabilized Gold Nanoparticles. *Journal of the American Chemical Society* **2000**, *122*, 12890-12891.
- (52) Yuan, Y.; Asakura, K.; Kozlova, A. P.; Wan, H.; Tsai, K.; Iwasawa, Y.: Supported gold catalysis derived from the interaction of a Au-phosphine complex with as-precipitated titanium hydroxide and titanium oxide. *Catalysis Today* **1998**, *44*, 333-342.
- (53) Battistoni, C.; Mattogno, G.; Zanoni, R.; Naldini, L.: Characterisation of some gold clusters by X-ray photoelectron spectroscopy. *Journal of Electron Spectroscopy and Related Phenomena* **1982**, *28*, 23-31.

- (54) Battistoni, C.; Mattogno, G.; Cariati, F.; Naldini, L.; Sgamellotti, A.: XPS photoelectron spectra of cluster compounds of gold. *Inorganica Chimica Acta* **1977**, *24*, 207-210.
- (55) Van Attekum, P. M. T. M.; Van der Velden, J. W. A.; Trooster, J. M.: X-ray photoelectron spectroscopy study of gold cluster and gold(I) phosphine compounds. *Inorganic Chemistry* **1980**, *19*, 701-704.
- (56) Boyen, H. G.; Ethirajan, A.; Kästle, G.; Weigl, F.; Ziemann, P.; Schmid, G.; Garnier, M. G.; Büttner, M.; Oelhafen, P.: Alloy Formation of Supported Gold Nanoparticles at Their Transition from Clusters to Solids: Does Size Matter? *Physical Review Letters* **2005**, *94*, 016804.
- (57) Ono, L. K.; Roldan Cuenya, B.: Formation and Thermal Stability of Au₂O₃ on Gold Nanoparticles: Size and Support Effects. *The Journal of Physical Chemistry C* **2008**, *112*, 4676-4686.
- (58) Turner, M.; Golovko, V. B.; Vaughan, O. P. H.; Abdulkin, P.; Berenguer-Murcia, A.; Tikhov, M. S.; Johnson, B. F. G.; Lambert, R. M.: Selective oxidation with dioxygen by gold nanoparticle catalysts derived from 55-atom clusters. *Nature* **2008**, *454*, 981-983.
- (59) Tsunoyama, H.; Ichikuni, N.; Sakurai, H.; Tsukuda, T.: Effect of electronic structures of Au clusters stabilized by poly(N-vinyl-2-pyrrolidone) on aerobic oxidation catalysis. *Journal of the American Chemical Society* **2009**, *131*, 7086-7179.
- (60) Rao, C. N. R.; Vijayakrishnan, V.; Aiyer, H. N.; Kulkarni, G. U.; Subbanna, G. N.: An investigation of well-characterized small gold clusters by photoelectron spectroscopy, tunneling spectroscopy, and cognate techniques. *The Journal of Physical Chemistry* **1993**, *97*, 11157-11160.
- (61) Santra, A. K.; Goodman, D. W.: Oxide-supported metal clusters: models for heterogeneous catalysts. *Journal of Physics: Condensed Matter* **2003**, *15*, R31.
- (62) Kitsudo, Y.; Iwamoto, A.; Matsumoto, H.; Mitsuhashi, K.; Nishimura, T.; Takizawa, M.; Akita, T.; Maeda, Y.; Kido, Y.: Final state effect for Au 4f line from gold-nano-particles grown on oxides and HOPG supports. *Surface Science* **2009**, *603*, 2108-2114.
- (63) Diebold, U.: The surface science of titanium dioxide. *Surface Science Reports* **2003**, *48*, 53-282.
- (64) Fong, Y.-Y.; Visser, B. R.; Gascooke, J. R.; Cowie, B. C. C.; Thomsen, L.; Metha, G. F.; Buntine, M. A.; Harris, H. H.: Photoreduction Kinetics of Sodium Tetrachloroaurate under Synchrotron Soft X-ray Exposure. *Langmuir* **2011**, *27*, 8099-8104.
- (65) Cowie, B.; Tadich, A.; Thomsen, L.: The Current Performance of the Wide Range (90–2500 eV) Soft X-ray Beamline at the Australian Synchrotron. *AIP Conference Proceedings* **2010**, *1234*, 307.
- (66) Shirley, D. A.: High-Resolution X-Ray Photoemission Spectrum of the Valence Bands of Gold. *Physical Review B* **1972**, *5*, 4709-4714.
- (67) Proctor, A.; Sherwood, P.: Data analysis techniques in x-ray photoelectron spectroscopy. *Analytical Chemistry* **1982**.
- (68) Shirley, D. A.: High-Resolution X-Ray Photoemission Spectrum of the Valence Bands of Gold. *Physical Review B* **1972**, *5*, 4709.
- (69) Hughes, H.; Scarfe, J.: Lineshapes in core-level photoemission from metals: I. Theory and computational analysis. *Journal of Physics: Condensed Matter* **1996**, *8*, 1421.
- (70) Briggs, D.; Seah, M. P.: Practical Surface Analysis. Macmillan Publishers Limited. All rights reserved, 1990.
- (71) Asami, K.: *Journal of Electron Spectroscopy and Related Phenomena* **1976**, *9*, 469-478.
- (72) Dücker, K.; Bonzel, H. P.: *Surface Science* **1989**, *213*, 25-48.

- (73) Thomas, T. D.; Weightman, P.: *Physical Review B* **1986**, *33*, 5406-5413.
- (74) Van Attekum, P.; Van der Velden, J.; Trooster, J.: X-ray photoelectron spectroscopy study of gold cluster and gold (I) phosphine compounds. *Inorganic Chemistry* **1980**, *19*, 701-1405.
- (75) Buttner, M.; Oelhafen, P.: XPS study on the evaporation of gold submonolayers on carbon surfaces. *Surface Science* **2006**, *600*, 1170-2347.
- (76) Lykhach, Y.; Plsek, J.: *Czech. Chem. Commun.* **2003**, *68*, 1791.
- (77) Battistoni, C.; Mattogno, G.; Zanoni, R.; Naldini, L.: *Journal of Electron Spectroscopy and Related Phenomena* **1982**, *28*, 23-31.
- (78) Boyen, H. G.; Ethirajan, A.; Kästle, G.; Weigl, F.; Ziemann, P.; Schmid, G.; Garnier, M.; Büttner, M.; Oelhafen, P.: Alloy formation of supported gold nanoparticles at their transition from clusters to solids: does size matter? *Physical review letters* **2005**, *94*, 16804.
- (79) Strydom, C. A.; Strydom, H. J.: *Inorganica Chimica Acta* **1989**, *159*, 191-195.
- (80) Juodkazis, K.; Juodkazytė, J.; Jasulaitienė, V.; Lukinskas, A.; Šebeka, B.: *Electrochemistry Communications* **2000**, *2*, 503-507.
- (81) Koslowski, B.; Boyen, H. G.; Wilderotter, C.; Kästle, G.; Ziemann, P.; Wahrenberg, R.; Oelhafen, P.: *Surface Science*, **2001**, *475*, 1-10.
- (82) Lim, D.-C.; Hwang, C.-C.; Ganteför, G.; Kim, Y.: Model catalysts of supported Au nanoparticles and mass-selected clusters. *Physical chemistry chemical physics : PCCP* **2010**, *12*, 15172-15252.
- (83) L.K.Ono; Cuenya, B. R.: *The Journal of Physical Chemistry C* **2008**, *112*, 4676 - 4686.
- (84) Lim, D. C.; Dietsche, R.; Ganteför, G.; Kim, Y. D.: *Chemical Physics Letters* **2008**, *457*, 391-395.
- (85) Stakheev, A. Y.; Kustov, L. M.: *Applied Catalysis A: General* **1999**, *188*, 3-35.
- (86) Lin, L.; Zheng, R. Y.; Xie, J. L.; Zhu, Y. X.; Xie, Y. C.: *Applied Catalysis B: Environmental* **2007**, *76*, 196-202.
- (87) Ohtani, B.; Prieto-Mahaney, O. O.; Li, D.; Abe, R.: What is Degussa (Evonik) P25? Crystalline composition analysis, reconstruction from isolated pure particles and photocatalytic activity test. *Journal of Photochemistry and Photobiology A: Chemistry* **2010**, *216*, 179-182.
- (88) Aliaga, C.; Park, J. Y.; Yamada, Y.; Lee, H. S.; Tsung, C.-K.; Yang, P.; Somorjai, G. A.: Sum Frequency Generation and Catalytic Reaction Studies of the Removal of Organic Capping Agents from Pt Nanoparticles by UV/Ozone Treatment. *The Journal of Physical Chemistry C*, **2009**, *113* (15), 6150–6155
- (89) Ho, K. Y.; Yeung, K. L.: Effects of ozone pretreatment on the performance of Au/TiO₂ catalyst for CO oxidation reaction. *Journal of Catalysis* **2006**, *242*, 131-141.

6 Catalytic behaviour of supported gold phosphine clusters

Objectives

Oxidation of alkenes, either at the double bond or at the adjacent allylic positions, can be undertaken by using a wide range of oxidants, such as potassium permanganate, osmium tetroxide, ozone, iodine, peroxy acids or ruthenium tetroxide.^{1,2} Catalytic oxidation of organic compounds using many transition metals as catalysts has been known for over a century.² The selective, partial oxidation of organic substrates is an important chemical transformation for production of both bulk and fine chemicals. The more efficient and environmentally benign reactions are increasingly being sought after due to the ever increasing costs for the production of organic molecules.³ New catalytic routes to common reagents and to novel chemical products are being investigated with a focus on their commercial viability, as rising costs of commodities and starting materials is making well-established and commonly used by industrial routes less profitable. Since the earliest reports by Haruta of the potential of supported gold nanoparticles for the oxidation of carbon monoxide and subsequent reports of selective partial oxidation using gold catalysts, the use of gold for oxidation of organic compounds has increasingly drawn more attention.^{4,5}

In this chapter, supported gold phosphine clusters were examined for their effectiveness for the partial oxidation of styrene under selected catalytic conditions. Each catalyst was investigated under various conditions of oxygen and/or the radical initiator tert-butyl hydrogen peroxide (TBHP). Our early experiments were focused on the development of robust and reliable methodology for oxidising alkenes in the liquid phase. Partial oxidation of styrene was chosen as an ideal model reaction to compare the reactivity of a large series of novel catalysts based on phosphine stabilised gold clusters and colloids. Styrene provides a range of challenges as a substrate in the catalytic oxidation, such as the control of product selectivity, due to wide of range of possible oxidation products.⁶

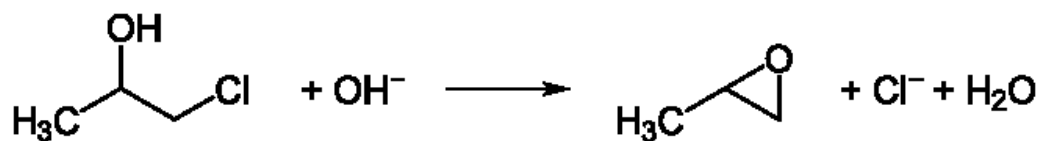
In the following pages, I will endeavour to discuss how the catalytic methodology was developed initially and then discuss the catalytic results under the standardised system. The comparison to the literature will be in general limited to heterogeneous systems that involve a metal oxide support. This chapter will attempt to:

- Illuminate the reactivity of supported gold clusters under three distinct catalytic conditions
- Compare the reactivity of gold clusters on two contrasting support materials (support effect)
- Compare the reactivity of catalysts made using gold clusters with of different nuclearity (size effect)
- Compare the effect of different catalyst activation methods on the reactivity (activation effect)
- Relate the electronic structure of the supported clusters to the observed reactivity.

Introduction

Alkene oxidation reactions are important chemical transformations in the laboratory, as well as in the chemical industry. Alkenes are often viewed as having latent functionality, which can be revealed under the right reaction conditions, at the appropriate stage during a multi-step process, with the desired functionality.⁷ One of the issues encountered in alkene oxidation reactions is the control of product selectivity, and often, the reaction can involve stoichiometric amounts of reactants. In the fine and bulk chemical synthesis,⁸ there is a significant demand for various terminal alcohols that can be formed from alkenes which is termed anti-Markovnikov alkene hydration. A common method for forming terminal alcohols involves hydroboration/oxidation which generates hydration products with anti-Markovnikov regioselectivity.⁹ This is a two-step process which requires stoichiometric amounts of borane reagents and generates boron-containing waste that is difficult to recycle. Furthermore, the peroxides used in the oxidation step raise safety and environmental concerns for large-scale industrial production. Most recently, Dong *et al.* have demonstrated a combined catalytic system that yields anti-Markovnikov alkene hydration products, which is based on a two-catalyst cooperative system involving an palladium-catalysed oxidation cycle followed by a reduction cycle enabled by ruthenium-based catalyst.¹⁰

Epoxidation



Epoxides are commercially important class of chemical intermediates in the production of a wide range of fine chemicals via various metal-catalysed oxidations of alkenes. They can easily be transformed in to a large variety of compounds by regioselective ring opening reactions.¹¹ Catalytic epoxidation of alkenes in the presence of molecular oxygen and hydrogen peroxide has attracted a lot of attention in recent years, due to the possible elegant and environmentally benign routes to a wide range of compounds.² The environmental benefits are mainly due to the high content of active oxygen in hydrogen peroxide and comparably few toxic by-products (water as the primary by-product in the case of hydrogen peroxide). Currently, one of the most common industrial routes for the production of simple epoxides is the chlorohydrin process, which is used to produce epoxides such as propylene oxide by the reaction with chlorine in the presence of sodium hydroxide (

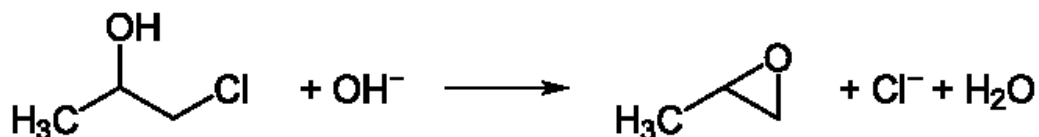


Figure 76). Typically for each tonne of propylene oxide produced there are two tonnes of sodium chloride and 0.1 tonnes of 1,2-dichloropropane produced as by-products.² Due to such large quantities of by-products being produced, greener methods for epoxidation of alkenes are being investigated as replacement for such inefficient industrial processes such as the chlorohydrin process and other stoichiometric methods.

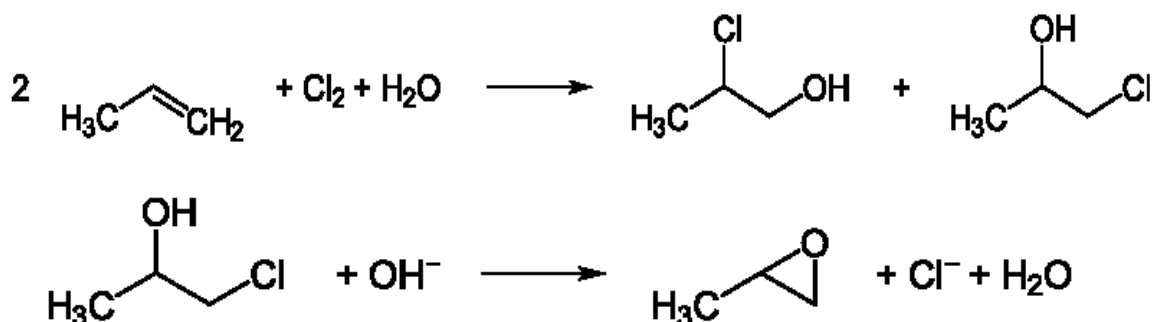


Figure 76: The chlorohydrin process for the production of epoxides.

In recent decades, a range of new methods involving various early transition metals have shown great potential as selective oxidation/epoxidation catalysts. In certain cases, new routes to propylene oxide which involve a $\text{Ti}^{\text{IV}}/\text{SiO}_2$ heterogeneous catalyst (TS-1), using ethylbenzene hydroperoxide as an oxidant, have been incorporated into new industrial plants.^{2,12} The latest generation of propylene oxide production plants are based on hydrogen peroxide as an oxidant or on recycling of cumene by the reduction of the co-product, cumyl alcohol with hydrogen concurrently. Direct epoxidation of propene with oxygen and hydrogen by heterogeneous gold catalysts is a promising process for propylene oxide synthesis, due to the simplicity of one-step reaction in gas phase.¹³⁻¹⁵

In parallel to the recent developments of heterogeneous epoxidation, asymmetric homogeneous catalysts have been improved significantly. Organometallic complexes with titanium (IV) and vanadium (V) have proven to be very selective for the epoxidation for a wide range of allylic alcohols. The Sharpless-Katsuki asymmetric epoxidation catalyst system is a well-known and historically significant catalyst, which proceeds *via* a dimeric organometallic complex from titanium isopropoxide in addition with a tartrate ester.¹⁶ Tert-butyl hydroperoxide is used as an oxidant during this process, as it is relatively safe and facile to use at the lab scale and improves the selectivity for the epoxide product.¹⁷ Recently, there have several further developments with similar vanadium complexes containing chiral salen ligands, which have demonstrated improved reactivity for a wider range of substrates, enhanced enantioselectivity and greater tolerance of water to such an extent that aqueous tert-butyl hydroperoxide can be used.^{18 19}

Although these homogeneous catalysts have found great use for synthesis of various fine chemicals on a relatively small scale, homogeneous catalysts suffer from a common problem – difficulty in separating catalyst and products, which leads to poor recycling of the catalyst material, contamination of products. Support immobilisation of homogeneous catalysts has been attempted through ion exchange, adsorption, covalent linkage, encapsulation, and substitution, depending on the nature of the metals and supports.²⁰ Some of these immobilized homogeneous systems have displayed significant disadvantages, such

as rapid loss in activity after immobilization, leaching of the catalytically active species, poor thermal stability, and poor recyclability.

The catalyst, either homogeneous or heterogeneous, in essence has two distinct functions:

- To generate the necessary active oxygen species for the desired reactivity
- To activate the organic substrate towards the desired product(s)

To tune these two separate aspects independently has proven difficult.

It was shown by DFT calculations that small gold clusters (Au_{13} , Au_{55}) can readily adsorb molecular oxygen; however, the activation of oxygen was shown to be difficult. The generation of the active oxygen species was shown to occur at the junction of the small gold clusters and the metal oxide supports.²⁴ Many gold-titania catalysts have gold particle sizes of 2-5 nm which have similar electronic properties to bulk gold; hence, the activation of oxygen does not occur. Recent studies have shown that small ligand stabilised gold cluster supported on silica were active for the oxidation of styrene and other organic compounds with only molecular oxygen.^{21,22}

The following section will provide a detailed summary on the current state of the selective partial catalytic oxidation of alkenes in the liquid phase by gold-based catalysts and other related catalyst systems, as the vast majority of the reported examples of gold-catalysed alkene oxidation have been achieved using heterogeneous catalyst systems.²³ Since the initial discovery of the catalytic activity of gold nanoparticles supported on metal oxide supports by Haruta *et al.*, gold-based heterogeneous catalysts have become increasingly important.²⁴ The potential of supported gold catalysts for the liquid phase oxidation of organic compounds has only been demonstrated in the last decade. Finally, it should be noted that there have been several very recent examples of unsupported gold nanoparticles being catalytically active for several reactions.²⁵⁻²⁷

Hughes *et al.* demonstrated that gold nanoparticles supported on carbon can be used for alkene oxidation and that under the right conditions the epoxide product can be generated in significant yields.²⁸ This study focused on the nanocrystalline gold with a broad particle size distribution (5- 50 nm), which was prepared by the reduction of tetrachloroauric

acid on a graphitic support in the presence of formaldehyde. This study focused on the oxidation of cyclohexene with various metal loadings (0.5 and 1 wt. %) of the Au/C catalyst. When the oxidation of cyclohexene was carried out in polar solvents (water, methanol, and tetrahydrofuran), the reaction yielded only the total oxidation products, such as carbon dioxide, formic acid and oxalic acid. Although conversions were much lower for the methanol and tetrahydrofuran systems as opposed to the aqueous system in which full conversion of the cyclohexene was observed. Following on from these results, a wide range of nonpolar solvents were employed which showed significantly improved selectivity for C₆ products. Typically, conversions of around 10-30 % were achieved with moderate selectivity for C₆ products. It was also shown that for the reaction to take place an initiator is required (either hydrogen peroxide or tert-butyl hydrogen peroxide). The highest selectivity for the cyclohexene oxide product (50%) was observed when aromatic solvents *i.e.* 1,2,3,5-tetramethylbenzene was used in combination with 1% Au/graphite as the catalyst. The strong solvent effect in such catalytic processes was later re-emphasised in the work by Valarie Caps, which showed that for the world gold council standard Au/TiO₂ catalyst the increase in the number of methyl groups within the structure of aromatic solvent can significantly increase the reactivity due the proposed radical type mechanism.²⁹ Further work by Hughes *et al.* showed that the initial product formed was the epoxide with other products being formed due to subsequent oxidations of epoxide.²⁸ Kinetic isotope studies, in which deuterated toluene was used, did not show any significant change in the rate of the reaction, which indicates that nonpolar solvents similar to toluene do not participate in the rate determining step of the reaction, by acting as sacrificial source of hydrogen. This contrasts significantly with the need to use sacrificial hydrogen in the gas phase oxidation of carbon monoxide and propene.¹³ Furthermore, Hughes *et al.* highlighted the sensitivity of gold-based catalysts to the presence of dopants.²⁸ The addition bismuth, as bismuth nitrate, to the catalyst was shown to significantly increase the yield of C₆ products (97.8%). Even with approximately 60 % loss of the bismuth dopant after the first run of the experiment, the catalyst was shown to be similarly effective over multiple runs. This observation emphasising that even tiny amounts of dopants can have a significant effect on selectivity of a catalyst.

Gold supported on titania has become the prevalent system for the studies on alkene oxidation in both the gas and liquid phase. Titania supports have been known to have a

much more noticeable electronic interaction with metal nanoparticles, which contrasts significantly with the inert carbon supports previously discussed. Caps *et al.* provided the first detailed proposal on the reaction mechanism for the oxidation of trans stilbene by the world gold council reference gold-titania catalyst.²⁹ The world gold council reference catalyst consists of gold nanoparticles supported on P-25 titania, prepared by precipitation-deposition method, with a gold loading of 1.5 % , a mean particle size of 3.9 nm (± 1.5 nm).³⁰ This stereoselective epoxidation of stilbene in the presence of 5 mol % of TBHP yielded 53 % of the epoxide product in the methylcyclohexane (MCH) solvent. Use of other solvents was also explored but did not result in improvement of the catalysts' selectivity, when compared to MCH. A free radical chain mechanism was proposed to explain the observed reactivity, in which the MCH peroxy radical is generated by hydrogen abstraction involving the gold nanoparticles. Further work by Caps *et al.* has also highlighted the importance of the support structure (*i.e.* porosity, chemical functionalities at the surface) and the effects of various preparative procedures, mentioned in chapter 4 on the effectiveness of the gold based titania catalysts.^{31,32} Citrate functionalised titania nanocrystallites were investigated for their effectiveness for the oxidation of stilbene, and the studies highlighted the importance of surface functionalisation of the titania support.³¹

Earlier work by Patil *et al.* investigated the selective oxidation of styrene by several gold - titania catalysts prepared by several modified deposition-precipitation methods. The gold loading varied significantly from 1 to 6 %, with relatively large particle sizes (5 to 20 nm) depending on the gold loading and preparation. TBHP was used as the active oxygen source, yielding moderate amounts of the styrene oxide product.^{33,34} As the large amounts TBHP were used in this system, there is very little need for small particles of gold for high catalytic activity, when compared to the previously described systems. With improved size of control of the gold particles, by decreasing the gold loading, it may be possible to decrease the mean particle diameter and improve reactivity significantly.

Turner *et al.* reported the first cluster-based gold catalyst systems supported on silica and BN being employed in the liquid phase oxidation of styrene.²¹ Gold phosphine cluster, Au₁₀₁, was deposited on fumed silica and also boron nitride, and heat treated at 200 °C. The gold loading for these systems was approximately 0.6 % by weight of gold, with an average

gold particle size of 1.7 nm. These cluster-based gold catalysts show surprising reactivity for styrene oxidation, in toluene with only molecular oxygen being used as the source of oxygen. The gold cluster based catalysts showed conversion of around 20-30 % with high selectivity for the benzaldehyde product. It is postulated that the main product is the epoxide, which is then further converted to other products. Comparisons between other gold nanoparticle preparations which generate increased particle sizes, such as the PVP-stabilised gold nanoparticle (3 nm), microemulsion (4 nm) and incipient wetness (≥ 30 nm) were also conducted. These catalysts showed little to no reactivity compared to the cluster-based catalysts under similar conditions. Previously, there have only been a handful of examples of supported gold catalysts on silica, and these examples have often required other sources of active oxygen. Some of the earliest examples of gold catalysis were of the hydrogenation of various alkenes and aromatic substrates by gold-silica catalyst, which showed moderate activity at high temperatures and pressures.³⁵ However, the catalysis potential of silica supported gold catalysts has largely been ignored when compared to the success of the titania supported gold catalysts pioneered by Haruta.^{36,37} It should be highlighted that in this study the loading of gold on the support material is only 0.6 % as compared to the World Gold Council (WGC) reference catalysts, which are much higher loaded and have larger mean gold particle diameter *e.g.* WGC Au-TiO₂ (1.5 wt. % of gold, 3.9 nm \pm 1.7nm) WGC Au-Fe₂O₃ (4.4 wt. % of gold, 4.0 nm \pm 0.9 nm), WGC Au-C (1 wt. % of gold, 10 nm \pm 0.9 nm).³⁸

Recently, several gold cluster-based catalytic systems have been developed on silica supports and investigated by Rongchao Jin. Since the biphasic alkane thiol method for the preparation of gold nanoparticles with tuneable size and functionality, a wide range of thiolate stabilised gold clusters have been prepared.^{39,40} Various supported gold thiolate clusters were studied for reactivity in the presence of oxygen, catalytic amounts of tert-butyl hydroperoxide (TBHP), and excess amounts of TBHP.⁴¹ The catalysts used in these studies were prepared by stirring a solution of the gold thiolate clusters (*i.e.* Au₂₅(SCH₂CH₂Ph)₁₈, Au₃₈(SCH₂CH₂Ph)₂₄, Au₁₄₄(SCH₂CH₂Ph)₆₀) in a slurry of fumed silica in dichloromethane. The samples were subsequently activated at 200 °C under vacuum. HR TEM analysis of the supported gold sample was unable to determine exact particle size, due to the small cluster sizes and distinguishing from the silica support. A size effect was observed where the smaller gold thiolate clusters were more effective for the conversion of styrene

with only molecular oxygen; whilst in the presence of catalytic amounts of TBHP much higher reactivity was observed in all cases. The size of cluster appears to have less of an effect in the presence of TBHP. The effect of *calcination* under vacuum was also investigated and shown to increase the reactivity of the silica supported gold clusters by approximately 6-10 % for the two smaller clusters, whilst in the case of the larger $\text{Au}_{144}(\text{SCH}_2\text{CH}_2\text{Ph})_{60}$, the reactivity decreased. Observed drop in reactivity was explained by the Au particle sintering which has decreased the ability of the cluster for oxygen activation. Three different catalytic methods were also compared for all the clusters, where the order of reactivity was TBHP only > Catalytic amounts of TBHP with O_2 as a main source of oxygen > oxygen only.

The proposed mechanism for the selective oxidation of styrene by gold thiolate cluster in all three systems goes by the common peroxo intermediate $\text{Au}_{25}\text{-O}_2$ species, which is generated in all systems (*i.e.* TBHP, TBHP/ O_2 , O_2), shown in Figure 77. Existence of such peroxo species was suggested by several computational studies of these catalysts in the gas and liquid phase.⁴² The activation of the oxygen is assumed to occur due to the electron rich Au_{13} core, and the Au_{12} shell which also activates the styrene nucleophile. Subsequent rearrangements and dissociation of the intermediates leads to three different possible products that were seen in the reaction.^{41,43} It should be noted that the proposed mechanism for this gold thiolate clusters assumes that no cluster sintering occurs, ignores the effect of the silica support and the fact that larger particles of gold have been shown to oxidise styrene in several previous reports.^{34,44,45}

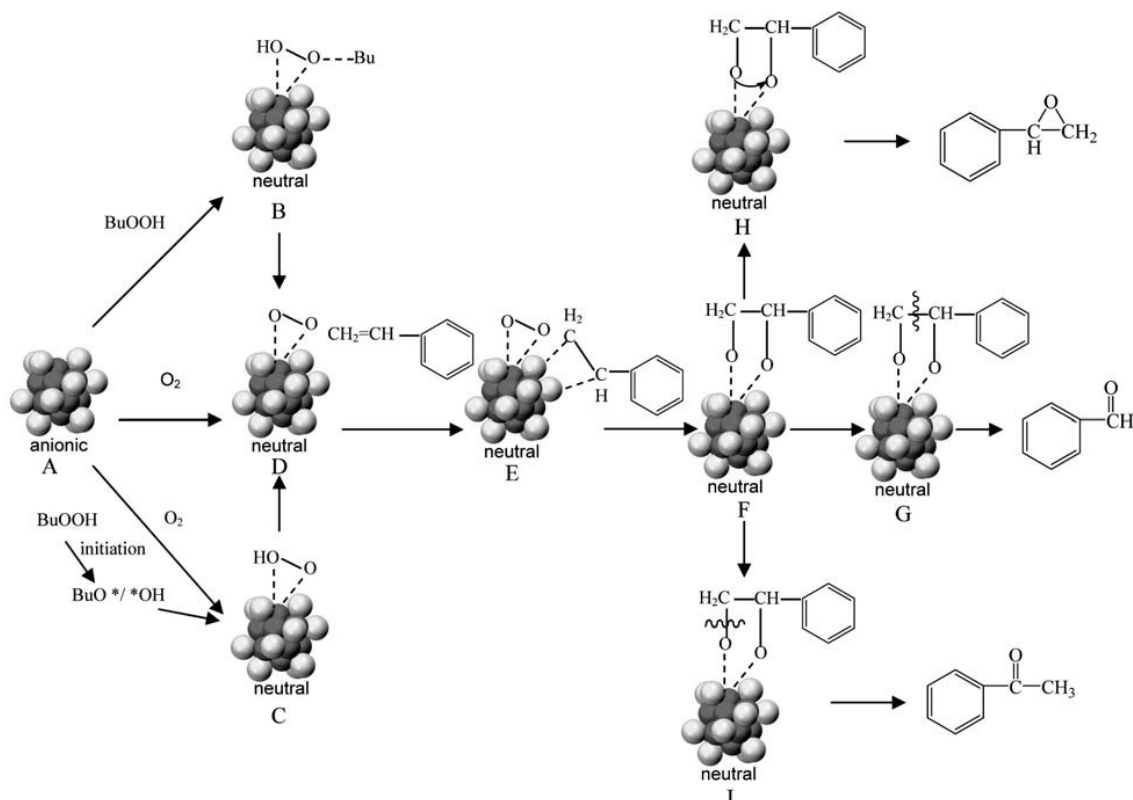


Figure 77; Proposed mechanism for the oxidation styrene by gold thiolate clusters reproduced from reference ⁴¹

Tsukuda *et al.* has recently shown that gold thiolate cluster immobilised on a hydroxyapatite support as a catalyst could lead to high conversions of styrene with high yields of the epoxide product using a high excess of anhydrous TBHP as the oxidant.^{46,47} It was proposed that the hydroxyapatite could be an ideal support material for the gold thiolate cluster (Au_{25}), due to the strong electrostatic interaction of the cluster with the PO_4^{3-} moiety of the support which could prevent sintering of the cluster on the support. Specifically, catalytic reactions were conducted using 0.5 wt. % Au loaded sample of the gold cluster on the hydroxyapatite support, which was *calcined* at 300 °C under vacuum for two hours resulting in formation of Au particles with dimensions of between 1.2–1.5 nm according to HRTEM data. The oxidation of styrene was conducted in anhydrous toluene and TBHP in test tubes at 80 °C. Dry toluene was shown to be essential for high yields of the epoxide product. Importantly, oxidation of toluene to benzaldehyde was also observed. The geometry and electronics of various modified supports were also shown to have an influence on the product selectivity. Further work in the presence of only molecular oxygen showed similar reactivity when compared to the gold phosphine cluster supported on silica.²¹

In contrast to this “*smaller is better*” idea for gold catalysis, Lambert *et al.* also highlighted that if nitrogen dioxide can also be used as the source of active oxygen for alkene oxidation reactions.⁴⁸ The authors were able to show that larger gold nanoparticles can catalyse the oxidation of styrene in the presence of nitrogen dioxide under mild conditions in toluene (100°C). Gold nanoparticles were prepared by a microemulsion technique and then deposited on to carbon support, which ensured that little or no support interaction as influencing the reactivity. The supported gold particles were dried at 85°C, the particle size was shown to be between 10-25 nm ($\sigma = 16$ nm). Under similar reaction conditions, it was shown that the large gold particles were not catalytically active towards oxidation of alkenes with oxygen alone, but under a 2 % nitrogen dioxide atmosphere moderate conversion of styrene with moderate selectivity towards the epoxide product was observed.

In summary, selective partial oxidation of styrene and related alkenes was catalysed by a range of supported gold nanoparticles in the liquid phase. A wide range of factors have been shown to influence the activity and product selectivity:

- Oxidant source
- Gold particle size
- Gold loading
- Support type and morphology
- Activation treatments
- Reaction conditions

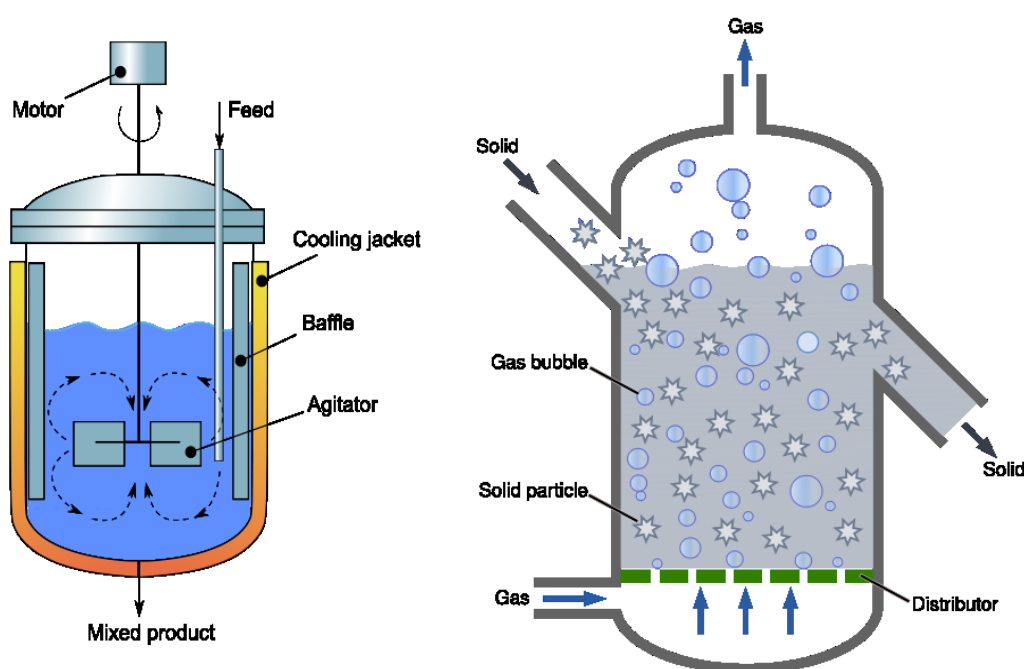
In the case of gold catalysts, using molecular oxygen as oxidant necessitates the design of catalysts with precise particle size of less than 1.5 nm, with better control over nanoparticle sintering, and a well understood support material than enhances selectivity of the formation of desired products. To date, it has been shown that there is a lot of potential for gold-based systems for the liquid phase partial oxidation of various alkene substrates. However, achieving precise control over morphology of model catalysts remains a major challenge. Hence, understanding of the activity and selectivity of these systems has proven elusive.

Experimental

I. Catalytic batch reactors

There are a wide range of methods available to assess the properties of new catalysts, such as continuously stirred tank reactors (CSTR), fluidised bed reactors and gradient free recycle reactors, which can be used for gas or liquid phase investigations.⁴⁹ CSTR and fluidised bed reactors are ideal for further development of promising catalysts. Fluidised bed reactors are ideal for multiphase chemical reactions, where components from different phases undergo transformations at the surface of a solid, heterogeneous catalyst.

Figure 78; Schematic representation of A) continuously stirred tank reactor and B) fluidised bed reactor



The initial focus of this research project was to develop various batch reactors in which a wide range of catalysts that were produced in our laboratory and obtained from various collaborators could be compared comprehensively against each other. A batch reactor typically consists of sealed vessel, a method to stir or agitate the solution or suspension and a source of heat, usually with a feedback loop temperature control. Due to mass transfer limitations, the rate of stirring can significantly affect the activity of the catalyst, which needs to be suspended evenly throughout the solution.

A Parr mini reactor series 4835 was inherited by our research group which was equipped with a digital pressure readout, isomantle heater controlled using internally submerged thermocouple using programmable digital temperature controller. The Parr reactor was modified in house to improve stirring rates from a maximum of 900 rpm to a calculated maximum of 1750 rpm. The reactor was connected to the in-house built gas manifold system which allowed a selection of gases (O_2 , H_2 , CO , C_2H_4) to be used during catalytic testing and running reactions under constant pressure using constant top-up mode. The reactor was made of type 316 stainless steel, which was corrosion resistant, but contains small amounts of nickel and chromium; hence, Teflon reactor cups were made and fitted for the reactor vessel with an aim to ensuring reproducibility of obtained results, due to better washing, avoiding cross-contamination and poisoning effects.

Sealed batch pressure reactors were produced in house using 316 stainless steel, comparable to the Parr reactor design. These were also fitted with Teflon liners, stirred magnetically with good control over stirring rate up to 700 rpm using normal magnetic stirring bars or up to 1200 rpm using rare-earth containing magnetic stirring bars. These reactors were heated using hotplate-stirrers with temperature control via feedback loop involving internally submerged thermocouple and microprocessor driven temperature controllers which allowed maintaining target temperature with precision of 1 °C. Glass batch reactors were used for ambient pressure experiments to increase productivity, which involved several iterations to optimise this system to achieve reproducibility. Our first design of catalytic testing system involving glass batch reactors involved a two-necked round bottomed flask (RBF) fitted with a jacketed condenser which had extra internal water-cooled spiral, with the gas flow introduced directly into the stirred liquid through the second neck *via* Pasteur pipette in the first instance. Later, a glass inlet tube fitted with a silica frit was used for better dispersion of gas. The outlet bubbler was connected to the top of the condenser to monitor flow. The oxygen gas was then slowly bubbled through the solution of the substrate (*ca.* 1 mL per min) with an aim to improve the oxygen saturation in the solvent (*i.e.* toluene).⁵⁰ These systems were heated using oil baths on hotplates with digital control of the temperature with precision to 1 °C. Once increased numbers of hotplate-stirrers were available, parallel catalytic tests were conducted. Ensuring that the gas flow was consistent for each glass batch reactor proved difficult as multiple reaction vessels were connected to a

single gas cylinder. However, it was found that the loss of solvent at elevated temperatures and high stirring rates was a significant issue to be aware of - in certain cases five to seven grams (out of total of 16.9 g) of solvent was lost. Attaching bubbler filled with limewater allowed to perform a qualitative check for carbon dioxide to prove that total oxidation of the reaction mixture was not occurring. Despite improving the seal at the ground glass joints, solvent loss remained an issue that kept recurring. After this method was abandoned, the gas inlet was moved to the top of the jacketed condenser connected to a single necked RBF, ensuring that the vessel was charged with an adequate supply of oxygen. Issues with slight solvent loss still reoccurred, which was assumed to be due to the elevated temperatures and high stirring rate. Eventually, it was found that Schlenk tube connected a vacuum double manifold proved adequate for running catalytic testing

II. Materials

Styrene (99.9 %, ReagentPlus®), cyclohexene (99.9 %, ReagentPlus®), cyclohexane (99.9 %, ReagentPlus®) were purchased from Sigma Aldrich. Styrene was filtered through activated basic alumina to remove the tert-butyl catechol inhibitor prior to use. Toluene (HPLC grade) was dried using an in-house solvent drying system which was fabricated by Nick Oliver according to literature methodology.⁵¹ Tert-butyl hydrogen peroxide (TBHP) was used in later experiments as a source of activated oxygen. TBHP was purchased as Luperox® 70 % solution in water from Sigma Aldrich, and was then further purified by azeotropic distillation using a Dean Stark apparatus to yield an anhydrous solution of TBHP in toluene with a concentration no greater than 4 M. The exact concentration was estimated using ¹H NMR.¹⁷ All gases are of instrument grade (99.9+ %) and were sourced from BOC. All glassware was cleaned in a caustic base bath consisting of potassium hydroxide in isopropanol/water (2:1), followed by washing in *aqua regia*, subsequently washing in distilled water and acetone, and finally dried in a glassware oven at 120°C or above overnight.

III. Experimental procedures

A 60 mM stock solution of styrene in toluene was prepared on a 500 mL scale. The stock solution was found to be stable from polymer formation due to the low concentration

of styrene in toluene and was stored at 4 °C in the absence of the catechol inhibitor in the refrigerator.

Oxygen only reactions

Stainless steel sealed pressure vessels were used for the catalytic tests under mild (5 bar) pressures of oxygen. Several modified versions of the mechanical stirrer attachment used in Parr reactor system were designed and fabricated in house to ensure homogenous stirring of the reaction. PTFE cups were also designed and made in house to minimise contamination of the reactor by the variety of catalysts investigated. Initially, the reactor cleaned vigorously by sonication with surfactant, scrubbed and then polished on a lath. The inlet ports and mechanical stirrer were disassembled for further cleaning. The reactor was tested for leaks and blank reactions were conducted to ensure that the catalyst contamination was eliminated.

Between catalytic runs, the detachable body of the Parr reactor was cleaned by sonication with surfactant and subsequent copious washing with distilled water and acetone, followed by drying in air. The stirrer was detached from the reactor head and cleaned by sonication and solvent washes as described above. The PTFE cup was cleaned by sonication and solvent washes as described above.

In a typical catalytic test a PTFE liner was charged with a solution of styrene (60 mM, 20 mL) in toluene and the appropriate catalyst (100 mg \pm 1 mg). The PTFE cup was then loaded in to the Parr pressure vessel and Parr reactor was assembled and sealed to ensure no loss of solvent or oxygen for the duration of the reaction. The vessel was first purged with argon (40 psi) three times whilst being stirred at a rate of 500 rpm. The reactor was checked for leaks by sealing the vessel with *ca.* 400 psi of argon and monitoring the digital pressure readout for any pressure change over a ten minute period. Subsequently, the vessel was vented, flushed three times with oxygen (75 psi) each time keeping a fresh portion of oxygen for a total of five minutes and then charged with oxygen at a pressure of 75 psi (5.1 bar). Once the reactor has been sealed with oxygen, the system was heated to 100 °C while stirring at a rate of 500 rpm. Once the reactor has reached the target temperature, the reaction mixture was stirred at 1000 rpm and left for 18 hours (typically, overnight). After this period the stirring was stopped and the heating mantle was removed and replaced with an ice-water

bath in order to ensure complete condensation of liquid inside the reactor prior to venting. Once the temperature has reached 20 °C, the reactor was vented, dismantled and the PTFE cup was removed. The reaction mixture was then centrifuged in a 50 mL falcon tube (PET) and the supernatant was stored at 4 °C (if required) prior analysis by gas chromatography. The washed and dried sample of a catalyst after reaction was stored at room temperature in a glass vial wrapped in tin foil for further analysis.

Catalytic amounts of tert-butyl hydroperoxide

Styrene solution (60 mM, 20 mL) was added to Schlenk tube containing magnetic stirrer bar and connected to a vacuum double manifold (Schlenk line), 5 mol. % (relative to styrene) of the TBHP (15 mg) as solution of known concentration in toluene was also added to the reaction flask. The flask was sealed, purged three times by vacuum/oxygen cycle and charged with oxygen under atmospheric pressure, whilst a stirred oil bath was preheated heated to 100 °C. Once the oil bath reached target temperature and stabilised the catalysis sample (100 mg) was quickly added and the Schlenk flask was lowered into the oil bath and stirred vigorously at 1000 rpm for 18 hours under an oxygen atmosphere. The Schlenk flask was lowered sufficiently that the oil bath heats all volume of the reaction mixture and that the stirring was stable and continuous. To prevent any possible solvent loss, the reaction vessel was additionally sealed using Teflon tape. Once the reaction was completed, the reaction mixture was cooled in an ice bath and the sample was then centrifuged as soon as possible. The supernatant is stored at 4°C for analysis by gas chromatography, whilst the catalyst is stored wrapped in tin foil for further analysis.

Excess tert-butyl hydroperoxide

The reactions in which TBHP was used as the primary source of active oxygen, the procedure was similar except the quantity of TBHP added was increased to 600 mg, which ensures the molar amount of TBHP was 200 % rather 5% of styrene.

IV. Analytical techniques

Gas chromatography (GC) was the technique of choice for the analysis of the reaction mixtures, which can be used for the separation and analysis of a wide range of volatile

compounds. Gas chromatography is a separation technique in which the components of a sample are distributed between two phases. One of these phases is a stationary bed with a large surface area and the other phase is a carrier gas that flows through the capillary column containing stationary phase. A sample is typically injected *via* the pre-heated injection port where it is vaporised and subsequently carried by the carrier gas phase (Helium) through the high surface area stationary phase or column. The different components of the sample equilibrate independently into the liquid (stationary) phase which is dependent on the temperature of the column at any given time. The components separate along the column due to differences in their relative vapour pressures and their different affinities for the material of stationary column.

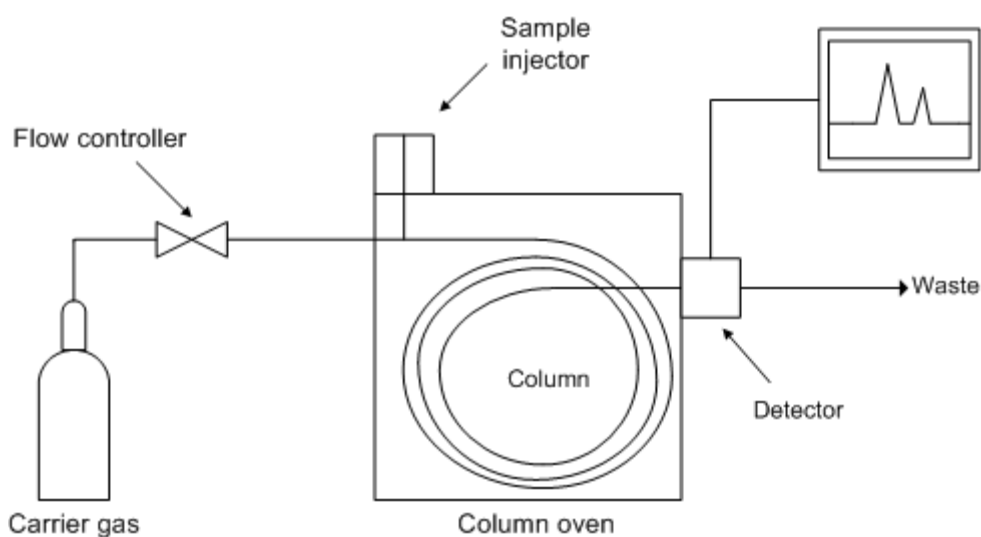


Figure 79; Schematic diagram of a gas chromatograph

There is a wide range of detectors that are used for the detection of various analytes. The flame ionisation detector (FID) was used for quantitative analysis of reaction product mixtures in the reported here study. The detection using mass spectrometer (MS) was also used for samples that generated unknown products.⁵² The FID detector is a popular detector that ionises the analytes to generate a signal. The analytes are typically burned in a small oxo-hydrogen flame (temperature) producing ions. These ions are collected and form a current that is used as the output signal. In the absence of an analytes the ionisation is negligible and is typically derived from traces of impurities (due to previous usage) eluted by the carrier gas from the column and from the impurities in the carrier gas and gasses used to generate flame. Low ionisation in the absence of analytes gives rise to an excellent flat background.

The injection port immediately before the FID detector was kept at 270 °C, to prevent the condensation of water and of high boiling analytes. FID is a very sensitive detector, (min detection sensitivity of ≈ 50 ppm) which is ideal for the detection of all organic compounds which burn in the oxo-hydrogen flame. The FID signal is proportional to the carbon content in the analyte, which gives the detector a large window of analyte concentrations within which the concentration of analyte is related to the peak area in a linear fashion.

Table 7; Summary of the optimised settings for the Shimadzu GC-2010 for analysis of styrene reactions

| Inlet | | Column | | Detector | |
|------------------|----------|--|-----------------|-------------------------------|------------|
| Temperature | 270 °C | Restek Rxi -5sil-5ms 30 m, 0.25 ID, 0.25 μ m film thickness | | Flame Ionising Detector (FID) | |
| Injection Volume | 1 mL | Column Flow | 1 mL/min | Temperature | 270 °C |
| Carrier Gas | Helium | Column Temperature | | Sampling time | 280 mS |
| Split Ratio | 100 | Temp. Initial | 95 °C – 3 min | Hydrogen | 40 mL/min |
| Purge flow | 5 mL/min | Ramping rate | + 20 °C per min | Air | 400 mL/min |
| | | Temp. Final | 250 °C – 20 min | Helium | 30 mL/min |

The signal generated is a distribution or peak whose shape is approximated as being Gaussian or normal in ideal circumstances. When the peak presents with non-symmetrical shapes, this can indicate there is an undesirable interaction with the stationary phase (fused silica in the Restek Rxi -5sil-5ms column). Peak broadening typically indicates that the mass transfer through the column is too slow. The shape of the peaks for the key components of the reaction mixture were optimised so that all of the peaks of interest were as symmetric as possible by carefully selecting the temperature profile of the gas chromatography oven, flow-rates of carrier gas, injection temperatures and volume of sample analysed. .

Table 7 gives values of the key parameters which were used on the Shimadzu GC-2010- FID giving rise to the optimum peak shape and separation. All of the key components of the reaction mixtures eluted within 10 minutes. However, several catalytic samples contained some much larger products that eluted much later compared to the typical low molecular weight partial oxidation products of styrene. Although exact chemical nature of these fractions remains elusive one could hypothesise that these are oligomers of styrene and/or highly functionalized with hydroxyl- or carboxy-functional groups molecules. As a

result, the gas chromatography method was adapted to include a period of temperature ramping to 250 °C, which resulted in the detection of several fractions corresponding to larger polyarene products. These heavier products were detected only very occasionally, yet the additional high temperature ramp was used to ensure that the column remained clean of any organic compounds. Column conditioning was undertaken after analysis of every hundred samples to ensure that the column performance was consistent.

Table 8: Summary of retention times for analytes of interest

| Compound | Styrene | Benzaldehyde | Decane | Benzyl OH | Styrene oxide | Acetophenone | Benzoic Acid |
|---------------------------|---------|--------------|--------|-----------|------------------|--------------|-----------------|
| Retention Time minutes | 3.93 | 5.22 | 6.03 | 7.17 | 8.09 | 8.58 | 18.01 |

Quantification by GC-FID

The magnitude of the signal generated by FID detector is proportional to the amount of analyte that is burned, which allows gas chromatography to be employed for quantitative analysis. Multiple methods are available for quantitative analysis by GC, such as normalisation of peak areas, use of internal standard and external standards *etc.* Early quantitative analysis of the reaction mixtures was performed using external standard method, where a known amount of a standard is added to known volume of reaction mixture collected after the catalytic test was finished. Later quantitative analysis of the reaction mixtures was performed by the internal standard method, where a known amount of a standard is added to each reaction mixture (usually as part of the stock solution of styrene) before the start of reaction. Several calibration mixtures with known amounts of the reactions products were prepared with the internal standard and analysed in parallel to the reaction mixtures. This allows accurate quantification of the amounts of products contained in the reaction to be determined by plotting the ratio of the peak area of the product and internal standard against the concentration. Decane was used as an internal standard because it was eluted with a similar retention time as the key products but was not consumed during the catalytic reaction. Another benefit of using internal (cf. external) standard was

that the solvent loss that affected the early reactions could be observed easily by comparing the ratio of the areas of the solvent vs. internal standard peaks in calibration samples and in samples after reaction.

It was found that the area normalisation method was sufficient to calculate the conversion of styrene and yields of each product. This calculation is based on the assumption that the percentage of the area of a peak is equal to the weight percentage of the analyte. This methodology is semi-quantitative, but due to the similarity of the response factors of each of the main products produced yields similar results to the internal standard method that was also used initially.

$$X\% = \frac{A_x}{\sum(A_i)} \times 100$$

Equation 5; Area normalisation calculation for product X, A_x is the area of peak X, which divided by the total area of all products

This method for this series of reactions proves reliable because:

- All products are eluted
- All products are detected
- All products have similar response factors

A more reliable method than the area normalisation procedure is to obtain the relative response factors, f , which eliminates any issues arising from variations in response factors. This procedure involves the use of a standard to which the response factors of all the products are compared to enabling precise calculation of relative response factors for each product.

$$f_x = f_s \left(\frac{A_s}{A_x} \right) \left(\frac{W_x}{W_s} \right)$$

Equation 6; Equation for calculating the relative response factor (f_x) of compound X, where f_s is the response factor of the standard, A_s and A_x are the areas of the standard and a product and W_x/W_s is the weight ratio of a product to the standard.

To calculate the yields of each product in a reaction sample, the peak area is multiplied by its corresponding relative response factor and then the percentage yield is calculated in a similar fashion to area normalization method discussed before.

$$X\% = \frac{A_x F_x}{\sum(A_i F_i)} \times 100$$

As similar product yields were being achieved by the area normalisation method the internal standard method for quantifying the amount of products was not employed. Decane was constantly used as an internal standard for the ensuring the solvent loss due to leaks was monitored.

Quantification by gas chromatography is a well-known, reliable technique for the analysis of wide range organic compounds. To ensure that the results are repeatable and reliable, each sample was analysed three times. It was found that although the peak areas did vary by up to 5 % in consecutive analyses of the same sample (suggesting that the injection volume was controlled to about this level) the relative amounts of the target products varied only marginally (< 1 %). Weekly column conditioning and injection port maintenance was carried to ensure that the sample repeatability was guaranteed. Calculating the yields of each compound with relative response factors requires that the standard sample is run in parallel to the catalytic samples.

V. GC-MS

GC-MS separates organic components of the reaction mixture in the same fashion as GC-FID; however, rather than detecting organic components by burning the sample in a hydrogen–oxygen flame, the sample is identified by a quadrupole time of flight mass spectroscope, allowing the products of the reaction sample to be identified by their mass spectrum; which can be compared to a library of known spectra on the NIST database. Shimadzu GCMS-QP2010 Plus was used for GC-MS analysis. Typically, only selected few samples were analysed using GC-MS in cases when there were significant product peaks that were unidentified such oligomers of styrene.

Results

The results of catalytic testing of a wide series of gold cluster-based catalysts are presented in the following pages. The series of catalysts studied encompass materials made *via* immobilisation of a range of atomically precise chemically synthesised gold clusters on a range of commercially available supports, termed “as made”, followed by activation using selected range of different treatments aimed at removal of organic protecting layer. Experimental results are discussed in the light of effects of the specific cluster used in preparation of the catalyst, type of support material, and observed changes due to activation treatments. Comparison to a range of relevant literature examples is presented with an aim to highlight differences and similarities in effects of various factors on the catalytic activity of gold-based catalysts. The catalytic studies discussed in this chapter are focused on the partial oxidation of styrene using three optimised catalytic testing methods that have been discussed in detail in the previous section. Our early experiments initially focused on the development of various methods for selective oxidation of a small range of alkene substrates, such as cyclohexene, styrene and monoterpene citral. However, due to the limited resources initially available, the focus of this work was on the selective oxidation of styrene. Toluene was used as the solvent, as it has been shown that selectivity towards epoxide can be quite high in toluene, despite the lower activity as compared to acetonitrile and methylcyclohexene systems.^{44,47} Toluene has also been shown to be particularly good for stabilising the tert-butoxy radical that can be generated in the reaction when TBHP is used, although other solvents can have better radical stabilisation.⁵³ A wide range of control reactions were conducted to ensure that the observed catalytic activity is due to the supported gold clusters rather than due to the TBHP alone or combination of the pure support material and TBHP.

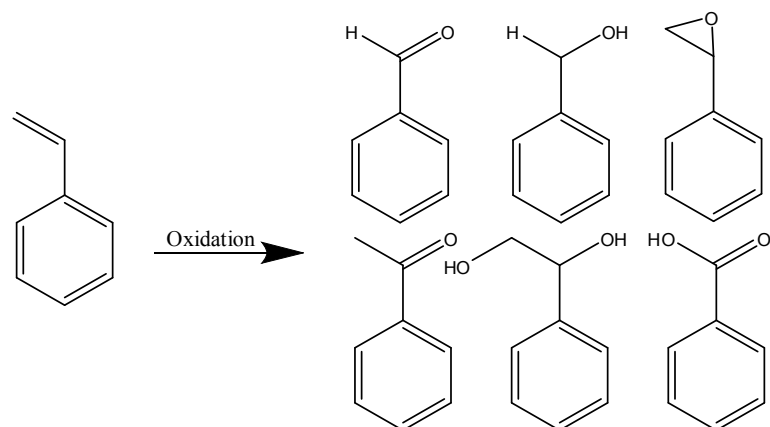
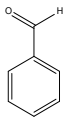
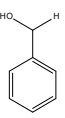
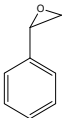
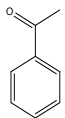


Figure 80; Common oxidation products of styrene; benzaldehyde, benzyl alcohol, styrene oxide, acetophenone, styrene glycol and benzoic acid.

Recent reports have also shown that toluene could be oxidised by oxygen in the presence of the supported gold and gold palladium catalysts at 160 °C.⁵⁴ However, under the conditions of these reactions conducted at 100 °C rather than 160 °C, no oxidation of toluene is observed in the presence of oxygen and catalysts used in this study. Importantly, no toluene oxidation occurs even in the presence of large amounts of TBHP under catalytic testing conditions used in this study. This observation is consistent with literature reports on the stability of TBHP in toluene at elevated temperatures.¹⁷

All reactions were conducted in duplicate. Typically differences in styrene conversions were within 3 % between two catalytic tests performed under the same conditions. The source of the error could be variability of mass measurement and transfer of catalysts, styrene and TBHP solutions, variability in stirring rates, possible inhomogeneity of the heterogeneous catalyst and variability in the times of heating up to the target temperature and quenching. A range of control reactions were conducted, as summarised in Table 9, demonstrating that the silica support material should have little or no activity for the oxidation of styrene under experimental conditions used in this study. However, the Evonik titania P-25 system showed moderate activity for styrene oxidation, which has been previously reported in the literature, particularly in the presence of TBHP.

Table 9: Summary of control reactions of both fumed silica and titania under various treatments and reaction conditions

| Substrate | Oxidant | Treatment | Conversion (%) |  |  |  |  | Minor products | |
|------------------------|-------------------------|-------------------------|----------------|---|--|---|---|----------------|-------|
| Fumed SiO ₂ | O ₂ 5 Bar | Calcined@ 200°, Air | – | – | – | – | – | – | |
| Fumed SiO ₂ | O ₂ 5 Bar | Heat treated @ 200°C | – | – | – | – | – | – | |
| Fumed SiO ₂ | 5 % TBHP | Calcined@ 200°, Air | – | – | – | – | – | – | |
| Fumed SiO ₂ | 5 % TBHP | Heat treated @ 200°C | – | – | – | – | – | – | |
| Fumed SiO ₂ | XS TBHP | Calcined@ 200°, Air | Trace | Trace | – | – | Trace | – | |
| Fumed SiO ₂ | XS TBHP | Heat treated @ 200°C | Trace | Trace | – | – | Trace | – | |
| P-25 titania | O ₂ 5 Bar | Calcined@ 200°, Air | – | – | – | – | – | Trace | |
| P-25 titania | O ₂ 5 Bar | Heat treated @ 200°C | – | – | – | – | – | Trace | |
| P-25 titania | 5 % TBHP | Calcined@ 200°, Air | < 1 % | 87.5 % | 7.1 % | – | Trace | Trace | |
| P-25 titania | 5 % TBHP | Heat treated @ 200°C | < 1 % | 91.2 % | 5.2 % | Trace | Trace | Trace | |
| P-25 titania | XS TBHP | Calcined@ 200°, Air | 6.4 % | 23.1% | < 1 % | Trace | < 1 % | Acid 71.2% | 4.1 % |
| P-25 titania | XS TBHP | Heat treated @ 200°C | 7.9 % | 22.5 % | 3.5 % | Trace | < 1% | Acid 65.1 % | 7.2 % |

Supported Au₁₀₁ cluster

Table 10 presents a summary of results for the oxidation of styrene using catalysts based on support-immobilised Au₁₀₁ cluster. The results will be compared and discussed in groups based on the reaction conditions with performance of catalysts compared across the range of supports and conditions used here and in context of previously published results. The oxidation of styrene can result in a wide range of possible catalytic products as illustrated in Figure 80; Common oxidation products of styrene, with some of the potential products being probable intermediates during the formation of the major products. In particular, the epoxide moiety, prized for its value as reactive functional group, can easily be converted to other products, making highly selective production of the epoxide a major challenge.

Results of catalytic tests using pure oxygen alone as an oxidant

Under moderate pressure of oxygen (5 bar), for both silica and titania samples the conversion of styrene was not significant (approximately 1 %) in the Parr batch reactors. In the case of the untreated samples, there was no reaction detected in the case of the titania supported gold phosphine cluster. This observation correlates well with previously published work which have shown that gold supported on titania requires a radical initiator for the oxidation of styrene to occur.⁴⁴ In the case of the untreated silica supported samples, there is a small amount of benzaldehyde detected as product with some trace amounts of benzyl alcohol. The untreated samples, which were refluxed in toluene in an attempted to remove the ligands under milder conditions, showed similar reactivity to the untreated samples, shown in Table 11. A recent report by Lopez- Sanchez *et al.* had demonstrated that by refluxing the supported gold nanoparticles in a solvent, which will solubilise the ligand or capping agent, one can produce active supported gold catalysts.⁵⁵ To prove successful removal of organic protecting layer by refluxing of the untreated catalyst in toluene, the supernatant obtained by centrifugation of the mixture was analysed by GC-MS confirming the presence of the small amounts of triphenylphosphine. The resulting supported gold clusters demonstrated slight increase in reactivity as compared to their corresponding untreated analogues. Further work on this method for developing active heterogeneous

catalysts could involve refluxing the supported nanoparticles under an inert (N₂, Ar) oxidising (O₂) or reducing (H₂) atmosphere.

Table 10; Summary of results of catalytic tests using Au₁₀₁ gold phosphine cluster (1.5 nm Au core) supported on fumed silica and Evonik P-25 titania.

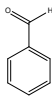
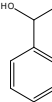
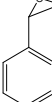
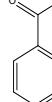
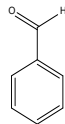
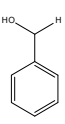
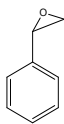
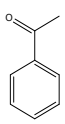
| Catalyst | Oxidant | Activation conditions | Conversion (%) |  |  |  |  | Minor products | |
|---|-------------------------|-------------------------|----------------|---|--|---|---|----------------|-------|
| Au ₁₀₁ Fumed SiO ₂ | O ₂ 5 Bar | Untreated | < 1 % | 98 % | Trace | – | – | – | |
| Au ₁₀₁ P-25 TiO ₂ | O ₂ 5 Bar | Untreated | – | Trace | – | – | – | – | |
| Au ₁₀₁ Fumed SiO ₂ | O ₂ 5 Bar | Calcined @ 200°, Air | 1.5 % | 99% | – | – | – | – | |
| Au ₁₀₁ P-25 TiO ₂ | O ₂ 5 Bar | Calcined @ 200°, Air | < 1 % | 99 % | Trace | – | – | – | |
| Au ₁₀₁ Fumed SiO ₂ | O ₂ 5 Bar | Heat treated @ 200°C | 7.8 % | 86.5 | 3.2 | – | – | Trace | |
| Au ₁₀₁ P-25 TiO ₂ | O ₂ 5 Bar | Heat treated @ 200°C | 2.5 % | 98 % | – | – | – | Trace | |
| Au ₁₀₁ Fumed SiO ₂ | 5% TBHP | Untreated | 2.7 % | 74 % | 1.6 % | 3.4 % | – | ≈ 10 % | |
| Au ₁₀₁ P-25 TiO ₂ | 5% TBHP | Untreated | < 1 % | 82 % | 5 % | – | – | Trace | |
| Au ₁₀₁ Fumed SiO ₂ | 5% TBHP | Calcined @ 200°, Air | 7.9 % | 77.5 % | 0.4 % | 7.5 % | 3.2 % | Trace | |
| Au ₁₀₁ P-25 TiO ₂ | 5% TBHP | Calcined @ 200°, Air | 12.6 % | 64.7% | .2 % | 3.1 % | Trace | ≈ 20% | |
| Au ₁₀₁ Fumed SiO ₂ | 5% TBHP | Heat treated @ 200°C | 13.2 % | 73.5 % | 3.8 % | 8.3 % | – | ≈ 3 % | |
| Au ₁₀₁ P-25 TiO ₂ | 5% TBHP | Heat treated @ 200°C | 11.5 % | 39.9 % | 9.2 % | < 1 % | – | – | |
| Au ₁₀₁ Fumed SiO ₂ | XS TBHP | Untreated | < 1 % | 99 % | Trace | – | – | – | |
| Au ₁₀₁ P-25 TiO ₂ | XS TBHP | Untreated | 34.6 % | 62.6 % | 8.5 % | 2.2 % | 5.2 % | Acid 17.5 % | ≈ 5 % |
| Au ₁₀₁ Fumed SiO ₂ | XS TBHP | Calcined @ 200°, Air | 32.4 % | 43.2 % | 3.5 % | 1.7 % | 6.5 % | 12.7 % | 10 % |
| Au ₁₀₁ P-25 TiO ₂ | XS TBHP | Calcined @ 200°, Air | 38.7 % | 65.7 % | 9.3 % | Trace | 3.0 % | 20 % | 10 % |
| Au ₁₀₁ Fumed SiO ₂ | XS TBHP | Heat treated @ 200°C | 46.3 % | 38.8 % | 4.6 % | 4.5 % | 9.7 % | 23.5% | 20% |
| Au ₁₀₁ P-25 TiO ₂ | XS TBHP | Heat treated @ 200°C | 36.5 % | 56.7 % | 9 % | 1.7 % | 6.6 % | 19.8% | 5 % |

Table 11; Summary of catalytic results of refluxed supported gold clusters

| Catalyst | Oxidant | Activation conditions | Conversion (%) |  |  |  |  | Minor products |
|--|-------------------------|-----------------------|----------------|---|--|---|---|----------------|
| Au ₁₀₁ Fumed SiO ₂ | O ₂ 5 Bar | Refluxed | <1 % | 98 % | Trace | – | – | – |
| Au ₁₀₁ P-25 TiO ₂ | O ₂ 5 Bar | Refluxed | – | trace | – | – | – | – |
| Au ₁₀₁ Fumed SiO ₂ | 5 % TBHP | Refluxed | 2.3 % | 69.7 % | 17.8 % | 5.4 % | 6.1 % | – |
| Au ₁₀₁ P-25 TiO ₂ | 5 % TBHP | Refluxed | 1.3 % | 86.3 % | 12.5 % | – | Trace | – |

Upon calcination of the support-immobilised clusters under air at 200 °C for two hours as previously described in chapter two, the conversion marginally increased in reactions catalysed by both SiO₂- and TiO₂- supported clusters with benzaldehyde as the only detectable product. The silica supported gold clusters appeared to be slightly more active than the titania supported sample. The minor increase in reactivity as compared to the untreated samples can be attributed to the calcination procedure, which partially removes the organic ligands from the surface of the gold clusters.

Results of the catalytic tests under ambient oxygen pressure with TBHP as initiator

In the presence of catalytic amounts of tert-butylhydroperoxide (5 mol %), the supported gold clusters appear to be more active for the oxidation styrene as compared to the reactions carried out without initiator under pure oxygen. In the case of the untreated supported gold samples, the observed styrene conversion was 2.7% and < 1% respectively for the silica and titania systems. The use of silica-supported catalyst resulted in formation of an increased amount of benzyl alcohol (11.6 %) with small, yet detectable amounts of the epoxide products also present. Whilst for the titania-supported sample, benzaldehyde was the only detected product. When compared to the control experiments (Table 9), the pure P-25 titania appears to be more active in the presence of TBHP (5 mol %), than the untreated supported gold phosphine cluster on P-25 titania. Upon calcination at 200 °C, the reactivity of Au₁₀₁-based catalysts moderately increased while the selectivity differed somewhat when compared to the oxygen only system. The silica sample showed a styrene conversion of 7.9 %,

with a slight increase in selectivity for the benzyl alcohol (10.4 %), acetophenone (3.2 %) and the epoxide (7.5%) products. On the other hand, the calcination of the titania sample resulted in a catalyst which had a conversion of 12.6 %, with benzaldehyde as the major product (64.7 %). Trace amounts of other products were also detected. In contrast to the calcined system, the heat treated samples yielded catalysts that differed in product selectivity. Although the styrene conversion is similar, benzyl alcohol (59.2 %) is the primary product for the titania supported gold system, with benzaldehyde (40 %) as the minor product and trace amounts of the epoxide product are also detected. However, for the silica supported samples, benzaldehyde (73.5 %) continued to be the major product, with benzyl alcohol (13.8 %) and benzyl oxide (8.3 %) as minor products.

It was observed that the activation conditions can significantly influence the reactivity and selectivity of the reaction. The untreated samples have shown very limited reactivity and benzaldehyde is the major product. In the presence TBHP (5mol %), the reactivity increases considerably in the case of activated catalysts. When TBHP is used as the catalytic initiator for the reaction at low molar percentages (5 mol %), it is assumed that the reaction goes by the free radical mechanism as proposed by Valarie Caps, in which the solvent forms a peroxy radical which is involved in the formation of carbon – oxygen bond in the substrate (in this case styrene).⁴⁴ Caps proposed this mechanism as an explanation for the reactivity of titania supported gold clusters, which have been shown to be active selective for epoxide and ketone products of analogous stilbene system. In the case of the silica supported samples, a similar mechanism can be applied in the presence of initiating amounts of TBHP.

Results of the catalytic tests under ambient oxygen pressure in the presence of excess TBHP

The reactivity of the supported gold phosphine clusters in the presence of excess of TBHP significantly increased as compared to the previous reaction conditions. In the case of the titania-supported clusters the reaction is only slightly influenced by the nature of the metal on the surface of the catalyst. TBHP was able to further oxidise the benzaldehyde to the benzoic acid product (≈ 20 %), although aldehyde was still the major product which contrasts greatly with the controls in which the benzoic acid product is the primary product.

The acid product was identified by GC-MS and confirmed by comparison against a benzoic acid standard using GC-FID. A range of other trace products, including several polyarene products, were identified by GC-MS. Presence of these minor products indicates that competing radical polymerisation side reaction occurs under these conditions in contrast to results observed under milder conditions earlier. However, none of these minor products was produced in significant quantities as compared to the key partial oxidation products. In the case of the silica supported samples, only the activated catalysts showed any activity which was comparable to the titania samples. The untreated sample showed no reactivity, which is in stark contrast with the untreated titania catalysts, which showed some reactivity.

Supported $\text{Au}_9(\text{PPh}_3)_8(\text{NO}_3)_3$

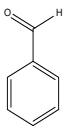
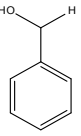
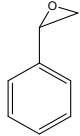
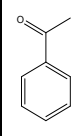
Results of catalytic tests using pure oxygen alone as an oxidant

Under moderate pressure of oxygen (5 bar), $\text{Au}_9\text{-SiO}_2$ samples were the only catalysts showing at least some conversion, with benzaldehyde as the major product again. However, in the most cases the sub-1% conversions obtained using $\text{Au}_9\text{-SiO}_2$ catalysts are comparable to performance of the pure support (control). The presence of the triphenyl phosphine ligands appears to have a minor effect on reactivity, when compared to the control reactions.

Upon calcining under relatively mild conditions (200 °C) in air, the $\text{Au}_9\text{-SiO}_2$ system becomes inactive towards oxidation of styrene. This is in stark contrast with the highest conversion (4.5%) for the Au_9 series of catalysts observed under O_2 only conditions for the material, which was heat treated under vacuum. Although the conversion is not high, the contrast with the calcined system is important to note. Extensive batch reactor cleaning was conducted, which has been described in the experimental section and several control reactions were conducted before and after reaction of concern, to confirm that the observed reactivity of the $\text{Au}_9\text{-SiO}_2$ samples was not caused by the presence of any contamination. Several different batches were also tested to ensure the reproducibility of the reaction which yielded similar results (2.6 % and 5.3 % for the untreated and heat treated samples respectively). We have shown that there is a small but significant difference in particle size in materials after these two different treatments *i.e.* the mean particle size was shown to be 1.8 nm for the heat treated system as opposed to 2.7 nm for the calcined system. The difference in particle size will lead to the significant difference in reactivity, due to the significant size

dependence for gold based catalysis. Although as discussed before the difficulty in distinguishing between the support material and the ultra-small gold clusters which have resisted agglomeration can give some uncertainty to these results.

Table 12; Summary of results for Au₉(PPh₃)₃(NO₃)₃ supported on fumed silica and P-25 titania. Reaction conditions are described in detail in the experimental section of this chapter.

| Catalyst | Oxidant | Activation conditions | Conversion (%) |  |  |  |  | Minor products | |
|---|-------------------------|--------------------------|----------------|---|--|---|---|--------------------------|--------|
| | | | | | | | | | |
| Au ₉ P-25 TiO ₂ | O ₂ 5 Bar | Untreated | – | – | – | – | – | – | |
| Au ₉ Fumed SiO ₂ | O ₂ 5 Bar | Untreated | 3.2 % | 94.5 % | Trace | – | – | Trace Phosphine oxide | |
| Au ₉ P-25 TiO ₂ | O ₂ 5 Bar | Calcined @ 200°, Air | < 1 % | 96.2 % | 2.7 % | – | – | Trace | |
| Au ₉ Fumed SiO ₂ | O ₂ 5 Bar | Calcined @ 200°, Air | < 1 % | 78.3 % | 18.7 % | – | – | Trace | |
| Au ₉ P-25 TiO ₂ | O ₂ 5 Bar | Heat treated @ 200°C | < 1 % | 92.6 % | 6.4 % | – | – | Trace | |
| Au ₉ Fumed SiO ₂ | O ₂ 5 Bar | Heat treated @ 200°C | 4.5 % | 71.4 % | 17.42 % | – | – | ≈ 7 % | |
| Au ₉ P-25 TiO ₂ | O ₂ 5 Bar | Calcined @ 400°C, Air | < 1 % | 96.7 % | 1.3 % | – | – | Trace | |
| Au ₉ Fumed SiO ₂ | O ₂ 5 Bar | Calcined @ 400°C, Air | < 1 % | 89.5 % | Trace | – | – | ≈ 6 % | |
| Au ₉ P-25 TiO ₂ | 5% TBHP | Untreated | 1.5 % | 91.2 % | 6.8 % | – | – | Trace | |
| Au ₉ Fumed SiO ₂ | 5% TBHP | Untreated | 4.2 % | 76.8 % | 15.7 % | – | Trace | ≈ 7.5 % | |
| Au ₉ P-25 TiO ₂ | 5% TBHP | Calcined @ 200°, Air | 10.6 % | 64.3 % | 22.8 % | 4.6 % | 7.5 % | Trace | |
| Au ₉ Fumed SiO ₂ | 5% TBHP | Calcined @ 200°, Air | < 1 % | 99 % | – | – | – | Trace | |
| Au ₉ P-25 TiO ₂ | 5% TBHP | Heat treated @ 200°C | 12.5 % | 29.4 % | 64.5 % | 2.5 % | 1.2 % | Trace | |
| Au ₉ Fumed SiO ₂ | 5% TBHP | Heat treated @ 200°C | 15.5 % | 81.1 % | 11.81 % | – | 6.4 % | ≈ 4 % | |
| Au ₉ P-25 TiO ₂ | 5% TBHP | Calcined @ 400°, Air | 3.6 % | 86.4 % | 11.2 % | Trace | 2.7 % | Trace | |
| Au ₉ Fumed SiO ₂ | 5% TBHP | Calcined @ 400°, Air | 11.5 % | 61.3 % | 17.3 % | 3.5 % | 9.1 % | ≈ 8 % | |
| Au ₉ P-25 TiO ₂ | XS TBHP | Untreated | 37.3 % | 68.2 % | 16.2 % | 2.4 % | 6.3 % | Acid 7.8 % | ≈ 6 % |
| Au ₉ Fumed SiO ₂ | XS TBHP | Untreated | ≈ 1 % | Trace | 97 % | – | – | – | – |
| Au ₉ P-25 TiO ₂ | XS TBHP | Calcined @ 200°, Air | 72.1 % | 35.1 % | 17.2 % | 2.4 % | 4.5 % | Acid 29.4 % | ≈ 11 % |
| Au ₉ Fumed SiO ₂ | XS TBHP | Calcined @ 200°, Air | 54.3 % | 47.7 % | 7.8 % | Trace | 19 % | Acid 23.5 % | Trace |
| Au ₉ P-25 TiO ₂ | XS TBHP | Heat treated @ 200°C | 65.1 % | 41.1 % | 22.1 % | 3.6 % | 8.1 % | Acid 33.6 % | ≈ 7 % |
| Au ₉ Fumed SiO ₂ | XS TBHP | Heat treated @ 200°C | 63.8 % | 56.8 % | 13.3 % | Trace | 19.6 % | Acid 4.0 % | ≈ 5 % |

As evidenced by the HRTEM, the calcined catalyst system does have a smaller population of small gold clusters (< 2 nm) present, as compared to the samples heated under vacuum. It can be difficult to ascribe directly whether the reactivity is due to the particle size alone or to the structure of the cluster species on the specific surface after activation. For example, Turner *et al.* described the reactivity of gold phosphine clusters support on various inert supports to the unique size of the gold clusters (1.7 nm), which was proposed as the site on which molecular oxygen is activated.²¹

The untreated titania samples were completely inactive, no products were detected, in addition, the reactivity of the activated samples (calcined and heat treated) was insignificant (<1 %). The activation of molecular oxygen with titania supported gold is known to require a radical initiator for the reaction to occur in the liquid phase; which corresponds well with the observations in these studies.⁵⁶ Multiple repeats with different batches of titania supported gold clusters were conducted, similar reactivity was observed.

Results of the catalytic tests under ambient oxygen pressure with TBHP as initiator

The reactivity of the supported gold clusters was radically different than oxygen only system upon addition of 5 mol % of TBHP to the reaction. Both untreated samples increased in activity, almost doubling in the case of the silica supported nonagold sample to 4.2 %. The catalysts calcined in oxygen differed markedly in the presence of catalytic amounts of TBHP, where the silica sample showed very little reactivity, and the titania sample increased in activity as compared to the untreated sample and the oxygen only system.

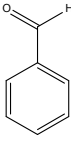
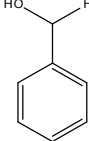
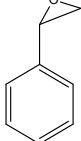
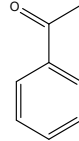
The heat treated silica sample was much more active than the sample calcined at 200 °C; however, the 400 °C calcined sample shows significantly more activity than the lower temperature sample. The higher temperature results in a more active catalyst due to the fact the triphenyl phosphine ligands are removed and the surface bound gold is more accessible by the substrates. For the heat treated sample, the observed activity could be a result of an anionic gold cluster species that is generated under a low oxygen atmosphere at high temperature. Due to issues of charging for photoelectron spectroscopy, the presence or absence of this species for the silica samples could not be confirmed conclusively.

In contrast, the titania supported nonagold clusters had very similar activity to each other. The presence of small gold nanoparticles (< 3 nm) ensured that the systems are still active for styrene oxidation with catalytic amounts of TBHP, despite the observed larger nanoparticles present in TEM. However, the product selectivity contrasts significantly with other reported systems. Patil *et al.* previously showed moderate selectivity for the epoxide product with several gold titania catalyst, with a high gold loading (1–6 %) and large particle size (2– 10 nm).

Results of the catalytic tests under ambient oxygen pressure in the presence of excess TBHP

When TBHP is used as the only source of oxidant, the activity for each catalyst increased, except in the case of the untreated nonagold cluster on silica, which was completely inactive. The corresponding titania sample was active, although significantly less than the activated samples, which correlates well with literature reports that titania supports and mesoporous titania materials are active for a various catalytic oxidation reactions, including styrene. In addition to the benzaldehyde, there was a approximately 25%-35% yield of the benzoic acid product in all systems except for the heat treated silica sample which only yielded 4 % benzoic acid.

Supported Au₈(PPH₃)₈(NO₃)₂Table 13; Summary of results for Au₈ supported on fumed silica and P-25 titania

| Catalyst | Oxidant | Activation conditions | Conversion (%) |  |  |  |  | Minor products | |
|---|-------------------------|-------------------------|----------------|---|---|---|---|----------------|-------|
| | | | | | | | | | |
| Au ₈ P-25 TiO ₂ | O ₂ 5 Bar | Untreated | Trace | 99 % | Trace | – | – | – | |
| Au ₈ Fumed SiO ₂ | O ₂ 5 Bar | Untreated | 2.1 % | 92 % | 11.5 % | – | – | Trace | |
| Au ₈ P-25 TiO ₂ | O ₂ 5 Bar | Calcined @ 200°, Air | – | Trace | – | – | – | – | |
| Au ₈ Fumed SiO ₂ | O ₂ 5 Bar | Calcined @ 200°, Air | < 1 % | 99 % | Trace | – | – | – | |
| Au ₈ P-25 TiO ₂ | O ₂ 5 Bar | Heat treated @ 200°C | < 1 % | Trace | – | – | – | – | |
| Au ₈ Fumed SiO ₂ | O ₂ 5 Bar | Heat treated @ 200°C | 3.7 % | 91 % | 3.1 % | 2.5 % | 1.7 % | Trace | |
| Au ₈ P-25 TiO ₂ | O ₂ 5 Bar | Calcined @ 400°, Air | < 1 % | 99 % | Trace | – | – | – | |
| Au ₈ Fumed SiO ₂ | O ₂ 5 Bar | Calcined @ 400°, Air | 2.2 % | 97.0 % | Trace | – | – | Trace | |
| Au ₈ P-25 TiO ₂ | 5% TBHP | Untreated | < 1 % | 93.1 % | 4.3 % | – | 2.1 % | – | |
| Au ₈ Fumed SiO ₂ | 5% TBHP | Untreated | 2.4 % | 82.2 % | 11.6 % | – | – | Trace | |
| Au ₈ P-25 TiO ₂ | 5% TBHP | Calcined @ 200°, Air | 16.2 % | 68.4 % | 16.8 % | 5.2 % | 8.1% | Trace | |
| Au ₈ Fumed SiO ₂ | 5% TBHP | Calcined @ 200°, Air | 9.8 % | 84.6 % | 8.3 % | Trace | 5.2 % | ≈ 4 % | |
| Au ₈ P-25 TiO ₂ | 5% TBHP | Heat treated @ 200°C | 14.5 % | 27.8 % | 43.6 % | 13.2 % | 7.0 % | ≈ 7 % | |
| Au ₈ Fumed SiO ₂ | 5% TBHP | Heat treated @ 200°C | 17.4 % | 32.4 % | 56.1 % | < 1 % | 6.8 % | Trace | |
| Au ₈ P-25 TiO ₂ | XS TBHP | Untreated | 32.5% | 73.2 % | 12.0 % | 1.6 % | 7.8 % | Acid 2.4 % | ≈ 4 % |
| Au ₈ Fumed SiO ₂ | XS TBHP | Untreated | ≈ 1 % | Trace | 98 % | – | – | – | Trace |
| Au ₈ P-25 TiO ₂ | XS TBHP | Calcined @ 200°, Air | 76.7 % | 42.5 % | 11.4 % | ≈ 1% | 3.6 % | Acid 31.2 % | 8 % |
| Au ₈ Fumed SiO ₂ | XS TBHP | Calcined @ 200°, Air | 47.9 % | 47.7 % | 7.8 % | Trace | 19.1 % | Acid 23.5 % | Trace |
| Au ₈ P-25 TiO ₂ | XS TBHP | Heat treated @ 200°C | 63.9 % | 46% | 6.5 % | Trace | 3.3 % | Acid 36.4 % | ≈ 6 % |
| Au ₈ Fumed SiO ₂ | XS TBHP | Heat treated @ 200°C | 61.8 % | 74.4 % | 12.0 % | 1.8 % | 4.1 % | Acid 4.7% | ≈ 5 % |

Results of catalytic tests using pure oxygen alone as an oxidant

Untreated Au₈ clusters don't demonstrate any significant activity, which is similar to what was observed for the Au₉ and Au₁₀₁ systems in the presence of only oxygen. Although, for the silica supported sample there is around a noticeable 2% conversion of the styrene, forming benzaldehyde as the only detectable product. The Au₈ samples treated by calcination at 200 °C showed no activity at all for any support, whilst the Au₈-silica sample treated by heat treatment at 200 °C showed a slight increase in conversion in styrene (3.7%). Increasing the calcination temperature to 400 °C, slightly increases the activity of the silica supported Au₈ sample to around 2%. As expected there is no reaction observed for any of the titania samples.

Results of the catalytic tests under ambient oxygen pressure with TBHP as initiator

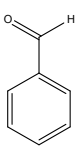
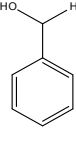
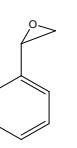
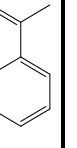
In the presence of catalytic amounts of TBHP, the reactivity of the titania supported gold clusters has increased significantly as compared to the oxygen system. Although for the untreated samples we don't see much conversion, upon calcination at 200 C, the titania supported sample is much more reactive with 16 % conversion of the styrene starting material. The main product formed is benzaldehyde (68 %), with small amounts of benzyl alcohol, acetophenone and styrene oxide formed. In contrast, the conversion for silica supported Au₈ sample is 10 %, with a higher selectivity for the benzaldehyde product. No styrene oxide product was formed for the silica sample. The heat-treated silica sample contrast significantly with the calcined sample, the styrene conversion increases to around 17 %, with much higher selectivity for the benzyl alcohol product (56 %). The heat treated titania sample demonstrated similar conversions of styrene; however, the main product of the reaction is now benzyl alcohol. A range of polymeric by-products were also formed.

Results of the catalytic tests under ambient oxygen pressure in the presence of excess TBHP

As with the Au₉ and Au₁₀₁ systems, when TBHP is employed as the primary oxidant the styrene conversion increased significantly. Benzaldehyde was the main product for the untreated titania sample, whilst no significant amount of the benzoic acid product was formed which was observed for the other treated titania samples. This trend was also observed for other gold clusters, which indicates that the presence of the gold cluster after post-deposition treatment improves the catalytic oxidation of the catalysts. The calcined titania sample was observed to have a styrene conversion of around 76 %, which contrasted with the heat treated sample, which demonstrated a 64 % conversion. A similar product selectivity was observed for each reaction. In contrast, the silica supported samples were not observed to be as reactive as the titania samples. The calcined sample showed a moderate styrene conversion around 50 %, with a 48 % yield of benzaldehyde. As with the Au₉ system, the calcined Au₈-silica sample also produces a small amount of the benzoic acid product (24%). The heat treated silica sample did not yield benzoic acid, which was typically observed when excess TBHP was used; along with benzaldehyde, acetophenone was the other main product.

Support pre-treatment

Table 14; Gold phosphine clusters supported on acid washed P-25 titania

| Catalyst | Oxidant | Activation conditions | Conversion (%) |  |  |  |  | Styrene oligomers |
|--|-------------------------|-------------------------|----------------|---|--|---|---|-------------------|
| Au ₁₀₁ P-25 TiO ₂ | O ₂ 5 Bar | Untreated | 82.0 % | < 1 % | Trace | – | – | >97 % |
| Au ₁₀₁ P-25 TiO ₂ | 5 % TBHP | Untreated | 97.6 % | < 1 % | Trace | – | – | > 97 % |
| Au ₁₀₁ P-25 TiO ₂ | O ₂ 5 Bar | Heat treated @ 200°C | 84.6 % | < 1 % | Trace | – | Trace | > 97 % |
| Au ₁₀₁ P-25 TiO ₂ | 5 % TBHP | Heat treated @ 200°C | 98.1 % | < 1 % | < 1 % | Trace | Trace | > 97 % |
| Au ₉ P-25 TiO ₂ | O ₂ 5 Bar | Untreated | 89.3 % | < 1 % | Trace | – | – | > 97 % |
| Au ₉ P-25 TiO ₂ | 5 % TBHP | Untreated | 98.5 % | < 1 % | < 1 % | – | – | > 97 % |
| Au ₉ P-25 TiO ₂ | O ₂ 5 Bar | Heat treated @ 200°C | 93.2 % | < 1 % | Trace | – | – | > 97 % |
| Au ₉ P-25 TiO ₂ | 5 % TBHP | Heat treated @ 200°C | 99.0 % | < 1 % | < 1 % | Trace | Trace | > 97 % |
| Au ₈ P-25 TiO ₂ | O ₂ 5 Bar | Untreated | 90.7 % | < 1 % | Trace | – | – | > 97 % |
| Au ₈ P-25 TiO ₂ | 5 % TBHP | Untreated | 97.2 % | < 1 % | < 1 % | – | – | > 97 % |
| Au ₈ P-25 TiO ₂ | O ₂ 5 Bar | Heat treated @ 200°C | 95.8 % | < 1 % | < 1 % | – | – | > 97 % |
| Au ₈ P-25 TiO ₂ | 5 %TBHP | Heat treated @ 200°C | 99.0 % | < 1 % | < 1 % | Trace | Trace | > 97 % |

In an attempt to improve the reactivity and selectivity of the titania supported gold clusters, slight modifications of the P-25 titania support material were undertaken and applied to the styrene oxidation reaction. Unmodified P-25 titania demonstrated slightly light sensitivity due light generated by light that can induce particle sintering. The P-25 support was washed with a 1 M solution of sulphuric acid as previously described by Lopez- Sanchez *et al.*, and the cluster deposited and activated as described in chapter two.⁵⁵ The acid washing of the titania increases coverage of the sulfonated (*i.e.* acidic) surface functionality, which was

shown to decrease the amount of agglomeration of the gold clusters on the surface due to the high temperature activation conditions and light.

The acid washed titania support samples showed very high reactivity but did not yield any expected oxidation products. The reactions were conducted under mild pressure of oxygen (5 bar) as well as in the presence of 5 mol % of the TBHP radical initiator. All the catalysts showed similar activity and selectivity, producing a wide range of styrene oligomers which proved difficult to isolate and characterise due to the similarity of individual products. Specifically, the GC-FID detected a wide range of products that eluted much slower than the typical oxidation products (normally between five and nine minutes). Approximately one hundred different product peaks were detected that appeared with the retention times ranging from eleven minutes to thirty minutes. An intense column conditioning programme was introduced to ensure that the peaks were not caused by other sources (*e.g.* impurities introduced due to earlier runs *etc.*), which would ensure that the observed peaks were coming from the reaction. The reaction samples were further analysed by GC-MS in attempt to identify the products with the help of MS. However, distinguishing between such similarly-structured products eluded us due to poor column separation resulting in failure to isolate each product fraction. Further attempts of characterising the oligo- or polymeric products were aimed at isolation of individual fractions by HPLC which was more appropriate for this proposed type of heavier molecular weight products. However, research in this direction was hampered and eventually had to be cancelled due to damage incurred due to the earthquakes and associated delays.

The catechol inhibitor, which is added (4-5 ppm) to styrene, prevents the radical polymerisation during storage. In the typical tests this inhibitor was removed by filtration through dried basic alumina. Once the catechol is removed, the styrene is diluted in toluene and stored in a dried volumetric flask at 4 °C in the dark. However, since oligomerization appeared to take place in the case of clusters supported on acid washed TiO₂, I have attempted study of the reactions involving the acid washed supported gold clusters were conducted in the presence of the catechol inhibitor in attempt to reduce the extent of the polymerisation reaction and allow formation of smaller partial oxidation products. The

conversion of styrene decreased slightly by approximately 7–9 %, with a slight increase in the yields for benzaldehyde and benzyl alcohol, in the presence of the TBHP initiator.

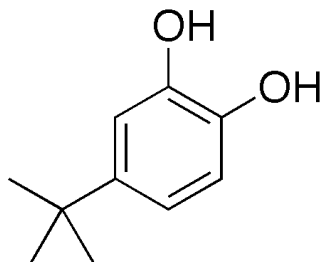


Figure 81; Tert butylcatechol is used to prevent styrene from undergoing radical polymerisation

Several reaction solutions were degassed and purged with argon. The aim of this additional step prior to setting up the reaction vessels was to improve the accuracy of the catalytic timing. However, it was observed when the samples were taken from the reaction prior to the addition of oxygen that the reaction had already begun. This observation confirmed that the reaction was being driven by the acid washed titania solely.

As the products were not of interest to us as partial oxidation products, other starting substrates were investigated to demonstrate that the acid washed supports could be employed as oxidation catalysts in other circumstances. With this in mind, styrene oxide and benzyl alcohol were used as substrates instead of styrene in toluene (60 mM). Au₉ on acid washed P-25 and Au₁₀₁ Acid washed P-25, which were heated at 200 °C in vacuum, showed surprisingly high yields (> 95 %) of the aldehyde product from the styrene oxide precursor with no polyarene products present at all. In the case of benzyl alcohol, much lower reactivity was observed which may be due to absence of a weak base which is known to require for benzyl alcohol oxidation. Further investigations in to the possibility of the oxidation of substituted alkenes (*i.e.* cyclohexene, citral), which are more stable to radical polymerisation than styrene; a well-known polymer precursor should be undertaken. The main issue with styrene as a model oxidation substrate is the sensitivity to polymerisation; however, it is a useful reaction which can highlight the selectivity or lack thereof for anti-Markonikov products of a catalyst.

Discussion

Overall, the titania supported clusters are not catalytically active for the oxidation of styrene when oxygen is used as the only source of active oxygen. This trend compares well with other literature examples of titania supported gold nanoparticle.^{30,32,44} In the case of the silica supported samples, moderate conversions of styrene were observed, even for the untreated samples. When compared to the analogous Au₅₅ by Tuner *et al.*, the observed conversions are about half that observed in this study.²¹ This lower reactivity could be attributed to the slightly lower gold loadings of the catalysts. In addition, the oxygen only reactions produced only small amounts of the styrene oxide product unlike the Au₅₅ which produced noticeably more (>10 % yield in some cases) The poor reactivity of the titania supported sample can be explained by the lack of radical initiator that was earlier postulated to be required for the activation molecular oxygen by a radical produced from the toluene solvent.⁴⁴ The calcined silica system was expected to be significantly more active for the oxidation of styrene in the presence of oxygen only.

In the presence of catalytic amounts of TBHP (5 mol %), the reactivity of the titania supported samples increases significantly. The conversions in this study are not high when compared to other literature reports; this is attributed to the relatively low gold loadings of the catalysts and also comparatively higher concentration of the styrene solution.(60mM vs 1mM) ^{29,32} In contrast to these literature reports on styrene and stilbene oxidation, we never achieved any high yields of styrene oxide product of any significance. We can attribute this to nature of the solvent, toluene, which was employed for this array of reactions. It has been proposed that the degree of methylation of the solvent could improve the selectivity for the epoxide product, by further stabilising the radicals present during the reaction.

In the presence of a threefold excess of the TBHP, we were expecting to observe an increase in the epoxide yield akin to the observations of by Liu *et al.*, highlighted that a Au₂₅ thiolate cluster supported on a hydroxyapatite which was activated at 200°C selectively oxidises styrene efficiently to the epoxide product in the presence of excess TBHP.⁴⁷ In contrast, we observed moderate yields of both benzaldehyde and benzoic acid whilst for the heat treated silica supported samples yielded acetophenone rather than benzoic acid.

Although the authors don't discuss the origins of this selectivity in mechanistic detail, the nature of the support and cluster ligand shell could explain observed differences in the reactivity with catalysts studied here.

What dictates the final electronic structure of the active components of these silica based catalysts have not yet been studied in detail. We have previously shown that silica based systems are difficult to analyse by photoelectron spectroscopy without the aid of a flood gun to neutralise the sample. Yet, resulting electron bombardment can also significantly damage the sample as was demonstrated by Goodman *et al.*, who used an electron stimulated desorption (ESD) to strip ligands of gold phosphine cluster (*i.e.* Au₆) deposited onto a flat titania (110) substrate.⁵⁷ Finally, our early attempts to use XPS for studies of porous silica-based catalysts were complicated by very low signal intensity, due to the gold species being mainly located deep inside the pores. TEM results, from chapter four, also showed that for the heat treated samples on silica, the average observed particle size is 2.3 nm whilst for calcined samples the particle size is 3.4 nm. For the titania samples, the measured particle size for the Au₁₀₁ samples was 3.2 nm for the heat treated sample and 3.8 nm for the calcined sample. The presence of oxygen, during the activation steps, appears to affect the electronic structure of the materials and also the degree of particle sintering; as well as the reactivity of the catalyst.

Recent reports by Turner *et al.* showed that certain silica supported gold phosphine clusters can activate molecular oxygen for the catalytic oxidation of styrene. However, the method of activation of their catalytic material involved the heating of untreated supported gold cluster in mild vacuum at 200 °C, similar to the method that has been designated as the “heat treatment” at 200 C in my study. The difference in observed reactivity could be explained by the differences in the morphology of the catalysts arising due differences in partial pressure of oxygen during thermal treatment, as particle aggregation is very significantly affected by the chemical atmosphere during thermal activation. The calcination under oxygen-rich conditions used in current study was aimed to facilitate ligand removal *via* oxidation. Hence, such treatment used in this study is expected to lead to increased aggregation of the gold particles present on the surface of support.

The supported gold clusters, which were heat treated at 200°C under a mild vacuum, show a moderate rise in conversion of styrene. For Au₁₀₁-TiO₂ sample, conversion increases to ≈ 2.5 % with benzaldehyde again present as the only major product detected. In the case of Au₁₀₁-SiO₂, the conversion increases to 7.8 % with both benzaldehyde and benzyl alcohol present as products. The reactivity for the heat treated sample is more akin to the previously reported reactivity of gold cluster supported on silica and BN.²¹ The contrast between the two thermal activation conditions indicates that the active species that are formed under vacuum are more active for the styrene oxidation under an oxygen atmosphere as compared to the calcination under air at the same temperature. It has been proposed that small gold clusters on silica are able to activate molecular oxygen to form oxygen adatoms on the surface of the active catalyst, which also forms a weak interaction with the styrene precursor.²¹

One of the big impediments to the performance of this series of catalysts was likely the triphenylphosphine ligand that was used to stabilise each of the clusters/nanoparticles. We observed by XPS that after treatment; heat treatment of calcination, the phosphorous peak was still observed, likely indicating that the triphenyl phosphine is still present on the surface. The treatment processes do improve the reactivity of the catalysts as compared to the untreated samples by rearranging the ligand shell. We briefly investigated the possibility of *washing* the ligands from the surface of the catalysts by refluxing under mild temperatures; however, the resulting materials were relatively inactive for styrene oxidation.⁵⁵ When comparing this series of catalysts to the thiol stabilised gold cluster catalysts, it is noticeable that the alkyl thiol ligands are much less sterically bulky which possibly accounts for the higher reported reactivity in similar reactions.^{22,58}

However, there are other avenues for achieving good selectivity and reactivity using phosphine stabilised clusters. One of the benefits of the phosphine gold clusters is their relative ease of preparation and characterisation as compared to the thiol gold clusters which often need ESI-MS to confirm the present of specific cluster nuclearities. A post-deposition reflux with a less sterically bulky ligand that can displace the bulky but labile triphenyl phosphine may help remedy this possibly issues. In addition, careful choice of electronic properties of the substituting ligand may also prove beneficial to the new catalytic material.

Overall, it was not possible to discern which effect was contributing to the reactivity of the different treatments; particle aggregation, rearrangement of the triphenyl phosphine ligand and formation of different oxygen species on the surface all could influence the reactivity of the catalysts in some way. A comparison to extended surface systems would help illuminate which factors have a greater influence on the reactivity of these materials, as would a more comprehensive STEM study on these materials.

Conclusion

In this chapter, various methods for catalytic oxidation were developed and used to study a matrix of supported gold clusters on silica and titania. Developments of the catalytic work were hindered due to solvent loss in reactions set-ups that involved a flow of air or oxygen through the reaction, investigations into the effect of the inhibitors present in starting reagents and other interruptions. Early studies focused on optimising the set-up for working under mild pressures of oxygen and understanding the limits of reaction set-up. The catalysts involved in these studies were prepared with low loadings (0.5 % by weight) as compared to other reported catalysts, where the reported metal loadings ranged from one to ten per cent. Styrene was chosen as a model substrate for catalytic investigations, due to the importance of the controlled partial oxidation of terminal alkenes for fine chemical synthesis.

The crux of this work was to attempt to understand the effect of cluster size and activation conditions on the reactivity of the catalytic system. There is no observable advantage to employing atomically precise gold phosphine over the larger Au₁₀₁ nanoparticles in the reactions studied in this chapter. Overall, benzaldehyde was formed as the main product in most of the reactions with slight variation in the amounts of other by-products formed, which was not dependent on the supported cluster used. More focused kinetic studies may help illuminate avenues for controlling the product selectivity.

Attempts to understand the light sensitivity of the titania supported gold clusters by prewashing the P-25 titania support with sulphuric acid yielded an active support for the

formation of styrene oligomers. The acidic surface functionality is known to modify the photocatalytic behaviour of the support, as well impeding nanoparticle sintering. Gold supported on the acid washed support didn't appear to greatly alter the polymerisation activity of the titania support, which after a 24 hour period had consumed all the styrene. However, when either styrene oxide or benzyl alcohol was used as the starting material, benzaldehyde was formed as the major product when gold supported on the acid washed supports was used. This acid washed supports should be investigated for catalytic activity in other systems where the radical polymerisation is not a competing side reaction.

Overall, the reactivity was seemingly low for this series of catalysts as compared to previous literature reports. To a certain extent, this can be explained by the use of lower loadings of gold cluster on the support material, a shorter run time for the catalytic reactions (16 hour as opposed to 18/24 hours) and possibly the presence of phosphine in the system. In certain cases, the pure support material was more active for gold oxidation than some of the gold containing samples which were not activated. The presence of the triphenyl phosphine ligands on the surface of the cluster, which we previously demonstrated was present on the surface was having a deactivating effect for the oxidation reaction.

Bridge

The following chapter will discuss the other areas that some supported gold phosphine clusters prepared in this thesis were used by our collaborators for other applications besides oxidation catalysis. In some systems, small gold clusters did prove advantageous over larger gold nanoparticle systems.

References

- (1) Mizuno, N.: *Modern heterogeneous oxidation catalysis*; Wiley Online Library, **2009**.
- (2) *Handbook of Heterogeneous Catalysis*; Ertl, G.; Knozinger, H.; Schuth, F.; Weitkamp, J., Eds.; Wiley-VCH Verlag GmbH & Co. : Weinheim, 2008; Vol. 1.
- (3) Thomas, J. M.: Heterogeneous Catalysis: Enigmas, Illusions, Challenges, Realities and Emergent Strategies of Design. *The Journal of Chemical Physics* **2008**, *128*, 182502.
- (4) Haruta, M.: Low-temperature oxidation of CO over gold supported on TiO₂, Fe₂O₃, and Co₃O₄. *Journal of Catalysis* **1993**, *144*, 175-192.
- (5) Haruta, M.; Yamada, N.; Kobayashi, T.; Iijima, S.: Gold catalysts prepared by coprecipitation for low-temperature oxidation of hydrogen and of carbon monoxide. *Journal of Catalysis* **1989**, *115*, 301-309.
- (6) Teo, P.; Wickens, Z.; Dong, G.; Grubbs, R.: Efficient and highly aldehyde selective wacker oxidation. *Organic letters* **2012**, *14*, 3237-3246.
- (7) Bäckvall, J.-E.: *Modern oxidation methods*; Wiley-VCH, **2011**.
- (8) Weissermel, K.; Arpe, H.-J.: *Industrial Organic Chemistry*; Third edition ed., **2003**.
- (9) Smith, M. B.; March, J.: *March's Advanced Organic Synthesis*; Fifth edition ed.; Wiley: New York, **2001**.
- (10) Dong, G.; Teo, P.; Wickens, Z.; Grubbs, R.: Primary alcohols from terminal olefins: formal anti-Markovnikov hydration via triple relay catalysis. *Science* **2011**, *333*, 1609-1621.
- (11) Sheldon, R.; Cornils, B.; Herrmann, W.: Applied Homogeneous Catalysis with Organometallic Compounds. *Wiley-VCH Verlag GmbH, Weinheim* **2002**, *1*, 412-427.
- (12) Spreight, J. G.: *Chemical and Process Design Handbook*; McGraw-Hill, **2002**.
- (13) Hayashi, T.; Tanaka, K.; Haruta, M.: Selective vapor-phase epoxidation of propylene over Au/TiO₂ catalysts in the presence of oxygen and hydrogen. *Journal of Catalysis* **1998**, *178*, 566-575.
- (14) Riegel, E. R.; Kent, J. A.: *Handbook of Industrial Chemistry*; Kluwer Academic/Plenum Publishers, **2003**.
- (15) Ertl, G.; Knözinger, H.: *Handbook of heterogeneous catalysis*; Wiley-VCH, **2008**.
- (16) Katsuki, T.; Sharpless, K. B.: The first practical method for asymmetric epoxidation. *Journal of the American Chemical Society* **1980**, *102*, 5974-5976.
- (17) Sharpless, K. B.; Rossiter, B. E.; Hill, J. G.: Anhydrous tert-Butyl Hydroperoxide in Toluene: The Preferred Reagent for Applications Requiring Dry TBHP. *Journal of Organic Chemistry* **1983**, *48*, 3607.
- (18) Jacobsen, E. N.; Pfaltz, A.; Yamamoto, H.: *Comprehensive Asymmetric Catalysis: Supplement 1*; Springer, **2003**; Vol. 1.
- (19) Zhang, W.; Basak, A.; Kosugi, Y.; Hoshino, Y.; Yamamoto, H.: Enantioselective epoxidation of allylic alcohols by a chiral complex of vanadium: An effective

controller system and a rational mechanistic model. *Angewandte Chemie International Edition* **2005**, *44*, 4389-4391.

(20) Mizuno, N.: *Modern Heterogeneous Oxidation Catalysis*; Wiley-VCH: Weinheim, 2009.

(21) Turner, M.; Golovko, V. B.; Vaughan, O. P. H.; Abdulkin, P.; Berenguer-Murcia, A.; Tikhov, M. S.; Johnson, B. F. G.; Lambert, R. M.: Selective oxidation with dioxygen by gold nanoparticle catalysts derived from 55-atom clusters. *Nature* **2008**, *454*, 981-983.

(22) Li, G.; Jin, R.: Atomically Precise Gold Nanoclusters as New Model Catalysts. *Accounts of Chemical Research* **2013**.

(23) Corma, A.; Garcia, H.: Supported gold nanoparticles as catalysts for organic reactions. *Chemical Society reviews* **2008**, *37*, 2096-2222.

(24) Haruta, M.; Kobayashi, T.; Sano, H.; Yamada, N.: Novel gold catalysts for the oxidation of carbon monoxide at a temperature far below 0°C. *Chem. Lett. (Jpn)* **1987**, *16*, 405-408.

(25) Mikami, Y.; Dhakshinamoorthy, A.; Alvaro, M.; Garcia, H.: Catalytic activity of unsupported gold nanoparticles. *Catalysis Science & Technology* **2012**.

(26) Boualleg, M.; Guillois, K.; Istria, B.; Burel, L.; Veyre, L.; Basset, J.-M.; Thieuleux, C.; Caps, V.: Highly efficient aerobic oxidation of alkenes over unsupported nanogold. *Chemical Communications* **2010**, *46*, 5361-5364.

(27) Haruta, M.: New Generation of Gold Catalysts: Nanoporous Foams and Tubes—Is Unsupported Gold Catalytically Active? *ChemPhysChem* **2007**, *8*, 1911-1913.

(28) Hughes, M. D.; Xu, Y.-J.; Jenkins, P.; McMorn, P.; Landon, P.; Enache, D. I.; Carley, A. F.; Attard, G. A.; Hutchings, G. J.; King, F.; Stitt, E. H.; Johnston, P.; Griffin, K.; Kiely, C. J.: Tunable gold catalysts for selective hydrocarbon oxidation under mild conditions. *Nature* **2005**, *437*, 1132-1135.

(29) Lignier, P.; Morfin, F.; Mangematin, S.; Massin, L.; Rousset, J.-L.; Caps, V.: Stereoselective stilbene epoxidation over supported gold-based catalysts. *Chemical Communications* **2007**, 186-194.

(30) Azar, M.; Caps, V.; Morfin, F.; Rousset, J.-L.; Piednoir, A.; Bertolini, J.-C.; Piccolo, L.: Insights into activation, deactivation and hydrogen-induced promotion of a Au/TiO₂ reference catalyst in CO oxidation. *Journal of Catalysis* **2006**, *239*, 307-312.

(31) Mendez, V.; Caps, V.; Daniele, S.: Design of hybrid titania nanocrystallites as supports for gold catalysts. *Chemical Communications* **2009**, 3116-3124.

(32) Lignier, P.; Comotti, M.; Schüth, F.; Rousset, J. L.; Caps, V.: Effect of the titania morphology on the Au/TiO₂ catalyzed aerobic epoxidation of stilbene. *Catalysis Today* **2009**, *141*, 355-715.

(33) Patil, N. S.; Uphade, B. S.; McCulloh, D. G.; Bhargava, S. K.; Choudhary, V. R.: Styrene epoxidation over gold supported on different transition metal oxides prepared by homogeneous deposition-precipitation. *Catalysis Communications* **2004**, *5*, 681-685.

(34) Patil, N. S.; Uphade, B. S.; Jana, P.; Sonawane, R. S.; Bhargava, S. K.; Choudhary, V. R.: Epoxidation of Styrene by Anhydrous t-Butyl Hydroperoxide over Au/TiO₂ Catalysts. *Catal Lett* **2004**, *94*, 89-93.

(35) Sermon, P. A.; Bond, G.; Wells, P.: Hydrogenation of Alkenes over supported gold *Journal of the Chemistry Society, Faraday Discussions* **1979**, *1*, 385-394.

(36) Haruta, M.: Catalysis: Gold rush. *Nature* **2005**, *437*, 1098-1099.

- (37) Haruta, M.: Catalysis of gold nanoparticles deposited on metal oxides. *CATTECH* **2002**, 6, 102-115.
- (38) Council, W. G.: Gold reference catalysts. *Gold Bulletin* **2003**, 36, 24.
- (39) Jin, R.: Quantum sized, thiolate-protected gold nanoclusters. *Nanoscale* **2010**, 2, 343-362.
- (40) Brust, M.; Fink, J.; Bethell, D.; Schiffrin, D.; Kiely, C.: Synthesis and reactions of functionalised gold nanoparticles. *Journal of the Chemical Society, Chemical Communications* **1995**, 1655-1656.
- (41) Zhu, Y.; Qian, H.; Jin, R.: An atomic-level strategy for unraveling gold nanocatalysis from the perspective of Au(n)(SR)_m nanoclusters. *Chemistry : A European Journal* **2010**, 16, 11455-11517.
- (42) Lopez-Acevedo, O.; Kacprzak, K. A.; Akola, J.; Häkkinen, H.: Quantum size effects in ambient CO oxidation catalysed by ligand-protected gold clusters. *Nature Chemistry* **2010**, 2, 329-334.
- (43) Yan, Z.; Huifeng, Q.; Rongchao, J.: Catalysis opportunities of atomically precise gold nanoclusters. *Journal of Materials Chemistry* **2011**, 21.
- (44) Lignier, P.; Morfin, F.; Mangematin, S.; Massin, L.; Rousset, J.-L.; Caps, V.: Stereoselective stilbene epoxidation over supported gold-based catalysts. *Chemical Communications* **2007**, 186-188.
- (45) Hughes, M. D.: Tunable gold catalysts for selective hydrocarbon oxidation under mild conditions. *Nature* **2005**, 437, 1132-1135.
- (46) Liu, Y.; Tsunoyama, H.; Akita, T.; Xie, S.; Tsukuda, T.: Aerobic Oxidation of Cyclohexane Catalyzed by Size-Controlled Au Clusters on Hydroxyapatite: Size Effect in the Sub-2 nm Regime. *ACS Catal.* **2011**, 1, 2-6.
- (47) Liu, Y.; Tsunoyama, H.; Akita, T.; Tsukuda, T.: Efficient and selective epoxidation of styrene with TBHP catalyzed by Au₂₅ clusters on hydroxyapatite. *Chemical Communications* **2010**, 46, 550-552.
- (48) Turner, M.; Vaughan, O. P. H.; Lambert, R.: Partial Oxidations with NO₂ Catalysed by Large Gold Particles. *Chemical Communications* **2008**, 2316.
- (49) Murzin, D.; Salmi, T.: *Catalytic Kinetics*; Elsevier: Amsterdam, **2005**.
- (50) Fischer, K.; Wilken, M.: Experimental determination of oxygen and nitrogen solubility in organic solvents up to 10 MPa at temperatures between 298 K and 398 K. *The Journal of Chemical Thermodynamics* **2001**, 33, 1285-1308.
- (51) Pangborn, A. B.; Giardello, M. A.; Grubbs, R. H.; Rosen, R. K.; Timmers, F. J.: Safe and convenient procedure for solvent purification. *Organometallics* **1996**, 15, 1518-3038.
- (52) David, D. J.: *Gas Chromatographic Detectors*; John Wiley & Sons: New York, **1974**.
- (53) Tsentelovich, Y. P.; Kulik, L. V.; Gritsan, N. P.; Yurkovskaya, A. V.: Solvent Effect on the Rate of β -Scission of the tert-Butoxyl Radical. *The Journal of Physical Chemistry A* **1998**, 102, 7975-7980.
- (54) Kesavan, L.; Tiruvalam, R.; Rahim, M. H. A.; bin Saiman, M. I.; Enache, D. I.; Jenkins, R. L.; Dimitratos, N.; Lopez-Sanchez, J. A.; Taylor, S. H.; Knight, D. W.; Kiely, C. J.; Hutchings, G. J.: Solvent-Free Oxidation of Primary Carbon-Hydrogen Bonds in Toluene Using Au-Pd Alloy Nanoparticles. *Science* **2011**, 331, 195-199.
- (55) Lopez-Sanchez, J.; Dimitratos, N.; Hammond, C.; Brett, G.; Kesavan, L.; White, S.; Miedziak, P.; Tiruvalam, R.; Jenkins, R.; Carley, A.; Knight, D.; Kiely, C.;

Hutchings, G.: Facile removal of stabilizer-ligands from supported gold nanoparticles. *Nature chemistry* **2011**, *3*, 551-557.

(56) Lignier, P.; Morfin, F.; Piccolo, L.; Rousset, J.-L.; Caps, V.: Insight into the free-radical chain mechanism of gold-catalyzed hydrocarbon oxidation reactions in the liquid phase. *Catalysis today* **2007**, *122*, 284-291.

(57) Chusuei, C.; Lai, X.; Davis, K.; Bowers, E.; Fackler, J.; Goodman, D.: A nanoscale model catalyst preparation: Solution deposition of phosphine-stabilized gold clusters onto a planar TiO₂ (110) support. *Langmuir* **2001**, *17*, 4113-8230.

(58) Jin, R.; Zhu, Y.; Qian, H.: Quantum-sized gold nanoclusters: bridging the gap between organometallics and nanocrystals. *Chemistry : A European Journal* **2011**, *17*, 6584-6677.

7 Further applications of supported gold clusters

Ligand-stabilised metal clusters have a wide range of novel applications in a vast array of disciplines due to their incredibly high surface area and unique size-dependent properties, which can be altered by the presence or absence of a single metal atom. There are many reviews on the potential uses of metal clusters and nanoparticles in cancer detection and treatment, as catalysts for new energy sources and as the building blocks for a range of new novel materials and for environmental amelioration.¹⁻⁴ In the previous chapter, we have shown that ligand-stabilised gold clusters on metal oxide supports are catalytically active for the oxidation of styrene. In collaboration with our international colleagues, we have also shown that these small gold clusters can be active for the photocatalytic production of hydrogen and as the active phase in photochromic gas sensors.

Hydrogen gas sensors based on gold clusters

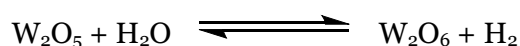
Overview

In collaboration with Professor Wojtek Wlodarski at RMIT University in Melbourne, gold phosphine clusters were investigated for their applications in photochromic hydrogen gas sensors. Samples of gold clusters deposited on tungsten oxide powders and samples of the pure unsupported gold clusters were prepared at the University of Canterbury, New Zealand. The gas sensing performance testing was conducted at RMIT, Melbourne, Australia

Hydrogen-based energy sources are currently being investigated as alternatives to the carbon based energy sources currently used.⁵ As an energy source, there are a wide range of benefits to hydrogen when compared to oil, such as benign by-products and plentiful supply in the form of water. With recent advances in the field of photocatalytic water splitting,^{6,7}

there is a need for improved methods for the detection of low concentrations of hydrogen gas, which has several associated potential risks such as a wide explosive concentration range, low ignition energy, large flame propagation velocity.⁸ Metal oxide materials have shown great potential as gasochromic sensors for hydrogen, where the optical properties of the metal oxides, such as ZnO, TiO₂ or WO₃ vary due to the injection/ejection of ions or electrons in the films.⁹ However, metal nanoparticles, such as platinum, palladium, copper and silver, are required as catalysts to improve the performance, reversibility, and selectivity of these metal oxide films as hydrogen sensors and fuel cells.¹⁰⁻¹² For this study, tungsten oxide was used as the metal oxide sensing layer on which gold clusters were deposited. Tungsten trioxide, an n-type semiconductor, is known to react with various gases. Therefore, a wide range of potential applications in photovoltaics, electrochromic devices and in water splitting have been demonstrated.¹³⁻¹⁶ Despite the improvements in hydrogen sensing the nature of the active site and the mechanism for the reaction on the surface of the sensor material is still poorly understood.¹⁷ Gold supported on WO₃ has been shown to be an excellent sensor for a wide range of gases such as hydrogen and hydrogen sulfide. The gasochromic transition of Au/WO₃ from transparent to a coloured state has been proposed to occur by dissociative chemisorption of molecular hydrogen onto the gold particles which reduces the hydrogen, forming hydrogen ions and releasing electrons in to the metal oxide layer. This results in the reduction of the W⁶⁺ (transparent) centre in the WO₃ crystal lattice to W⁵⁺ (blue colour) and the formation of water vapour from the combination of 2H⁺ with surface bound O²⁻ ions produced by the reduction of W⁶⁺ to W⁵⁺:

The reverse reaction occurs when hydrogen gas is purged from the system at elevated temperatures with synthetic air, restoring the stoichiometry of the WO₃, i.e. W⁵⁺ → W⁶⁺.



It has been shown that Au/WO₃ based systems can significantly outperform comparable Pt/WO₃ sensors.¹⁸ Gold systems have been shown to be giving an improved response and improved detection limits have also been achieved.¹⁸⁻²¹ The cause of the

improved sensor performance has not been conclusively proven, but it has been proposed that the gold nanoparticles which interact with the metal oxide support at the interface with gold where activation (or dissociation) of the hydrogen and other gases occurs, which aligns well with the proposed mechanism for the activation of supported gold particles on titania.^{21,22}

The benefits of using noble metal nanoparticles, supported on tungsten oxide films, are illustrated in Figure 82. The absorbance spectrum of tungsten oxide films (500 nm thick) is shown without and with gold catalyst, as shown in Figure 82A. The supported gold clusters slightly shift the spectrum towards the blue region while also increasing the magnitude of the absorbance (Figure 82A)

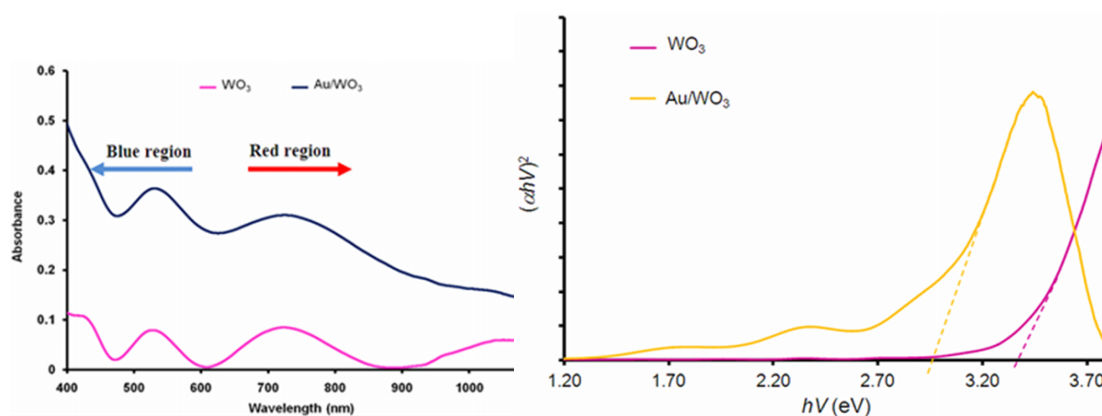


Figure 82: A) Absorbance versus optical wavelength of sputtered WO₃ coated with ligand-stabilised gold clusters on quartz substrates as compared to only sputtered WO₃; B) Estimated optical band gap of sputtered WO₃ (3.36 eV) and Au/WO₃ (3.00 eV) This data was collected by Muhammad Z. Ahmad at RMIT, Melbourne

The alteration in the absorbance spectra of the WO₃ films coated with the gold clusters demonstrates the modification of the optical band gap of the films. The optical band gap of the sputtered tungsten oxide films was estimated with reference to their absorbance spectra measured at room temperature according to the Tauc method.^{23,24} The band gap estimation curves, which were derived from the films absorbance spectra, are shown in Figure 82B. Using the Tauc method, the band gap is the value where the tangent to the curve intersects the band gap energy axis as shown by the extrapolation of the dashed lines in the figure. As shown in Figure 82B, the optical band gap of the tungsten oxide layer reduces after deposition and subsequent annealing of the gold clusters. The optical band gap of the single layer sputtered WO₃ was found to be 3.36 eV; this value is within the range of 3.00 – 3.40 eV

reported in the literature.²⁵ Upon deposition of the gold layer, the band gaps reduced to 3.00 eV, possibly due to the formation of the gold oxide interaction with the support, as recently proposed.²⁶

Overall, there has been tremendous momentum in the fabrication of novel sensor materials in recent years; however, further development of these model systems with nanostructured morphologies is required to improve reversibility, repeatability, selectivity and lifetimes of these sensor materials. Our collaborative research was aimed at using atomically precise ligand-stabilised gold clusters as the active species supported on a variety of nanostructured tungsten oxide materials (*i.e.* nanofilms, nanoparticles and nanofibres). In the following pages, I will summarise some of our recent results of supported $[\text{Au}_9(\text{PPh}_3)_8](\text{NO}_3)_3$ on tungsten oxide nanofilms.

Hydrogen gas-sensing experiments

The performance of two nanostructured sensors, termed S_1 and S_2 , for the detection of hydrogen gas, from room temperature to 450 °C, was conducted on the experimental set-up outlined in Figure 82. A constant gas flow of 200 sccm was maintained by the mass flow controllers in the enclosed test chamber during the sensor experiments. An external heater (connected to a thermocouple for in-situ measurements) was employed throughout the test to vary the operating temperatures of the sensors, as shown in Figure 83B. A computerized gas calibration system was used for to adjust the hydrogen concentrations (in v/v %) to 0.06, 0.13, 0.25, 0.50, 0.75, and 1.00 balanced in synthetic air.

The ideal operational temperatures were identified by exposing each sensor (S_1 and S_2) to hydrogen (0.06 v/v %) balanced in synthetic air during a series of on/off cycles, with a cycle step duration (either on or off) of 180 seconds at room temperature. Upon completion, the temperature was increased stepwise at an interval of 50 °C for the next measurement.

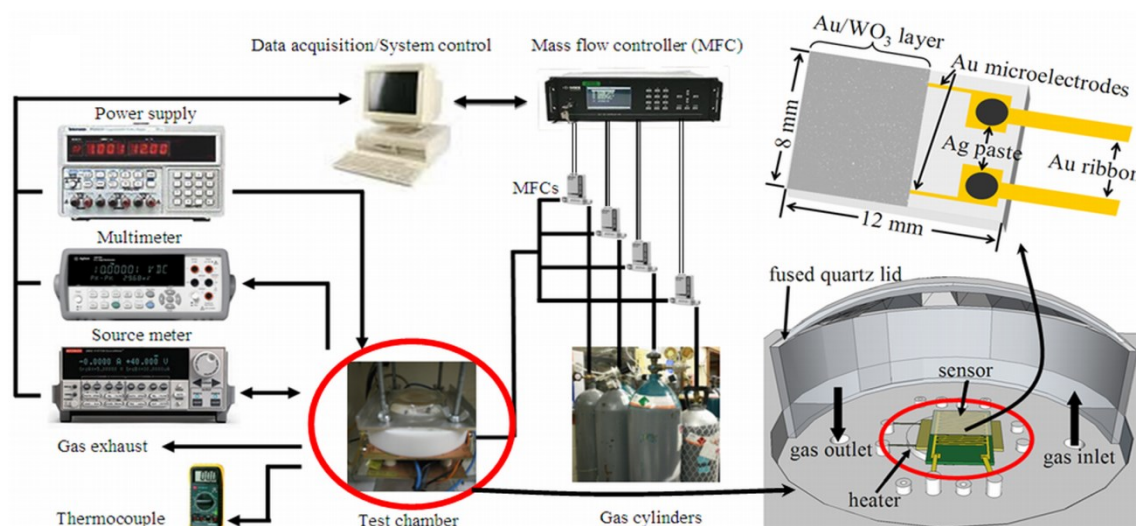


Figure 83: Hydrogen sensing performance of various nanostructured layers was conducted at RMIT, Melbourne Australia on a set-up illustrated above (a) Gas testing setup; (b) sketch of test chamber, and (c) Au/WO₃ based sensor on gold interdigitated electrode

During the cycles at the optimised temperature for each sensor (S1 and S2), the sensors were exposed to gaseous hydrogen balanced in synthetic air of various concentrations. These concentrations were chosen based on a 25 % decrease from the highest obtainable hydrogen concentration (1 %) to 0.25 % and followed by a 50 % decrease from 0.25 % to 0.13 % and 0.13 % to 0.06 %, respectively. A computer with data logger software was used to log the data in real time. The sensor response (S) was calculated according to the equation $S = R_a/R_g$, where R_a and R_g are the resistance of the sensor in air and hydrogen–synthetic air mixture, respectively.

Preparation of photochromic sensor

Gold interdigitated electrode (IDT) was prepared according to the method previously described by Wlodarski at RMIT.²⁶ The IDT was cleaned with acetone, methanol, and de-ionized (DI) water and blow-dried with nitrogen (N₂) prior to deposition of the tungsten oxide layer by radio-frequency (RF) sputtering. The RF sputtering deposition parameters used to obtain *ca.* 500 nm WO₃-film are given in Table 15.

Table 15: Deposition parameters for WO₃ film by RF sputtering.

| Tungsten target purity | Sample target distance (mm) | Base pressure (Torr) | Pressure during deposition (Torr) | Gas (%) | Substrate temperature (°C) | RF power (W) | Thickness (nm) |
|------------------------|-----------------------------|----------------------|-----------------------------------|--------------------------------|----------------------------|--------------|----------------|
| 99.95% | 70 | 10 ⁻⁵ | 2 × 10 ⁻² | Ar (10) O ₂ (90) | 300 | 80 | 500 |

The gold IDT with the annealed RF sputtered tungsten trioxide film were dip-coated using solutions of [Au₉(PPh₃)₈](NO₃)₃ clusters in methanol at two different concentrations: 0.01 and 0.1 mg/mL, giving rise to series of samples codenamed S₁ and S₂ respectively. The samples were dipped into the gold cluster solution for thirty minutes, quickly followed by blow-drying under nitrogen.

The samples of as-immobilised Au₉ clusters on WO₃ films were annealed in static air at 400 °C for two hours with a temperature ramp up/down of 2 °C/min. This activation process was analogous to the calcination of the previous titania and silica samples. The high temperature activation process is expected to sinter the particles as was observed with our previous results. Once completed, the annealed samples (S₁ and S₂) were attached to gold contact ribbons using silver paste and resin (1:1 ratio). A subsequent heat treatment at 100 °C (hot plate) for 15 – 20 minutes solidified the paste between the electrodes and the IDT.

Characterisation of the photochromic sensors

Scanning Electron Microscopy (SEM) images were obtained using a FEI Nova NanoSEM. SEM imaging revealed the presence of WO_3 nanostructures with the average size of *ca.* 50 nm in the images of the pure, RF-sputtered WO_3 films thin film after annealing to 400 °C. SEM images of the WO_3 films modified with Au clusters (after annealing) suggest presence of relatively large gold nanoparticles of their aggregates sparsely and reasonably uniformly scattered at the surface. Although SEM is clearly not ideal for imaging ultra-small atomically precise clusters, such as nonagold cluster used in this study, it is useful nevertheless as a non-destructive technique which allows imaging over large areas.

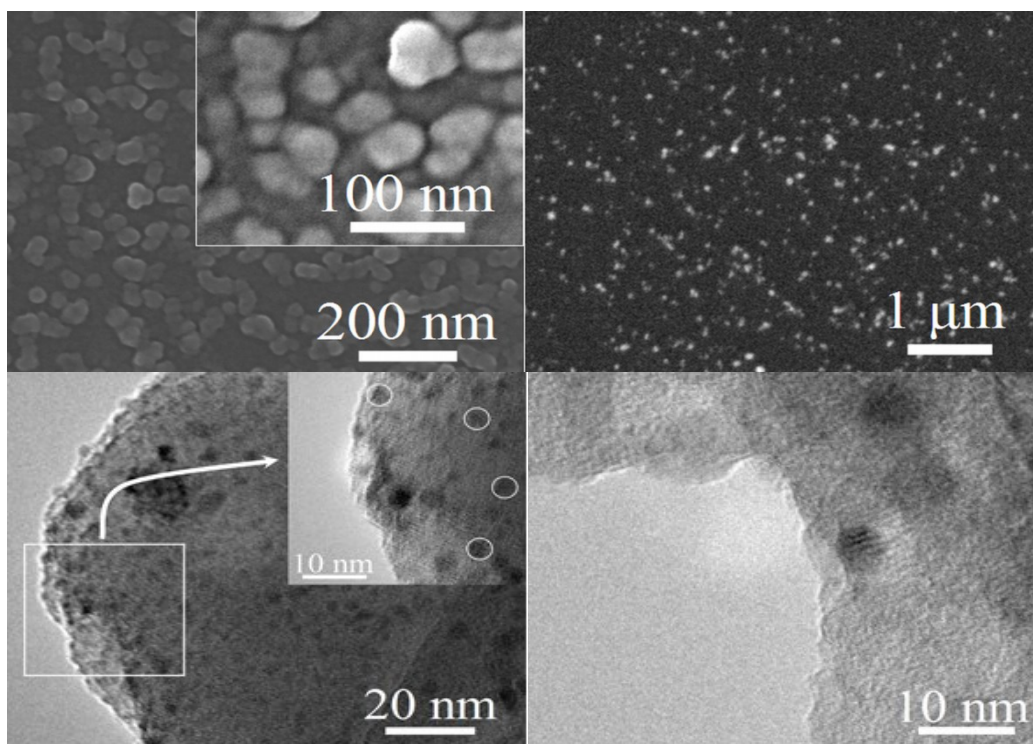


Figure 84; SEM images of A) RF sputtered WO_3 thin film after annealing to 400 °C prior to gold cluster deposition. Inset: higher magnification image of the WO_3 film highlighting its nanostructured nature with approximately 50 nm average size of the crystallite; B) Large Au nanoparticles (white spots) dispersed on WO_3 thin films after deposition and calcination; C) & D) HRTEM images of < 5 nm Au nanoparticles on WO_3 support.

HRTEM images show a significant proportion of the sub-5 nm gold nanoclusters on WO_3 support (in addition to rather large Au particles observed earlier by SEM. Imaging of ultra-small gold clusters on oxide supports using conventional HRTEM becomes progressively more challenging as particle sizes decrease due to the instrumental limitations

and difficulties associated with diminishing differences in contrast between particles and support. The inset of Figure 4a shows a zoomed-in image on a selected area with selected sub-5 nm gold nanoclusters highlighted.

Photoelectron spectroscopy of gold clusters on tungsten oxide films

X-ray photoelectron spectroscopy (XPS) data was collected at room temperature using Cu K α radiation ($\lambda = 1.54178 \text{ \AA}$) by Dr. Günther Anderson on a lab based machine at Flinders University, Australia. The ultra-high vacuum apparatus, built by SPECS (Berlin, Germany), is equipped with a non-monochromatic X-ray source for Mg and Al K α radiation. The spectra of the electrons emitted from the samples are recorded with a hemispherical Phoibos 100 energy analyser from SPECS. High resolution XP spectra were collected using pass energy of 10 eV. The angle between the X-ray irradiation and the analyser is 54° . The base pressure of the UHV chamber was the 10^{-10} mbar range.

Peak analysis was performed in a fashion comparable to the photoelectron data from chapter 5.

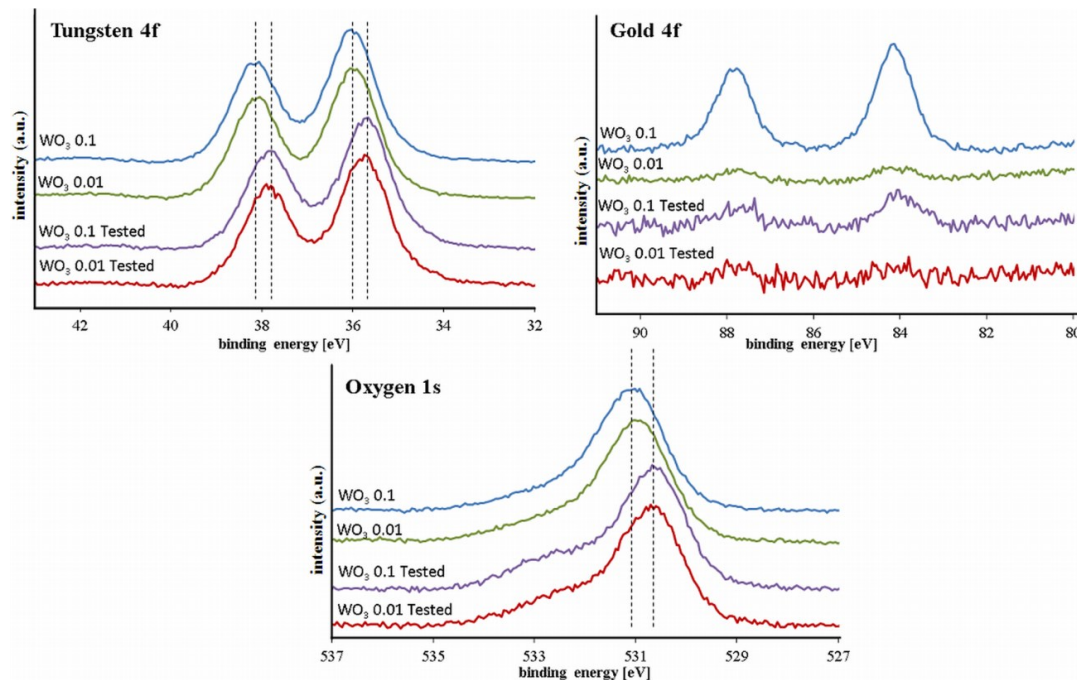


Figure 85; XPS spectra of Au/WO₃ annealed samples (a) tungsten 4f spectra, (b) gold 4f spectra, (c) oxygen 1s spectra. Energy scale has been calibrated with first carbon peak which is attributed to adventitious carbon. S₁ is low concentration sample (0.01) while S₂ is the higher concentration sample (0.1)

The binding energy (BE) of the tungsten $4f_{7/2}$ peak was observed to be at 36.2 ± 0.1 for the S_1 and S_2 samples prior to the calcination of the deposited gold layers, which is similar to reported literature values.²⁷ This value correlates to a mixture both of orthorhombic and monoclinic phases of tungsten trioxide. However, the BE of the tungsten $4f_{7/2}$ of the calcinated, tested S_1 and S_2 samples has a minute shift of -0.3 eV. This shift to 35.78 ± 0.1 eV could be due to loss of oxygen during the second annealing. Similar peak positions have been reported for WO_3 deposited employing various techniques, such as thermal evaporation,²⁸ chemical vapour deposition,²⁹ and sputtering (RF and DC).³⁰ This shift could be influenced by the film thickness as well as by band-bending that occurs due to WO_3 –gold interaction at high metal loadings.¹⁷ It is well known that exposure of the WO_3 thin films to at elevated temperature (> 350 °C) leads to higher peak intensity, which is due to the removal of adventitious carbon,³¹ however, it is the broadening of peaks that is associated with the change in stoichiometry of the sample surface.³² Formation of the oxygen vacancies can be ruled out as one of the dominant factors for materials for films with good gas sensing capabilities.³³

The peak for the O 1s core level in the high resolution photoelectron spectra of the tested and untested S_1 and S_2 samples, Figure 85, was observed at 531.0 eV for untested samples shifting to 530.6 eV after hydrogen sensing testing, which involved exposure to high temperature. Values of the O 1s binding energy reported in the literature vary from 530.7 to 530.4 eV, with variations explained by the thickness, specific nature of materials as well as their preparation (conditions of annealing, temperature and duration etc.).³² A small shoulder centred at about 532.1 eV is observed in the as-deposited and 400 °C annealed films. This shoulder becomes more pronounced when the film is annealed at temperature higher than 400 °C. This peak was attributed to an oxide species present directly on the surface of the sensor.

In the Au spectra, the observed peak position shift could be due to the sintering of a certain proportion of the total population of the gold clusters into larger particles, as alluded to by SEM and TEM, due to the high temperature regime of the experiment and the annealing process. Importantly, detection of ultra-small Au clusters using bulk surface sensitive XPS techniques is challenging when larger Au particles account for a significant

proportion of total gold atomic percentage and contrast with metal oxide materials.³⁴ Diffusion of the gold into the depth of the 500 nm thick WO_3 film upon testing at elevated temperatures might account for the observed diminution of the intensity in case of S_1 series samples.

Performance of nanostructured gold hydrogen sensors

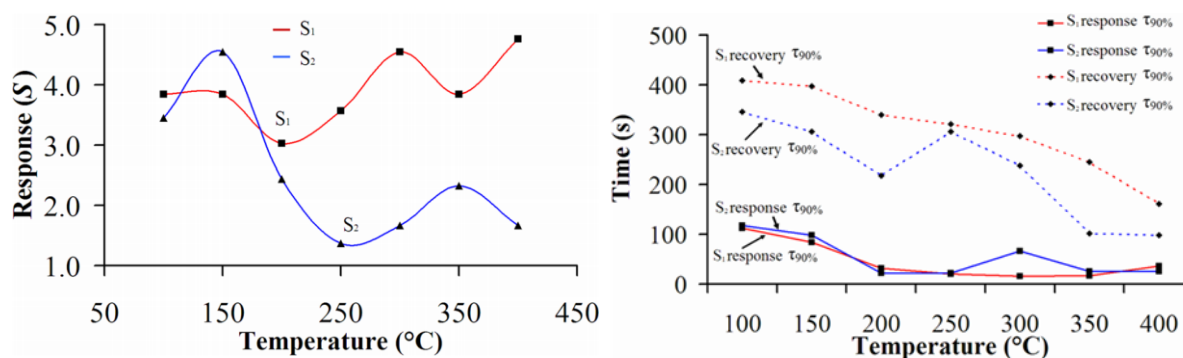


Figure 86: Response of S_1 and S_2 sensors to hydrogen exposure (0.06 v/v% in air) in the wide range of temperatures (100 – 400 °C).

Figure 87 summarises the hydrogen sensing performance of the nanostructured Au/ WO_3 -based sensors, S_1 and S_2 . The response (S) towards hydrogen is shown for temperatures between 100 °C and 400 °C, because of the poor response at low (< 100 °C) and at high (> 400 °C) temperatures. $\tau_{90\%}$ is defined as the time needed to achieve 90% of the maximum change in Figure 86B. We have selected 300 and 350 °C as optimal higher range temperatures for systematic testing of S_1 and S_2 sensors respectively. Although lower temperature may be ideal in terms of response magnitude, at around 150 °C, slower response times are observed at these conditions.

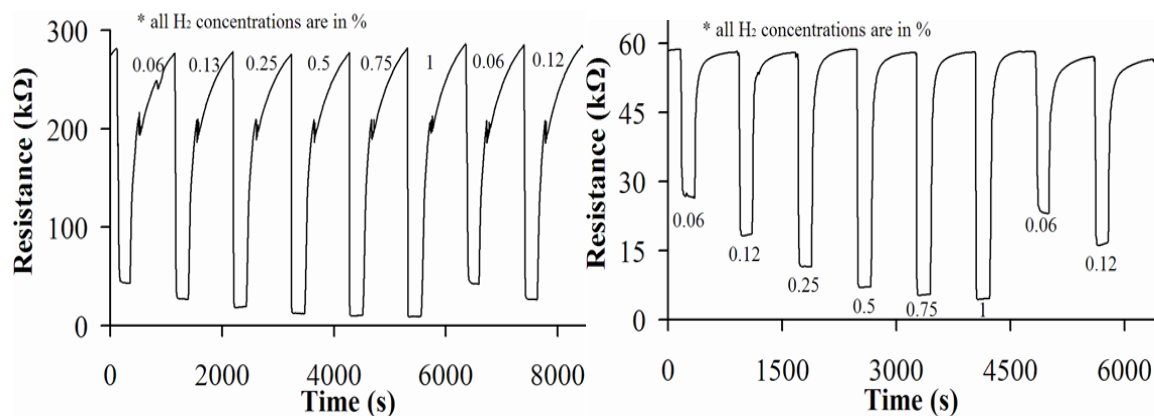


Figure 88: Dynamic performance of the nanostructured Au/WO₃-based sensor A) S₁ towards H₂ of various concentrations at the optimized operating temperature (300 °C); B) sensor S₂ towards H₂ of various concentrations at the optimized operating temperature (350 °C).

In Figure 88, the S₁ and S₂ sensors were systematically tested towards a wider, industrially relevant range of hydrogen concentrations at the optimal operating temperatures, illustrating the dynamic response of the Au/WO₃-based sensor S₁ at the optimized operating temperature of 300 °C in Figure 88A and sensor S₂ at its optimized operating temperature in Figure 88B.

In Figure 86A, the highest magnitude of response of S₁ sensor to hydrogen occurred at 150 °C. However, at this operating temperature poor response and recovery ($\tau_{90\%}$) time of over 500 s were observed (Figure 86B); hence, 350 °C was preferred as the optimized sensor operating temperature, which showed faster response and recovery times very close to complete return of the signal to the baseline level upon switching off the hydrogen flow. The dynamic response of S₁ to various hydrogen concentrations at the optimized operating temperature is shown in Figure 88A. At this temperature, the Au/WO₃-based sensor S₁ showed excellent performance upon exposure to hydrogen at six different concentrations (0.06, 0.13, 0.25, 0.5, 0.75, and 1%). Specifically, pronounced decrease in resistance of up to 90% or more accompanied hydrogen exposure.

Figure 88B demonstrated the dynamic performance of the Au/WO₃-based sensor S₂ which also demonstrates significant responses to hydrogen in the range of tested concentrations. Interestingly, the Au/WO₃-based sensor S₂ has lower starting levels of resistance. The S₂ sensor, (the higher concentration samples) may have a higher loading of the small Au₉ cluster, but because of the calcination process the agglomeration of the clusters

resulted in greater amount of particle sintering. These larger particles were much less effective for catalysing the activation of hydrogen at the surface of the sensor. Au/WO₃-based sensor S₁ demonstrates much greater relative decreases in resistance (*cf.* S₂) indicating that in this case “less is more” when it comes to the effect of Au loading on observed dynamic performance of sensors.

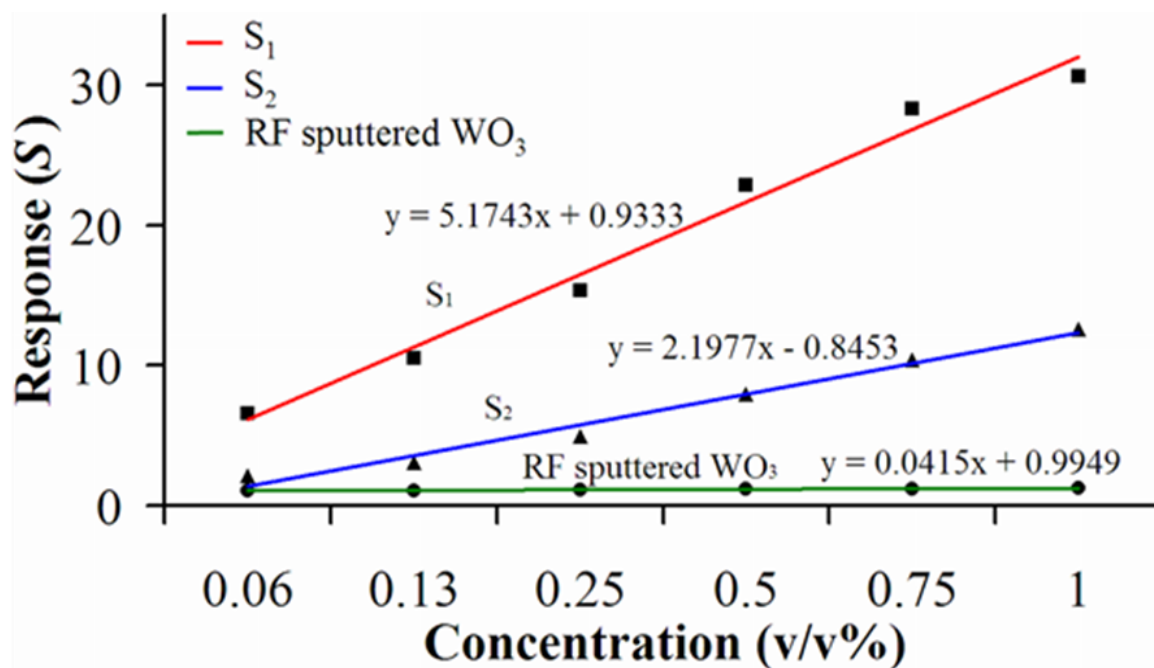


Figure 89: Response towards hydrogen Vs. concentration range of 0.06 – 1 v/v% for the S₁ and S₂ as well as the RF sputtered WO₃ (as comparison) at their respective optimized operating temperatures

The experimental data of the sensor response (S) versus hydrogen concentrations at their respective optimized operating temperatures shows that sensor made with low quantities demonstrated far superior relative response when compared to the control WO₃ film and higher quantities of gold (S₂), shown in Figure 89. It was noted that the experimentally observed trends displayed a linear dependence on hydrogen concentrations throughout the investigated range. This plot confirms that the higher loaded S₂ had a diminished response at temperatures above 200 °C, which was attributed to cluster sintering at elevated temperatures. At high operating temperatures (>150 °C), the issue of humidity was ignored as water desorption was found to occur at a faster rate³⁵. Importantly, the sensor response of S₁ was approximately three times greater than the response of S₂. On comparing the slope coefficients of the fitting equations, it was observed that the rate of

increase in the S_1 response towards hydrogen is approximately 2.5 higher than the response of S_2 . The linear correlation between sensor response and concentration of H_2 , as seen in Figure 89, can be perfectly fitted by the typical relationship observed for metal oxide sensors

$$S(\text{response}) = A(\text{gas concentration})^B,$$

where A and B are defined as a constant typical of the sensing element *i.e.* hydrogen and B values are usually 1 or 1/2, respectively.^{36,37} These constants could also depend on the charge of the surface species and the stoichiometry of the involved reactions.³⁸

Summary

This collaborative project aimed to show the potential of small, atomically precise gold clusters in sensors for hydrogen gas. Preliminary results showed that this approach could be successful in the fabrication of reversible, low-temperature devices as hydrogen sensors. By employing chemically synthesised, atomically precise Au nanoclusters deposited onto WO_3 nanostructured thin film, we have demonstrated proof of concept fabrication for a series of H_2 sensors. Promising performance was shown for an industrially important range of hydrogen concentrations, 0.06 – 1 %. Lower concentrations of gold cluster on the surface yielded a device that outperformed a device with a tenfold increase of gold cluster present on the surface. Characterisation of samples by electron microscopy and XPS showed agglomeration of the clusters occurred; further work on a low temperature sensing regime is warranted in an attempt to distinguish the effect of the un-sintered cluster from the observed larger (≈ 5 nm) nanoparticles. Both sensors showed temperature dependent, high relative responses towards hydrogen at various concentrations tested. Finally, the sensors reported here are promising for industrial applications due to their excellent stability and reproducibility. Further investigations into the performance of these sensors in the presence of other competing gases is required to assess the potential of these devices in practical, real-world applications

There are still many aspects of these devices, however, that still need to be investigated in more depth. A sensor designed with larger gold nanoparticles (> 5 nm) is needed to compare with S_1 and S_2 to confirm or exclude the size effect of the small gold clusters. From a mechanistic viewpoint, there is little information on the interaction of gold

cluster or nanoparticles with hydrogen. The effect of the triphenyl phosphine ligand should also be investigated, as there is potential for the ligand to co-ordinate and interfere with or promote the activation of hydrogen in the sensor device. Post-fabrication modification of the surface with acid or base may also be an interesting avenue to pursue toward further optimisation of these devices.

Photocatalytic hydrogen production from ethanol

Photocatalytic hydrogen production from organic compounds is proving to be a promising route for energy production.⁶ Photocatalysts based upon supported metal nanoparticles on a semi-conductor, such as titania and zinc oxide, have been shown to active for photocatalytic hydrogen production.³⁹ Recent work by Murdoch *et al.* highlighted gold nanoparticles with size range of 2-30 nm on titania are very active for the production of hydrogen from ethanol.⁴⁰ The reactivity of these photocatalysts appeared to be dependent on the morphology and dimensions of the titania support and less sensitive to the gold nanoparticles size. The photocatalytic reaction involves the excitation of the semi-conductor support by photons of equal or higher energy than the band-gap energy. The photoexcitation produces electron-hole pairs that can react with the adsorbed chemical species on the surface. The supported metal nanoparticles help to trap the photo-excited electrons from the conduction band and transfer them to the adsorbed species.⁴¹

A small selection of our gold cluster catalysts, supported on Evonik P-25 titania, were tested for their photocatalytic activity for hydrogen production from ethanol.

Experimental set-up

The photocatalytic reactions were conducted by Dr. Jeff Waterhouse at the University of Auckland. The photocatalytic reactions were conducted in a liquid slurry reactor under nitrogen with ethanol (30 mL) and our supplied catalysts (20 mg). The catalysts were pre-reduced under hydrogen at 673 K at 1 atm. UV-light source consisted of a concentric set of six tubular lamps, with 15 W power and a wavelength of 350 nm position approximately 5 cm from the reactor. Analysis of the reaction products was conducted with two gas

chromatographs equipped with thermal conductivity detectors. Preliminary photocatalytic results

Table 16 presents a summary of the results from the photocatalytic tested conducted at the University of Auckland. These preliminary tests were conducted to ascertain whether there is any improvement in reactivity when using small ligand-stabilised gold clusters. Previous reports by Murdoch *et al.* investigated a range of gold catalysts supported on anatase and rutile.⁴⁰ It was observed that the optimal size of the gold nanoparticles was around 12 nm, and the reaction rate was independent of the gold particle size above 12 nm. In addition, gold nanoparticles supported on anatase were found to be two orders of magnitude higher than that of rutile supported catalysts. In comparison, Evonik P-25 titania consists of a mixture of anatase and rutile was used as the support material for this series of catalysts.⁴² The control reactions with the P-25 support demonstrated moderate reaction rates, upon acid washing with 1 m sulfuric acid, the reaction rate decreased significantly. This can be attributed to the fact that the surface charge of surface is an important contributing factor to the generation of surface radicals.⁴³

Table 16: Summary of results of photocatalytic production of hydrogen of supported gold clusters on titania.

| Sample | Rate ($\mu\text{mol min}^{-1}$) Day 1 | Rate ($\mu\text{mol min}^{-1}$) Day 2 |
|---|---|---|
| Evonik P-25 TiO ₂ | 4.17×10^{-3} | - |
| Evonik P-25 TiO ₂ Acid Washed | 4.69×10^{-4} | - |
| Au ₁₀₁ -TiO ₂ Refluxed at 100 °C for 2 hours | 1.23×10^{-2} | 1.62×10^{-2} |
| Au ₁₀₁₅ -TiO ₂ (Acid Washed) Refluxed at 100 °C for 2 | 4.27×10^{-3} | 6.98×10^{-3} |
| Au ₁₀₁ -TiO ₂ 0.05% Calcined | 1.34×10^{-2} | - |
| Au ₉ -TiO ₂ 0.5% Unheated | 2.49×10^{-3} | - |
| Au ₉ -TiO ₂ 0.5% Heated at 200 °C | 3.56×10^{-3} | - |
| Au ₉ -TiO ₂ 0.5% Calcined at 200 °C | 6.12×10^{-3} | - |

The deposition of the Au₉ cluster appears not to increase the reaction rate, even after various activation procedures are applied. The calcination of the P-25 supported Au₉ cluster appears to have the highest reactivity as compared to the heat treated and untreated Au₉ catalytic samples. TEM and photoelectron studies of the similar samples indicated that calcination under air leads to more cluster sintering on the support. The higher reaction rate of the calcined Au₉ sample can be attributed to the presence of these larger gold particles.

In the case of the supported Au₁₀₁ nanoparticles, the reaction rate is much greater for the Au₁₀₁ supported on P-25 titania as compared to the acid washed system, which were activated by refluxing at 100 °C for two hours. These samples were also tested for two days; and the reactivity doesn't decrease on the second day of testing. A sample was prepared with ten times less gold as compared to the 0.5 % typically used for our series of catalysts. At the lower loading, the catalyst appears to have similar reactivity to the higher loaded refluxed sample.

Overall, these preliminary results indicate that the supported Au₉ does not show any significant increase in reactivity. The larger Au₁₀₁ nanoparticles supported on titania appear to be more reactive than the smaller Au₉ clusters. The surface charge of the titania support also appears to influence the subsequent photocatalytic activity. Acid-washing of the titania support decreases the photocatalytic reactivity. Overall, these preliminary results don't provide any evidence that small gold cluster would be advantageous for photocatalytic production of hydrogen as compared to the recent study by Murdoch *et al.* which indicated that the optimum gold nanoparticle size for this reaction was around 12 nm. More detailed comparisons with larger gold nanoparticles supported on anatase with comparable gold loadings would provide a better picture of how active our catalysts are. Further investigations into the effectiveness of such small gold clusters should attempt to modify the organic ligand. The large, bulky triphenyl phosphine ligand in this system was largely ignored but photoelectron studies have shown that the ligand is present on the surface. Various ligand exchange protocols with thiol ligands could help remove the sterically bulky ligand and improve reactivity.

References

- (1) Femoni, C.; Iapalucci, M. C.; Kaswalder, F.; Longoni, G.; Zacchini, S.: The possible role of metal carbonyl clusters in nanoscience and nanotechnologies. *Coordination Chemistry Reviews* **2006**, *250*, 1580-1604.
- (2) Murty, B. S.; Shankar, P.; Rath, B.; Murday, J.: *Textbook of Nanoscience and Nanotechnology*; Springer, **2012**.
- (3) Frey, N. A.; Peng, S.; Cheng, K.; Sun, S.: Magnetic nanoparticles: synthesis, functionalization, and applications in bioimaging and magnetic energy storage. *Chemical Society Reviews* **2009**, *38*, 2532-2542.
- (4) Dobrovolskaia, M. A.; McNeil, S. E.: *Handbook of Immunological Properties of Engineered Nanomaterials*; World Scientific, **2012**.
- (5) Winter, C.-J.: Energy policy is technology politics—The hydrogen energy case (with an eye particularly on safety comparison of hydrogen energy to current fuels). *International journal of hydrogen energy* **2006**, *31*, 1623-1631.
- (6) Lewis, N. S.; Nocera, D. G.: Powering the planet: Chemical challenges in solar energy utilization. *Proceedings of the National Academy of Sciences* **2006**, *103*, 15729-15735.
- (7) Heyduk, A. F.; Nocera, D. G.: Hydrogen produced from hydrohalic acid solutions by a two-electron mixed-valence photocatalyst. *Science* **2001**, *293*, 1639-1641.
- (8) Rosyid, O. A.; Jablonski, D.; Hauptmanns, U.: Risk analysis for the infrastructure of a hydrogen economy. *International Journal of Hydrogen Energy* **2007**, *32*, 3194-3200.
- (9) Shanak, H.; Schmitt, H.: Fast coloration in sputtered gasochromic tungsten oxide films. *Physica Status Solidi (a)* **2006**, *203*, 3748-3753.
- (10) Zhang, C.; Boudiba, A.; Navio, C.; Bittencourt, C.; Olivier, M.-G.; Snyders, R.; Debliquy, M.: Highly sensitive hydrogen sensors based on co-sputtered platinum-activated tungsten oxide films. *International Journal of Hydrogen Energy* **2011**, *36*, 1107-1114.
- (11) Simon, Q.; Barreca, D.; Bekermann, D.; Gasparotto, A.; Maccato, C.; Comini, E.; Gombac, V.; Fornasiero, P.; Lebedev, O. I.; Turner, S.: Plasma-assisted synthesis of Ag/ZnO nanocomposites: First example of photo-induced H₂ production and sensing. *International Journal of Hydrogen Energy* **2011**, *36*, 15527-15537.
- (12) Al-Saleh, M.; Gultekin, S.; Al-Zakri, A.; Khan, A.: Steady state performance of copper impregnated Ni/PTFE gas diffusion electrode in alkaline fuel cell. *International journal of hydrogen energy* **1996**, *21*, 657-661.
- (13) Lee, E.; Lee, J. M.; Koo, J. H.; Lee, W.; Lee, T.: Hysteresis behavior of electrical resistance in Pd thin films during the process of absorption and desorption of hydrogen gas. *international journal of hydrogen energy* **2010**, *35*, 6984-6991.
- (14) Granqvist, C. G.: Electrochromic tungsten oxide films: review of progress 1993–1998. *Solar Energy Materials and Solar Cells* **2000**, *60*, 201-262.
- (15) Samerjai, T.; Tamaekong, N.; Liewhiran, C.; Wisitsoraat, A.; Tuantranont, A.; Phanichphant, S.: Selectivity towards hydrogen gas by flame-made Pt-loaded WO₃ sensing films. *Sensors and Actuators B: Chemical* **2011**, *157*, 290-297.
- (16) Huang, K.; Pan, Q.; Yang, F.; Ni, S.; Wei, X.; He, D.: Controllable synthesis of hexagonal WO₃ nanostructures and their application in lithium batteries. *Journal of Physics D: Applied Physics* **2008**, *41*, 155417.
- (17) Dwyer, D. J.: Surface chemistry of gas sensors: H₂S on WO₃ films. *Sensors and Actuators B: Chemical* **1991**, *5*, 155-159.
- (18) Zhang, J.; Liu, X.; Wu, S.; Cao, B.; Zheng, S.: One-pot synthesis of Au-supported ZnO nanoplates with enhanced gas sensor performance. *Sensors and Actuators B: Chemical* **2012**, *169*, 61-66

- (19) Stoycheva, T.; Vallejos, S.; Blackman, C.; Moniz, S.; Calderer, J.; Correig, X.: Important considerations for effective gas sensors based on metal oxide nanoneedles films. *Sensors and Actuators B: Chemical* **2012**, *161*, 406-413.
- (20) Della Gaspera, E.; Buso, D.; Guglielmi, M.; Martucci, A.; Bello, V.; Mattei, G.; Post, M. L.; Cantalini, C.; Agnoli, S.; Granozzi, G.: Comparison study of conductometric, optical and SAW gas sensors based on porous sol-gel silica films doped with NiO and Au nanocrystals. *Sensors and Actuators B: Chemical* **2010**, *143*, 567-573.
- (21) Della Gaspera, E.; Buso, D.; Martucci, A.: Gold nanoparticles to boost the gas sensing performance of porous sol-gel thin films. *Journal of sol-gel science and technology* **2011**, *60*, 366-377.
- (22) Buso, D.; Post, M.; Cantalini, C.; Mulvaney, P.; Martucci, A.: Gold nanoparticle-doped TiO₂ semiconductor thin films: Gas sensing properties. *Advanced Functional Materials* **2008**, *18*, 3843-3849.
- (23) Tauc, J.; Menth, A.: States in the gap. *Journal of Non-Crystalline Solids* **1972**, *8-10*, 569-585.
- (24) Kako, T.; Kikugawa, N.; Ye, J.: Photocatalytic activities of AgSbO₃ under visible light irradiation. *Catalysis Today* **2008**, *131*, 197-202.
- (25) Granqvist, C. G.: *Handbook of inorganic electrochromic materials*; Elsevier Science, **1995**.
- (26) Della Gaspera, E.; Martucci, A.; Yaacob, M.; Ou, J.; Kalantar-Zadeh, K.; Wlodarski, W.: WO₃-Au-Pt Nanocrystalline Thin Films as Optical Gas Sensors. *Sensor Letters* **2011**, *9*, 595-599.
- (27) Orsini, G.; Tricoli, V.: Mesoporous, high-surface-area tungsten oxide monoliths with mixed electron/proton conductivity. *Journal of Materials Chemistry* **2010**, *20*, 6299-6308.
- (28) Lozzi, L.; Passacantando, M.; Santucci, S.; La Rosa, S.; Svechnikov, N. Y.: Surface and in depth chemistry of polycrystalline WO₃ thin films studied by X-ray and soft X-ray photoemission spectroscopies. *Sensors Journal, IEEE* **2003**, *3*, 180-188.
- (29) Cross, W. B.; Parkin, I. P.; O'Neill, S. A.; Williams, P. A.; Mahon, M. F.; Molloy, K. C.: Tungsten Oxide Coatings from the Aerosol-Assisted Chemical Vapor Deposition of Photocatalytically Active γ -WO₃ Films. *Chemistry of materials* **2003**, *15*, 2786-2796.
- (30) Frühberger, B.; Grunze, M.; Dwyer, D.: Surface chemistry of H₂ sensitive tungsten oxide films. *Sensors and Actuators B: Chemical* **1996**, *31*, 167-174.
- (31) Dezelah, C. L.; El-Kadri, O. M.; Kukli, K.; Arstila, K.; Baird, R. J.; Lu, J.; Niinistö, L.; Winter, C. H.: A low valent metalorganic precursor for the growth of tungsten nitride thin films by atomic layer deposition. *Journal of Materials Chemistry* **2007**, *17*, 1109-1116.
- (32) Maffei, T.; Yung, D.; LePennec, L.; Penny, M.; Cobley, R.; Comini, E.; Sberveglieri, G.; Wilks, S.: STM and XPS characterisation of vacuum annealed nanocrystalline WO₃ films. *Surface Science* **2007**, *601*, 4953-4957.
- (33) Barton, D. G.; Shtein, M.; Wilson, R. D.; Soled, S. L.; Iglesia, E.: Structure and electronic properties of solid acids based on tungsten oxide nanostructures. *The Journal of Physical Chemistry B* **1999**, *103*, 630-640.
- (34) Herzing, A.; Kiely, C.; Carley, A.; Landon, P.; Hutchings, G.: Identification of active gold nanoclusters on iron oxide supports for CO oxidation. *Science (New York, N.Y.)* **2008**, *321*, 1331-1336.
- (35) Ou, J. Z.; Yaacob, M. H.; Breedon, M.; Zheng, H. D.; Campbell, J. L.; Latham, K.; Plessis, J. d.; Wlodarski, W.; Kalantar-zadeh, K.: In situ Raman spectroscopy of H₂ interaction with WO₃ films. *Physical Chemistry Chemical Physics* **2011**, *13*, 7330-7339.
- (36) Barreca, D.; Carraro, G.; Comini, E.; Gasparotto, A.; Maccato, C.; Sada, C.; Sberveglieri, G.; Tondello, E.: Novel synthesis and gas sensing performances of CuO-TiO₂ nanocomposites functionalized with Au nanoparticles. *The Journal of Physical Chemistry C* **2011**, *115*, 10510-10517.

(37) Barreca, D.; Comini, E.; Ferrucci, A. P.; Gasparotto, A.; Maccato, C.; Maragno, C.; Sberveglieri, G.; Tondello, E.: First Example of ZnO-TiO₂ Nanocomposites by Chemical Vapor Deposition: Structure, Morphology, Composition, and Gas Sensing Performances. *Chemistry of Materials* **2007**, *19*, 5642-5649.

(38) Madou, M. J.; Morrison, S. R.: Chemical Physics of Surfaces. *Academic Press Inc.* **1988**.

(39) Bamwenda, G. R.; Tsubota, S.; Nakamura, T.; Haruta, M.: Photoassisted hydrogen production from a water-ethanol solution: a comparison of activities of Au/TiO₂ and Pt/TiO₂. *Journal of Photochemistry and Photobiology A: Chemistry* **1995**, *89*, 177-189.

(40) Murdoch, M.; Waterhouse, G.; Nadeem, M.; Metson, J.; Keane, M.; Howe, R.; Llorca, J.; Idriss, H.: The effect of gold loading and particle size on photocatalytic hydrogen production from ethanol over Au/TiO₂ nanoparticles. *Nature chemistry* **2011**, *3*, 489-581.

(41) Fujishima, A.; Zhang, X.; Tryk, D. A.: TiO₂ photocatalysis and related surface phenomena. *Surface Science Reports* **2008**, *63*, 515-582.

(42) Ohtani, B.; Prieto-Mahaney, O. O.; Li, D.; Abe, R.: What is Degussa (Evonik) P25? Crystalline composition analysis, reconstruction from isolated pure particles and photocatalytic activity test. *Journal of Photochemistry and Photobiology A: Chemistry* **2010**, *216*, 179-182.

(43) Hadjiivanov, K. I.; Klissurski, D. G.: Surface chemistry of titania (anatase) and titania-supported catalysts. *Chemical Society Reviews* **1996**, *25*, 61-69.

8

Concluding summary and further research

In this thesis, a series of investigations into chemistry of supported, ligand-stabilised gold clusters were conducted. A range of phosphine stabilised gold clusters were prepared with differing core nuclearities, and were characterised in detail. In particular, it was hoped that with improved control of the gold particle size that a distinct particle size effect would be observed for the catalytic oxidation of styrene. A comprehensive study of the electronic structure of the supported gold clusters on titania was conducted, in an effort to understand the effect of various post-deposition treatments had on the electronic structure of the supported gold particles.

In chapter 2, the preparation and characterisation of the atomically precise ligand-stabilised gold clusters was described in detail. The first high resolution far-infrared spectroscopy study of the metal-metal vibrations and metal-ligand vibrations of ligand stabilised gold clusters is presented in chapter 3. In these experiments, the vibrational modes of interest were identified by comparison to their simulated spectrum which was calculated by Jason Alvino and Dr. Gregory Metha at the University of Adelaide. These preliminary studies showed that the far-IR spectroscopy could be used to characterise cluster materials, however, due the strength of the vibrational modes of interest studies on supported gold clusters was not possible. Further studies on the binding of molecular oxygen with the gold clusters may provide a route for identifying the potential active intermediates and transition-states that so far have only been postulated in the literature for ligand stabilised gold clusters

Chapter 4 described the preparation of heterogeneous catalyts derived from ligand protected gold clusters. A range of supports and actviation conditions were employed to generate active heterogeneous catalysts using gold clusters. The nature of the support and type of post-deposition treatment used were discussed and explored. The materials were characterised by HRTEM, which failed to show gold particles smaller than 1.3~1.5 nm accurately, mainly due to the contrast with the metal oxide supports. STEM experiments in Australia on several samples highlighted that in many samples, the population of ~ 1nm was much greater than what was shown by HRTEM

As microscopy of these materials proved difficult to accurately detail the particle size of the gold particles, electronic properties of the heterogeneous gold catalysts were studied using X-Ray photoelectron spectroscopy in chapter 5. This surface sensitive technique provided a range of details on the gold metal oxidation state and also the range of particle sizes present on the surface of the support. Using this bulk sample spectroscopic technique, we were able to do a series of systematic studies, particularly on the titania supported samples. Due to excessive sample charging of the silica samples, a comparative study was not completed.

Finally, chapter 6 discussed the catalytic behaviour of the supported gold clusters for the catalytic oxidation of styrene. A select range of catalysts and reaction conditions with various sources of active oxygen were chosen for this study. The reactivity of the catalysts was shown to be dependent on the source of active oxygen, either molecular oxygen or organic peroxide. The small phosphine clusters (Au_8 and Au_9) should very similar reactivity but differed slightly from the larger Au_{101} nanoparticle system. It was concluded that for the catalytic oxidation of styrene under these reactions conditions, adding a single atom of gold does not make an appreciable difference to the reaction selectivity, until bulk material characteristics become more dominant as the particle size is increased.

In addition, chapter 7 details the further applications of the gold phosphine clusters as hydrogen sensors and as catalysts for the catalytic reduction of alcohol to form hydrogen gas. Overall, the small Au_9 phosphine cluster demonstrated potential as active, reversible hydrogen sensors, when deposited on tungsten trioxide substrates. One area of research that we regrettably did not have the time to pursue was the post-deposition ligand exchange of the supported gold clusters. In this thesis, we purposely used triphenyl phosphine as the ligand for all of the clusters. We showed in this work that after various activation treatments that the triphenyl phosphine was still present on the surface of the catalyst. By using a ligand that is a stronger donor such as trimethyl phosphine or even an alkyl thiol, we could remove the sterically bulky triphenyl phosphine under the right reaction conditions through a ligand substitution from the surface of the metal oxide support.

The nature of the surface charge of the support was not explored in the depth throughout this work; however, modification of the surface charge of the support after

deposition of the gold clusters may also influence the subsequent catalytic activity of the supported gold clusters. A wash treatment of the supported gold clusters, with either acid or base, would lead to different reactivity and also differing cluster sintering kinetics, which has been reported upon previously in various extended surfaces systems. This avenue for research was put on hold due to the difficulty in characterising the surface charge of these materials with adequate equipment, even with synchrotron based XPS and NEXAFS.

Although this thesis was largely concerned with supported phosphine clusters, the unsupported gold phosphine clusters should also be investigated for their catalytic potential. Recent reports of naked gold cluster consisting of thirteen atoms of gold have shown moderate turnover frequencies. The clusters used in this thesis, with sterically bulky triphenyl phosphine, will in all likelihood not show significant activity without some sort of ligand exchange with a less sterically bulky ligand or capping group. In addition, the environmental impact of using such small particles of gold or any metal should also be an important consideration for any further commercial applications. Mixed metal nanoparticles or cluster of gold are also potential area of further interest, particularly with lanthanides and actinides due to their interesting oxidation chemistry. The chemistry of these mixed metal particles is has only just begun to be explored in detail in UHV systems, there are very few reports on the wet-chemical preparation of similar system.

The potential applications of gold based catalysts or devices in industry are still to be exploited fully. Though there are several examples of gold catalysts being employed for large scale epoxidation; more extensive use of gold based systems is limited by several factors such as thermal stability, selectivity and cost. Many of these issues should rapidly be solved over the upcoming years, which should make gold based systems an attractive option for applications as industrial catalysts and devices. In conclusion, the recent gold rush in chemistry has generated a range of new catalytic routes towards chemical targets, new possibilities for sensors, and range of potential applications in medicine. If the gold is to deliver on its many promises, the gulf between many model-extended surface studies and industrially relevant catalysts needs to be bridged. This thesis attempted to bridge some of that gap and also showed that gold based devices have the potential for applications in industry.